


REPORT DOCUMENTATION PAGE			Form Approved OMB No 0704-0188	
<small>Public reporting burden for this collection of information is estimated to average 1 hour per response, including the time for reviewing instructions, searching existing data sources, gathering and maintaining the data needed, and completing and reviewing the collection of information. Send comments regarding this burden estimate or any other aspect of this collection of information, including suggestions for reducing the burden, to Washington Headquarters Services, Directorate for Information Operations and Reports, 1215 Jefferson Davis Highway, Suite 1204, Arlington, VA 22202-4302, and to the Office of Management and Budget, Paperwork Reduction Project (0704-0188), Washington, DC 20503.</small>				
1.  PB97 121354	2. REPORT DATE August 1996	3. REPORT TYPE AND DATES COVERED Final		
4. TITLE AND SUBTITLE Active Control for Seismic-Resistant Structures on Embedded Foundation in Layered Half-Space			5. FUNDING NUMBERS (G) NSF BCS 9302201 NCEER R-35696	
6. AUTHOR(S) Franklin Y. Cheng and Sukit Suthiwong				
7. PERFORMING ORGANIZATION NAME(S) AND ADDRESS(ES) Department of Civil Engineering University of Missouri-Rolla Rolla, MO 65409-0030			8. PERFORMING ORGANIZATION REPORT NUMBER 96-2	
9. SPONSORING/MONITORING AGENCY NAME(S) AND ADDRESS(ES) National Science Foundation 4201 Wilson Blvd./Arlington, VA 22230 National Center for Earthquake Engineering Research State University of New York Buffalo, NY 14260			10. SPONSORING/MONITORING AGENCY REPORT NUMBER	
11. SUPPLEMENTARY NOTES				
12a. DISTRIBUTION AVAILABILITY STATEMENT			12b. DISTRIBUTION CODE	
13. ABSTRACT (Maximum 200 words) The response behavior of seismically excited frame structures with active control and boundless soil is investigated. Mathematical models based on the existence or absence of structure-soil interaction (SSI) and/or control are presented. With SSI consideration, the frequency-dependent property of unbounded nonhomogeneous soil and foundation embedment is applied. Optimal closed-loop laws are established based on the generalized performance index. In the control system considering SSI effects, foundation translation and rocking are included in the control rule. Algorithms are implemented in the time domain. Studies indicate the strong influence of foundation embedment and depth of soil layer on soil-rocking coefficients and consequently on structural response. In a certain structure, additional modes as a result of the foundation's degrees of freedom dominate and hence result in distinct structural response behavior. For example, the rocking mode is important in a massive and/or high-rise structure while the translation mode dominates in a low-rise structure. In a massive low-rise structure such as a nuclear reactor, the combination of these two dominant modes leads to large structural responses. In the control system including SSI effects, reduction of structural response is a result of the decrease in foundation rocking rather than relative floor translation which occurs where the structure is fixed at its base. Furthermore, the effect of control force in strengthening the system's stiffness and damping is reduced in the case of a structure founded on soft soil.				
14. SUBJECT TERMS Active control Earthquake Half-space Soil structure interaction			Foundation Rocking Embedment Optimization	15. NUMBER OF PAGES 261
			Closed loop Performance index	16. PRICE CODE
17. SECURITY CLASSIFICATION OF REPORT Unclassified	18. SECURITY CLASSIFICATION OF THIS PAGE Unclassified	19. SECURITY CLASSIFICATION OF ABSTRACT Unclassified	20. LIMITATION OF ABSTRACT	



FB97 121 354

Civil Engineering Study Structural Series 96-2

**ACTIVE CONTROL FOR SEISMIC-RESISTANT STRUCTURES
ON EMBEDDED FOUNDATION IN LAYERED HALF-SPACE**

by


Franklin Y. Cheng
Curators' Professor

Sukit Suthiwong
Former Ph.D. Student

Department of Civil Engineering
University of Missouri-Rolla
Rolla, MO 65409-0030



Report Series Prepared for the National Science Foundation
under Grant No. NSF BCS 9302201
National Center for Earthquake Engineering Research
under Grant No. NCEER R35696

REPRODUCED BY: 
U.S. Department of Commerce
National Technical Information Service
Springfield, Virginia 22161

Civil Engineering Study Structural Series 96-2



PB97-121354

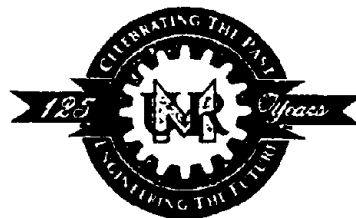
**ACTIVE CONTROL FOR SEISMIC-RESISTANT STRUCTURES
ON EMBEDDED FOUNDATION IN LAYERED HALF-SPACE**

by

Franklin Y. Cheng
Curators' Professor

Sukit Suthiwong
Former Ph.D. Student

Department of Civil Engineering
University of Missouri-Rolla
Rolla, MO 65409-0030



Report Series Prepared for the National Science Foundation
under Grant No. NSF BCS 930221
National Center for Earthquake Engineering Research
under Grant No. NCEER R35696

PROTECTED UNDER INTERNATIONAL COPYRIGHT
ALL RIGHTS RESERVED.
NATIONAL TECHNICAL INFORMATION SERVICE
U.S. DEPARTMENT OF COMMERCE

ABSTRACT

The response behavior of seismically excited frame structures with active control and boundless soil is investigated. Mathematical models based on the existence or absence of structure-soil interaction (SSI) and/or control are presented. With SSI consideration, the frequency-dependent property of unbounded nonhomogeneous soil and foundation embedment is applied. Optimal closed-loop laws are established based on the generalized performance index. In the control system considering SSI effects, foundation translation and rocking are included in the control rule. Algorithms are implemented in the time domain.

Studies indicate the strong influence of foundation embedment and depth of soil layer on soil rocking coefficients and consequently on structural response. In a certain structure, additional modes as a result of the foundation's degrees of freedom dominate and hence result in distinct structural response behavior. For example, the rocking mode is important in a massive and/or high-rise structure while the translation mode dominates in a low-rise structure. In a massive low-rise structure such as a nuclear reactor, the combination of these two dominant modes leads to large structural responses. In the control system including SSI effects, reduction of structural response is a result of the decrease in foundation rocking rather than relative floor translation which occurs where the structure is fixed at its base. Furthermore, the effect of control force in strengthening the system's stiffness and damping is reduced in the case of a structure founded on soft soil.

ACKNOWLEDGEMENTS

This report is mainly supported by the National Science Foundation under grant no. NSF BCS-930221 and partially supported by the National Center for Earthquake Engineering under grant no. NCEER R35696. Actual soil data were obtained at the Takenaka Experimental Building Site in Japan. The authors gratefully acknowledge this support and assistance.

TABLE OF CONTENTS

	Page
ABSTRACT	iii
ACKNOWLEDGMENTS	iv
LIST OF ILLUSTRATIONS	x
LIST OF TABLES	xviii
NOMENCLATURE	xix
SECTION	
I. INTRODUCTION	1
A. OBJECTIVE	1
B. LITERATURE REVIEW	2
C. OVERVIEW	5
II. DYNAMIC SYSTEM MODELING	8
A. TOTAL DYNAMIC SYSTEM	8
B. STRUCTURE SYSTEM	11
C. SOIL SYSTEM	13
1. Free-field System	13
2. Excavated Part of System	15
3. Ground System	15
D. MODELING DIAGRAM	16
III. STATE EQUATIONS FOR FIX- AND SSI-MODEL WITH / WITHOUT CONTROL	19

A.	FORMULATION FOR FIXED BASE MODEL	19
B.	FORMULATION FOR STRUCTURE-SOIL INTERACTION MODEL	23
1.	Single-story Equation of Motion	23
2.	Multistory Equation of Motion	24
3.	Interaction Force at Foundation-soil Interface	28
4.	State Equation of SSI-model	31
C.	SOLUTION TECHNIQUE FOR STATE EQUATIONS	35
IV.	OPTIMAL CONTROL LAW	41
A.	GENERALIZED PERFORMANCE INDEX	42
1.	Transversality Condition	43
2.	Euler's Equation	46
B.	FEEDBACK GAIN MATRIX	46
C.	WEIGHTING MATRIX	48
V.	FREQUENCY-DEPENDENT COEFFICIENTS OF SOIL SYSTEMS ..	53
A.	FREE-FIELD SYSTEM'S STIFFNESS MATRIX	53
1.	Definition and Concept	53
2.	Generalized Strain-displacement Matrix	59
3.	Flexibility Matrix	62
4.	Integration Technique	68
B.	EXCAVATED PART'S STIFFNESS MATRIX	70
1.	Definition and Concept	70
2.	Element Stiffness Matrix	79

3.	Element Mass Matrix	85
C.	GROUND SYSTEM'S STIFFNESS AND FLEXIBILITY MATRICES	86
1.	Dynamic Stiffness Matrix	86
2.	Time-derivative Dynamic Flexibility Matrix	87
3.	Impulse Velocity Matrix	89
VI	INVESTIGATION OF DYNAMIC STIFFNESS COEFFICIENTS OF SOIL SYSTEMS	97
A.	SCOPE OF INVESTIGATION	97
1.	Study Parameters and Actual Site Data	97
2.	Nondimensionalized Spring and Damping Coefficients	99
B.	INVESTIGATION OF EXCAVATED PART'S COEFFICIENTS	100
1.	Effects of Hysteretic Damping	102
2.	Effects of Foundation Embedment	108
C.	INVESTIGATION OF FREE-FIELD SYSTEM COEFFICIENTS	113
1.	Effects of Foundation Embedment	115
2.	Effects of Layer's Depth	120
D.	INVESTIGATION OF GROUND SYSTEM COEFFICIENTS	126
1.	Dynamic Stiffness Coefficients	126
a.	Effects of Foundation Embedment	127
b.	Effects of Layer's Depth	132
2.	Time-derivative Flexibility Coefficients	133

3.	Impulse Velocity Coefficients	137
VII.	INVESTIGATION OF TOTAL DYNAMIC SYSTEMS WITH AND WITHOUT CONTROL	143
A.	SCOPE OF INVESTIGATION	143
1.	Concerning Parameters	143
2.	Governing Parameters	146
B.	INVESTIGATION OF SINGLE STORY WITHOUT CONTROL	147
1.	Structural Response vs. Time	147
2.	Effects of Floor Mass and Slenderness Ratio	152
3.	Effects of Fixed-base Frequency	160
4.	Effects of Soil's Layer Depth	166
C.	INVESTIGATION OF 10-STORY STRUCTURE WITH CONTROL	169
VIII.	CONCLUSIONS	182
A.	MATHEMATICAL MODELS	182
B.	STUDY OF SOIL SYSTEMS	184
1.	System's Excavated Part	185
2.	Free-field System	185
3.	Ground System	187
C.	BEHAVIOR OF TOTAL DYNAMIC SYSTEMS	188
1.	System without Control	188
2.	System with Control	190

APPENDICES

A. GREEN'S INFLUENCE FUNCTION 192

B. STIFFNESS MATRICES OF LAYER AND HALF-PLANE 224

C. WAVE EQUATIONS IN CARTESIAN COORDINATES 241

REFERENCES 259

BIBLIOGRAPHY 261

LIST OF ILLUSTRATIONS

Figure	Page
1 Multistory Controlled Building Embedded in Unbounded Soil	9
2 Two-dimensional Dynamic System	10
3 Structure System Modeling	12
4 Free-field System with Rigid Interface	14
5 Excavated Part of System with Rigid Interface	15
6 Ground System with Rigid Interface	16
7 Fixed-base Diagram	16
8 Controlled Fixed-base Diagram	17
9 Structure-soil Interaction Diagram	17
10 Controlled Structure-soil Interaction Diagram	18
11 Single-story SSI-model	21
12 Free-body Diagram of Single-story SSI-model	22
13 Structure System with Fictitious Springs Subjected to Equivalent Forces	32
14 Forces and Displacements of Free-field System with Rigid Interface	53
15 Prescribed Displacements along Rigid Interface	55
16 Linearly Distributed Loads along Assumed Line	56
17 Flexibility Matrix Diagram	68
18 Diagonal Integrand of Submatrix [1-1] vs. k Wave-number	71
19 Off-diagonal Integrand of Submatrix [1-1] vs. k Wave-number	71
20 Diagonal Integrand of Submatrix [1-3] vs. k Wave-number	72

21	Off-diagonal Integrand of Submatrix [1-3] vs. k Wave-number	72
22	Forces and Displacements of Excavated Part of System with Rigid Interface ...	73
23	Discretization of Excavated Part of System	74
24	Rigid Body Degrees of Freedom of Excavated Part of System	78
25	Four-node Rectangular Element	80
26	Forces and Displacements of Ground System with Rigid Interface	87
27	Spring Coefficient (K_x) of Excavated Part of System, $D/B=2.0$, with Indicated Damping Ratio	104
28	Damping Coefficient (C_x) of Excavated Part of System, $D/B=2.0$, with Indicated Damping Ratio	104
29	Spring Coefficient (K_{xy}) of Excavated Part of System, $D/B=2.0$, with Indicated Damping Ratio	105
30	Damping Coefficient (C_{xy}) of Excavated Part of System, $D/B=2.0$, with Indicated Damping Ratio	105
31	Spring Coefficient (K_y) of Excavated Part of System, $D/B=2.0$, with Indicated Damping Ratio	106
32	Damping Coefficient (C_y) of Excavated Part of System, $D/B=2.0$, with Indicated Damping Ratio	106
33	Spring Coefficient (K_z) of Excavated Part of System, $D/B=2.0$, with Indicated Damping Ratio	107
34	Damping Coefficient (C_z) of Excavated Part of System, $D/B=2.0$, with Indicated Damping Ratio	107
35	Spring Coefficient (K_x) of Excavated Part of System, Indicated D/B , with 5% Damping Ratio	109
36	Damping Coefficient (C_x) of Excavated Part of System, Indicated D/B , with 5% Damping Ratio	109
37	Spring Coefficient (K_{xy}) of Excavated Part of System, Indicated D/B , with 5% Damping Ratio	110

38	Damping Coefficient (C_{xy}) of Excavated Part of System, Indicated D/B, with 5% Damping Ratio	110
39	Spring Coefficient (K_y) of Excavated Part of System, Indicated D/B, with 5% Damping Ratio	111
40	Damping Coefficient (C_y) of Excavated Part of System, Indicated D/B, with 5% Damping Ratio	111
41	Spring Coefficient (K_z) of Excavated Part of System, Indicated D/B, with 5% Damping Ratio	112
42	Damping Coefficient (C_z) of Excavated Part of System, Indicated D/B, with 5% Damping Ratio	112
43	Spring Coefficient (K_x) of Free-field System, Half-plane, Indicated D/B, with 5% Damping Ratio	116
44	Damping Coefficient (C_x) of Free-field System, Half-plane, Indicated D/B, with 5% Damping Ratio	116
45	Spring Coefficient (K_{xy}) of Free-field System, Half-plane, Indicated D/B, with 5% Damping Ratio	117
46	Damping Coefficient (C_{xy}) of Free-field System, Half-plane, Indicated D/B, with 5% Damping Ratio	117
47	Spring Coefficient (K_y) of Free-field System, Half-plane, Indicated D/B, with 5% Damping Ratio	118
48	Damping Coefficient (C_y) of Free-field System, Half-plane, Indicated D/B, with 5% Damping Ratio	118
49	Spring Coefficient (K_z) of Free-field System, Half-plane, Indicated D/B, with 5% Damping Ratio	119
50	Damping Coefficient (C_z) of Free-field System, Half-plane, Indicated D/B, with 5% Damping Ratio	119
51	Spring Coefficient (K_x) of Free-field System, Layer on Rock, Indicated H/B, D/B=0.5, with 5% Damping Ratio	121
52	Damping Coefficient (C_x) of Free-field System, Layer on Rock, Indicated H/B, D/B=0.5, with 5% Damping Ratio	121

53	Spring Coefficient (K_{xy}) of Free-field System, Layer on Rock, Indicated H/B, D/B=0.5, with 5% Damping Ratio	122
54	Damping Coefficient (C_{xy}) of Free-field System, Layer on Rock, Indicated H/B, D/B=0.5, with 5% Damping Ratio	122
55	Spring Coefficient (K_y) of Free-field System, Layer on Rock, Indicated H/B, D/B=0.5, with 5% Damping Ratio	123
56	Damping Coefficient (C_y) of Free-field System, Layer on Rock, Indicated H/B, D/B=0.5, with 5% Damping Ratio	123
57	Spring Coefficient (K_z) of Free-field System, Layer on Rock, Indicated H/B, D/B=0.5, with 5% Damping Ratio	124
58	Damping Coefficient (C_z) of Free-field System, Layer on Rock, Indicated H/B, D/B=0.5, with 5% Damping Ratio	124
59	Spring Coefficient (K_x) of Ground System, with 5% Damping Ratio	128
60	Damping Coefficient (C_x) of Ground System, with 5% Damping Ratio	128
61	Spring Coefficient (K_{xy}) of Ground System, with 5% Damping Ratio	129
62	Damping Coefficient (C_{xy}) of Ground System, with 5% Damping Ratio	129
63	Spring Coefficient (K_y) of Ground System, with 5% Damping Ratio	130
64	Damping Coefficient (C_y) of Ground System, with 5% Damping Ratio	130
65	Spring Coefficient (K_z) of Ground System, with 5% Damping Ratio	131
66	Damping Coefficient (C_z) of Ground System, with 5% Damping Ratio	131
67	Real Part of Horizontal Dynamic Stiffness Coefficients, Ground System with 5% Damping Ratio	134
68	Imaginary Part of Horizontal Dynamic Stiffness Coefficients, Ground System with 5% Damping Ratio	134
69	Real Part of Coupling Dynamic Stiffness Coefficients, Ground System with 5% Damping Ratio	135
70	Imaginary Part of Coupling Dynamic Stiffness Coefficients, Ground System with 5% Damping Ratio	135

71	Real Part of Rocking Dynamic Stiffness Coefficients, Ground System with 5% Damping Ratio	136
72	Imaginary Part of Rocking Dynamic Stiffness Coefficients, Ground System with 5% Damping Ratio	136
73	Real Part of Time-derivative Horizontal Flexibility Coefficients, Ground System with 5% Damping Ratio	138
74	Imaginary Part of Time-derivative Horizontal Flexibility Coefficients, Ground System with 5% Damping Ratio	138
75	Real Part of Time-derivative Coupling Flexibility Coefficients, Ground System with 5% Damping Ratio	139
76	Imaginary Part of Time-derivative Coupling Flexibility Coefficients, Ground System with 5% Damping Ratio	139
77	Real Part of Time-derivative Rocking Flexibility Coefficients, Ground System with 5% Damping Ratio	140
78	Imaginary Part of Time-derivative Rocking Flexibility Coefficients, Ground System with 5% Damping Ratio	140
79	Horizontal Impulse Velocity Coefficients of Ground System, with 5% Damping Ratio	141
80	Coupling Impulse Velocity Coefficients of Ground System, with 5% Damping Ratio	141
81	Rocking Impulse Velocity Coefficients of Ground System, with 5% Damping Ratio	142
82	Acceleration Records of 1940 El Centro Earthquake, North-south and 1985 Mexico Earthquake, East-west (50-70sec)	148
83	Maximum Displacement Response vs. Fixed-base Frequency, 2% Damping FIX-model, El Centro and Mexico Earthquakes	148
84	FIX Response and SSI Response (Ds), 5h-slenderness Ratio, $f=1.25\text{Hz}$, Floor & Footing Mass Ratio=10.0 & 2.0, S0-soil Condition, El Centro Earthquake ...	151
85	FIX Response and SSI Response (Dg), 5h-slenderness Ratio, $f=1.25\text{Hz}$, Floor & Footing Mass Ratio=10.0 & 2.0, S0-soil Condition, El Centro Earthquake ...	151

86	FIX Response and SSI Response (Ds), 5h-slenderness Ratio, $f=0.7\text{Hz}$, Floor & Footing Mass Ratio=10.0 & 2.0, S0-soil Condition, Mexico Earthquake	153
87	FIX Response and SSI Response (Dg), 5h-slenderness Ratio, $f=0.7\text{Hz}$, Floor & Footing Mass Ratio=10.0 & 2.0, S0-soil Condition, Mexico Earthquake	153
88	System Properties vs. Floor Mass Ratio, S0-soil Condition, $f=1.25\text{Hz}$, Footing Mass Ratio=2.0, El Centro Earthquake	154
89	Maximum Responses vs. Floor Mass Ratio, S0-soil Condition, $f=1.25\text{Hz}$, Footing Mass Ratio=2.0, El Centro Earthquake	154
90	Maximum Horizontal Forces vs. Floor Mass Ratio, S0-soil Condition, $f=1.25\text{Hz}$, Footing Mass Ratio=2.0, El Centro Earthquake	155
91	Maximum Moments vs. Floor Mass Ratio, S0-soil Condition, $f=1.25\text{Hz}$, Footing Mass Ratio=2.0, El Centro Earthquake	155
92	Maximum Responses vs. Floor Mass Ratio, S0-soil Condition, $f=0.70\text{Hz}$, Footing Mass Ratio=2.0, Mexico Earthquake	158
93	Maximum Horizontal Forces vs. Floor Mass Ratio, S0-soil Condition, $f=0.70\text{Hz}$, Footing Mass Ratio=2.0, Mexico Earthquake	159
94	Maximum Moments vs. Floor Mass Ratio, S0-soil Condition, $f=0.70\text{Hz}$, Footing Mass Ratio=2.0, Mexico Earthquake	159
95	System Properties vs. Floor Mass Ratio, h5-slenderness Ratio, S0-soil Condition, Footing Mass Ratio=2.0, El Centro Earthquake	161
96	Maximum Responses vs. Floor Mass Ratio, h5-slenderness Ratio, S0-soil Condition, Footing Mass Ratio=2.0, El Centro Earthquake	161
97	Maximum Horizontal Forces vs. Floor Mass Ratio, S0-soil Condition, h5-slenderness Ratio, Footing Mass Ratio=2.0, El Centro Earthquake	162
98	Maximum Moments vs. Floor Mass Ratio, h5-slenderness Ratio, S0-soil Condition, Footing Mass Ratio=2.0, El Centro Earthquake	162
99	System Properties vs. Floor Mass Ratio, h1-slenderness Ratio, S0-soil Condition, Footing Mass Ratio=2.0, El Centro Earthquake	163
100	Maximum Responses vs. Floor Mass Ratio, h1-slenderness Ratio, S0-soil Condition, Footing Mass Ratio=2.0, El Centro Earthquake	163

101	Maximum Horizontal Forces vs. Floor Mass Ratio, S0-soil Condition, h1-slenderness Ratio, Footing Mass Ratio=2.0, El Centro Earthquake	164
102	Maximum Moments vs. Floor Mass Ratio, h1-slenderness Ratio, S0-soil Condition, Footing Mass Ratio=2.0, El Centro Earthquake	164
103	System Properties vs. Floor Mass Ratio, h5-slenderness Ratio, f=1.25Hz, Footing Mass Ratio=2.0, El Centro Earthquake	167
104	Maximum Responses vs. Floor Mass Ratio, h5-slenderness Ratio, f=1.25Hz, Footing Mass Ratio=2.0, El Centro Earthquake	167
105	Maximum Horizontal Forces vs. Floor Mass Ratio, f=1.25Hz, h5-slenderness Ratio, Footing Mass Ratio=2.0, El Centro Earthquake	168
106	Maximum Moments vs. Floor Mass Ratio, h5-slenderness Ratio, f=1.25Hz, Footing Mass Ratio=2.0, El Centro Earthquake	168
107	10-story Shear Structure with Active Tendon System Embedded in Half-plane	170
108	Fundamental Frequency and Damping Ratio vs. s1/r Ratio, 10-story Controlled Structure, FIX-model	172
109	Fundamental Frequency and Damping Ratio vs. s1/r Ratio, 10-story Controlled Structure, SSI-model	173
110	Top Floor Displacement Relative to Footing of FIX-model and SSI-model (Excluding Rotational Effect), without Control	175
111	Top Floor Displacement Relative to Footing of FIX-model and SSI-model (Excluding Rotational Effect), with Control (s1/r=0.6)	176
112	Maximum Top Floor Displacement and Horizontal Control Force vs. s1/r Ratio, FIX-model	177
113	Maximum Top Floor Relative Displacement with and without Rotational Effect and Horizontal Control Force vs. s1/r Ratio, SSI-model	178
114	Footing Rotation of System with Control (s1/r=0.6) and without Control	179
115	Maximum Horizontal Interaction Force and Interaction Moment vs. s1/r Ratio, SSI-model	181
116	Linearly Distributed Loads on Vertical Assumed Line	194

117	Loaded Layer with Reaction Forces (Part I)	194
118	Total Soil System with External Forces (Part II)	195
119	Total Soil System in k -domain	205
120	Linearly Distributed Loads on Horizontal Assumed Line	210
121	Displacements, Stresses, and External Forces on Layer i	226
122	Displacements, Stresses, and External Forces on Half-plane	232
123	Infinitesimal Cube in Harmonic Motion	242
124	Cross Section of Incident P-wave	249
125	Displacement Associated with Incident P-wave	250
126	Cross Section of Incident S-wave	253
127	Displacement Associated with Incident S-wave	253
128	Typical Earthquake Record	255
129	In-plane Displacement for Horizontal Layer	257

LIST OF TABLES

Table		Page
I	Soil Profile at Takenaka Experimental Building Site (TEBS)	98
II	Dimensionless Natural Frequencies of Undamped Bounded Domain with $D/B \approx 2.0$	102
III	Floor Mass and Mass Moment of Inertia	150

NOMENCLATURE

ω_0	dimensionless frequency
$\{a_i\}$	real part of plant matrix's i^{th} eigenvector
A_P, A_{SV}	amplitudes of incident P- and SV-wave traveling in negative z -direction / amplitudes of general P- and SV-wave
A_{SH}	amplitudes of general SH-wave
\bar{A}	complex variable equal to $1/(k^2 \gamma^* f^2 \bar{D})$
$[A]$	matrix-related degrees of freedom of nodes along rigid interface to rigid-body degrees of freedom at point 0
$[A_1]$	submatrix-related degrees of freedom of nodes along left vertical rigid interface to rigid-body degrees of freedom at point 0
$[A_2]$	submatrix-related degrees of freedom of nodes along left portion of horizontal rigid interface to rigid-body degrees of freedom at point 0
$[A_3]$	submatrix-related degrees of freedom of nodes along right portion of horizontal rigid interface to rigid-body degrees of freedom at point 0
$[A_4]$	submatrix-related degrees of freedom of nodes along right vertical rigid interface to rigid-body degrees of freedom at point 0
$[\hat{A}], [\check{A}]$	characteristic matrix of FIX-model and SSI-model, respectively
b	length of horizontal element on structure-soil interface
b_e	width of discretizing element in excavated part of domain
$\{b_i\}$	imaginary part of plant matrix's i^{th} eigenvector
B	half-width of rectangular mat foundation
B_P, B_{SV}	amplitudes of incident P- and SV-wave traveling in positive z -direction
$[\hat{B}], [\check{B}]$	matrices related to controller-location for FIX-model and SSI-model, respectively

\bar{B}	complex variable equal to $(1 - 1/\bar{D})/(k^3 \Upsilon^* d f^2 s^2)$
$[\bar{B}]$	element strain nodal-displacement matrix in excavated part of system
C_x, C_y, C_z	nondimensionalized damping coefficients in horizontal direction, rocking, and vertical direction, respectively
C_{xy}	nondimensionalized coupling damping coefficients of horizontal direction and rocking
c_1	translational damping coefficient of single-story shear structure
C	phase velocity of wave traveling in soil domain
C_x, C_y, C_z	components of vector $\{C\}$
C_P	P-wave velocity, dilatational wave velocity
C_S	S-wave velocity, shear wave velocity
\bar{C}	complex variable equal to $1/(k^2 \Upsilon^* s^2)$
$\{C\}$	vector associated with wave amplitudes
$\{C_{ss}\}$	proportional damping matrix corresponding to structure degrees of freedom
$\{C_{so}\}, \{C_{os}\}$	damping matrix corresponding to structure and foundation degrees of freedom
$\{C_{oo}\}$	damping matrix corresponding to foundation degrees of freedom
$[\bar{C}]$	matrix containing nondimensionalized damping coefficients
$\{\hat{c}\}, \{\check{c}\}$	vectors related to structure-base's acceleration
D5	half-plane having foundation embedment to half-width ratio equal to 0.5
D10	half-plane having foundation embedment to half-width ratio equal to 1.0
D5H10	layer on rock having foundation embedment to half-width ratio equal to 0.5 and layer's depth to foundation half-width ratio equal to 1.0

D5H20	layer on rock having foundation embedment to half-width ratio equal to 0.5 and layer's depth to foundation half-width ratio equal to 2.0
d, d_i	depth of soil layer, and depth of soil layer i
d_e	depth of discretizing element in excavated part of domain
D	depth of foundation embedment
Dg	floor displacement relative to ground system
Ds	floor relative displacement excluding rigid motion effect due to foundation rotation
\bar{D}	complex value equal to C_p^2/C_s^2
$[D], [\hat{D}], [\check{D}]$	plant matrix, FIX-model's plant matrix, and SSI-model's plant matrix
$[\bar{D}]$	element stress-strain matrix in excavated part of system
e	volumetric strain
$[\exp([\Lambda])]$	exponential of matrix $[\Lambda]$
E, E_i, E_R	Young's modulus of elasticity, Young's modulus of elasticity of layer i and of half-space
$\{\hat{E}\}, \{\check{E}\}$	external disturbance vectors for FIX-model and SSI-model, respectively
f	scalar equal to $\sqrt{1/P_x^2 - 1}$
$f(\)$	quadratic energy functional
$F(\)$	augmented functional of functional f
FEM	Finite Element Method
FIX	fixed-base
F_x^e, F_z^e	horizontal force and vertical force at point 0 of rigid interface of system's excavated part
F_x^g, F_z^g	horizontal force and vertical force at point 0 of rigid interface of ground system

F_x^l, F_z^l	horizontal force and vertical force at point 0 of rigid interface of free-field system
$\dot{F}_{xx}^g, \dot{F}_{x\theta}^g,$ $\dot{F}_{\theta x}^g, \dot{F}_{\theta\theta}^g, \dot{F}_{zz}^g$	ground system's time-derivative displacement coefficients corresponding to the first subscript's degree of freedom due to a unit force excitation corresponding to the second subscript's degree of freedom
F, F_e, F_o	impulse velocity function, its even part, and odd part
$F_{xx}^g, F_{x\theta}^g,$ $F_{\theta x}^g, F_{\theta\theta}^g, F_{zz}^g$	ground system's impulse velocity coefficients corresponding to the first subscript's degree of freedom due to a unit force excitation corresponding to the second subscript's degree of freedom
[F]	soil flexibility matrix (strain-stress relationship)
$[\bar{\mathbf{F}}]_i$	element soil flexibility matrix (strains on i^{th} element in relation to stresses on i^{th} element)
$[F_{00}^g]$	dynamic-flexibility matrix of ground system with rigid interface
$[\dot{F}_{00}^g]$	ground system's time-derivative dynamic-flexibility matrix
$[F_{00}^g]$	impulse velocity matrix of ground system
$g(\)$	quadratic function related to state vector at t_n
$G(\)$	augmented function of function g
[G]	feedback gain matrix
$[G^{\text{FIX}}], [G^{\text{SSI}}]$	feedback gain matrices for FIX-model and SS-model, respectively
h_0	depth of rectangular mat foundation
h_{ai}	accumulated height from rotational point 0 to the centroid of mass m_i
h_i	structure height at i^{th} floor
H	depth of homogeneous layer on rock
IBEM	Indirect Boundary Element Method

I_0	foundation mass moment of inertia with respect to point 0
I_i	i^{th} floor mass moment of inertia with respect to point 0
$[I]$	identity matrix
J, J_n	performance index and performance index of n^{th} time interval
K_x, K_y, K_z	nondimensionalized spring coefficients in horizontal direction, rocking, and vertical direction, respectively
K_{xy}	nondimensionalized coupling spring coefficients of horizontal direction and rocking
k	wave number
k_i, k_1	translational spring-stiffness coefficient of multistory shear structure at i^{th} floor and of single-story shear structure, respectively
$[K_{SS}]$	symmetrical spring-stiffness matrix corresponding to structure degrees of freedom
$[K_{SO}], [K_{OS}]$	spring-stiffness matrix corresponding to structure and foundation degrees of freedom
$[K_{OO}]$	spring-stiffness matrix corresponding to foundation degrees of freedom
$[K^e]$	stiffness matrix of system's excavated part
$[\bar{K}^e]_j$	j^{th} element stiffness matrix of system's excavated part
$[\check{K}_{OO}]$	arbitrary diagonal static-stiffness matrix
$[\check{K}_{OO}]$	symmetric spring-stiffness matrix corresponding to foundation degrees of freedom using in state weighting matrix [Q]
$[\check{K}]$	matrix containing nondimensionalized spring coefficients
$[\bar{K}_{OO}]$	pseudo-static-stiffness matrix of ground system
l	time-instant number where impulse velocity functions approach zero
l_x, l_y, l_z	propagating directional cosine to x-, y-, z-axis of incident P-wave

l	half number of elements on horizontal part of structure-soil interface
le	half number of even portions along width of system's excavated part
$[L]$	interpolation matrix of distributed forces
$[\bar{L}]_i$	interpolation matrix of distributed forces on i^{th} element
m_0	mass of rectangular mat foundation
m_i	structure lumped mass at i^{th} floor
m_x, m_y, m_z	propagating directional cosine to x -, y -, z -axis of incident S-wave
M	number of soil layers above horizontal structure-soil interface
Me	number of even portions along depth of excavated part of system
$M_{base}^{FIX}, M_{base}^{SSI}$	base moments for FIX-model and SSI-model
M_y^e	moment around y -axis at point 0 of rigid interface of excavated part
M_y^g	moment around y -axis at point 0 of rigid interface of ground system
M_y^f	moment around y -axis at point 0 of rigid interface of free-field system
$[M_{SS}]$	diagonal lumped-mass matrix corresponding to structure degrees of freedom
$[M_{S0}], [M_{0S}]$	mass matrix corresponding to structure and foundation degrees of freedom
$[M_{00}]$	mass matrix corresponding to foundation degrees of freedom
$[M^e]$	mass matrix of system's excavated part
$[\bar{M}^e]_j$	j^{th} element mass matrix of system's excavated part
nl	minimum of n and l
$N-1$	number of soil layers in total soil system
NCR	number of controllers

NN	number of nodal points along structure-soil interface
NO	number of structure floors
NS	number of sampling steps in discrete Fourier transform
NT	number of time intervals
$N\emptyset$	integer equal to NO for FIX-model and $NO+2$ for SSI-model
$[\bar{N}]$	displacement shape function matrix of element in excavated part of system
$[N]$	rigid-body kinematics matrix of rigid interface
$[\bar{N}]_i$	rigid-body kinematics matrix of rigid interface along i^{th} element
ONC	one of nodes to which controller attaches
p	horizontal linearly distributed load
p_i	horizontal load intensity at node i
P-	primary
P_i	horizontal force at node i
P_j^I	part I horizontal reaction force at node j
P_j^H	homogeneous part of horizontal reaction force at node j
P_j^P	particular part of horizontal reaction force at node j
$\{PR_B\}$	force vector on nodes along interface (boundary) of system's excavated part
$\{PR_I\}$	force vector on interior nodes of system's excavated part
$[PRpr^*]_{M,l}$	matrix-related nodal forces P_{M+1}, R_{M+1} to distributed loads p, r along horizontal element l underneath layer M
$[PRpr^I]_j$	matrix-related part I nodal forces P_j, R_j, P_{j+1} , and R_{j+1} to distributed loads p, r along vertical assumed line in layer j

$\{PRpr^H\}_j$	matrix-related homogeneous part of nodal forces P_j, R_j, P_{j+1} , and R_{j+1} to distributed loads p, r along vertical assumed line in layer j
$\{PRpr^P\}_j$	matrix-related particular part of nodal forces P_j, R_j, P_{j+1} , and R_{j+1} to distributed loads p, r along vertical assumed line in layer j
$\{Q\}$	state weighting matrix
r	vertical linearly distributed load
r_i	vertical load intensity at node i
R_i	vertical force at node i
R_x, R_z	horizontal and vertical interaction force at point 0 between structure system and ground system
R_j^i	part I vertical reaction force at node j
R_j^H	homogeneous part of vertical reaction force at node j
R_j^P	particular part of vertical reaction force at node j
R_θ	interaction moment around y -axis at point 0 between structure system and ground system
$\{R\}$	control weighting matrix
$\{R_0\}$	vector consisting of horizontal interaction force and interaction moment
$\{\mathcal{R}_0\}$	dynamic-equivalent-force vector
s	scalar equal to $\sqrt{1/m_x^2 - 1}$
$sub_M(\{X\})$	submatrix of dimension 4×2 consisting of elements in matrix $\{X\}$ from row $4i-3^{\text{th}}$ to row $4i^{\text{th}}$ and from column $4M-1^{\text{th}}$ to column $4M^{\text{th}}$
SSI	structure-soil interaction
S-	secondary
SH-	secondary horizontal
SV-	secondary vertical

$S_{base}^{FIX}, S_{base}^{SSI}$	horizontal base shear for FIX-model and SSI-model
$S_{xx}^e, S_{x\theta}^e,$ $S_{\theta x}^e, S_{\theta\theta}^e, S_{zz}^e$	system's excavated part's force coefficients corresponding to the first subscript's degree of freedom due to a unit displacement excitation corresponding to the second subscript's degree of freedom
$S_{xx}^f, S_{x\theta}^f,$ $S_{\theta x}^f, S_{\theta\theta}^f, S_{zz}^f$	free-field system's force coefficients corresponding to the first subscript's degree of freedom due to a unit displacement excitation corresponding to the second subscript's degree of freedom
$S_{xx}^g, S_{x\theta}^g,$ $S_{\theta x}^g, S_{\theta\theta}^g, S_{zz}^g$	ground system's force coefficients corresponding to the first subscript's degree of freedom due to a unit displacement excitation corresponding to the second subscript's degree of freedom
$SU/B_j([X])$	submatrix of dimension 4×4 consisting of elements in matrix $[X]$ from row $4j-3^{th}$ to row $4j^{th}$ and from column $4j-3^{th}$ to column $4j^{th}$
$[S]$	weighting matrix
$[S^e]$	dynamic-stiffness matrix of system's excavated part corresponding to all nodal points
$[S_{00}]$	dynamic-stiffness matrix of system with rigid interface
$[S_{00}^e]$	dynamic-stiffness matrix of system's excavated part with rigid interface
$[S_{00}^g]$	dynamic-stiffness matrix of ground system with rigid interface
$[S_{00}^f]$	dynamic-stiffness matrix of free-field system with rigid interface
$[S_{BB}^e]$	dynamic-stiffness matrix of system's excavated part corresponding to nodes along interface (boundary)
$[S_{P-SV}^L]_i$	dynamic-stiffness matrix of layer i associated with P- and SV-wave
$[S_{P-SV}^R]$	dynamic-stiffness matrix of half-plane associated with P- and SV-wave
$[S_{P-SV}^T]$	dynamic-stiffness matrix of total soil system associated with P- and SV-wave

$[\bar{S}_{BB}]$	dynamic-stiffness submatrix of system's excavated part corresponding to nodes along interface (boundary)
$[\bar{S}_{BI}]$	dynamic-stiffness submatrix of system's excavated part corresponding to nodes along interface (boundary) and interior nodes
$[\bar{S}_{IB}]$	dynamic-stiffness submatrix of system's excavated part corresponding to interior nodes and nodes along interface (boundary)
$[\bar{S}_{II}]$	dynamic-stiffness submatrix of system's excavated part corresponding to interior nodes
$[\bar{S}^e]_j$	j^{th} element dynamic-stiffness matrix of system's excavated part
TEBS	Takenaka Experimental Building Site
t, t_i	time variable and time instant
t_0, t_f	initial time-instant and final time-instant
T_F	time range of impulse velocity function
$[T]$	transformation matrix
$[T]$	generalized strain-displacement matrix
$[\bar{T}]_i$	i^{th} element strain-displacement matrix
u	horizontal displacement / prescribed horizontal displacement / displacement in x-direction
u_i	nodal horizontal displacement at node i
\bar{u}_i	horizontal control force corresponding to i^{th} controller
u^H	homogeneous part of horizontal displacement
u^P, u_j^P	particular part of horizontal displacement and of nodal horizontal displacement at node j
u_{pr}	horizontal displacement due to distributed loads p, r
u_{pr}^I	part I horizontal displacement due to distributed loads p, r

u_{pr}^{II}	part II horizontal displacement due to distributed loads p, r
$\{uw_B\}$	displacement vector on nodes along interface (boundary) of system's excavated part
$\{uw_I\}$	displacement vector on interior nodes of system's excavated part
u_P, u_S	x-direction's displacements associated with P- and S-wave
u_{SH}, u_{SV}	x-direction's displacements associated with SH- and SV-wave
$[uwAB]_j$	matrix-related displacements u, w along vertical assumed line in layer j to wave amplitudes $A_P, A_{SV}, B_P,$ and B_{SV}
$[uwAB*]_j$	matrix-related nodal displacements $u_j, w_j, u_{j+1},$ and w_{j+1} to wave amplitudes $A_P, A_{SV}, B_P,$ and B_{SV}
$[uwpr]'_j$	Green's influence function matrix in k -domain related displacements u, w along vertical assumed line in layer i to distributed loads p, r along vertical assumed line in layer j
$[uwpr]'_{M,l}$	Green's influence function matrix in k -domain related displacements u, w along vertical assumed line in layer i to distributed loads p, r along horizontal element l underneath layer M
$[uwpr*]'_{M,l}$	matrix-related nodal displacements u_i, w_i, u_{i+1} and w_{i+1} to distributed loads p, r along horizontal element l underneath layer M
$[uwpr^I]_j$	matrix-related part I displacements u, w along vertical assumed line in layer j to distributed loads p, r along same line
$[uwpr^{II}]'_j$	matrix-related part II displacements u, w along vertical assumed line in layer i to distributed loads p, r along vertical assumed line in layer j
$[uwpr^H]_j$	matrix-related homogeneous part of displacements u, w along vertical assumed line in layer j to distributed loads p, r along same line
$[uwpr^P]_j$	matrix-related particular part of displacements u, w along vertical assumed line in layer j to distributed loads p, r along same line
$[uwpr^P]_j$	matrix-related particular part of nodal displacements $u_j, w_j, u_{j+1},$ and w_{j+1} to distributed loads p, r along vertical assumed line in layer j

$[uw\tau\sigma_i^{i+1}]$	transfer matrix-related $u_i, w_i, \tau_i,$ and σ_i to $u_{i+1}, w_{i+1}, \tau_{i+1},$ and σ_{i+1}
$[uw\tau\sigma AB_i]$	matrix-related $u_i, w_i, \tau_i,$ and σ_i to wave amplitudes $A_P, A_{SV}, B_P,$ and B_{SV}
$[uwpr]$	Green's influence function matrix in space-domain-related displacements u, w along assumed line to distributed loads p, r along same line
$[uwpr'_u]$	Green's influence function matrix in space-domain-related displacements u, w along assumed line on element i to distributed loads p, r along assumed line on element ii
$[uwpr]'_j$	Green's influence function matrix in space-domain-related displacements u, w in layer i to distributed loads p, r along vertical assumed line in layer j
$[uwpr]'^i_{M,l}$	Green's influence function matrix in space-domain-related displacements u, w in layer i to distributed loads p, r along horizontal element l underneath layer M
$\{\vec{U}\}$	horizontal control force vector
v	displacement in y -direction
v_P, v_S	y -direction's displacements associated with P- and S-wave
v_{SH}, v_{SV}	y -direction's displacements associated with SH- and SV-wave
w	vertical displacement / prescribed vertical displacement / displacement in z -direction
w_i	nodal vertical displacement at node i
w^{Hj}	homogeneous part of vertical displacement
w^P, w_i^P	particular part of vertical displacement and of nodal vertical displacement at node j
w_{pr}	vertical displacement due to distributed loads p, r
w^I_{pr}	part I vertical displacement due to distributed loads p, r
$w^{II}_{pr}(k, z)$	part II vertical displacement due to distributed loads p, r
w_P, w_S, w_{SV}	z -direction's displacements associated with P-, S-, and SV-wave

[W]	weighting matrix used in indirect boundary element method
\ddot{x}^b	horizontal acceleration of structure-base
x_0^e	horizontal displacement at point 0 of rigid interface of system's excavated part
x_0^g	horizontal displacement at point 0 of rigid interface of ground system
x_0^f	horizontal displacement at point 0 of rigid interface of free-field system
x_0^t	horizontal displacement at point 0 of rigid interface of total system
x_i^t	horizontal i^{th} floor displacement of total system
x_i^{tb}	horizontal i^{th} floor displacement of total system which is relative to structure-base's displacement
x_i^{tg}	horizontal i^{th} floor displacement of total system which is relative to horizontal displacement of ground system with rigid interface
$\{X_0^{tg}\}$	foundation displacement vector of total dynamic system which is relative to that of ground system
$\{X_S^t\}$	floor displacement vector of total dynamic system
$\{X_S^{tb}\}$	floor displacement vector of total dynamic system which is relative to that of structure-base
$\{X_S^{tg}\}$	floor displacement vector of total dynamic system which is relative to that of ground system
z_i	vertical displacement corresponding to node i
z_0^e	vertical displacement at point 0 of rigid interface of excavated part
z_0^g	vertical displacement at point 0 of rigid interface of ground system
z_0^f	vertical displacement at point 0 of rigid interface of free-field system
z_0^t	vertical displacement at point 0 of rigid interface of total system
{Z}	state vector

$\{Z_{n-1}\}$	state vector of the previous step
$\{Z^{ib}\}, \{Z^{ig}\}$	state vector for FIX-model and SSI-model
α_i	real part of i^{th} eigenvalue
α_m	damping-mass ratio
$\{\alpha\}$	polynomial coefficient vector
β_i	imaginary part of i^{th} eigenvalue
β_k	damping-stiffness ratio
$\frac{\partial}{\partial x}, \frac{\partial}{\partial y}$	partial derivative with respect to successive variable(s)
δ	Dirac-delta function
$\{\hat{\delta}_0\}$	horizontal base-acceleration coefficient vector for foundation
$\{\hat{\delta}_S\}$	horizontal base-acceleration coefficient vector for superstructure
Δt	time increment
$\Delta \omega$	frequency increment
$\epsilon_x, \epsilon_y, \epsilon_z$	normal strains in x -, y -, z -direction, respectively
$\{\Phi\}$	solution vector of transformed state equation
$\gamma_{xy}, \gamma_{xz}, \gamma_{yz}$	shear strains in direction of first subscript on infinitesimal area, normal in direction of second subscript
$[\gamma_0]$	controller-location matrix for foundation
$[\gamma_S]$	controller-location matrix for superstructure
$\{\Gamma\}$	resultant vector of $[T]^{-1}\{E\}$
η_i, η_1	damping ratio of translational mode i for multistory shear structure and of translational mode for single-story shear structure, respectively
Υ	shear modulus of elasticity
Υ^*	complex shear modulus of elasticity

η_1, η_2	proportional damping ratios of two translational modes
i	imaginary number = $\sqrt{-1}$
ϑ	coordinates along structure-soil interface
λ	Lame constant
$[\Lambda]$	matrix consisting of plant matrix's eigenvalues
λ^*	complex Lame's constant
$\{\lambda_g\}, \{\lambda_f\}$	multiplier vectors for quadratic function g and functional f , respectively
$\{\Pi\}$	recursive form of term using in $\{\Phi\}$
θ_0^e	rotation around y -axis at point 0 of rigid interface of excavated part
θ_0^g	rotation around y -axis at point 0 of rigid interface of ground system
θ_0^f	rotation around y -axis at point 0 of rigid interface of free-field system
θ_0^t	rotation around y -axis at point 0 of rigid interface of total system
θ_0^{tg}	rotation around y -axis at point 0 of rigid interface of total system which is relative to that of ground system with rigid interface
$\{\Theta_g\}$	boundary condition vector
ρ, ρ_i, ρ_R	mass density, soil mass density of layer i and of half-space
$\sigma_x, \sigma_y, \sigma_z$	normal stresses in x -, y -, z -direction
$\sigma_{z(i)}$	normal stress at node i in z -direction
σ_z^p	particular part of normal stress in z -direction
τ	time variable
$\tau_{xy}, \tau_{xz}, \tau_{yz}$	shear stresses in direction of first subscript on infinitesimal area, normal in direction of second subscript
$\tau_{xz(i)}$	shear stress at node i in x -direction on infinitesimal area, normal in z -direction

τ_x^p	particular part of shear stress in x -direction on infinitesimal area, normal in z -direction
ν, ν_i, ν_R	Poisson's ratio, Poisson's ratio of soil layer i and of half-space
ω	harmonic excitation frequency
ω_i	harmonic excitation frequency corresponding to i mode
$\Omega_x, \Omega_y, \Omega_z$	components of rotational-strain vector
Ω_T	truncated frequency
$\{\Omega\}$	rotational-strain vector
$\{\Xi_f\}$	constraint vector
ψ_P, ψ_S	angles of incident P- and S-wave measured from positive x -axis
$\zeta, \zeta_i, \zeta_R, \zeta_j$	hysteretic damping ratio, hysteretic damping ratio of soil layer i , of half-space, and discretizing soil element j

I. INTRODUCTION

A. OBJECTIVE

Understanding the response behavior of a dynamic system, with control and boundless soil domain is necessary prior to the construction implementation of such an integrated control in civil engineering structure. In the past, studies of structural dynamic controlled system were based on the fixed-base (FIX) model for which the structure is assumed to be fixed at its base. This model may be well-founded where the structure is built on rock. If the structure is constructed on soft soil, the dynamic system should include structure-soil interaction (SSI) which covers the foundation's translational and rotational degrees of freedom. Added modes as a result of the foundation degrees of freedom could lead to various changes in structural response behavior and accordingly control behavior and effectiveness. Especially, a rocking (rotation) mode which is omitted in the FIX-model may dominate in a particular structure.

The objective of this study is first to develop mathematical models representing the regarded dynamic system. Four models are developed based on the existence or absence of the structure-soil interaction and control. They are regarded as a FIX-model, SSI-model, FIX-model with control, and SSI-model with control. To represent closely an actual system, the frequency-dependent coefficients of nonhomogeneous unbounded soil are considered in the SSI-model and SSI-model with control. The foundation embedment is also taken into account. Yet the algorithms used in determining structural response are formulated on the basis of time domain since it is more familiar to most civil engineers

than frequency domain. More importantly, the implementation of an active control must be carried out in real-time fashion. The concept of a closed-loop control is applied to both FIX-model with control and SSI-model with control. The optimum control rules are developed by minimizing a generalized performance index. In the SSI-model with control, not only structural response but also foundation response is included in the control rule.

Prior to the investigation of a total dynamic system's behavior, the influence of parametric soil conditions on the soil dynamic stiffness coefficients is studied. The soil condition parameters are damping ratio, foundation embedment, and layer depth. The soil condition of an actual site is also examined. The soil profile of Takenaka Experimental Building in Japan is used. Finally, the effects of structure-soil interaction on structural response and control are assessed.

B. LITERATURE REVIEW

An active control has recently gained recognition in civil engineering. The control algorithm has a few general approaches such as Riccati matrix, instantaneous optimal control, and generalized optimal control (Cheng and Tian, 1993; Soong, 1990; Cheng, 1988; Yang et al., 1987; Cheng and Pantelides, 1986). These control algorithms have been developed based on the FIX-model. Among these three approaches, only a generalized optimal control yields a control law which is neither a function of time nor time increment (Cheng et al., 1992). Consequently the control force driven by a digital-type actuator is not depend upon its time interval.

As for the calculation of soil stiffness coefficients required in a structure-soil interaction consideration, a few well-known approaches are discussed. The estimated

spring constant based on soil's shear modulus is used in an approximate approach. This estimated coefficient lacks a crucial frequency-dependent property and leads to an unjustified solution. Furthermore, the role of foundation configuration and embedment are not included. More complicated approaches that yield a frequency-dependent coefficient are the finite element method and the boundary element method. Both methods take foundation configuration and embedment into account. In the finite element method, the fictitious boundary attaching dash-pot is imposed at some distance from a vibrating structure to create a bounded region since soil is a semi-infinite medium. The dash-pot does not allow waves originating from the structure to reflect back into the region. The large discretized domain in the finite element method requires numerous data and computing storage. Without utilizing the fictitious boundary and without introducing nodes in the interior, the boundary element method (Wolf and Darbre, 1984a,b; 1983) is appropriately applied to the unbounded domain.

With respect to response solution technique, two major approaches can be applied. One is carried out in the frequency domain and the other in the time domain. The former seems to be suitable since the soil system has frequency-dependent property. But this method requires the transformation of input excitation in the time domain into its corresponding pair in the frequency domain. Therefore the complete series of an input excitation needs to be known prior to the calculation. This approach cannot be executed in a real-time fashion which is required in the implementation of an actual active control system. Furthermore, the second transformation is needed for output response. The latter requires the transformation of the frequency-dependent soil coefficient. By applying the

special technique (Hayashi and Katukura, 1990), only the frequency band limited soil coefficient is exercised. In this technique, the static component of the coefficient is not needed.

Recently there has been some research on structural control including structure-soil interaction. A limited number of control devices, strategies and algorithms have been studied. Wong and Luco (1991) formulated their algorithm in the frequency domain which is not suitable for the actual active control system. An active control device is introduced as the absorbing boundary such that all upward propagating waves are absorbed and no downward propagating waves are reflected. Alam and Baba (1993) presented an active optimal control algorithm taking structure-soil interaction into account. Their optimal closed-open-loop control law is formulated to satisfy the stationary Riccati equation. An approximate frequency-independent soil coefficient is used in structure-soil interaction application. Smith et al. (1994) developed an optimal closed-loop control algorithm considering structure-soil interaction effects. In their studies, an optimal control rule is based on the Riccati equation. To incorporate this control rule into the frequency-domain formulation, only a harmonic ground motion was considered. Cheng and Suthiwong (1994) and Cheng et al. (1994) developed a generalized optimal active control algorithm including structure-soil interaction effects. Their algorithm can be implemented in real-time fashion while frequency-dependent soil coefficient obtained by the boundary element method is taken into account. An active tendon is used as a control device in this closed-loop control. These publications are also part of the author's research study.

C. OVERVIEW

In Section II, the various models and systems used in this study and their assumptions are defined. Their symbols and notations are described as well. Modeling diagrams are included.

Section III contains the formulations of state equations for a FIX- and SSI-model with and without control. The transformation to their canonical form and solution technique of the first-order differential equation are demonstrated. In addition, the derivation of interaction forces at foundation-soil interface based on a convolution integral technique is presented. This method requires the impulse velocity coefficients formulated in Section V. A physical interpretation of SSI-model's motion equation is given as well.

In Section IV, the optimal control rules or feedback gain matrices for a FIX-model and SSI-model are established. A generalized performance index as objective functional is defined. Euler's equation and transversality condition are formulated and enforced to obtain an optimal solution. The weighting matrices used in the performance index and the feedback gain matrix are presented.

Section V describes the methods of determining frequency-dependent coefficients of various soil systems. The indirect boundary element method is discussed for a free-field system's dynamic stiffness coefficients. This method requires the displacement Green's influence function formulated in Appendix A. Numerical integration techniques such as an adaptive quadrature and Simpson's method are addressed as well. The finite element method is detailed for the dynamic stiffness coefficients of a system's excavated part. Four-node rectangular element and consistent mass matrix are employed. For a ground

system's dynamic stiffness coefficients, the subtraction method and its cautious measure are pointed out. Then the time-derivative dynamic flexibility coefficient of ground system is defined. Finally, the discussion of the discrete Fourier transform with causality condition is given. This technique is used in transforming the time-derivative dynamic flexibility coefficients in frequency domain to impulse velocity coefficients in time domain.

In Section VI, the nondimensionalized dynamic stiffness coefficients of various soil systems are examined. The parameters studied include soil hysteretic damping, foundation embedment, and depth of a soil layer on rock base. In addition to the parametric study, the actual site of Takenaka Experimental Building in Japan is investigated. For a ground system, the dynamic stiffness, time-derivative flexibility, and impulse velocity coefficients are presented. Coefficients of the systems with half-plane and a varying depth layer on rock are compared as well.

Section VII involves the investigation of total dynamic systems with and without control. The investigating parameters are classified as concerning parameters and governing parameters. The former relate to the parameters indicating structure and foundation failures. The latter may be described as the parameters affecting structural response and control behavior. Effects of the governing parameters on the concerning parameters are discussed. Effects of structure-soil interaction on control are also pointed out.

In Section VIII, the work is summarized. Then conclusions are given. Some suggestions are included as well.

In Appendix A, the displacement-Green's-influence-functions as fundamental solutions of indirect boundary element method are derived. These functions relate the displacements along the assumed line of a nonhomogenous semi-infinite medium to the applied linearly distributed loads acting on the same line. The assumed line consists of vertical and horizontal lines which subsequently form a structure-soil interface. Green's functions are first formulated in the k wave-number domain and then transformed to the space domain. Dynamic stiffness matrices in the k -domain of a layer and half-plane given in Appendix B are part of the formulation. The in-plane displacement equations in Appendix C are used as well. Included is a special case corresponding to the vertically incident wave ($k=0$).

Appendix B presents the derivation of dynamic stiffness matrices in k -domain of an unbounded layer and half-plane. Both mediums are homogeneous. The displacement equations in Appendix C are needed. Special cases corresponding to $k = 0$ are provided. For a half-plane, the formulations in both negative and positive k wave-number are demonstrated.

In Appendix C, the primary- and secondary-wave equations are formulated based upon the dynamic-equilibrium equations of an infinitesimal cube. For an in-plane problem, the displacement equations of an unbounded horizontal layer are established. Their required boundary condition and the definition of a k wave-number are given.

II. DYNAMIC SYSTEM MODELING

A multistory controlled building sits on a rectangular mat foundation embedded in unbounded soil, as shown in Figure 1. The building is equipped with an intelligent control of active tendon system. This system consists of response sensors connected to a computerized control panel and actuators with a tendon linked to hydraulic equipment operated by the control panel. The unbounded soil domain is modeled by layered half-space made up of stacking horizontal unbounded layers resting on a half-space. The soil domain is assumed to be an isotropic viscoelastic medium with hysteretic damping. Its properties may vary with depth but remain constant within the individual layers.

The origin of the global Cartesian coordinate system with z -axis pointing downward is at the bottom center of the foundation. In general, it is assumed that incident P- and S-wave (see details in Appendix C), composing earthquake excitation, have directions of propagation lying on the same vertical plane. It is also assumed that this vertical plane is on x - z plane, parallel to the face of the building.

A. TOTAL DYNAMIC SYSTEM

To investigate response behavior, a two-dimensional system on x - z plane shown in Figure 2 is selected to represent the physical properties in x - and z -direction for the whole system. This system is subjected to only the body P- and SV-wave, since the amplitude of SH-wave is in y -direction. A N -story seismic shear structure equipped with an active tendon system rests on a rigid rectangular foundation embedded in a layered half-space. The layered half-space consists of $N-1$ horizontal layers having infinite length in x -

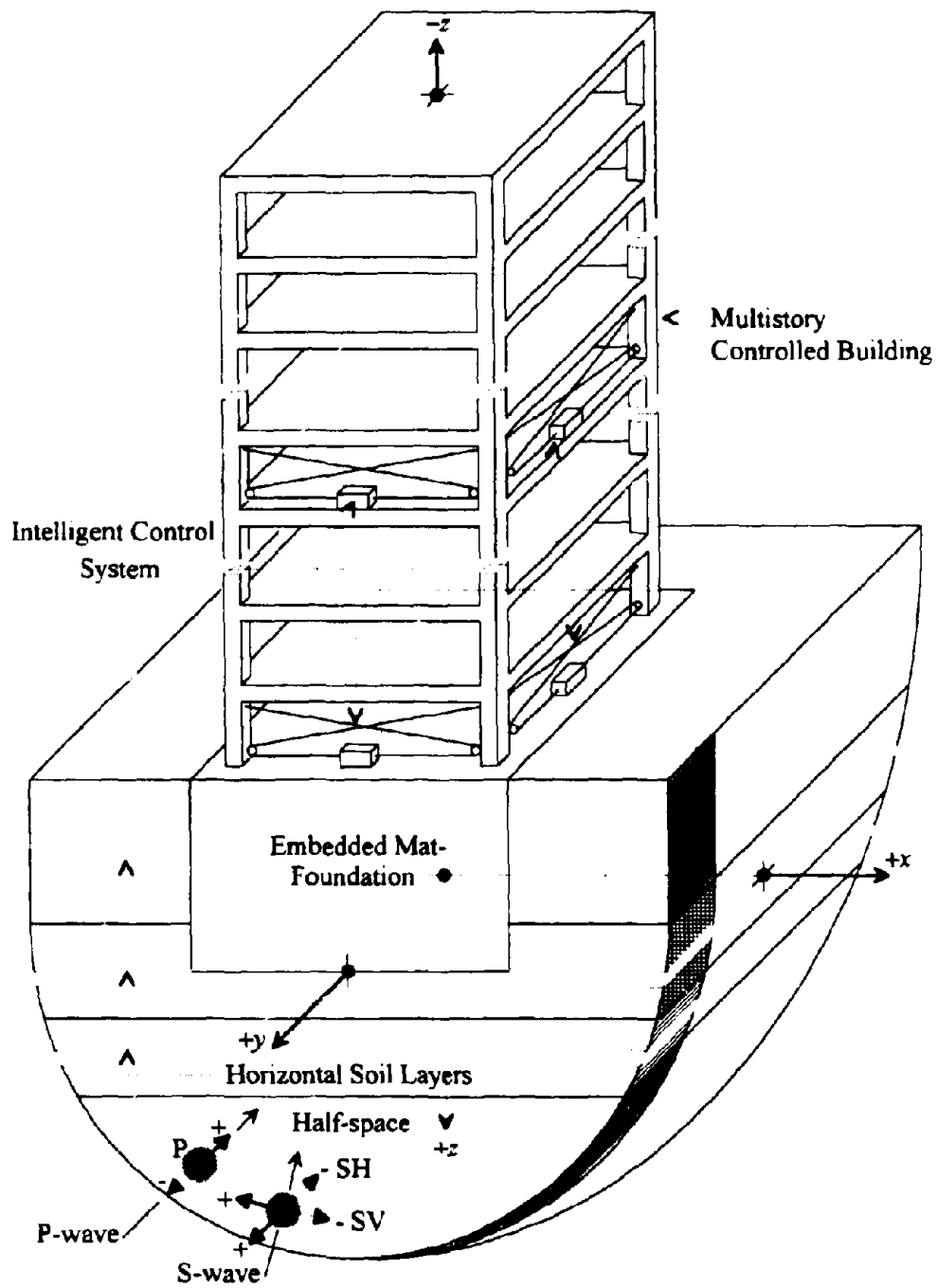


Figure 1. Multistory Controlled Building Embedded in Unbounded Soil

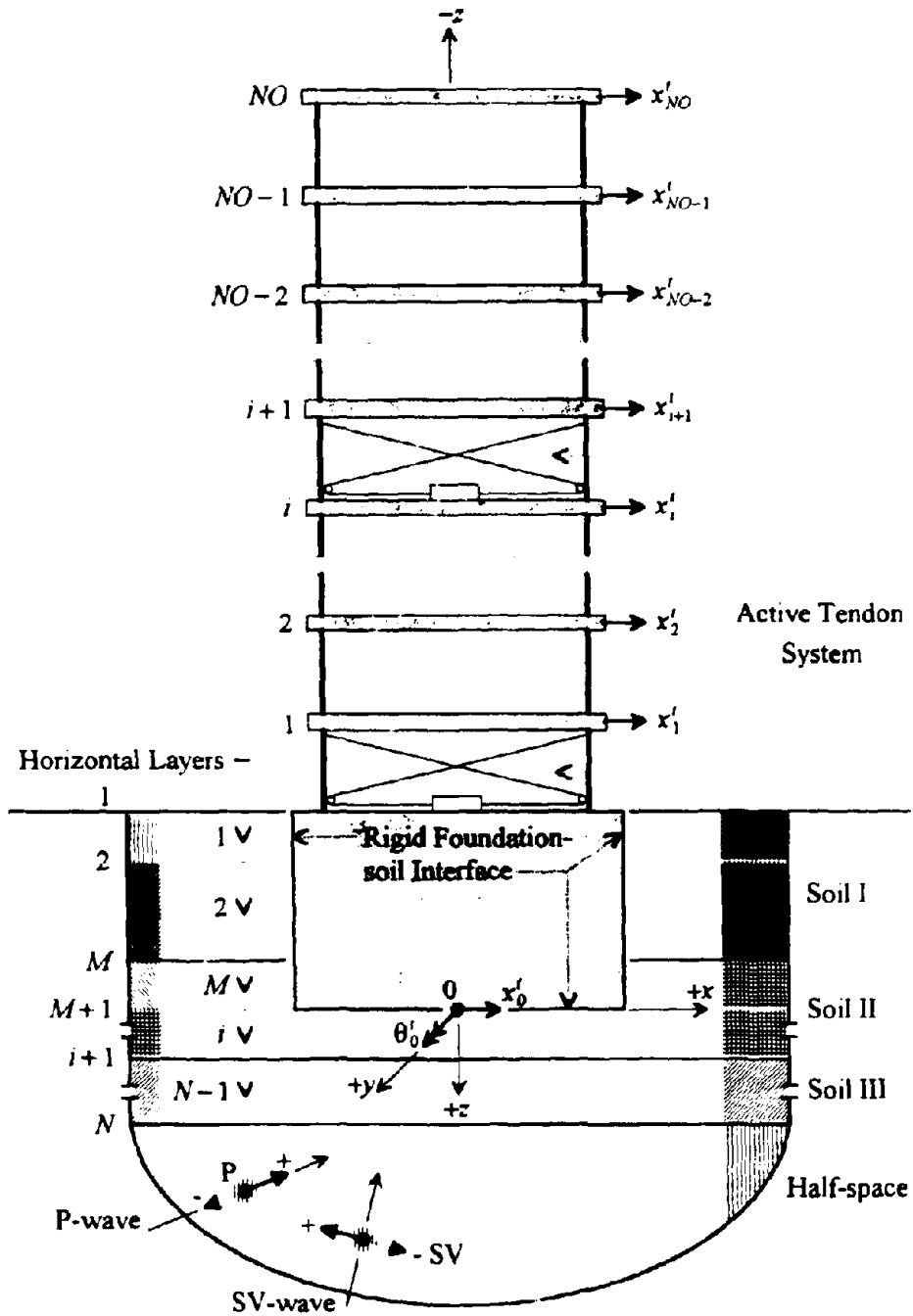


Figure 2. Two-dimensional Dynamic System

direction and a half-space. By introducing artificial horizontal interfaces, the amount of horizontal layers may be larger than that of given soil layers. For example, interfaces 2 and $M+1$ are added in Figure 2. The horizontal interface on which the bottom of the foundation rests is called interface $M+1$, lying underneath the designated layer M

Since the foundation is assumed to be rigid, only two degrees of freedom at point 0, a horizontal translation x_0^t and a rotation θ_0^t around y -axis, can be used to represent the degrees of freedom along the foundation-soil interface. To investigate response behavior of the shear structure, a vertical translation at point 0 is neglected. For the superstructure, horizontal translations x_i^t , for $i=1,2,\dots,NO$, are used to describe the degree of freedom on each floor i . Superscript t stands for total dynamic system.

At the foundation-soil interface, the total dynamic system is divided into two systems, a structure system and a ground system. The former consists of a two-dimensional NO -story shear structure equipped with an active tendon system and its foundation. The latter is soil with excavation comprising horizontal unbounded layers and a half-space. By using the substructure method, both systems are separately analyzed, based on an assumption that the interface between these two systems is in complete contact.

B. STRUCTURE SYSTEM

Two models in Figure 3 can be used to represent the structure system, a structure-soil interaction model (SSI) and a fixed-base model (FIX). The former, taking structure-soil interaction into consideration, involves a rigorous mathematical soil model

The latter, a relatively simple model, assumes that a structure is fixed at its support and thus may be valid only where a structure is built on rock.

For both models, structure masses m_i are lumped on each floor i , for $i=1,2,\dots,NO$. Floor translational spring stiffness are represented by two columns on each floor, each column having a stiffness of $k_i/2$. Proportional damping ratios of two translational modes.

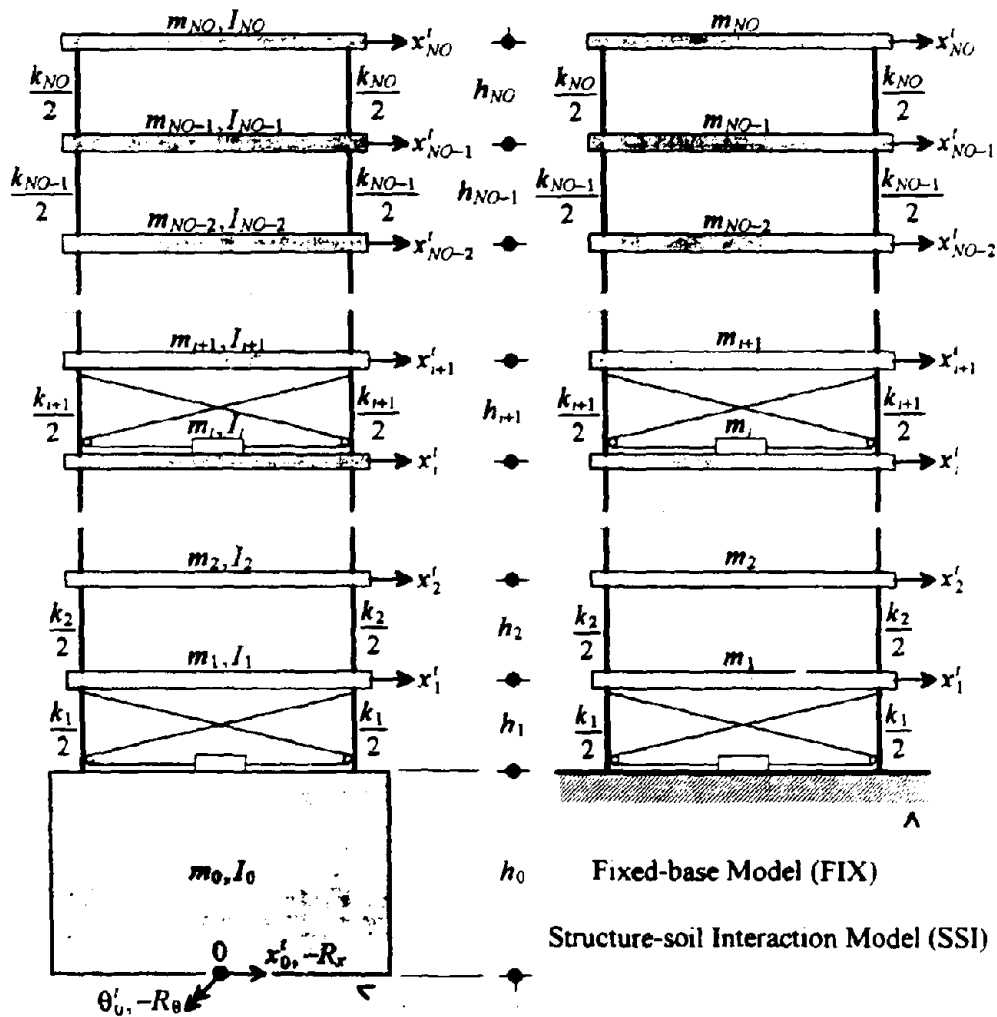


Figure 3. Structure System Modeling

η_1 and η_2 , are used to determine viscous damping of the structure. Floor heights are equal to h_i . Only horizontal translations x_i^f are used to describe floor degrees of freedom. Included in the models are NCR number of digital-type active tendon controllers, where NCR can be equal to or less than NO . These models will be analyzed on the basis of time-domain procedure.

Only for an SSI-model do foundation properties and foundation degrees of freedom need to be included. The former are foundation mass m_0 , foundation mass moment of inertia with respect to point 0, I_0 , and foundation depth h_0 . The latter consist of, at point 0, a translation x_0^f in x -direction and a rotation θ_0^f around y -axis. Furthermore, the floor mass moments of inertia with respect to point 0, I_i , are taken into account. The SSI-model has its interface connected to the ground system. Interaction here leads to an interaction force R_x and an interaction moment R_θ at point 0 in x -direction and around y -axis, respectively

C. SOIL SYSTEM

1. **Free-field System.** In Figure 4, the site prior to excavation and construction is called a free-field system which is an unbounded continuous domain represented by $N-1$ unbounded horizontal layers resting on a half-space. Each layer i , for $i=1,2,\dots,N-1$, has constant properties: soil density ρ_i , modulus of elasticity E_i , Poisson's ratio ν_i , hysteretic damping ratio ζ_i , and layer depth d_i . The half-space has the following properties: soil density ρ_R , modulus of elasticity E_R , Poisson's ratio ν_R , and hysteretic damping ratio ζ_R . Since the half-space is mostly used to represent rock bed, subscript R is introduced. The system is subjected to incident P- and SV-wave.

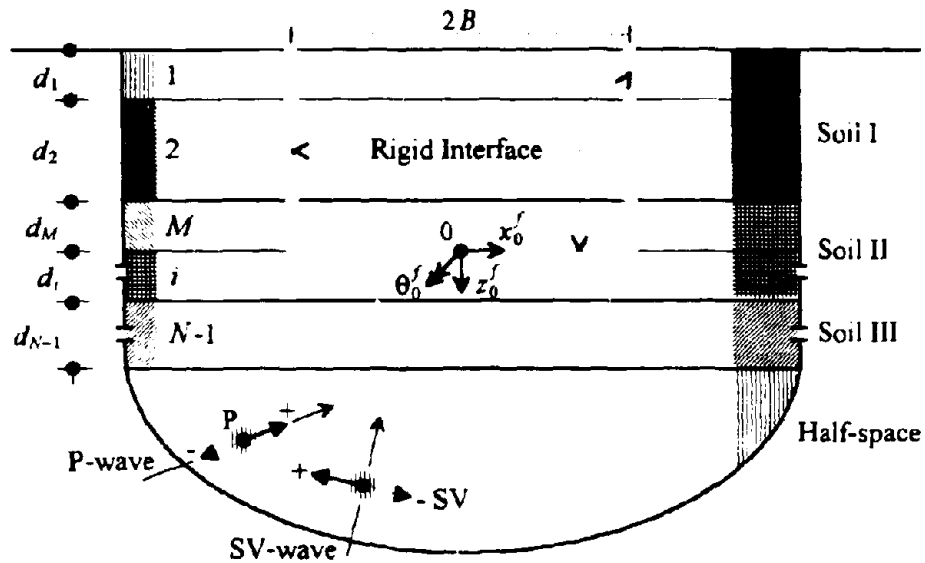


Figure 4. Free-field System with Rigid Interface

After inserting rigid interface along the line which subsequently forms structure-soil interface, three degrees of freedom at point 0, a horizontal translation x_0^f , a vertical translation z_0^f , and a rotation θ_0^f , suffice to represent the degrees of freedom along inserted rigid interface. Superscript f denotes the free-field system. Length of the horizontal interface is equal to width of the foundation, $2B$. Length of the vertical interface, D , can be determined by the summation of d_i , for $i=1,2,\dots,M$, which may be equal to foundation depth, h_0 , in case of full embedment of the foundation.

Since the properties of this unbounded system are frequency-dependent, the indirect boundary element method in frequency domain is appropriately applied without using a fictitious boundary and without introducing the system's interior nodes.

2. **Excavated Part of System.** Excavated soil, which will be replaced by the foundation, defines this system as shown in Figure 5. It has a dimension of $D = \sum_{i=1}^M d_i$ by $2B$. Three degrees of freedom at point 0, x_0^e , z_0^e , and θ_0^e in x -, z -direction and around y -direction, represent the degrees of freedom along the rigid interface. Superscript e denotes the excavated part of the system. Since this system is a bounded medium, the finite element method in the frequency domain is employed.

3. **Ground System.** This system, shown in Figure 6, is described as a free-field system with excavation. Degrees of freedom along the rigid interface are represented at point 0 by x_0^g , z_0^g , and θ_0^g in x -, z -direction and around y -direction, respectively. Superscript g denotes the ground system.

Even though soil systems behave nonlinearly when subjected to high levels of earthquake excitation, the behavior of a linear system has to be fully understood. As the superposition principle is valid for a linear system, the linear properties of this system (for example, linear system's stiffness) can be obtained by subtracting those of the system's excavated part from those of the free-field system.

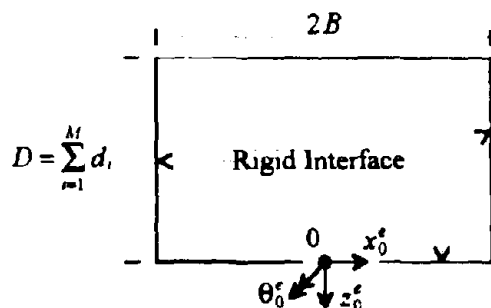


Figure 5. Excavated Part of System with Rigid Interface

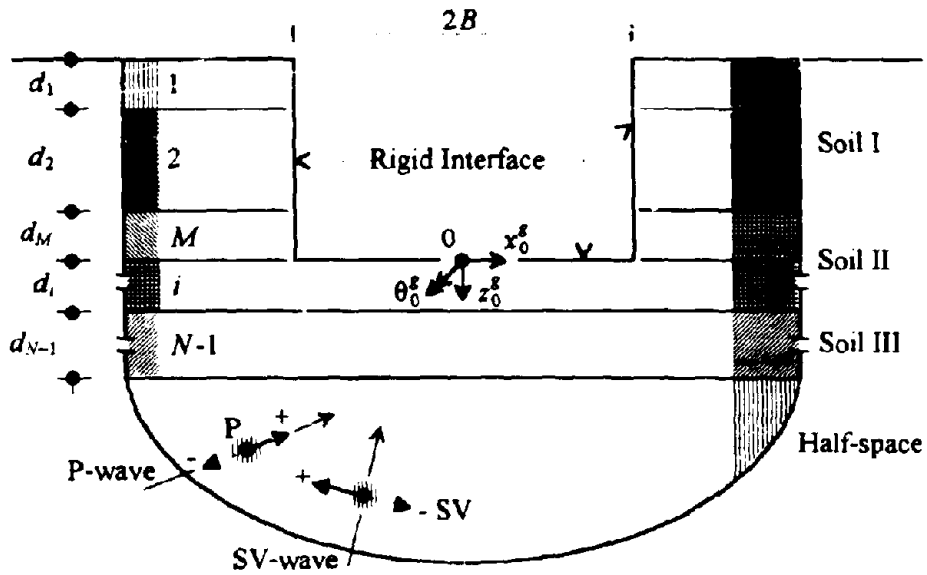


Figure 6. Ground System with Rigid Interface

D. MODELING DIAGRAM

The two aforementioned models (FIX-model and SSI-model) representing the structure system are integrated with a closed-loop control system. Therefore the modeling diagrams can be summarized as shown in Figures 7, 8, 9, and 10.

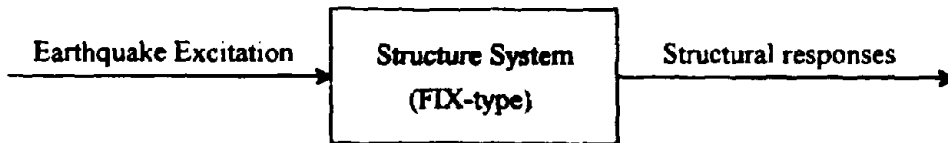


Figure 7. Fixed-base Diagram

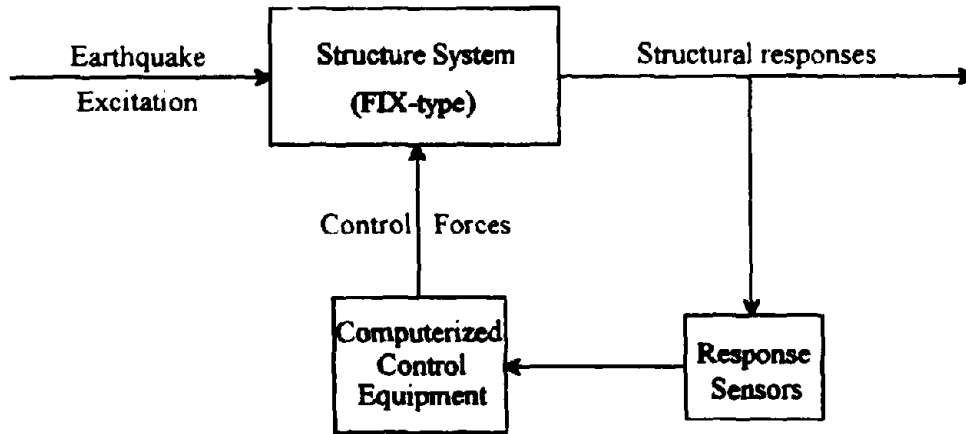


Figure 8. Controlled Fixed-base Diagram

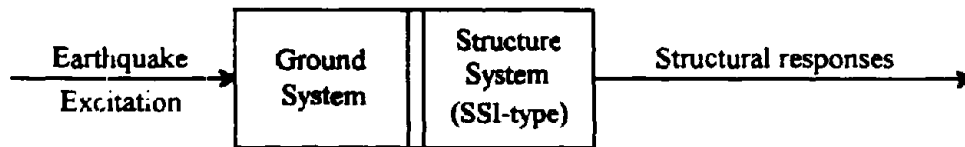


Figure 9. Structure-soil Interaction Diagram

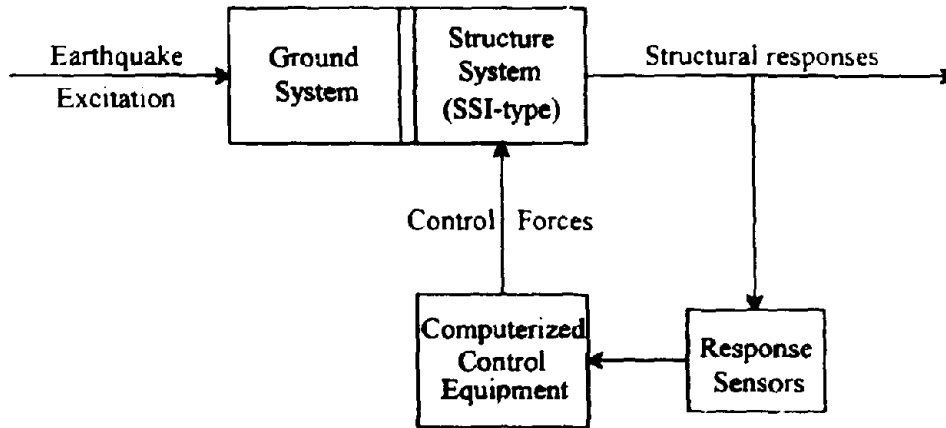


Figure 10. Controlled Structure-soil Interaction Diagram

III. STATE EQUATIONS FOR FIX- AND SSI-MODEL WITH / WITHOUT CONTROL

A. FORMULATION FOR FIXED BASE MODEL

For a fixed-base model (see FIX-type in Figure 3), the motion equation of a NO -story seismic shear structure equipped with an active tendon control, at any n^{th} time-instant, may be expressed as

$$[M_{SS}]\{\ddot{X}_S^{tb}(n)\} + [C_{SS}]\{\dot{X}_S^{tb}(n)\} + [K_{SS}]\{X_S^{tb}(n)\} = [\gamma_S]\{\ddot{U}(n)\} + \{\delta_S\}\ddot{x}^b(n) \quad (1)$$

where $[M_{SS}]$, $[C_{SS}]$, and $[K_{SS}]$ of dimension NO by NO are diagonal lumped-mass, proportional damping, and symmetrical spring-stiffness matrices, respectively. $\{X_S^{tb}\}$ of dimension NO by 1 is floor displacement vector, $[x_{NO}^{tb} \ x_{NO-1}^{tb} \ \dots \ x_1^{tb} \ \dots \ x_2^{tb} \ x_1^{tb}]^T$. Superscript tb indicates values in the response vector are of the total dynamic system and relative to those of the structure-base. Subscript S or SS indicates that elements in the denoted vector or matrix correspond to the superstructure's degrees of freedom. At this state of formulation, these notations may appear to be unnecessary. A dot and a double dot over a symbol denote the first derivative and second derivative in relation to time, respectively. $[\gamma_S]$ of dimension NO by NCR is a controller-location matrix, where NCR is the number of active controllers. $\{\ddot{U}\}$ of dimension NCR by 1 is the vector of horizontal control forces, $[\ddot{u}_{NCR} \ \dots \ \ddot{u}_i \ \dots \ \ddot{u}_1]^T$. $\{\delta_S\}$ of dimension NO by 1 is a horizontal base-acceleration coefficient vector, each row equals the negative value of a lumped mass corresponding to the row number of a degree of freedom. \ddot{x}^b is a horizontal acceleration

of the structure-base. For the formulation of a system without control, the term associated with control force vector is omitted.

An example of a controller-location matrix $[\gamma_S]$ for a two-controller system, having controller no.1 attached between structure-base and first floor (node no.1) and controller no.2 attached between second floor (node no.2) and third floor (node no.3), is shown as

$$[\gamma_S] = \begin{bmatrix} 0 & 0 \\ \vdots & \vdots \\ 0 & 0 \\ -1 & 0 \\ 1 & 0 \\ 0 & -1 \end{bmatrix} \quad (2)$$

The motion Equation (1) can be rewritten in form of a state equation as

$$\begin{Bmatrix} \{\dot{X}_S^{tb}(n)\} \\ \{\ddot{X}_S^{tb}(n)\} \end{Bmatrix} = \begin{bmatrix} [0] & [I] \\ -[M_{SS}]^{-1}[K_{SS}] & -[M_{SS}]^{-1}[C_{SS}] \end{bmatrix} \begin{Bmatrix} \{X_S^{tb}(n)\} \\ \{\dot{X}_S^{tb}(n)\} \end{Bmatrix} + \begin{bmatrix} [0] \\ [M_{SS}]^{-1}[\gamma_S] \end{bmatrix} \{\vec{U}(n)\} + \begin{Bmatrix} \{0\} \\ [M_{SS}]^{-1}\{\delta_S\} \end{Bmatrix} \ddot{x}^b(n) \quad (3)$$

where $[I]$ is an identity matrix of dimension NO by NO . In compact form, the state Equation (3) can be written as

$$\{\dot{Z}^{tb}(n)\} = [\hat{A}]\{Z^{tb}(n)\} + [\hat{B}]\{\vec{U}(n)\} + \{\hat{C}\}\ddot{x}^b(n) \quad (4)$$

with

$$\{Z^{tb}(n)\} = \begin{Bmatrix} \{X_S^{tb}(n)\} \\ \{X_S^{tb}(n)\} \end{Bmatrix} \quad (5)$$

$$[\dot{A}] = \begin{bmatrix} [0] & [I] \\ -[M_{SS}]^{-1}[K_{SS}] & -[M_{SS}]^{-1}[C_{SS}] \end{bmatrix} \quad (6)$$

$$[\dot{B}] = \begin{bmatrix} [0] \\ [M_{SS}]^{-1}[\gamma_S] \end{bmatrix} \quad (7)$$

$$\{\dot{C}\} = \begin{Bmatrix} \{0\} \\ [M_{SS}]^{-1}\{\delta_S\} \end{Bmatrix} \quad (8)$$

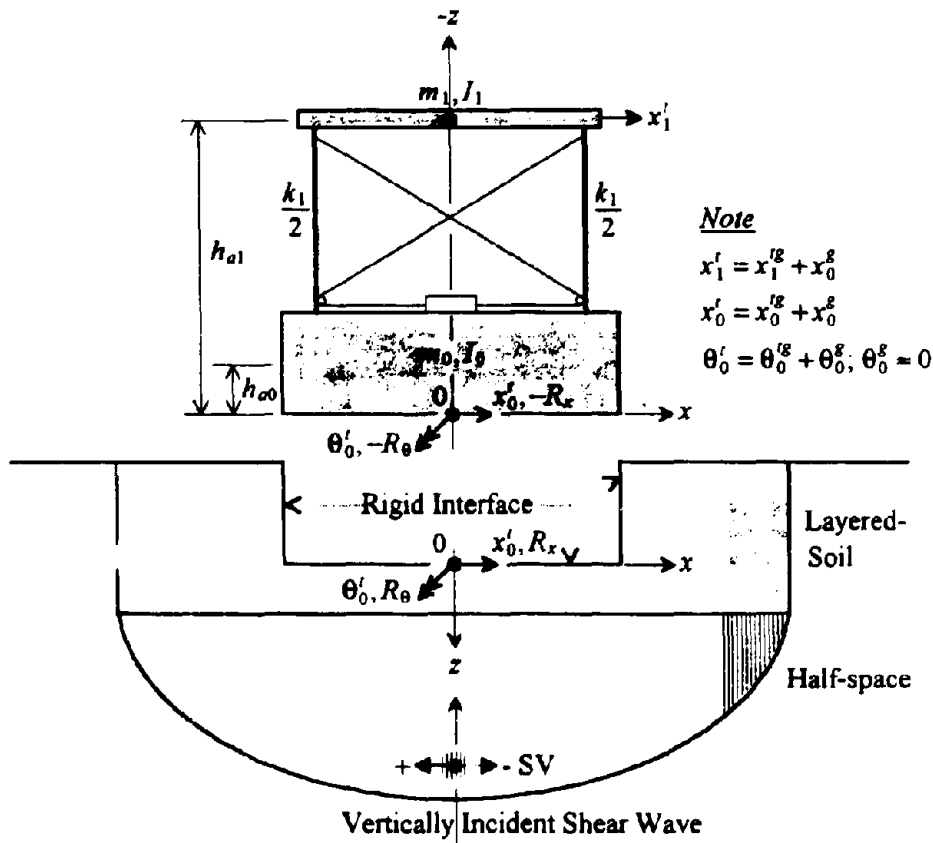
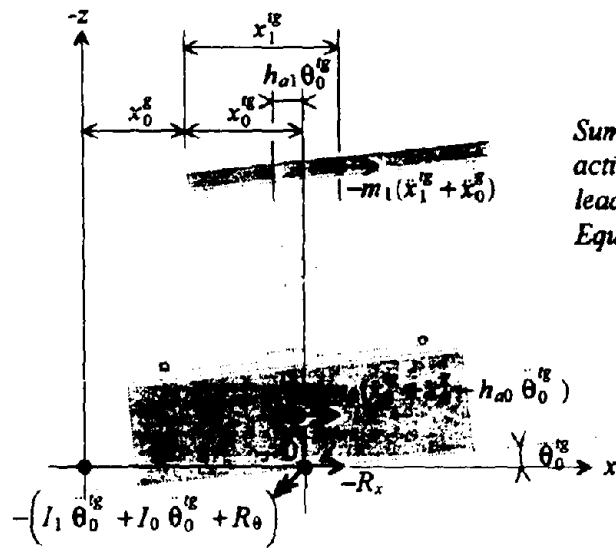


Figure 11. Single-story SSI-model

$$\begin{aligned}
 & \vec{u}_1 \leftarrow m_1(\ddot{x}_1^{ig} + \ddot{x}_0^g) \\
 & \leftarrow k_1(x_1^{ig} - x_0^g + h_{a1}\theta_0^{ig}) \\
 & \leftarrow c_1(\dot{x}_1^{ig} - \dot{x}_0^g + h_{a1}\dot{\theta}_0^{ig})
 \end{aligned}$$

Summation of horizontal forces acting on mass m_1 leads to first row of Equation of Motion (3.9)



Summation of moments acting around node 0 leads to third row of Equation of Motion (3.9)

$$\begin{aligned}
 & c_1(\dot{x}_1^{ig} - \dot{x}_0^g + h_{a1}\dot{\theta}_0^{ig}) \rightarrow \\
 & k_1(x_1^{ig} - x_0^g + h_{a1}\theta_0^{ig}) \rightarrow \\
 & \vec{u}_1 \rightarrow \\
 & R_x
 \end{aligned}$$

Summation of horizontal forces acting on mass m_0 leads to second row of Equation of Motion (3.9)

Figure 12. Free-body Diagram of Single-story SSI-model

where $\{Z^n\}$ is a state vector of dimension $2NO$ by 1. A dot over a letter denotes a derivative with respect to time. The characteristic matrix $[\hat{A}]$ of dimension $2NO$ by $2NO$ is a time-independent matrix as are matrix $[\hat{B}]$ of dimension $2NO$ by NCR and vector $\{\hat{C}\}$ of dimension $2NO$ by 1.

B. FORMULATION FOR STRUCTURE-SOIL INTERACTION MODEL

1. **Single-story Equation of Motion.** For a structure-soil interaction model subjected to a vertically incident shear wave, rotational seismic input may be omitted. Therefore, at any n^{th} time-instant, the motion equation of a single-story seismic shear structure equipped with an active tendon system (see Figures 11 and 12) can be obtained as

$$\begin{bmatrix} m_1 & 0 & 0 \\ 0 & m_0 & -h_{a0}m_0 \\ -h_{a1}m_1 & -h_{a0}m_0 & I_1 + I_0 + h_{a0}^2m_0 \end{bmatrix} \begin{Bmatrix} \dot{x}_1^{ig}(n) \\ \dot{x}_0^{ig}(n) \\ \dot{\theta}_0^{ig}(n) \end{Bmatrix} + \begin{bmatrix} c_1 & -c_1 & h_{a1}c_1 \\ -c_1 & c_1 & -h_{a1}c_1 \\ 0 & 0 & 0 \end{bmatrix} \begin{Bmatrix} x_1^{ig}(n) \\ x_0^{ig}(n) \\ \theta_0^{ig}(n) \end{Bmatrix} \\ + \begin{bmatrix} k_1 & -k_1 & h_{a1}k_1 \\ -k_1 & k_1 & -h_{a1}k_1 \\ 0 & 0 & 0 \end{bmatrix} \begin{Bmatrix} x_1^{ig}(n) \\ x_0^{ig}(n) \\ \theta_0^{ig}(n) \end{Bmatrix} = \begin{Bmatrix} -m_1 \\ -m_0 \\ h_{a1}m_1 + h_{a0}m_0 \end{Bmatrix} \ddot{x}_0^g(n) \\ + \begin{Bmatrix} -1 \\ 1 \\ 0 \end{Bmatrix} \ddot{u}_1(n) + \begin{Bmatrix} 0 \\ -R_x(n) \\ -R_\theta(n) \end{Bmatrix} \quad (9)$$

where m_1 and m_0 are floor lumped mass and foundation lumped mass, respectively. I_1 and I_0 are floor and foundation mass moments of inertia around point 0. h_{a1} and h_{a0} are accumulated heights from rotational point 0 to the centroid of floor lumped mass and foundation lumped mass, respectively. k_1 is translational spring-stiffness coefficient. c_1 is

ite vector of dimension $2NO$ by 1. A dot over a letter denotes a
 ct to time. The characteristic matrix $[\hat{A}]$ of dimension $2NO$ by $2NO$
 matrix as are matrix $[\hat{B}]$ of dimension $2NO$ by NCR and vector $\{\hat{C}\}$
 1.

ON FOR STRUCTURE-SOIL INTERACTION MODEL

ory Equation of Motion. For a structure-soil interaction model
 tically incident shear wave, rotational seismic input may be omitted
 n^{th} time-instant, the motion equation of a single-story seismic shear
 ith an active tendon system (see Figures 11 and 12) can be obtained

$$\begin{aligned}
 & \begin{bmatrix} 0 \\ -h_{a0}m_0 \\ I_1 + I_0 + h_{a0}^2m_0 \end{bmatrix} \begin{Bmatrix} \ddot{x}_1^g(n) \\ \ddot{x}_0^g(n) \\ \ddot{\theta}_0^g(n) \end{Bmatrix} + \begin{bmatrix} c_1 & -c_1 & h_{a1}c_1 \\ -c_1 & c_1 & -h_{a1}c_1 \\ 0 & 0 & 0 \end{bmatrix} \begin{Bmatrix} \dot{x}_1^g(n) \\ \dot{x}_0^g(n) \\ \dot{\theta}_0^g(n) \end{Bmatrix} \\
 & \begin{bmatrix} k_1 & -k_1 & h_{a1}k_1 \\ -k_1 & k_1 & -h_{a1}k_1 \\ 0 & 0 & 0 \end{bmatrix} \begin{Bmatrix} x_1^g(n) \\ x_0^g(n) \\ \theta_0^g(n) \end{Bmatrix} = \begin{Bmatrix} -m_1 \\ -m_0 \\ h_{a1}m_1 + h_{a0}m_0 \end{Bmatrix} \ddot{x}_0^g(n) \\
 & + \begin{Bmatrix} -1 \\ 1 \\ 0 \end{Bmatrix} \ddot{u}_1(n) + \begin{Bmatrix} 0 \\ -R_x(n) \\ -R_\theta(n) \end{Bmatrix} \quad (9)
 \end{aligned}$$

e floor lumped mass and foundation lumped mass, respectively.
 d foundation mass moments of inertia around point O. h_{a1} and h_{a0}
 hts from rotational point O to the centroid of floor lumped mass and
 ass, respectively. k_1 is translational spring-stiffness coefficient c_1 is

$$[M_{SS}] = \begin{bmatrix} m_{NO} & \dots & 0 & \dots & 0 \\ \vdots & \ddots & \vdots & \ddots & \vdots \\ 0 & \dots & m_1 & \dots & 0 \\ \vdots & \ddots & \vdots & \ddots & \vdots \\ 0 & \dots & 0 & \dots & m_1 \end{bmatrix} \quad (11)$$

$$[M_{SO}] = [0]; \quad [M_{OS}] = \begin{bmatrix} 0 & \dots & 0 & \dots & 0 \\ -h_{aNO}m_{NO} & \dots & -h_{a1}m_1 & \dots & -h_{a1}m_1 \end{bmatrix} \quad (12)$$

$$[M_{OO}] = \begin{bmatrix} m_0 & -h_{a0}m_0 \\ -h_{a0}m_0 & \sum_{i=0}^{NO} I_i + h_{a0}^2 m_0 \end{bmatrix} \quad (13)$$

$$[K_{SS}] = \begin{bmatrix} k_{NO} & -k_{NO} & 0 & \dots & 0 & \dots & 0 & 0 \\ -k_{NO} & k_{NO} + k_{NO-1} & -k_{NO-1} & \dots & 0 & \dots & 0 & 0 \\ 0 & -k_{NO-1} & k_{NO-1} + k_{NO-2} & \dots & 0 & \dots & 0 & 0 \\ \vdots & \vdots & \vdots & \ddots & \vdots & \ddots & \vdots & \vdots \\ 0 & 0 & 0 & \dots & k_1 + k_{r-1} & \dots & 0 & 0 \\ \vdots & \vdots & \vdots & \ddots & \vdots & \ddots & \vdots & \vdots \\ 0 & 0 & 0 & \dots & 0 & \dots & k_3 + k_2 & -k_2 \\ 0 & 0 & 0 & \dots & 0 & \dots & -k_2 & k_2 + k_1 \end{bmatrix} \quad (14)$$

$$[K_{SO}] = \begin{bmatrix} 0 & h_{NO}k_{NO} \\ 0 & h_{NO-1}k_{NO-1} - h_{NO}k_{NO} \\ 0 & h_{NO-2}k_{NO-2} - h_{NO-1}k_{NO-1} \\ \vdots & \vdots \\ 0 & h_1k_1 - h_{r-1}k_{r-1} \\ \vdots & \vdots \\ 0 & h_2k_2 - h_3k_3 \\ -k_1 & h_{a1}k_1 - h_2k_2 \end{bmatrix} \quad (15)$$

$$[K_{OS}] = \begin{bmatrix} 0 & 0 & 0 & \dots & 0 & \dots & 0 & -k_1 \\ 0 & 0 & 0 & \dots & 0 & \dots & 0 & 0 \end{bmatrix} \quad (16)$$

$$[K_{OO}] = \begin{bmatrix} k_1 & -h_{a1}k_1 \\ 0 & 0 \end{bmatrix} \quad (17)$$

$$[M_{SS}] = \begin{bmatrix} m_{NO} & \dots & 0 & \dots & 0 \\ \vdots & \ddots & \vdots & \ddots & \vdots \\ 0 & \dots & m_1 & \dots & 0 \\ \vdots & \ddots & \vdots & \ddots & \vdots \\ 0 & \dots & 0 & \dots & m_1 \end{bmatrix} \quad (11)$$

$$[M_{SO}] = [0]; \quad [M_{OS}] = \begin{bmatrix} 0 & \dots & 0 & \dots & 0 \\ -h_{aNO}m_{NO} & \dots & -h_{a1}m_1 & \dots & -h_{a1}m_1 \end{bmatrix} \quad (12)$$

$$[M_{OO}] = \begin{bmatrix} m_0 & -h_{a0}m_0 \\ -h_{a0}m_0 & \sum_{i=0}^{NO} I_i + h_{a0}^2 m_0 \end{bmatrix} \quad (13)$$

$$[K_{SS}] = \begin{bmatrix} k_{NO} & -k_{NO} & 0 & \dots & 0 & \dots & 0 & \dots & 0 & \dots & 0 & \dots & 0 & \dots & 0 \\ -k_{NO} & k_{NO} + k_{NO-1} & -k_{NO-1} & \dots & 0 & \dots & 0 & \dots & 0 & \dots & 0 & \dots & 0 & \dots & 0 \\ 0 & -k_{NO-1} & k_{NO-1} + k_{NO-2} & \dots & 0 & \dots & 0 & \dots & 0 & \dots & 0 & \dots & 0 & \dots & 0 \\ \vdots & \vdots & \vdots & \ddots & \vdots & \ddots & \vdots & \ddots & \vdots & \ddots & \vdots & \ddots & \vdots & \ddots & \vdots \\ 0 & 0 & 0 & \dots & k_1 + k_{i-1} & \dots & 0 & \dots & 0 & \dots & 0 & \dots & 0 & \dots & 0 \\ \vdots & \vdots & \vdots & \ddots & \vdots & \ddots & \vdots & \ddots & \vdots & \ddots & \vdots & \ddots & \vdots & \ddots & \vdots \\ 0 & 0 & 0 & \dots & 0 & \dots & k_3 + k_2 & \dots & -k_2 & \dots & 0 & \dots & 0 & \dots & 0 \\ 0 & 0 & 0 & \dots & 0 & \dots & -k_2 & \dots & k_2 + k_1 & \dots & 0 & \dots & 0 & \dots & 0 \end{bmatrix} \quad (14)$$

$$[K_{SO}] = \begin{bmatrix} 0 & h_{NO}k_{NO} \\ 0 & h_{NO-1}k_{NO-1} - h_{NO}k_{NO} \\ 0 & h_{NO-2}k_{NO-2} - h_{NO-1}k_{NO-1} \\ \vdots & \vdots \\ 0 & h_1k_1 - h_{i+1}k_{i+1} \\ \vdots & \vdots \\ 0 & h_2k_2 - h_3k_3 \\ -k_1 & h_{a1}k_1 - h_2k_2 \end{bmatrix} \quad (15)$$

$$[K_{OS}] = \begin{bmatrix} 0 & 0 & 0 & \dots & 0 & \dots & 0 & -k_1 \\ 0 & 0 & 0 & \dots & 0 & \dots & 0 & 0 \end{bmatrix} \quad (16)$$

$$[K_{OO}] = \begin{bmatrix} k_1 & -h_{a1}k_1 \\ 0 & 0 \end{bmatrix} \quad (17)$$

0 indicate that elements in the denoted vector or matrix correspond to the degrees of freedom of superstructure and foundation, respectively. α_m and β_k can be determined by solving $\alpha_m + \beta_k \omega_i^2 = 2\omega_i \eta_i$, for $i = 1, 2$ where η_i are damping ratios of translational mode of frequency ω_i . $\{\delta_S\}$ of dimension NO by 1 and $\{\delta_0\}$ of dimension 2 by 1 are horizontal ground-acceleration coefficient vectors for superstructure and foundation, respectively. h_{ai} , $i = 0, 1, \dots, NO$, are accumulated heights from rotational point 0 to the centroid of mass m_i . h_i , $i = 1, \dots, NO$, are the i^{th} floor height.

Vector $\{X_S^{tg}\}$ of dimension NO by 1 is the floor translation vector. $[x_{NO}^{tg} \ x_{NO-1}^{tg} \ \dots \ x_i^{tg} \ \dots \ x_2^{tg} \ x_1^{tg}]^T$. $\{X_0^{tg}\}$ of dimension 2 by 1 is a vector consisting of foundation translation and rotation at point 0, $[x_0^{tg} \ \theta_0^{tg}]^T$. Superscript tg indicates all responses are of the total dynamic system and relative to those of ground system. A dot and a double dot over a symbol denote the first derivative and second derivative in relation to time, respectively. \ddot{x}_0^g is the horizontal acceleration, at point 0, of the ground system with rigid interface. $\{R_0\}$ of dimension 2 by 1 is a vector consisting of horizontal interaction force and interaction moment at point 0, $[R_x \ R_\theta]^T$.

Matrices $[\gamma_S]$ of dimension NO by NCR and $[\gamma_0]$ of dimension 2 by NCR are controller-location matrices for superstructure and foundation, respectively. NCR is the number of active controllers. $\{\vec{U}\}$ of dimension NCR by 1 is the vector of horizontal control forces, $[\vec{u}_{NCR} \ \dots \ \vec{u}_i \ \dots \ \vec{u}_1]^T$. An example of matrices $[\gamma_S]$ and $[\gamma_0]$ for a two-controller system, having controller no.1 attached between rigid foundation and first floor (node no.1) and controller no.2 attached between second floor (node no.2) and third floor (node no.3), is shown as

0 indicate that elements in the denoted vector or matrix correspond to the degrees of freedom of superstructure and foundation, respectively. α_m and β_k can be determined by solving $\alpha_m + \beta_k \omega_i^2 = 2\omega_i \eta_i$, for $i = 1, 2$ where η_i are damping ratios of translational mode of frequency ω_i . $\{\delta_S\}$ of dimension NO by 1 and $\{\delta_0\}$ of dimension 2 by 1 are horizontal ground-acceleration coefficient vectors for superstructure and foundation, respectively. h_{ai} , $i = 0, 1, \dots, NO$, are accumulated heights from rotational point 0 to the centroid of mass m_i . h_i , $i = 1, \dots, NO$, are the i^{th} floor height.

Vector $\{X_S^{ig}\}$ of dimension NO by 1 is the floor translation vector, $[x_{NO}^{ig} \ x_{NO-1}^{ig} \ \dots \ x_i^{ig} \ \dots \ x_2^{ig} \ x_1^{ig}]^T$. $\{X_0^{ig}\}$ of dimension 2 by 1 is a vector consisting of foundation translation and rotation at point 0, $[x_0^g \ \theta_0^g]^T$. Superscript ig indicates all responses are of the total dynamic system and relative to those of ground system. A dot and a double dot over a symbol denote the first derivative and second derivative in relation to time, respectively. \ddot{x}_0^g is the horizontal acceleration, at point 0, of the ground system with rigid interface. $\{R_0\}$ of dimension 2 by 1 is a vector consisting of horizontal interaction force and interaction moment at point 0, $[R_x \ R_\theta]^T$.

Matrices $[\gamma_S]$ of dimension NO by NCR and $[\gamma_0]$ of dimension 2 by NCR are controller-location matrices for superstructure and foundation, respectively. NCR is the number of active controllers. $\{\vec{U}\}$ of dimension NCR by 1 is the vector of horizontal control forces, $[\vec{u}_{NCR} \ \dots \ \vec{u}_i \ \dots \ \vec{u}_1]^T$. An example of matrices $[\gamma_S]$ and $[\gamma_0]$ for a two-controller system, having controller no.1 attached between rigid foundation and first floor (node no.1) and controller no.2 attached between second floor (node no.2) and third floor (node no.3), is shown as

$$\{\dot{X}_0^g(t)\} = \int_0^t [\dot{F}_{00}^g(\tau)] \{R_0(t-\tau)\} d\tau \quad (26)$$

with

$$[\dot{F}_{00}^g(\tau)] = \begin{bmatrix} \dot{F}_{zx}^g & \dot{F}_{x0}^g \\ \dot{F}_{0x}^g & \dot{F}_{00}^g \end{bmatrix} \quad (27)$$

where t and τ are time variables. $[\dot{F}_{00}^g]$ is the ground system's impulse velocity matrix with rigid interface (see Subsection C.3 of Section V). Coefficients \dot{F}_{zx}^g , \dot{F}_{x0}^g , \dot{F}_{0x}^g , and \dot{F}_{00}^g are velocities, at time equals τ , corresponding to the first subscript's degree of freedom due to a unit impulse force, at time equals zero, corresponding to the second subscript's degree of freedom. Based on causality conditions, interaction forces and velocities under a unit impulse force, prior to time equal to zero, must be zero. Thus τ varies from 0 to t .

Since the solution procedure of a state equation is carried on in the discrete time domain, the convolution integral can be replaced by summation as

$$\{\dot{X}_0^g(n)\} = \Delta t \sum_{m=0}^n [\dot{F}_{00}^g(m)] \{R_0(n-m)\} \quad (28)$$

where Δt and n are time increment and time-instant number, respectively. m varies from zero to n . To reduce the number of operations in Equation (28), one may take advantage of the fact that a ground system with half-space has radiation damping. Then the amplitude of velocity under a unit impulse load (impulse velocity function) attenuates as time proceeds. At time-instant number equals l , for instance, all elements in the impulse velocity

$$\{X_0^g(t)\} = \int_0^t [F_{00}^g(\tau)]\{R_0(t-\tau)\}d\tau \quad (26)$$

with

$$[F_{00}^g(\tau)] = \begin{bmatrix} F_{xx}^g & F_{x0}^g \\ F_{0x}^g & F_{00}^g \end{bmatrix} \quad (27)$$

where t and τ are time variables. $[F_{00}^g]$ is the ground system's impulse velocity matrix with rigid interface (see Subsection C.3 of Section V). Coefficients $F_{xx}^g, F_{x0}^g, F_{0x}^g,$ and F_{00}^g are velocities, at time equals τ , corresponding to the first subscript's degree of freedom due to a unit impulse force, at time equals zero, corresponding to the second subscript's degree of freedom. Based on causality conditions, interaction forces and velocities under a unit impulse force, prior to time equal to zero, must be zero. Thus τ varies from 0 to t .

Since the solution procedure of a state equation is carried on in the discrete time domain, the convolution integral can be replaced by summation as

$$\{X_0^g(n)\} = \Delta t \sum_{m=0}^n [F_{00}^g(m)]\{R_0(n-m)\} \quad (28)$$

where Δt and n are time increment and time-instant number, respectively. m varies from zero to n . To reduce the number of operations in Equation (28), one may take advantage of the fact that a ground system with half-space has radiation damping. Then the amplitude of velocity under a unit impulse load (impulse velocity function) attenuates as time proceeds. At time-instant number equals l , for instance, all elements in the impulse velocity

$$\{R_0(n)\} = [\bar{K}_{00}] \{X_0^g(n)\} - \{R_0(n-1)\} \quad (32)$$

with

$$[\bar{K}_{00}] = \frac{2}{\Delta t^2} [\dot{F}_{00}^g(0)]^{-1} \quad (33)$$

$$\begin{aligned} \{R_0(n-1)\} = & [\bar{K}_{00}] \left[\{X_0^g(n-1)\} \right. \\ & \left. + \frac{\Delta t}{2} \left(\{\dot{X}_0^g(n-1)\} + \Delta t \sum_{m=1}^{n-1} [\dot{F}_{00}^g(m)] \{R_0(n-m)\} \right) \right] \quad (34) \end{aligned}$$

where the time-independent matrix $[\bar{K}_{00}]$ of dimension 2 by 2 is a pseudo-static-stiffness matrix of ground system. Vector $\{R_0\}$ of dimension 2 by 1 is a dynamic-equivalent-force vector making up for the ground system's dynamic effect. This vector depends only upon the events prior to n^{th} time-instant.

4. State Equation of SSI-model. Substituting interaction force vector [Equation (32)] in the multistory equation of motion [Equation (10)] results in

$$\begin{aligned} & \begin{bmatrix} [M_{SS}] & [M_{S0}] \\ [M_{0S}] & [M_{00}] \end{bmatrix} \begin{Bmatrix} \{\dot{X}_S^g(n)\} \\ \{\dot{X}_0^g(n)\} \end{Bmatrix} + \begin{bmatrix} [C_{SS}] & [C_{S0}] \\ [C_{0S}] & [C_{00}] \end{bmatrix} \begin{Bmatrix} \{X_S^g(n)\} \\ \{X_0^g(n)\} \end{Bmatrix} \\ & + \begin{bmatrix} [K_{SS}] & [K_{S0}] \\ [K_{0S}] & [K_{00}] + [\bar{K}_{00}] \end{bmatrix} \begin{Bmatrix} \{X_S^g(n)\} \\ \{X_0^g(n)\} \end{Bmatrix} = \begin{Bmatrix} \{\delta_S\} \\ \{\delta_0\} \end{Bmatrix} \ddot{x}_0^g(n) \\ & + \begin{bmatrix} [\gamma_S] \\ [\gamma_0] \end{bmatrix} \{\ddot{U}(n)\} + \begin{Bmatrix} \{0\} \\ \{R_0(n-1)\} \end{Bmatrix} \quad (35) \end{aligned}$$

$$\{R_0(n)\} = [\bar{K}_{00}] \{X_0^g(n)\} - \{R_0(n-1)\} \quad (32)$$

with

$$[\bar{K}_{00}] = \frac{2}{\Delta t^2} [\dot{F}_{00}^g(0)]^{-1} \quad (33)$$

$$\{R_0(n-1)\} = [\bar{K}_{00}] \left[\{X_0^g(n-1)\} + \frac{\Delta t}{2} \left(\{X_0^g(n-1)\} + \Delta t \sum_{m=1}^n [F_{00}^g(m)] \{R_0(n-m)\} \right) \right] \quad (34)$$

where the time-independent matrix $[\bar{K}_{00}]$ of dimension 2 by 2 is a pseudo-static-stiffness matrix of ground system. Vector $\{R_0\}$ of dimension 2 by 1 is a dynamic-equivalent-force vector making up for the ground system's dynamic effect. This vector depends only upon the events prior to n^{th} time-instant.

4. State Equation of SSI-model. Substituting interaction force vector [Equation (32)] in the multistory equation of motion [Equation (10)] results in

$$\begin{aligned} & \begin{bmatrix} [M_{SS}] & [M_{SO}] \\ [M_{OS}] & [M_{OO}] \end{bmatrix} \begin{Bmatrix} \{X_S^g(n)\} \\ \{X_0^g(n)\} \end{Bmatrix} + \begin{bmatrix} [C_{SS}] & [C_{SO}] \\ [C_{OS}] & [C_{OO}] \end{bmatrix} \begin{Bmatrix} \{X_S^g(n)\} \\ \{X_0^g(n)\} \end{Bmatrix} \\ & + \begin{bmatrix} [K_{SS}] & [K_{SO}] \\ [K_{OS}] & [K_{OO}] + [\bar{K}_{00}] \end{bmatrix} \begin{Bmatrix} \{X_S^g(n)\} \\ \{X_0^g(n)\} \end{Bmatrix} = \begin{Bmatrix} \{\delta_S\} \\ \{\delta_0\} \end{Bmatrix} X_0^g(n) \\ & + \begin{bmatrix} [\gamma_S] \\ [\gamma_0] \end{bmatrix} \left\{ \dot{U}(n) \right\} + \begin{Bmatrix} \{0\} \\ \{R_0(n-1)\} \end{Bmatrix} \end{aligned} \quad (35)$$

Taking $[\bar{K}_{00}]$ in the total system's stiffness matrix could be physically interpreted as attaching a set of fictitious springs, having coefficients of \bar{K}_{xx} , $\bar{K}_{x\theta}$, $\bar{K}_{\theta x}$, and $\bar{K}_{\theta\theta}$ (elements of $[\bar{K}_{00}]$), to a structure system's rigid foundation as shown in Figure 13. Meanwhile the total system is subjected to the equivalent forces of amplitude $-m_i \ddot{x}_0^g$ at the centroid of each mass i , where $i = 0, 1, \dots, NO$, and is subjected to an equivalent moment of amplitude $\sum_{m=0}^{NO} h_{0i} m_i \ddot{x}_0^g$ around point 0 (contribution of $\{\delta_S\} \ddot{x}_0^g$ and $\{\delta_0\} \ddot{x}_0^g$). Furthermore, at point 0, dynamic-equivalent force R_x and moment R_θ ($\{R_0\} = [R_x \ R_\theta]^T$) are added to compensate for the ground system's dynamic effect.

Rearranging Equation (35), acceleration vector can be expressed as

$$\begin{aligned}
 \begin{Bmatrix} \{\ddot{X}_S^g(n)\} \\ \{\ddot{X}_0^g(n)\} \end{Bmatrix} &= - \begin{bmatrix} [M_{SS}] & [M_{S0}] \\ [M_{0S}] & [M_{00}] \end{bmatrix}^{-1} \begin{bmatrix} [C_{SS}] & [C_{S0}] \\ [C_{0S}] & [C_{00}] \end{bmatrix} \begin{Bmatrix} \{\dot{X}_S^g(n)\} \\ \{\dot{X}_0^g(n)\} \end{Bmatrix} \\
 &- \begin{bmatrix} [M_{SS}] & [M_{S0}] \\ [M_{0S}] & [M_{00}] \end{bmatrix}^{-1} \begin{bmatrix} [K_{SS}] & [K_{S0}] \\ [K_{0S}] & [K_{00}] + [\bar{K}_{00}] \end{bmatrix} \begin{Bmatrix} \{X_S^g(n)\} \\ \{X_0^g(n)\} \end{Bmatrix} \\
 &+ \begin{bmatrix} [M_{SS}] & [M_{S0}] \\ [M_{0S}] & [M_{00}] \end{bmatrix}^{-1} \begin{Bmatrix} \{\delta_S\} \\ \{\delta_0\} \end{Bmatrix} \ddot{x}_0^g(n) \\
 &+ \begin{bmatrix} [M_{SS}] & [M_{S0}] \\ [M_{0S}] & [M_{00}] \end{bmatrix}^{-1} \begin{bmatrix} [\gamma_S] \\ [\gamma_0] \end{bmatrix} \{\tilde{U}(n)\} \\
 &+ \begin{bmatrix} [M_{SS}] & [M_{S0}] \\ [M_{0S}] & [M_{00}] \end{bmatrix}^{-1} \begin{Bmatrix} \{0\} \\ \{R_0(n-1)\} \end{Bmatrix} \quad (36)
 \end{aligned}$$

Taking $[\bar{K}_{00}]$ in the total system's stiffness matrix could be physically interpreted as attaching a set of fictitious springs, having coefficients of \bar{K}_{xx} , $\bar{K}_{x\theta}$, $\bar{K}_{\theta x}$, and $\bar{K}_{\theta\theta}$ (elements of $[\bar{K}_{00}]$), to a structure system's rigid foundation as shown in Figure 13. Meanwhile the total system is subjected to the equivalent forces of amplitude $-m_i \ddot{x}_0^g$ at the centroid of each mass i , where $i = 0, 1, \dots, NO$, and is subjected to an equivalent moment of amplitude $\sum_{i=0}^{NO} h_{ai} m_i \ddot{x}_0^g$ around point 0 (contribution of $\{\delta_S\} \ddot{x}_0^g$ and $\{\delta_0\} \ddot{x}_0^g$). Furthermore, at point 0, dynamic-equivalent force R_x and moment R_θ ($\{R_0\} = [R_x \ R_\theta]^T$) are added to compensate for the ground system's dynamic effect.

Rearranging Equation (35), acceleration vector can be expressed as

$$\begin{aligned}
 \begin{Bmatrix} \{\ddot{X}_S^g(n)\} \\ \{\ddot{X}_0^g(n)\} \end{Bmatrix} &= \begin{bmatrix} [M_{SS}] & [M_{S0}] \\ [M_{OS}] & [M_{00}] \end{bmatrix}^{-1} \begin{bmatrix} [C_{SS}] & [C_{S0}] \\ [C_{OS}] & [C_{00}] \end{bmatrix} \begin{Bmatrix} \{\dot{X}_S^g(n)\} \\ \{\dot{X}_0^g(n)\} \end{Bmatrix} \\
 &- \begin{bmatrix} [M_{SS}] & [M_{S0}] \\ [M_{OS}] & [M_{00}] \end{bmatrix}^{-1} \begin{bmatrix} [K_{SS}] & [K_{S0}] \\ [K_{OS}] & [K_{00}] + [\bar{K}_{00}] \end{bmatrix} \begin{Bmatrix} \{X_S^g(n)\} \\ \{X_0^g(n)\} \end{Bmatrix} \\
 &+ \begin{bmatrix} [M_{SS}] & [M_{S0}] \\ [M_{OS}] & [M_{00}] \end{bmatrix}^{-1} \begin{Bmatrix} \{\delta_S\} \\ \{\delta_0\} \end{Bmatrix} \ddot{x}_0^g(n) \\
 &+ \begin{bmatrix} [M_{SS}] & [M_{S0}] \\ [M_{OS}] & [M_{00}] \end{bmatrix}^{-1} \begin{bmatrix} [\gamma_S] \\ [\gamma_0] \end{bmatrix} \{\ddot{U}(n)\} \\
 &+ \begin{bmatrix} [M_{SS}] & [M_{S0}] \\ [M_{OS}] & [M_{00}] \end{bmatrix}^{-1} \begin{Bmatrix} \{0\} \\ \{R_0(n-1)\} \end{Bmatrix} \quad (36)
 \end{aligned}$$

$$\{\ddot{\mathbf{R}}_0(n-1)\} = \left\{ \begin{array}{c} \{0\} \\ \left[\begin{array}{cc} [M_{SS}] & [M_{SO}] \\ [M_{OS}] & [M_{OO}] \end{array} \right]^{-1} \left\{ \begin{array}{c} \{0\} \\ \{\mathbf{R}_0(n-1)\} \end{array} \right\} \end{array} \right\} \quad (44)$$

where the characteristic matrix $[\ddot{A}]$ of dimension $2(NO+2)$ by $2(NO+2)$ is a time-independent matrix as are matrix $[\ddot{B}]$ of dimension $2(NO+2)$ by NCR and vector $\{\ddot{C}\}$ of dimension $2(NO+2)$ by 1. Acceleration vector $\{\ddot{\mathbf{R}}_0\}$ of dimension $2(NO+2)$ by 1 is associated with dynamic-equivalent forces, depending only upon the outcomes prior to n^{th} time-instant.

C. SOLUTION TECHNIQUE FOR STATE EQUATIONS

As discussed in Section IV, for a closed-loop control, control forces and structural responses are related to an optimal control law as

$$\{\vec{U}(n)\} = [G^{FIX}]\{Z^{ib}(n)\} \quad \text{for FIX-model} \quad (45)$$

$$\{\vec{U}(n)\} = [G^{SSI}]\{Z^{is}(n)\} \quad \text{for SSI-model} \quad (46)$$

where $[G^{FIX}]$ of dimension NCR by $2NO$ and $[G^{SSI}]$ of dimension NCR by $2(NO+2)$ are time-independent feedback gain matrices for FIX-model and SSI-model, respectively.

Therefore the state Equations (4) and (38) can be written in a similar form as

$$\{\dot{Z}^{ib}(n)\} = [\hat{D}]\{Z^{ib}(n)\} + \{\hat{E}(n)\} \quad \text{for FIX-model} \quad (47)$$

$$\{\dot{Z}^{is}(n)\} = [\check{D}]\{Z^{is}(n)\} + \{\check{E}(n)\} \quad \text{for SSI-model} \quad (48)$$

with

$$\{\ddot{\mathbf{R}}_0(n-1)\} = \left\{ \begin{array}{c} \{0\} \\ \left[\begin{array}{cc} [M_{SS}] & [M_{S0}] \\ [M_{0S}] & [M_{00}] \end{array} \right]^{-1} \left\{ \begin{array}{c} \{0\} \\ \{\mathbf{R}_0(n-1)\} \end{array} \right\} \end{array} \right\} \quad (44)$$

where the characteristic matrix $[\check{\mathbf{A}}]$ of dimension $2(NO+2)$ by $2(NO+2)$ is a time-independent matrix as are matrix $[\check{\mathbf{B}}]$ of dimension $2(NO+2)$ by NCR and vector $\{\check{\mathbf{C}}\}$ of dimension $2(NO+2)$ by 1. Acceleration vector $\{\check{\mathbf{R}}_0\}$ of dimension $2(NO+2)$ by 1 is associated with dynamic-equivalent forces, depending only upon the outcomes prior to n^{th} time-instant.

C. SOLUTION TECHNIQUE FOR STATE EQUATIONS

As discussed in Section IV, for a closed-loop control, control forces and structural responses are related to an optimal control law as

$$\{\vec{\mathbf{U}}(n)\} = [G^{FIX}]\{Z^{ib}(n)\} \quad \text{for FIX-model} \quad (45)$$

$$\{\vec{\mathbf{U}}(n)\} = [G^{SSI}]\{Z^{is}(n)\} \quad \text{for SSI-model} \quad (46)$$

where $[G^{FIX}]$ of dimension NCR by $2NO$ and $[G^{SSI}]$ of dimension NCR by $2(NO+2)$ are time-independent feedback gain matrices for FIX-model and SSI-model, respectively.

Therefore the state Equations (4) and (38) can be written in a similar form as

$$\{Z^{ib}(n)\} = [\hat{\mathbf{D}}]\{Z^{ib}(n)\} + \{\hat{\mathbf{E}}(n)\} \quad \text{for FIX-model} \quad (47)$$

$$\{Z^{is}(n)\} = [\check{\mathbf{D}}]\{Z^{is}(n)\} + \{\check{\mathbf{E}}(n)\} \quad \text{for SSI-model} \quad (48)$$

with

pseudo-spring-stiffness. The plant matrix yields $N\mathcal{O}$ complex conjugate pairs of eigenvalues $\alpha_i \pm i\beta_i$, and their corresponding eigenvectors $\{a_i\} \pm i\{b_i\}$, where $i = \sqrt{-1}$, α_i, β_i are real scalars; $\{a_i\}, \{b_i\}$ are real vectors of dimension $2N\mathcal{O}$ by 1, and $i = 1, 2, \dots, N\mathcal{O}$.

Transformation matrix $[T]$ is needed to transform the state equation into canonical form. $[T]$ is a real matrix of dimension $2N\mathcal{O}$ by $2N\mathcal{O}$, consisting of real parts $\{a_i\}$ and imaginary parts $\{b_i\}$ of the plant matrix's eigenvectors, and can be expressed as

$$[T] = \left[\begin{array}{cc|cc|cc} \{a_1\} & \{b_1\} & \dots & \{a_i\} & \{b_i\} & \dots & \{a_{N\mathcal{O}}\} & \{b_{N\mathcal{O}}\} \end{array} \right] \quad (54)$$

Transformation matrix $[T]$ and plant matrix $[D]$ are related to matrix $[\Lambda]$, consisting of real parts α_i and imaginary parts β_i of the plant matrix's eigenvalues, as

$$[T]^{-1}[D][T] = [\Lambda] \quad (55)$$

where $[\Lambda]$ of dimension $2N\mathcal{O}$ by $2N\mathcal{O}$ is a real matrix of the following form.

$$[\Lambda] = \left[\begin{array}{cccc|cccc} [\Lambda_1] & \dots & [0] & \dots & [0] & & & \\ \vdots & & \vdots & & \vdots & & & \\ [0] & \dots & [\Lambda_i] & \dots & [0] & & & \\ \vdots & & \vdots & & \vdots & & & \\ [0] & \dots & [0] & \dots & [\Lambda_{N\mathcal{O}}] & & & \end{array} \right] \quad (56)$$

$$[\Lambda_i] = \left[\begin{array}{cc} \alpha_i & \beta_i \\ -\beta_i & \alpha_i \end{array} \right] \quad (57)$$

Let solution of the state Equation (53) be expressed as

$$\{Z(n)\} = [T]\{\Phi(n)\} \quad (58)$$

pseudo-spring-stiffness. The plant matrix yields $N\mathcal{O}$ complex conjugate pairs of eigenvalues $\alpha_i \pm i\beta_i$, and their corresponding eigenvectors $\{a_i\} \pm i\{b_i\}$, where $i = \sqrt{-1}$. α_i, β_i are real scalars; $\{a_i\}, \{b_i\}$ are real vectors of dimension $2N\mathcal{O}$ by 1, and $i = 1, 2, \dots, N\mathcal{O}$.

Transformation matrix $[T]$ is needed to transform the state equation into canonical form. $[T]$ is a real matrix of dimension $2N\mathcal{O}$ by $2N\mathcal{O}$, consisting of real parts $\{a_i\}$ and imaginary parts $\{b_i\}$ of the plant matrix's eigenvectors, and can be expressed as

$$[T] = \left[\begin{array}{cc|cc|cc} \{a_1\} & \{b_1\} & \dots & \{a_i\} & \{b_i\} & \dots & \{a_{N\mathcal{O}}\} & \{b_{N\mathcal{O}}\} \end{array} \right] \quad (54)$$

Transformation matrix $[T]$ and plant matrix $[D]$ are related to matrix $[\Lambda]$, consisting of real parts α_i and imaginary parts β_i of the plant matrix's eigenvalues, as

$$[T]^{-1}[D][T] = [\Lambda] \quad (55)$$

where $[\Lambda]$ of dimension $2N\mathcal{O}$ by $2N\mathcal{O}$ is a real matrix of the following form.

$$[\Lambda] = \left[\begin{array}{cccc|cccc} [\Lambda_1] & \dots & [0] & \dots & [0] & & & \\ \vdots & \ddots & \vdots & \ddots & \vdots & & & \\ [0] & \dots & [\Lambda_i] & \dots & [0] & & & \\ \vdots & \ddots & \vdots & \ddots & \vdots & & & \\ [0] & \dots & [0] & \dots & [\Lambda_{N\mathcal{O}}] & & & \end{array} \right] \quad (56)$$

$$[\Lambda_i] = \left[\begin{array}{cc} \alpha_i & \beta_i \\ -\beta_i & \alpha_i \end{array} \right] \quad (57)$$

Let solution of the state Equation (53) be expressed as

$$\{Z(n)\} = [T]\{\Phi(n)\} \quad (58)$$

By assuming $\{\exp([0])\}$ is equal to an identity matrix $[I]$ and using Taylor polynomial expansion at $[\Lambda]t$ equals $[0]$, matrix $\{\exp([\Lambda]t)\}$ of dimension $2N\mathcal{O}$ by $2N\mathcal{O}$ can be approximated as

$$\{\exp([\Lambda]t)\} = \begin{bmatrix} \{\exp([\Lambda_1]t)\} & \cdots & [0] & \cdots & [0] \\ \vdots & \ddots & \vdots & \ddots & \vdots \\ [0] & \cdots & \{\exp([\Lambda_i]t)\} & \cdots & [0] \\ \vdots & \ddots & \vdots & \ddots & \vdots \\ [0] & \cdots & [0] & \cdots & \{\exp([\Lambda_{N\mathcal{O}}]t)\} \end{bmatrix} \quad (65)$$

with

$$\{\exp([\Lambda_i]t)\} = \exp(\alpha_i t) \begin{bmatrix} \cos(\beta_i t) & \sin(\beta_i t) \\ -\sin(\beta_i t) & \cos(\beta_i t) \end{bmatrix} \quad (66)$$

Applying the initial conditions in Equations (61) and (62) and utilizing trapezoidal rule with time increment Δt , the solution Equation (64) at n^{th} time-instant can be written as

$$\begin{aligned} \{\Phi(n\Delta t)\} &= \{\exp([\Lambda]n\Delta t)\}\{\Phi(0)\} + \frac{\Delta t}{2}\{\exp([\Lambda]n\Delta t)\}\{\Gamma(0)\} \\ &\quad + \Delta t \sum_{m=1}^{n-1} \{\exp([\Lambda](n-m)\Delta t)\}\{\Gamma(m\Delta t)\} + \frac{\Delta t}{2}\{\Gamma(n\Delta t)\} \\ &= \Delta t \sum_{m=1}^{n-1} \{\exp([\Lambda](n-m)\Delta t)\}\{\Gamma(m\Delta t)\} + \frac{\Delta t}{2}\{\Gamma(n\Delta t)\} \end{aligned} \quad (67)$$

In compact form, the solution Equation (67) can be derived as

$$\{\Phi(n)\} = \{\Pi(n-1)\} + \frac{\Delta t}{2}\{\Gamma(n)\} \quad (68)$$

By assuming $[\exp(\{0\})]$ is equal to an identity matrix $[I]$ and using Taylor polynomial expansion at $[\Lambda]t$ equals $[0]$, matrix $[\exp([\Lambda]t)]$ of dimension $2N\mathcal{O}$ by $2N\mathcal{O}$ can be approximated as

$$[\exp([\Lambda]t)] = \begin{bmatrix} [\exp([\Lambda_1]t)] & \dots & [0] & \dots & [0] \\ [0] & & [\exp([\Lambda_i]t)] & & [0] \\ \vdots & & \vdots & & \vdots \\ [0] & & [0] & & [\exp([\Lambda_{N\mathcal{O}}]t)] \end{bmatrix} \quad (65)$$

with

$$[\exp([\Lambda_i]t)] = \exp(\alpha_i t) \begin{bmatrix} \cos(\beta_i t) & \sin(\beta_i t) \\ -\sin(\beta_i t) & \cos(\beta_i t) \end{bmatrix} \quad (66)$$

Applying the initial conditions in Equations (61) and (62) and utilizing trapezoidal rule with time increment Δt , the solution Equation (64) at n^{th} time-instant can be written as

$$\begin{aligned} \{\Phi(n\Delta t)\} &= [\exp([\Lambda]n\Delta t)]\{\Phi(0)\} + \frac{\Delta t}{2}[\exp([\Lambda]n\Delta t)]\{\Gamma(0)\} \\ &\quad + \Delta t \sum_{m=1}^{n-1} [\exp([\Lambda](n-m)\Delta t)]\{\Gamma(m\Delta t)\} + \frac{\Delta t}{2}\{\Gamma(n\Delta t)\} \\ &= \Delta t \sum_{m=1}^{n-1} [\exp([\Lambda](n-m)\Delta t)]\{\Gamma(m\Delta t)\} + \frac{\Delta t}{2}\{\Gamma(n\Delta t)\} \end{aligned} \quad (67)$$

In compact form, the solution Equation (67) can be derived as

$$\{\Phi(n)\} = \{\Pi(n-1)\} + \frac{\Delta t}{2}\{\Gamma(n)\} \quad (68)$$

IV. OPTIMAL CONTROL LAW

The time-continuous version of state Equations (4) for FIX-model and (38) for SSI-model can be written in a parallel format as

$$\{\dot{Z}^{fb}(t)\} = [\hat{A}]\{Z^{fb}(t)\} + [\hat{B}]\{\vec{U}(t)\} + \{\hat{E}(t)\} \quad \text{for FIX-model} \quad (71)$$

$$\{\dot{Z}^{ss}(t)\} = [\check{A}]\{Z^{ss}(t)\} + [\check{B}]\{\vec{U}(t)\} + \{\check{E}(t)\} \quad \text{for SSI-model} \quad (72)$$

with

$$\{\hat{E}(t)\} = \{\hat{C}\}\dot{x}^b(t) \quad (73)$$

$$\{\check{E}(t)\} = \{\check{C}\}\dot{x}_0^s(t) + \{\check{R}_0(t-\Delta t)\} \quad (74)$$

where $\{\hat{E}\}$ and $\{\check{E}\}$ of dimension $2N\mathcal{O}$ by 1 are external disturbance vectors for FIX-model and SSI-model, respectively. $N\mathcal{O}$ equals NO for FIX-model and $NO+2$ for SSI-model, where NO is the number of a structure's floors. $[\hat{A}]$ and $[\check{A}]$ of dimension $2N\mathcal{O}$ by $2N\mathcal{O}$ are characteristic matrices for FIX-model and SSI-model, respectively. $\{Z^{fb}\}$ and $\{Z^{ss}\}$ of dimension $2N\mathcal{O}$ by 1 are state vectors for FIX-model and SSI-model, respectively. $[\hat{B}]$ and $[\check{B}]$ of dimension $2N\mathcal{O}$ by NCR are the matrices associated with a controller's location for FIX-model and SSI-model, respectively. NCR is the number of active controllers. $\{\vec{U}\}$ of dimension NCR by 1 is the vector consisting of horizontal control forces.

IV. OPTIMAL CONTROL LAW

The time-continuous version of state Equations (4) for FIX-model and (38) for SSI-model can be written in a parallel format as

$$\{Z^{fb}(t)\} = [\hat{A}]\{Z^{fb}(t)\} + [\hat{B}]\{\tilde{U}(t)\} + \{\hat{E}(t)\} \quad \text{for FIX-model} \quad (71)$$

$$\{Z^{ss}(t)\} = [\check{A}]\{Z^{ss}(t)\} + [\check{B}]\{\tilde{U}(t)\} + \{\check{E}(t)\} \quad \text{for SSI-model} \quad (72)$$

with

$$\{\hat{E}(t)\} = \{\hat{C}\}x^b(t) \quad (73)$$

$$\{\check{E}(t)\} = \{\check{C}\}x_0^s(t) + \{\check{R}_0(t-\Delta t)\} \quad (74)$$

where $\{\hat{E}\}$ and $\{\check{E}\}$ of dimension $2N\mathcal{O}$ by 1 are external disturbance vectors for FIX-model and SSI-model, respectively. $N\mathcal{O}$ equals NO for FIX-model and $NO+2$ for SSI-model, where NO is the number of a structure's floors. $[\hat{A}]$ and $[\check{A}]$ of dimension $2N\mathcal{O}$ by $2N\mathcal{O}$ are characteristic matrices for FIX-model and SSI-model, respectively. $\{Z^{fb}\}$ and $\{Z^{ss}\}$ of dimension $2N\mathcal{O}$ by 1 are state vectors for FIX-model and SSI-model, respectively. $[\hat{B}]$ and $[\check{B}]$ of dimension $2N\mathcal{O}$ by NCR are the matrices associated with a controller's location for FIX-model and SSI-model, respectively. NCR is the number of active controllers. $\{\tilde{U}\}$ of dimension NCR by 1 is the vector consisting of horizontal control forces.

with

$$J_n(\{Z(t)\}, \{\tilde{U}(t)\}) = \frac{1}{2} \int_{t_{n-1}}^{t_n} (\{Z(t)\}^T [Q] \{Z(t)\} + \{\tilde{U}(t)\}^T [R] \{\tilde{U}(t)\}) dt \quad (78)$$

For each time interval n , the amplitude of state variables $z_i(t)$ for $i=1,2,\dots,2N\mathcal{O}$ and control forces $\tilde{u}_i(t)$, at time t_{n-1} , are specified from the previous time interval; those at time t_n are not. This leads to the problem of minimizing a variable-end-point functional for which the unknown amplitude of state vector $\{Z(t)\}$ at time t_n should also be minimized. Therefore the function of this state vector needs to be included in the expression of performance index. A new objective functional or generalized performance index at time interval $[t_{n-1}, t_n]$ can be defined as

$$J_n(\{Z(t_n)\}, \{Z(t)\}, \{\tilde{U}(t)\}) = g(\{Z(t_n)\}) + \int_{t_{n-1}}^{t_n} f(t, \{Z(t)\}, \{\tilde{U}(t)\}) dt \quad (79)$$

with

$$g(\{Z(t_n)\}) = \frac{1}{2} \{Z(t_n)\}^T [S] \{Z(t_n)\} \quad (80)$$

$$f(t, \{Z(t)\}, \{\tilde{U}(t)\}) = \frac{1}{2} (\{Z(t)\}^T [Q] \{Z(t)\} + \{\tilde{U}(t)\}^T [R] \{\tilde{U}(t)\}) \quad (81)$$

To ensure a positive value for Equation (80), the weighting matrix $[S]$ of dimension $2N\mathcal{O}$ by $2N\mathcal{O}$ is a positive semi-definite.

1. **Transversality Condition.** To minimize the generalized performance index J_n in Equation (79) with a free endpoint condition and consequently the performance

with

$$J_n(\{Z(t)\}, \{\tilde{U}(t)\}) = \frac{1}{2} \int_{t_{n-1}}^{t_n} \left(\{Z(t)\}^T [Q] \{Z(t)\} + \{\tilde{U}(t)\}^T [R] \{\tilde{U}(t)\} \right) dt \quad (78)$$

For each time interval n , the amplitude of state variables $z_i(t)$ for $i=1, 2, \dots, 2N\mathcal{O}$ and control forces $\tilde{u}_i(t)$, at time t_{n-1} , are specified from the previous time interval; those at time t_n are not. This leads to the problem of minimizing a variable-end-point functional for which the unknown amplitude of state vector $\{Z(t)\}$ at time t_n should also be minimized. Therefore the function of this state vector needs to be included in the expression of performance index. A new objective functional or generalized performance index, at time interval $[t_{n-1}, t_n]$ can be defined as

$$J_n(\{Z(t_n)\}, \{Z(t)\}, \{\tilde{U}(t)\}) = g(\{Z(t_n)\}) + \int_{t_{n-1}}^{t_n} f(t, \{Z(t)\}, \{\tilde{U}(t)\}) dt \quad (79)$$

with

$$g(\{Z(t_n)\}) = \frac{1}{2} \{Z(t_n)\}^T [S] \{Z(t_n)\} \quad (80)$$

$$f(t, \{Z(t)\}, \{\tilde{U}(t)\}) = \frac{1}{2} \left(\{Z(t)\}^T [Q] \{Z(t)\} + \{\tilde{U}(t)\}^T [R] \{\tilde{U}(t)\} \right) \quad (81)$$

To ensure a positive value for Equation (80), the weighting matrix $[S]$ of dimension $2N\mathcal{O}$ by $2N\mathcal{O}$ is a positive semi-definite.

1. **Transversality Condition.** To minimize the generalized performance index J_n in Equation (79) with a free endpoint condition and consequently the performance

$$G = \frac{1}{2} \{Z(t_n)\}^T [S] \{Z(t_n)\} + \{\lambda_g\}^T \left\{ \begin{array}{l} t_{n-1} - t_0 - (n-1)\Delta t \\ \{Z(t_{n-1})\} - \{Z_{n-1}\} \\ t_n - t_0 - n\Delta t \end{array} \right\} \quad (85)$$

$$F = \frac{1}{2} \left(\{Z(t)\}^T [Q] \{Z(t)\} + \{\tilde{U}(t)\}^T [R] \{\tilde{U}(t)\} \right) \\ + \{\lambda_f(t)\}^T \left(\{\dot{Z}(t)\} - [A] \{Z(t)\} - [B] \{\tilde{U}(t)\} - \{E(t)\} \right) \quad (86)$$

Applying the fundamental necessary condition (variation of $J_n = 0$) to Equation (84) with unknown endpoints leads to the transversality condition as

$$dG + \left[\left(F - \{F_{,Z(t)}\}^T \{Z(t)\} \right) dt \right]_{t_{n-1}}^{t_n} + \left[\{F_{,Z(t)}\}^T \{d\{Z(t)\}\} \right]_{t_{n-1}}^{t_n} = 0 \quad (87)$$

where the letter d represents differential of function or variable following it. A comma denotes a partial derivative with respect to the subscript following it.

Since t_{n-1} , $\{Z(t_{n-1})\}$, and t_n are known and fixed, their differentials dt_{n-1} , $d\{Z(t_{n-1})\}$ and dt_n equal zero. Therefore the transversality condition in Equation (87) can be reduced as

$$\left\{ \{G_{,Z(t_n)}\} + \{F_{,Z(t)}\}_{t_n}^T \right\} \{d\{Z(t_n)\}\} = 0 \quad (88)$$

Substituting Equations (85) and (86) in Equation (88), and knowing that $\{d\{Z(t_n)\}\} \neq \{0\}$, leads to

$$[S] \{Z(t_n)\} + \{\lambda_f(t_n)\} = \{0\} \quad (89)$$

$$G = \frac{1}{2} \{Z(t_n)\}^T [S] \{Z(t_n)\} + \{\lambda_g\}^T \left\{ \begin{array}{c} t_{n-1} - t_0 - (n-1)\Delta t \\ \{Z(t_{n-1})\} - \{Z_{n-1}\} \\ t_n - t_0 - n\Delta t \end{array} \right\} \quad (85)$$

$$F = \frac{1}{2} \left(\{Z(t)\}^T [Q] \{Z(t)\} + \{\tilde{U}(t)\}^T [R] \{\tilde{U}(t)\} \right) \\ + \{\lambda_f(t)\}^T \left(\{\dot{Z}(t)\} - [A] \{Z(t)\} - [B] \{\tilde{U}(t)\} - \{E(t)\} \right) \quad (86)$$

Applying the fundamental necessary condition (variation of $J_n = 0$) to Equation (84) with unknown endpoints leads to the transversality condition as

$$dG + \left[\left(F - \{F_{,Z(t)}\}^T \{\dot{Z}(t)\} \right) dt \right]_{t_{n-1}}^{t_n} + \left[\{F_{,Z(t)}\}^T \{d\{Z(t)\}\} \right]_{t_{n-1}}^{t_n} = 0 \quad (87)$$

where the letter d represents differential of function or variable following it. A comma denotes a partial derivative with respect to the subscript following it.

Since t_{n-1} , $\{Z(t_{n-1})\}$, and t_n are known and fixed, their differentials dt_{n-1} , $d\{Z(t_{n-1})\}$ and dt_n equal zero. Therefore the transversality condition in Equation (87) can be reduced as

$$\left\{ \{G_{,Z(t_n)}\} + \{F_{,Z(t)}\}^T \right\}_{t_n}^T \{d\{Z(t_n)\}\} = 0 \quad (88)$$

Substituting Equations (85) and (86) in Equation (88), and knowing that $\{d\{Z(t_n)\}\} \neq \{0\}$, leads to

$$[S] \{Z(t_n)\} + \{\lambda_f(t_n)\} = \{0\} \quad (89)$$

index which can be done by satisfying the Euler equations and the transversality condition previously described.

At each endpoint n ($t = t_n$) for $n = 1, 2, \dots, NT$, the Euler Equation (92) can be written as

$$\{\vec{U}(t_n)\} = [R]^{-1}[B]^T\{\lambda_r(t_n)\} \quad (94)$$

Substituting transversality condition from Equation (89) in Equation (94) leads to

$$\{\vec{U}(t_n)\} = -[R]^{-1}[B]^T[S]\{Z(t_n)\} \quad (95)$$

By comparing Equations (95) to (93), the feedback gain matrix at each endpoint n can be expressed as

$$[G(t_n)] = -[R]^{-1}[B]^T[S] \quad (96)$$

Gain matrix $[G(t_n)]$ is constant and neither a function of time t nor time increment Δt . Therefore it is valid at every endpoint n .

Analogous to $[G(t_n)]$, feedback gain matrices for FIX-model and SSI-model can be expressed as

$$[G^{FIX}] = -[\hat{R}]^{-1}[\hat{B}]^T[\hat{S}] \quad \text{for FIX-model} \quad (97)$$

$$[G^{SSI}] = -[\check{R}]^{-1}[\check{B}]^T[\check{S}] \quad \text{for SSI-model} \quad (98)$$

index which can be done by satisfying the Euler equations and the transversality condition previously described.

At each endpoint n ($t = t_n$) for $n = 1, 2, \dots, NT$, the Euler Equation (92) can be written as

$$\{\vec{U}(t_n)\} = [R]^{-1}[B]^T\{\lambda_j(t_n)\} \quad (94)$$

Substituting transversality condition from Equation (89) in Equation (94) leads to

$$\{\vec{U}(t_n)\} = -[R]^{-1}[B]^T[S]\{Z(t_n)\} \quad (95)$$

By comparing Equations (95) to (93), the feedback gain matrix at each endpoint n can be expressed as

$$[G(t_n)] = -[R]^{-1}[B]^T[S] \quad (96)$$

Gain matrix $[G(t_n)]$ is constant and neither a function of time t nor time increment Δt . Therefore it is valid at every endpoint n .

Analogous to $[G(t_n)]$, feedback gain matrices for FIX-model and SSI-model can be expressed as

$$[G^{FIX}] = -[\check{R}]^{-1}[\check{B}]^T[\check{S}] \quad \text{for FIX-model} \quad (97)$$

$$[G^{SSI}] = -[\check{R}]^{-1}[\check{B}]^T[\check{S}] \quad \text{for SSI-model} \quad (98)$$

where $[K_{SS}]$, $[K_{SO}]$, $[M_{SS}]$, $[M_{OO}]$, $[\gamma_S]$ and $[\gamma_0]$ are given in Equations (14), (15), (11), (13), (24), and (25), respectively.

A weighting matrix $[S]$ of dimension $2NO$ by $2NO$ is selected as an arbitrary row-matrix as

$$[\hat{S}] = [\check{S}] = \begin{bmatrix} [0] & [0] \\ [S_D] & [S_V] \end{bmatrix} \quad (104)$$

where elements on the R^{th} row of submatrices $[S_D]$ and $[S_V]$ of dimension NO by NO equal the arbitrary constants s_D and s_V , respectively, which satisfy a positive semi-definite assumption. For each controller, R equals $NO - ONC + 1$, where ONC is one of the controller's node numbers which does not allow any two consecutive rows of the matrix to be filled.

To assure a positive semi-definite condition of matrix $[S]$, alternately, a symmetrical matrix can be chosen as

$$[\hat{S}] = \gamma_D \begin{bmatrix} \beta_V^{-1} [K_{SS}] & [K_{SS}] \\ [K_{SS}] & \beta_V [K_{SS}] \end{bmatrix} \quad \text{for FIX-model} \quad (105)$$

$$[\check{S}] = \gamma_D \begin{bmatrix} \beta_V^{-1} [\check{K}] & [\check{K}] \\ [\check{K}] & \beta_V [\check{K}] \end{bmatrix} \quad \text{for SSI-model} \quad (106)$$

with

$$[\check{K}] = \begin{bmatrix} [K_{SS}] & [K_{SO}] \\ [K_{SO}]^T & [K_{OO}] \end{bmatrix} \quad (107)$$

where γ_D and β_V are a stiffness scaling factor and a damping scaling factor, respectively.

The influence of s_D, s_V and γ_D, β_V on the total system can be demonstrated by using a fixed-base single-story shear structure as an example. Substituting the gain matrix of the FIX single-story structure [Equation (97)] in the plant matrix Equation (49) leads to

$$[\hat{D}] = [\hat{A}] - \frac{1}{\hat{R}} \{\hat{B}\} \{\hat{B}\}^T [\hat{S}] \quad (108)$$

with

$$[\hat{A}] = \begin{bmatrix} 0 & 1 \\ -(k_1/m_1) & -(c_1/m_1) \end{bmatrix} \quad (109)$$

$$\{\hat{B}\} = \begin{bmatrix} 0 \\ -1/m_1 \end{bmatrix} \quad \text{and} \quad \hat{R} = \frac{1}{k_1} \quad (110)$$

where $[\hat{A}]$, $\{\hat{B}\}$, and \hat{R} are obtained for the FIX single-story structure by using Equations (6), (7), and (101), respectively. Then inserting the row and symmetrical weighting matrices $[\hat{S}]$ in Equations (104) and (105) into Equation (108) leads to

$$[\hat{D}] = \begin{bmatrix} 0 & 1 \\ -(k_1/m_1)(1+s_D/m_1) & -(c_1/m_1)(1+s_V k_1/c_1 m_1) \end{bmatrix} \quad \text{for row matrix } [\hat{S}] \quad (111)$$

$$[\hat{D}] = \begin{bmatrix} 0 & 1 \\ -(k_1/m_1)(1+\gamma_D k_1/m_1) & -(c_1/m_1)(1+\beta_V \gamma_D k_1^2/c_1 m_1) \end{bmatrix} \quad \text{for symmetrical matrix } [\hat{S}] \quad (112)$$

By comparing the characteristic matrix $[\hat{A}]$ of the structure system in Equation (109) to the plant matrices $[\hat{D}]$ of the structure system with control [Equations (111) and (112)], the constants s_D, γ_D and s_V, γ_V increase the stiffness and damping coefficients of the new system, respectively. As the stiffness and damping coefficients correspond to displacement and velocity vectors, s_D, γ_D and s_V, γ_V can also be described as displacement control and velocity control factors, respectively. The complex conjugate pairs of eigenvalues of the plant matrices in Equations (111) and (112) can be expressed as $\alpha \pm i\beta$, where

$$\alpha = -\frac{c_1(1 + s_V k_1 / c_1 m_1)}{2m_1} \quad \text{for Equation (111)} \quad (113)$$

$$\alpha = -\frac{c_1(1 + \beta_V \gamma_D k_1^2 / c_1 m_1)}{2m_1} \quad \text{for Equation (112)} \quad (114)$$

and

$$\beta = \sqrt{\frac{k_1(1 + s_D / m_1)}{m_1} - \left(\frac{c_1(1 + s_V k_1 / c_1 m_1)}{2m_1}\right)^2} \quad \text{for Equation (111)} \quad (115)$$

$$\beta = \sqrt{\frac{k_1(1 + \gamma_D k_1 / m_1)}{m_1} - \left(\frac{c_1(1 + \beta_V \gamma_D k_1^2 / c_1 m_1)}{2m_1}\right)^2} \quad \text{for Equation (112)} \quad (116)$$

For a subcritical damping system, an imaginary part of the root, β , can be interpreted as a damped free vibration frequency ω and $-\alpha/\beta$ as a damping ratio. In order to maintain the

system in the subcritical range (β is a real number $\neq 0$), s_D, s_V or γ_D, β_V must be selected according to the following inequality condition.

$$s_V < \frac{2m_1}{k_1} \sqrt{m_1 k_1 \left(1 + \frac{s_D}{m_1}\right)} - c_1 \quad (117)$$

$$\beta_V < \frac{2m_1}{\gamma_D k_1^2} \sqrt{m_1 k_1 \left(1 + \frac{\gamma_D k_1}{m_1}\right)} - \frac{c_1}{\gamma_D k_1} \quad (118)$$

V. FREQUENCY-DEPENDENT COEFFICIENTS OF SOIL SYSTEMS

A. FREE-FIELD SYSTEM'S STIFFNESS MATRIX

1. **Definition and Concept.** The dynamic-stiffness matrix $[S_{00}^f(\omega)]$ of the continuous free-field system with rigid interface is represented in Figure 14. It specifies the amplitude of forces F_x^f, M_y^f, F_z^f due to unit amplitude of displacements x_0^f, θ_0^f, z_0^f applied at node 0 of the rigid interface for harmonic motion with excitation frequency ω as

$$\begin{Bmatrix} F_x^f \\ M_y^f \\ F_z^f \end{Bmatrix} = [S_{00}^f(\omega)] \begin{Bmatrix} x_0^f \\ \theta_0^f \\ z_0^f \end{Bmatrix} \quad (119)$$

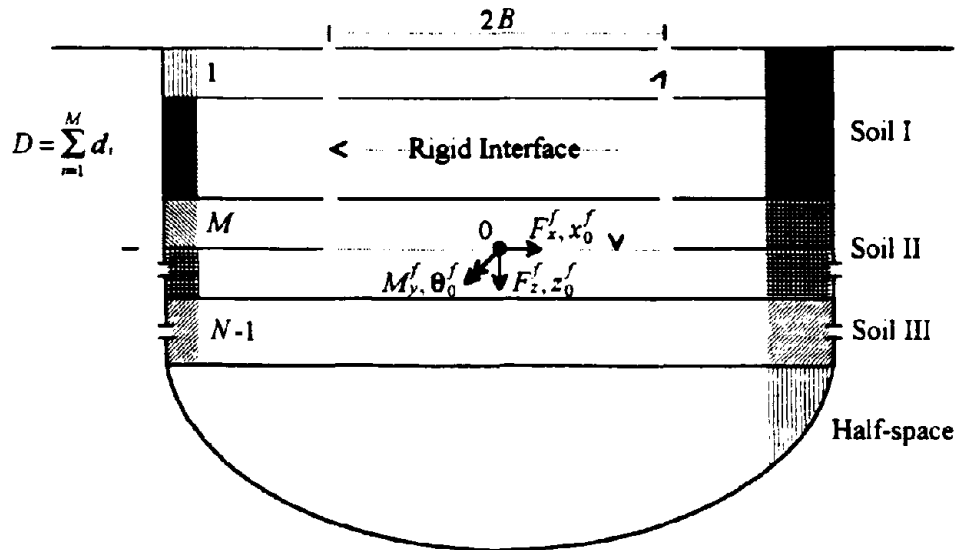


Figure 14. Forces and Displacements of Free-field System with Rigid Interface

The concept of the indirect boundary element method, a special case of weighted-residual technique, can be applied to the free-field system even though the rigid interface is not a boundary. Assume that loading patterns acting along the rigid interface do exist and that these loads result, along the same interface, in the prescribed displacements of unit nodal values x_0^f , θ_0^f , z_0^f . This can be achieved by adjusting load intensities to satisfy this condition. Integrating loading patterns with prescribed displacements will lead to the dynamic-stiffness matrix. Since only a finite number of load intensities can be chosen, an approximate solution results.

In Figure 15, the rigid interface consists of two vertical interfaces for length D and a horizontal interface for length $2B$. As additional horizontal interfaces are introduced into the system, the former is divided into elements of length d_i , for $i=1,2,\dots,M$, on each of the vertical interfaces. The latter is equally divided into $2L$ elements, each of length b . The elements are numbered from 1 to $2(M+L)$. Element 1 is started from the top element of the left vertical interface to the bottom one, element M . Elements $M+1,\dots,M+2L$ define the elements of the horizontal interface from the left element to the right one. On the right vertical interface, elements $M+2L+1,\dots,2(M+L)$ are used to describe the elements from top to bottom.

Rigid body kinematics relate the prescribed displacement amplitudes $u(\vartheta)$, $w(\vartheta)$ along the rigid interface (see Figure 15) to the rigid body degrees of freedom associated with the dynamic-stiffness's definition as

$$\begin{Bmatrix} u(\vartheta) \\ w(\vartheta) \end{Bmatrix} = [N(\vartheta)] \begin{Bmatrix} x_0^f \\ \theta_0^f \\ z_0^f \end{Bmatrix} \quad (120)$$

where ϑ denotes symbolically a point on the assumed line which subsequently forms the rigid interface. A bold letter in the matrix used in Subsection A indicates the corresponding matrix is in the space domain.

On the continuous system in Figure 16, load amplitudes $p(\vartheta)$, $r(\vartheta)$ along the assumed line are related to the initially unknown intensities p_i , r_i on node i as

$$\begin{Bmatrix} p(\vartheta) \\ r(\vartheta) \end{Bmatrix} = [L(\vartheta)] \begin{Bmatrix} p_1 \\ r_1 \\ \vdots \\ p_i \\ r_i \\ \vdots \\ p_{NN} \\ r_{NN} \end{Bmatrix} \quad (121)$$

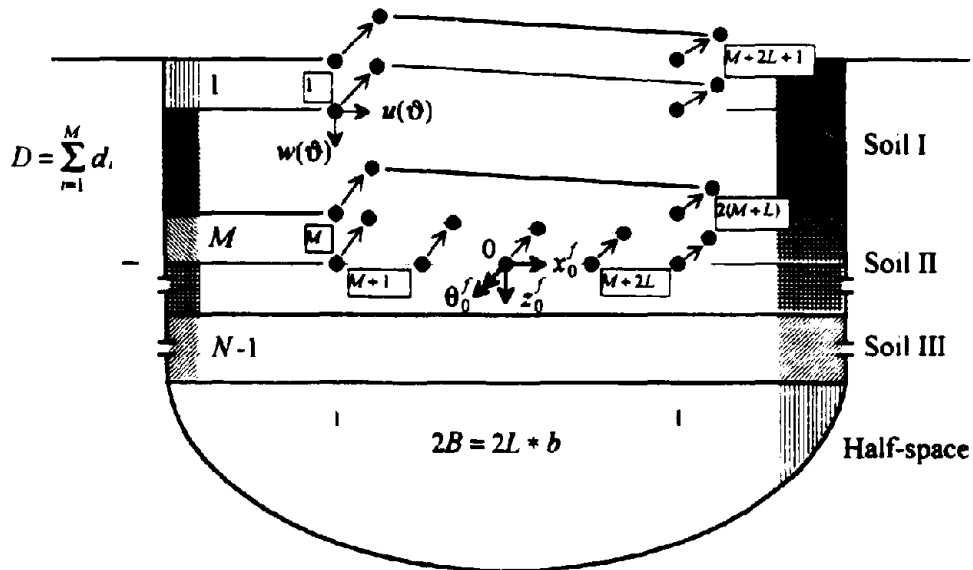


Figure 15. Prescribed Displacements along Rigid Interface

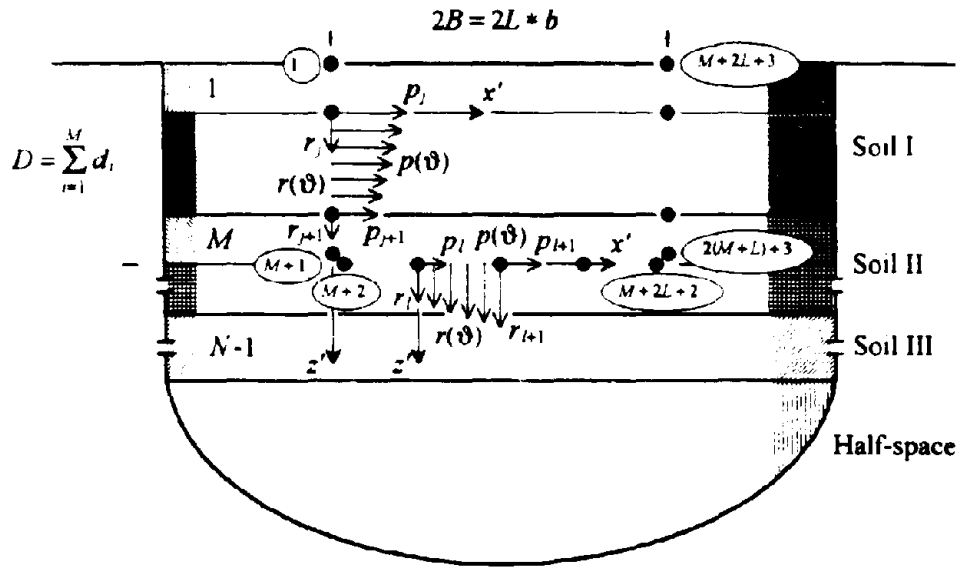


Figure 16. Linearly Distributed Loads along Assumed Line

$[L(\vartheta)]$ represents a selected interpolation function (for example, a linearly distributed function). Nodes are numbered from 1 to NN , where NN is a number of the nodes along the assumed line and equals $2(M+L)+3$ as the discontinuities of load patterns are introduced at the corners of the assumed line. Node 1 goes from the top node of the left vertical interface to the bottom one, node $M+1$. Nodes $M+2, \dots, M+2L+2$ define the nodes of the horizontal interface from the left node to the right one. On the right vertical interface, nodes $M+2L+3, \dots, 2(M+L)+3$ are used to describe the nodes from top to bottom.

Green's influence functions relate the amplitudes of displacements $u_{pr}(\vartheta)$, $w_{pr}(\vartheta)$ along the assumed line to initially unknown intensities p, r , on node i as

$$\begin{Bmatrix} u_{pr}(\vartheta) \\ w_{pr}(\vartheta) \end{Bmatrix} = [\mathbf{uwpr}(\vartheta)] \begin{Bmatrix} p_1 \\ r_1 \\ \vdots \\ p_i \\ r_i \\ \vdots \\ p_{NN} \\ r_{NN} \end{Bmatrix} \quad (122)$$

Since only a finite number of load intensities p, r , can be introduced, the displacement-boundary condition on the interface cannot be satisfied exactly but is expressed in an average sense as

$$\int_{\vartheta} [\mathbf{W}(\vartheta)]^T \left(\begin{Bmatrix} u_{pr}(\vartheta) \\ w_{pr}(\vartheta) \end{Bmatrix} - \begin{Bmatrix} u(\vartheta) \\ w(\vartheta) \end{Bmatrix} \right) d\vartheta = \{0\} \quad (123)$$

In order to guarantee the symmetry of the dynamic-stiffness matrix, for indirect boundary element method, the weighting matrix $[\mathbf{W}(\vartheta)]$ is chosen to be equal to $[\mathbf{L}(\vartheta)]$.

Substituting Equations (120) and (122) in Equation (123), the load intensities p, r , which satisfy the condition in Equation (123) can be determined as

$$\begin{Bmatrix} p_1 \\ r_1 \\ \vdots \\ p_i \\ r_i \\ \vdots \\ p_{NN} \\ r_{NN} \end{Bmatrix} = [\mathbf{F}]^{-1} [\mathbf{T}] \begin{Bmatrix} x_0^f \\ \theta_0^f \\ z_0^f \end{Bmatrix} \quad (124)$$

where

$$[\mathbf{F}] = \int_{\vartheta} [\mathbf{L}(\vartheta)]^T [\mathbf{u}\mathbf{w}\mathbf{p}\mathbf{r}(\vartheta)] d\vartheta \quad (125)$$

$$[\mathbf{T}] = \int_{\vartheta} [\mathbf{L}(\vartheta)]^T [\mathbf{N}(\vartheta)] d\vartheta \quad (126)$$

The flexibility matrix $[\mathbf{F}]$ of a dimension $2(NN)$ by $2(NN)$, where $NN=2(M+L)+3$, is symmetric. The generalized strain-displacement matrix $[\mathbf{T}]$ has a dimension of $2(NN)$ by 3.

As is well known from virtual work consideration, amplitudes of the concentrated loads F_x^f, M_y^f, F_z^f can be obtained by integrating loading patterns with prescribed displacements as

$$\begin{Bmatrix} F_x^f \\ M_y^f \\ F_z^f \end{Bmatrix} = \int_{\vartheta} [\mathbf{N}(\vartheta)]^T \begin{Bmatrix} p(\vartheta) \\ r(\vartheta) \end{Bmatrix} d\vartheta \quad (127)$$

Using Equations (121) and (124) in Equation (127) leads to the dynamic-stiffness matrix of free-field system with rigid interface as

$$\begin{Bmatrix} F_x^f \\ M_y^f \\ F_z^f \end{Bmatrix} = [S_{00}^f(\omega)] \begin{Bmatrix} x_0^f \\ \theta_0^f \\ z_0^f \end{Bmatrix} \quad (128)$$

where

$$[S_{00}^f(\omega)] = [\mathbf{T}]^T [\mathbf{F}]^{-1} [\mathbf{T}] \quad (129)$$

2. **Generalized Strain-displacement Matrix.** Integration in Equation (126) is performed, along the rigid interface, on each element based on its local coordinates. Origin of the local coordinates is located at the top node for the vertical element and at the left node for the horizontal element.

By using the geometric configuration shown in Figure 15, the rigid body kinematics in Equation (120) can be broken down into one of each element as

$$[\bar{\mathbf{N}}(z)]_i = \begin{bmatrix} 1 - \left(\sum_{n=1}^M d_n \right) + z & 0 \\ 0 & B & 1 \end{bmatrix} \text{ for element } i, i=1, \dots, M \quad (130)$$

$$[\bar{\mathbf{N}}(x)]_i = \begin{bmatrix} 1 & 0 & 0 \\ 0 & \left(\sum_{n=1}^{M+L} b \right) - x & 1 \end{bmatrix} \text{ for element } i, i=M+1, \dots, M+L \quad (131)$$

$$[\bar{\mathbf{N}}(x)]_i = \begin{bmatrix} 1 & 0 & 0 \\ 0 & - \left(\sum_{n=M+L+1}^i b \right) + b - x & 1 \end{bmatrix} \text{ for element } i, i=M+L+1, \dots, M+2L \quad (132)$$

$$[\bar{\mathbf{N}}(z)]_i = \begin{bmatrix} 1 - \left(\sum_{n=M-2L}^M d_n \right) + z & 0 \\ 0 & -B & 1 \end{bmatrix} \text{ for element } i, i=M+2L+1, \dots, 2(M+L) \quad (133)$$

where a horizontal bar on top of a letter denotes that the given matrix is element matrix. As an example, the determination of the terms on the first row and second column of the matrix in Equation (130) is described as follows. The term $\sum_{n=1}^M d_n$ represents the distance from the top node of i^{th} element to the level of point 0. Subtracting z (distance from the top node of i^{th} element to a considering point) from $\sum_{n=1}^M d_n$ results in $\sum_{n=1}^M d_n - z$ which

represent the distance from a considering point to the level of point 0. Multiplying $\sum_{n=1}^M d_n - z$ by θ'_0 (rotation at point 0) leads to a negative horizontal displacement at a considering point. The expression on the first row and second column of this matrix relates to the horizontal displacement at a considering point, $u(z)$, to the rotation at point 0, θ'_0 , therefore it equals $-\sum_{n=1}^M d_n + z$.

For linearly distributed loads in Figure 16, a two-node element is employed. Since only the nodal values on these two corresponding nodes dictate loading patterns on the element, the interpolation matrix in Equation (121) can be written as

$$[\bar{\mathbf{L}}(z)]_i = \begin{bmatrix} 1 - z/d_i & 0 & z/d_i & 0 \\ 0 & 1 - z/d_i & 0 & z/d_i \end{bmatrix} \text{ for element } i \text{ on vertical interface} \quad (134)$$

$$[\bar{\mathbf{L}}(x)]_i = \begin{bmatrix} 1 - x/b & 0 & x/b & 0 \\ 0 & 1 - x/b & 0 & x/b \end{bmatrix} \text{ for element } i \text{ on horizontal interface} \quad (135)$$

Using Equations (130) to (135), the element strain-displacement matrix $[\bar{\mathbf{T}}]_i$ can be obtained as

$$[\bar{\mathbf{T}}]_i = \int_0^{d_i} [\bar{\mathbf{L}}(z)]_i^T [\bar{\mathbf{N}}(z)]_i dz, \text{ for element } i \text{ on vertical interfaces} \quad (136)$$

$$[\bar{\mathbf{T}}]_i = \int_0^b [\bar{\mathbf{L}}(x)]_i^T [\bar{\mathbf{N}}(x)]_i dx, \text{ for element } i \text{ on horizontal interface} \quad (137)$$

represent the distance from a considering point to the level of point 0. Multiplying $\sum_{n=1}^M d_n - z$ by θ'_0 (rotation at point 0) leads to a negative horizontal displacement at a considering point. The expression on the first row and second column of this matrix relates to the horizontal displacement at a considering point, $u(z)$, to the rotation at point 0, θ'_0 , therefore it equals $-\sum_{n=1}^M d_n + z$.

For linearly distributed loads in Figure 16, a two-node element is employed. Since only the nodal values on these two corresponding nodes dictate loading patterns on the element, the interpolation matrix in Equation (121) can be written as

$$[\bar{\mathbf{L}}(z)]_i = \begin{bmatrix} 1-z/d_i & 0 & z/d_i & 0 \\ 0 & 1-z/d_i & 0 & z/d_i \end{bmatrix} \text{ for element } i \text{ on vertical interface} \quad (134)$$

$$[\bar{\mathbf{L}}(x)]_i = \begin{bmatrix} 1-x/b & 0 & x/b & 0 \\ 0 & 1-x/b & 0 & x/b \end{bmatrix} \text{ for element } i \text{ on horizontal interface} \quad (135)$$

Using Equations (130) to (135), the element strain-displacement matrix $[\bar{\mathbf{T}}]_i$ can be obtained as

$$[\bar{\mathbf{T}}]_i = \int_0^{d_i} [\bar{\mathbf{L}}(z)]_i^T [\bar{\mathbf{N}}(z)]_i dz, \text{ for element } i \text{ on vertical interfaces} \quad (136)$$

$$[\bar{\mathbf{T}}]_i = \int_0^b [\bar{\mathbf{L}}(x)]_i^T [\bar{\mathbf{N}}(x)]_i dx, \text{ for element } i \text{ on horizontal interface} \quad (137)$$

Completing the integration in Equations (136) and (137) results, for element i , in

$$[\bar{\mathbf{T}}]_i = \begin{bmatrix} d_i/2 - \left(\sum_{n=1}^M d_n\right) d_i/2 + d_i^2/6 & 0 \\ 0 & Bd_i/2 & d_i/2 \\ d_i/2 - \left(\sum_{n=1}^M d_n\right) d_i/2 + d_i^2/3 & 0 \\ 0 & Bd_i/2 & d_i/2 \end{bmatrix} \quad i = 1, \dots, M, \quad (138)$$

$$[\bar{\mathbf{T}}]_i = \begin{bmatrix} b/2 & 0 & 0 \\ 0 & \left(\sum_{n=1}^{M+L} b\right) b/2 - b^2/6 & b/2 \\ b/2 & 0 & 0 \\ 0 & \left(\sum_{n=1}^{M+L} b\right) b/2 - b^2/3 & b/2 \end{bmatrix} \quad i = M+1, \dots, M+L, \quad (139)$$

$$[\bar{\mathbf{T}}]_i = \begin{bmatrix} b/2 & 0 & 0 \\ 0 & -\left(\sum_{n=M+L+1}^i b\right) b/2 + b^2/3 & b/2 \\ b/2 & 0 & 0 \\ 0 & -\left(\sum_{n=M+L+1}^i b\right) b/2 + b^2/6 & b/2 \end{bmatrix} \quad i = M+L+1, \dots, M+2L, \quad (140)$$

$$[\bar{\mathbf{T}}]_i = \begin{bmatrix} d_i/2 - \left(\sum_{n=M-2L}^M d_n\right) d_i/2 + d_i^2/6 & 0 \\ 0 & -Bd_i/2 & d_i/2 \\ d_i/2 - \left(\sum_{n=M-2L}^M d_n\right) d_i/2 + d_i^2/3 & 0 \\ 0 & -Bd_i/2 & d_i/2 \end{bmatrix} \quad i = M+2L+1, \dots, 2(M-L). \quad (141)$$

Therefore the generalized strain-displacement matrix $[\mathbf{T}]$ of a dimension of $2(NN)$ by 3 can be obtained by assembling the element strain-displacement matrices. In the

assembling process, the element matrices of two adjacent elements are overlapped on the rows corresponding to the same node. This overlapping does not apply to the nodes corresponding to the corners of the assumed line since discontinuities in loading patterns were introduced.

3. **Flexibility Matrix.** Integration in Equation (125) is performed in the same manner as that of Equation (126) for generalized strain-displacement matrix.

As noted in Appendix A, Green's influence function relates amplitudes of displacements u_{pr} , w_{pr} in layer i to initially unknown intensities of linearly distributed loads on the vertical assumed line in layer j (see Figure 16) as

$$\begin{Bmatrix} u_{pr}(x', z) \\ w_{pr}(x', z) \end{Bmatrix}'_j = [\mathbf{uwpr}(x', z)]'_j \begin{Bmatrix} p_j \\ r_j \\ p_{j+1} \\ r_{j+1} \end{Bmatrix} \quad (142)$$

with

$$[\mathbf{uwpr}(x', z)]'_j = \int_{-\infty}^{\infty} [\mathbf{uwpr}(k, z)]'_j \exp(-ikx') dk \quad (143)$$

where

$$[\mathbf{uwpr}(k, z)]_j'^{LW} = -[\mathbf{uwAB}(k, z)]_j [\mathbf{uwAB}_j(k)]_j^{-1} \mathbf{SUB}_j \left([\mathbf{S}_{P-SV}^T(k)]_j^{-1} \right) \\ \left([\mathbf{PRpr}_j^P(k)]_j, -[\mathbf{S}_{P-SV}^L(k)]_j [\mathbf{uwpr}_j^P(k)]_j \right) \quad (144)$$

$$\begin{aligned}
[uwpr(k, z)]_j^{i+j} &= [uwpr^p(k, z)]_j - [uwAB(k, z)]_j [uwAB_*(k)]_j^{-1} [uwpr^p(k)]_j \\
&\quad - [uwAB(k, z)]_j [uwAB_*(k)]_j^{-1} SUB_y \left([S_{P-SV}^T(k)]^{-1} \right) \\
&\quad \left([PRpr^p(k)]_j - [S_{P-SV}^L(k)]_j [uwpr^p(k)]_j \right) \quad (145)
\end{aligned}$$

$$\begin{aligned}
[uwpr(k=0, z)]_j^{i+j} &= -[uwAB(z)]_j^{k=0} [uwAB_*]_j^{k=0}^{-1} \\
&\quad SUB_y \left([[S_{P-SV}^T]^{k=0}]^{-1} \right) [PRpr^p]_j^{k=0} \quad (146)
\end{aligned}$$

$$\begin{aligned}
[uwpr(k=0, z)]_j^{i+j} &= [uwpr^l(z)]_j^{k=0} - [uwAB(z)]_j^{k=0} [uwAB_*]_j^{k=0}^{-1} \\
&\quad SUB_y \left([[S_{P-SV}^T]^{k=0}]^{-1} \right) [PRpr^l]_j^{k=0} \quad (147)
\end{aligned}$$

Details of formulation and nomenclature of Equations (142) to (147) can be found in Equations (419), (420), (358), (360), (412), and (414), respectively.

As for linearly distributed loads on the horizontal element with node l and node $l+1$, which are on the horizontal interface underneath layer M (see Figure 16), Green's influence function in layer i can be obtained as

$$\left\{ \begin{array}{l} u_{pr}(x', z) \\ w_{pr}(x', z) \end{array} \right\}_{M,i}^i = [uwpr(x', z)]_{M,i}^i \left\{ \begin{array}{l} p_l \\ r_l \\ p_{l+1} \\ r_{l+1} \end{array} \right\} \quad (148)$$

with

$$[uwpr(x', z)]_{M,i}^i = \int_{-\infty}^{\infty} [uwpr(k, z)]_{M,i}^i \exp(-ikx') dk \quad (149)$$

where

$$[uwpr(k, z)]'_{M,i} = [uwAB(k, z)]_i [uwAB_*(k)]_i^{-1} sub_{iM} \left([S_{P-SV}^T(k)]^{-1} \right) [PRpr_*(k)]_{M,i} \quad (150)$$

$$[uwpr(k=0, z)]'_{M,i} = [uwAB(z)]_i^{k=0} [uwAB_*(z)]_i^{k=0}^{-1} sub_{iM} \left([S_{P-SV}^T]^{k=0} \right) [PRpr_*(z)]_{M,i}^{k=0} \quad (151)$$

Equations (148) to (151) are duplicated from Equations (421), (422), (369), and (418), respectively. Since the horizontal interface is evenly divided, identical Green's influence functions for loads on the horizontal element arise.

The z -axes in Equations (142) to (151) are based on that of layer i . But the x' -axes are based on that of distributed loads, as shown in Figure 16, on that of layer j for loads on vertical interface, and on that of element l for loads on horizontal interface. By using axis transformation and Equations (142) and (148), Green's influence function based on the local coordinates of element i due to the linearly distributed loads on element ii can be obtained as follows.

Element ii on vertical left interface, for $ii = 1, \dots, M$

$$[uwpr(z)]'_i = [uwpr(0, z)]'_i, \quad i = 1, \dots, M \quad (152)$$

$$[uwpr(x)]'_i = [uwpr(\{i-M-1\}b + x, d_M)]'_i, \quad i = M+1, \dots, M+2L \quad (153)$$

$$[uwpr(z)]'_i = [uwpr(2B, z)]'_i^{i-M-2L}, \quad i = M+2L+1, \dots, 2(M+L) \quad (154)$$

Element ii on horizontal interface, for $ii = M+1, \dots, M+2L$

$$[\mathbf{uwpr}(z)'_{ii}] = [\mathbf{uwpr}(\{M+1-ii\}b, z)]'_{M,ii} , i = 1, \dots, M \quad (155)$$

$$[\mathbf{uwpr}(x)'_{ii}] = [\mathbf{uwpr}(\{i-ii\}b + x, d_M)]^M_{M,ii} , i = M+1, \dots, M+2L \quad (156)$$

$$[\mathbf{uwpr}(z)'_{ii}] = [\mathbf{uwpr}(\{M-2L+1-ii\}b, z)]^{i-M-2L}_{M,ii} , i = M+2L+1, \dots, 2(M+L) \quad (157)$$

Element ii on vertical right interface, for $ii = M+2L+1, \dots, 2(M+L)$

$$[\mathbf{uwpr}(z)'_{ii}] = [\mathbf{uwpr}(-2B, z)]'_{ii-M-2L} , i = 1, \dots, M \quad (158)$$

$$[\mathbf{uwpr}(x)'_{ii}] = [\mathbf{uwpr}(\{i-M+2L-1\}b + x, d_M)]^M_{ii-M-2L} , i = M+1, \dots, M+2L \quad (159)$$

$$[\mathbf{uwpr}(z)'_{ii}] = [\mathbf{uwpr}(0, z)]^{i-M-2L}_{ii-M-2L} , i = M+2L+1, \dots, 2(M+L) \quad (160)$$

In the Green's influence matrices on the left side of Equations (152) to (160), superscript i denotes displacements on the element i and subscript ii indicates that the displacements on element i are due to the distributed loads on element ii . The coordinates used in these matrices are based on those of element i . Taking Equation (155) as an example, element i of this equation is on the vertical left interface and element ii is on the horizontal interface. Therefore, Green's influence matrix of layer i (superscript i of the matrix on the right side of the equation) due to the distributed loads on the horizontal element having node ii and $ii+1$, which is on the horizontal interface underneath layer M , is used. Since the z -axis used in this matrix is based on that of layer i (element i), no transformation is needed. However, the x' -axis is referred to that of element ii on the horizontal interface (see Figure 16). To obtain the displacement of element i , the distance

from the left node of element ii (origin of x' -axis) to the vertical left interface is substituted into x' -ordinate. $M+1$ is the element number of the element having its left node aligned with the vertical left interface (see Figure 15). Therefore, $ii-M-1$ is equal to a number of elements between the vertical left interface and the left node of element ii . Then $\{M+1-ii\}b$ is determined as the negative distance from the left node of element ii to the vertical left interface.

Substituting the interpolation matrices in Equations (134), (135) and Green's influence matrices in Equations (152) to (160) into Equation (125), the element flexibility matrix $[\bar{\mathbf{F}}]_{ii}'$ relating nodal strains of element i to nodal stresses of element ii can be expressed as follows.

Element i on vertical left interface, for $i=1, \dots, M$

$$[\bar{\mathbf{F}}]_{ii}' = \int_0^{d_i} [\mathbf{L}(z)]_i^T [\mathbf{uwpr}(0, z)]_{ii}' dz, \quad ii=1, \dots, M \quad (161)$$

$$[\bar{\mathbf{F}}]_{ii}' = \int_0^{d_i} [\mathbf{L}(z)]_i^T [\mathbf{uwpr}(\{M+1-ii\}b, z)]_{M,ii}' dz, \quad ii=M+1, \dots, M+2L \quad (162)$$

$$[\bar{\mathbf{F}}]_{ii}' = \int_0^{d_i} [\mathbf{L}(z)]_i^T [\mathbf{uwpr}(-2B, z)]_{ii-M-2L}' dz, \quad ii=M+2L+1, \dots, 2(M+L) \quad (163)$$

Element i on horizontal interface, for $i=M+1, \dots, M+2L$

$$[\bar{\mathbf{F}}]_{ii}' = \int_0^b [\mathbf{L}(x)]_i^T [\mathbf{uwpr}(\{i-M-1\}b+x, d_M)]_{ii}^M dx, \quad ii=1, \dots, M \quad (164)$$

$$[\bar{\mathbf{F}}]_{ii}' = \int_0^b [\mathbf{L}(x)]_i^T [\mathbf{uwpr}(\{i-ii\}b+x, d_M)]_{M,ii}^M dx, \quad ii=M+1, \dots, M+2L \quad (165)$$

$$[\bar{\mathbf{F}}]_{ii}^i = \int_0^b [\mathbf{L}(x)]_i^T [\mathbf{uwpr}(\{i-M+2L-1\}b+x, d_M)]_{ii-M-2L}^M dx$$

$$ii = M+2L+1, \dots, 2(M+L) \quad (166)$$

Element i on vertical right interface, for $i = M+2L+1, \dots, 2(M+L)$

$$[\bar{\mathbf{F}}]_{ii}^i = \int_0^{d_i} [\mathbf{L}(z)]_i^T [\mathbf{uwpr}(2B, z)]_{ii-M-2L}^{i-M-2L} dz, \quad ii = 1, \dots, M \quad (167)$$

$$[\bar{\mathbf{F}}]_{ii}^i = \int_0^{d_i} [\mathbf{L}(z)]_i^T [\mathbf{uwpr}(\{M-2L+1-ii\}b, z)]_{ii-M-2L}^{i-M-2L} dz, \quad ii = M+1, \dots, M+2L \quad (168)$$

$$[\bar{\mathbf{F}}]_{ii}^i = \int_0^{d_i} [\mathbf{L}(z)]_i^T [\mathbf{uwpr}(0, z)]_{ii-M-2L}^{i-M-2L} dz, \quad ii = M+2L+1, \dots, 2(M+L) \quad (169)$$

Thus assembling the element flexibility matrix $[\bar{\mathbf{F}}]_{ii}^i$ of a 4 by 4 dimension leads to the flexibility matrix $[\mathbf{F}]$ of a dimension of $2(NN)$ by $2(NN)$. In the assembling process, element matrices are overlapped on the matrix's elements corresponding to the same nodes. Rows of the element flexibility matrix correspond to the nodal strains of element i , and columns to the nodal stresses of element ii .

Since integration of the element flexibility matrix $[\bar{\mathbf{F}}]_{ii}^i$ in Equations (161) through (169) is intricate and time-consuming, one may take advantage of the symmetry of the flexibility matrix $[\mathbf{F}]$ and interface configuration. Not all elements in the flexibility matrix need to be determined. For examples, the flexibility matrix may be divided into nine submatrices as shown in Figure 17; each relates strains along vertical or horizontal interface to stresses along vertical or horizontal interface. As the flexibility matrix is symmetrical, the submatrices [1-2], [3-1], [3-2] are identical to the transposed

submatrices $[2-1]^T, [1-3]^T, [2-3]^T$, respectively. Submatrix $[3-3]$ is identical to submatrix $[1-1]$ due to identical vertical interfaces on the left and right.

4. **Integration Technique.** To obtain the flexibility matrix $[F]$, unlike the generalized strain-displacement matrix $[T]$, a numerical integration needs to be employed. This is due to rigorous mathematical form of Green's influence functions [see Equations (142) to (151)] in the flexibility matrix $[F]$. Substituting Equation (143) or (149) into Equations (161) through (169), the element flexibility matrix $[\bar{F}]_{ij}$ can be expressed in a double integration form as follows.






	Stresses on vertical left interface	Stresses on horizontal interface	Stresses on vertical right interface	Rows
Strains on vertical left interface		$[1-2]$ identical to $[2-1]^T$		1 $2M+2$
Strains on horizontal interface				$2M+3$ $2M+4L+4$
Strains on vertical right interface	$[3-1]$ identical to $[1-3]^T$	$[3-2]$ identical to $[2-3]^T$	$[3-3]$ identical to $[1-1]$	$2M+4L+5$ $4(M+L)+6$
Columns	1 $2M+2$	$2M+3$ $2M+4L+4$	$2M+4L+5$ $4(M+L)+6$	

Figure 17. Flexibility Matrix Diagram

Element i on vertical left interface, for $i = 1, \dots, M$

$$[\bar{\mathbf{F}}]_{ii}' = \int_0^{d_i} \int_{-\infty}^{\infty} [\mathbf{L}(z)]_i^T [uwpr(k, z)]_{ii}' dk dz, \quad ii = 1, \dots, M \quad (170)$$

$$[\bar{\mathbf{F}}]_{ii}' = \int_0^{d_i} \int_{-\infty}^{\infty} [\mathbf{L}(z)]_i^T [uwpr(k, z)]_{M,ii}' \exp(-ik\{M+1-ii\}b) dk dz$$

$$ii = M+1, \dots, M+2L \quad (171)$$

$$[\bar{\mathbf{F}}]_{ii}' = \int_0^{d_i} \int_{-\infty}^{\infty} [\mathbf{L}(z)]_i^T [uwpr(k, z)]_{n-M-2L}' \exp(2ikB) dk dz$$

$$ii = M+2L+1, \dots, 2(M+L) \quad (172)$$

Element i on horizontal interface, for $i = M+1, \dots, M+2L$

$$[\bar{\mathbf{F}}]_{ii}' = \int_0^b \int_{-\infty}^{\infty} [\mathbf{L}(x)]_i^T [uwpr(k, d_M)]_{ii}^M \exp[-ik\{(i-M-1)b+x\}] dk dx$$

$$ii = 1, \dots, M \quad (173)$$

$$[\bar{\mathbf{F}}]_{ii}' = \int_0^b \int_{-\infty}^{\infty} [\mathbf{L}(x)]_i^T [uwpr(k, d_M)]_{M,ii}^M \exp[-ik\{(i-ii)b+x\}] dk dx$$

$$ii = M+1, \dots, M+2L \quad (174)$$

$$[\bar{\mathbf{F}}]_{ii}' = \int_0^b \int_{-\infty}^{\infty} [\mathbf{L}(x)]_i^T [uwpr(k, d_M)]_{ii-M-2L}^M \exp[-ik\{(i-M+2L-1)b+x\}] dk dx$$

$$ii = M+2L+1, \dots, 2(M+L) \quad (175)$$

Element i on vertical right interface, for $i = M+2L+1, \dots, 2(M+L)$

$$[\bar{\mathbf{F}}]_{ii}' = \int_0^{d_i} \int_{-\infty}^{\infty} [\mathbf{L}(z)]_i^T [uwpr(k, z)]_{ii}^{M-2L} \exp(-2ikB) dk dz, \quad ii = 1, \dots, M \quad (176)$$

$$[\bar{\mathbf{F}}]_{ii}' = \int_0^{d_i} \int_{-\infty}^{\infty} [\mathbf{L}(z)]_i^T [uwpr(k, z)]_{M,ii}^{M-2L} \exp(-ik\{M-2L+1-ii\}b) dk dz$$

$$ii = M+1, \dots, M+2L \quad (177)$$

$$[\bar{\mathbf{F}}]_{ii}' = \int_0^{d_i} \int_{-\infty}^{\infty} [\mathbf{L}(z)]_i^T [uwpr(k, z)]_{ii-M-2L}^{M-2L} dk dz, \quad ii = M+2L+1, \dots, 2(M+L) \quad (178)$$

To optimize accuracy and computational time for integration in Equations (170) to (178), the adaptive quadrature numerical integration [Burden and Faires, 1988] is applied along k -axis due to the fluctuated nature and variation of functions along this axis (see Figures 18, 19, 20, and 21). This efficient technique can distinguish the amount of functional variation and adapt step size to varying requirements. Therefore the approximation error is uniformly distributed.

Also along k -axis, the functions diminish in both positive and negative directions when the absolute value of k increases. Thus certain values of k are used as upper and lower limits. Note the case of an interval corresponding to a large absolute value of k . Here, if percentage of the area under the interval to the area under the whole range is equal to or less than the desired value, the corresponding k defines the limits.

Since the contours of the functions along x - and z -axis are quite smooth, Simpson's method is adequately employed.

B. EXCAVATED PART'S STIFFNESS MATRIX

1. **Definition and Concept.** For harmonic motion with excitation frequency ω , the dynamic-stiffness matrix $[S_{00}^s(\omega)]$ of the bounded excavated part of the system with

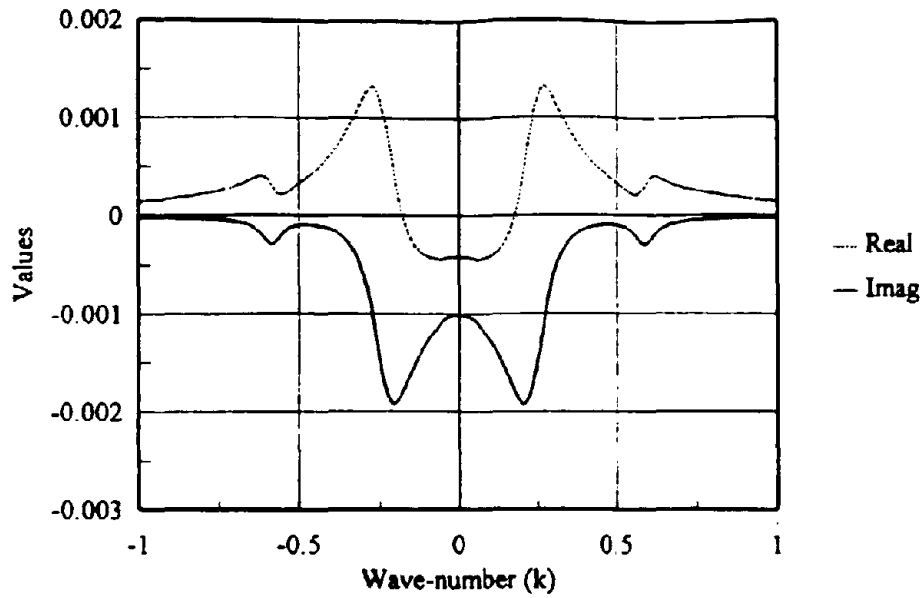


Figure 18. Diagonal Integrand of Submatrix [1-1] vs. Wave-number (k)

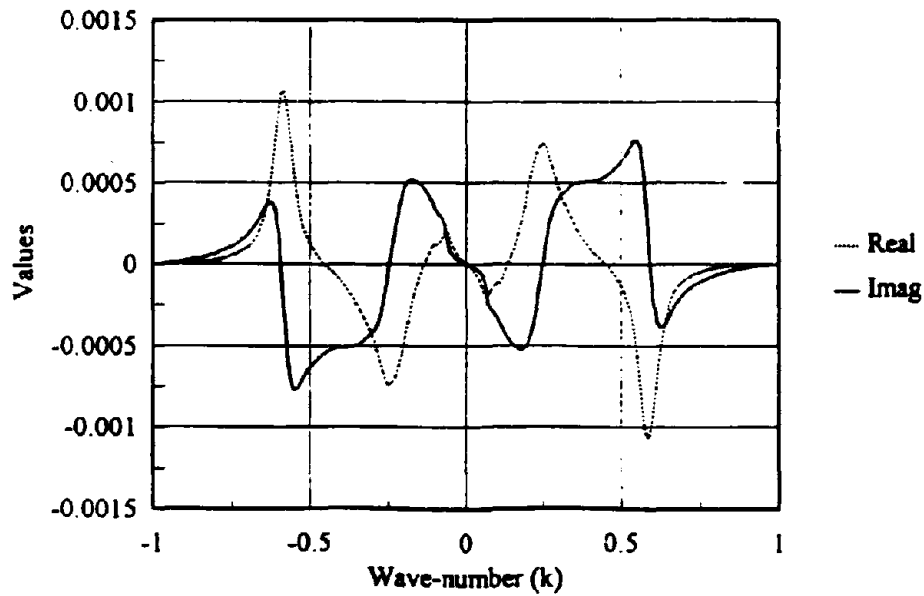


Figure 19. Off-diagonal Integrand of Submatrix [1-1] vs. Wave-number (k)

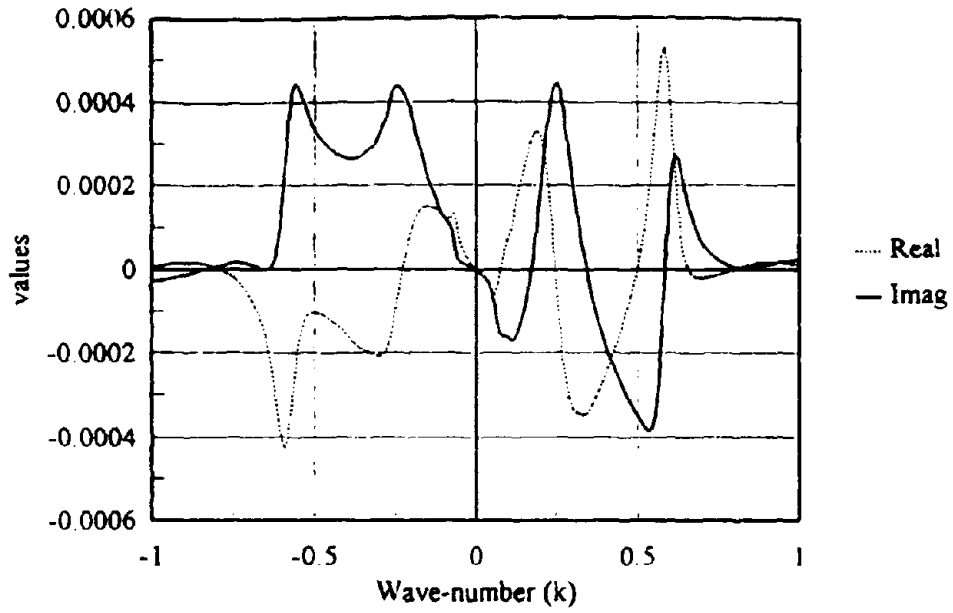


Figure 20. Diagonal Integrand of Submatrix [1-3] vs. Wave-number (k)

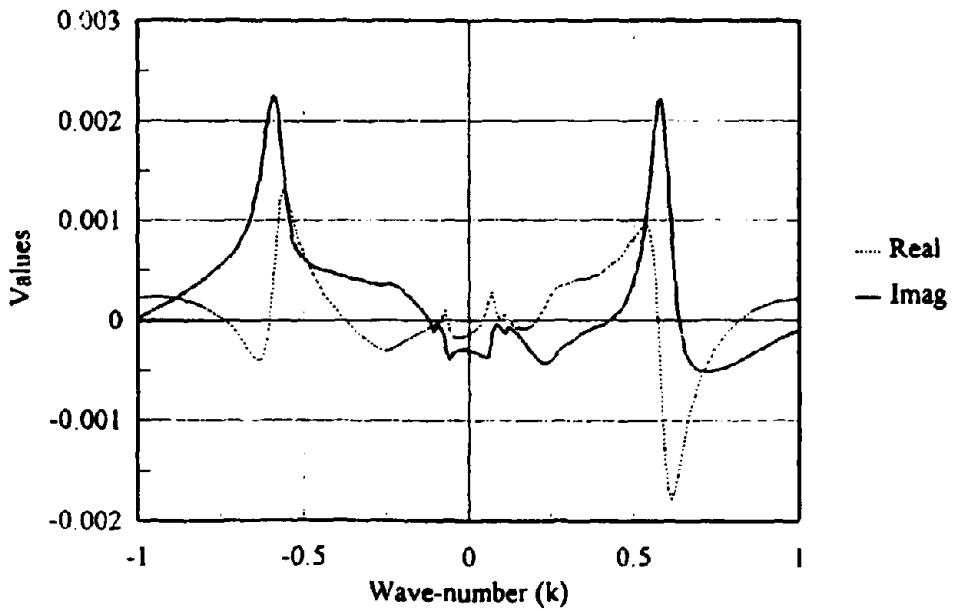


Figure 21. Off-diagonal Integrand of Submatrix [1-3] vs. Wave-number (k)

rigid interface is demonstrated in Figure 22. It defines amplitude of forces F_x^e, M_y^e, F_z^e due to unit amplitude of displacements x_0^e, θ_0^e, z_0^e applied at node 0 of the rigid interface as

$$\begin{Bmatrix} F_x^e \\ M_y^e \\ F_z^e \end{Bmatrix} = [S_{00}^e(\omega)] \begin{Bmatrix} x_0^e \\ \theta_0^e \\ z_0^e \end{Bmatrix} \quad (179)$$

with

$$[S_{00}^e(\omega)] = [K^e](1 + 2\zeta i) - \omega^2[M^e] \quad (180)$$

where $[K^e]$ and $[M^e]$ are the stiffness matrix and the mass matrix of the excavated part of the system, respectively. Symbols ζ and i represent the linear hysteretic damping ratio and $\sqrt{-1}$, respectively

As the excavated part of the system represents a bounded domain, the concept of the finite element method can be applied. First, the domain is discretized into elements connected to each other at nodal points. Determining and assembling the element dynamic-stiffness matrix leads to the dynamic-stiffness matrix corresponding to the degrees of freedom of all nodal points. Then the condensation process is needed to

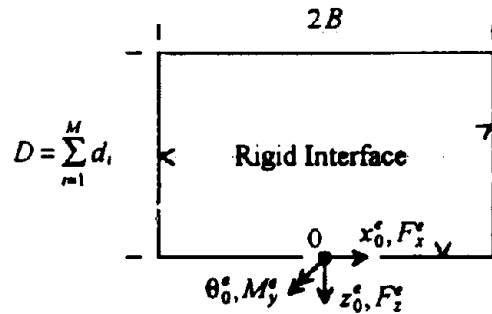


Figure 22. Forces and Displacements of Excavated Part of System with Rigid Interface

eliminate the degrees of freedom of the nodes not lying on the rigid interface. Finally, relating the degrees of freedom of the nodes along the interface to the rigid-body degrees of freedom at point 0 yields the desired dynamic-stiffness matrix.

As shown in Figure 23, depth D of the excavated domain is equally divided into Me portions, each of length d_e . And the domain's width at length $2B$ is evenly divided into $2Le$ portions, each of length b_e . This results in $2LeMe$ rectangular elements of dimension d_e by b_e , each having four nodal points.

Shown in the same figure, rectangular elements are numbered from 1 to $2LeMe$ starting from left to right and top to bottom. The nodes are categorized into two groups: nodes along the interfaces (subscript B) and nodes in the domain's interior, including those along the top boundary (subscript I). The former are numbered from 1 to $Me+1$, going from top to bottom of the vertical left interface, from $Me+1$ to $Me+2Le+1$ going from left

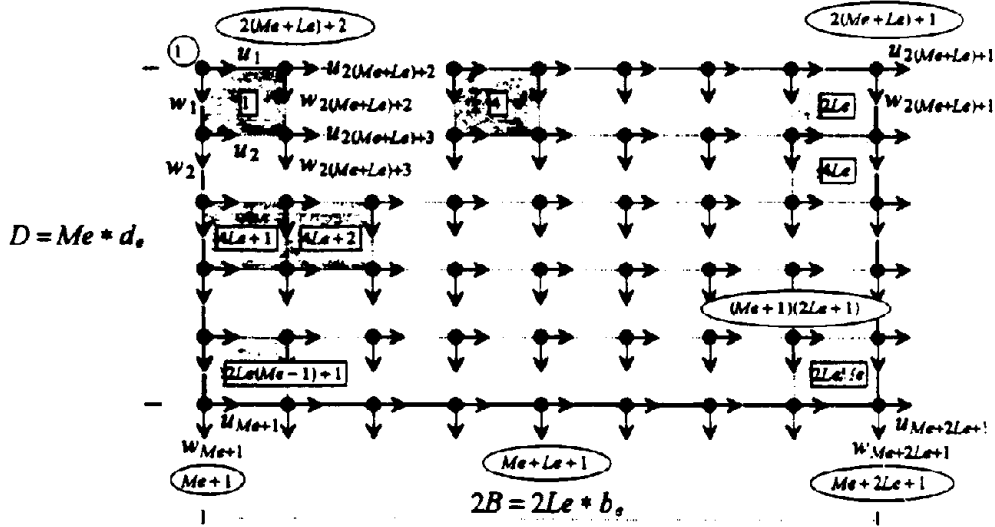


Figure 23. Discretization of Excavated Part of System

to right of the horizontal interface, and from $Me+2Le+1$ to $2(Me+Le)+1$ going from bottom to top of the vertical right interface. The latter are numbered from $2(Me+Le)+2$ to $(Me+1)(2Le+1)$ going from top to bottom and left to right for the interior.

The 8×8 dynamic-stiffness matrix $[\bar{S}^e(\omega)]_j$ of element j , where $j=1, \dots, 2LeMe$, can be obtained as

$$[\bar{S}^e(\omega)]_j = [\bar{K}^e]_j (1 + 2\zeta_j \tau) - \omega^2 [\bar{M}^e]_j \quad (181)$$

where $[\bar{K}^e]_j$ and $[\bar{M}^e]_j$ are the stiffness matrix and mass matrix of element j . They are discussed in the next two subsections (2 and 3).

In the standard assembling process, the element dynamic-stiffness matrices $[\bar{S}^e(\omega)]$ of adjacent discretizing elements are overlapped on the matrix's elements corresponding to the same nodes. The resulting matrix can be expressed as

$$\begin{Bmatrix} \{PR_B\} \\ \{PR_I\} \end{Bmatrix} = [S^e(\omega)] \begin{Bmatrix} \{uw_B\} \\ \{uw_I\} \end{Bmatrix} \quad (182)$$

with

$$\{PR_B\} = \begin{Bmatrix} P_1 \\ R_1 \\ \vdots \\ P_i \\ R_i \\ \vdots \\ P_{2(Me+Le)+1} \\ R_{2(Me+Le)+1} \end{Bmatrix} \quad \text{and} \quad \{PR_I\} = \begin{Bmatrix} P_{2(Me+Le)+2} \\ R_{2(Me+Le)+2} \\ \vdots \\ P_i \\ R_i \\ \vdots \\ P_{(Me+1)(2Le+1)} \\ R_{(Me+1)(2Le+1)} \end{Bmatrix} \quad (183)$$

$$[S^e(\omega)] = \begin{bmatrix} [\bar{S}_{BB}] & [\bar{S}_{BI}] \\ [\bar{S}_{IB}] & [\bar{S}_{II}] \end{bmatrix} \quad (184)$$

$$\{u w_B\} = \begin{Bmatrix} u_1 \\ w_1 \\ \vdots \\ u_i \\ w_i \\ \vdots \\ u_{2(Me+Le)+1} \\ w_{2(Me+Le)+1} \end{Bmatrix} \quad \text{and} \quad \{u w_I\} = \begin{Bmatrix} u_{2(Me+Le)+2} \\ w_{2(Me+Le)+2} \\ \vdots \\ u_i \\ w_i \\ \vdots \\ u_{(Me+1)(2Le+1)} \\ w_{(Me+1)(2Le+1)} \end{Bmatrix} \quad (185)$$

where P_i and R_i are the horizontal and vertical forces at node i , respectively. u_i and w_i are the horizontal and vertical displacements at node i , respectively. The dynamic-stiffness matrix $[S^e(\omega)]$ of dimension $2(Me+1)(2Le+1)$ by $2(Me+1)(2Le+1)$ consists of four submatrices, each corresponding to the degrees of freedom of subscripts' nodes. Subscript B indicates the nodes along the interfaces. Subscript I stands for the interior nodes, including those along the top boundary. Superscript e denotes the excavated part system.

Since no external forces act on the nodes in the interior ($\{PR_I\} = 0$), Equation (182) can be condensed and expressed as

$$\{PR_B\} = [S_{BB}^e(\omega)]\{u w_B\} \quad (186)$$

with

$$[S_{BB}^e(\omega)] = [\bar{S}_{BB}] - [\bar{S}_{BI}][\bar{S}_{II}]^{-1}[\bar{S}_{IB}] \quad (187)$$

where $[S_{BB}^e(\omega)]$ has a dimension of $4(Me+Le)+2$ by $4(Me+Le)+2$.

Since the interface is rigid, as shown in Figure 24, the degrees of freedom of the nodes along the interface relate to the rigid body degrees of freedom at point 0 as

$$\{uw_B\} = [A] \begin{Bmatrix} x_0^e \\ \theta_0^e \\ z_0^e \end{Bmatrix} \quad (188)$$

with

$$[A] = \begin{bmatrix} [A_1] \\ [A_2] \\ [A_3] \\ [A_4] \end{bmatrix} \quad (189)$$

where

$$[A_1] = \begin{bmatrix} \vdots & \vdots & \vdots \\ 1 & -\left(\sum_{n=1}^{Me} d_n\right) & 0 \\ 0 & B & 1 \\ \vdots & \vdots & \vdots \end{bmatrix} \quad \text{for node } i, i=1, \dots, Me \quad (190)$$

$$[A_2] = \begin{bmatrix} \vdots & \vdots & \vdots \\ 1 & 0 & 0 \\ 0 & \sum_{n=1}^{Me+Le} b_n & 1 \\ \vdots & \vdots & \vdots \end{bmatrix} \quad \text{for node } i, i=Me+1, \dots, Me+Le \quad (191)$$

$$[A_3] = \begin{bmatrix} \vdots & \vdots & \vdots \\ 1 & 0 & 0 \\ 0 & -\left(\sum_{n=Me+Le+1}^i b_n\right) + b_i & 1 \\ \vdots & \vdots & \vdots \end{bmatrix} \quad \text{for node } i, i=Me+Le+1, \dots, Me+2Le+1 \quad (192)$$

$$[A_4] = \begin{bmatrix} \vdots & \vdots & \vdots \\ 1 & -\left(\sum_{Me+2Le+2}^i d_e\right) & 0 \\ 0 & -B & 1 \\ \vdots & \vdots & \vdots \end{bmatrix} \text{ for node } i, i = Me+2Le+2, \dots, 2(Me+Le)+1 \quad (193)$$

Matrix $[A]$ of dimension $4(Me+Le)+2$ by 3 consists of 4 submatrices, $[A_1]$, $[A_2]$, $[A_3]$, and $[A_4]$. Matrix $[A_1]$, having a dimension of $2Me$ by 3 , corresponds to the degrees of freedom along the vertical left interface. Matrix $[A_2]$, having a dimension of $2Le$ by 3 , corresponds to the degrees of freedom along the left portion of the horizontal interface. Matrix $[A_3]$, having a dimension of $2Le+2$ by 3 , corresponds to the degrees of freedom along the right portion of the horizontal interface. Matrix $[A_4]$, having a dimension of $2Me$ by 3 , corresponds to the degrees of freedom along the vertical right interface. These submatrices can be determined by using geometric consideration in Figure 24. For example, the term $-\sum_{Me+2Le+2}^i d_e$ in Equation (193) relates a horizontal displacement at node

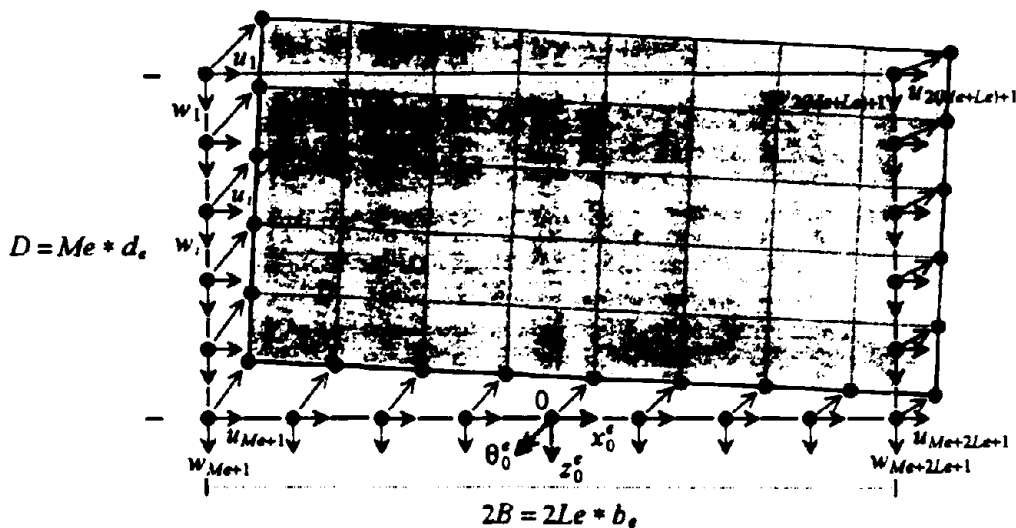


Figure 24. Rigid Body Degrees of Freedom of Excavated Part of System

i of the vertical right interface, u_i , to the rotation at point 0, θ_0^e . This term represents the negative distance from node i to the level of point 0 as the positive rotation results in the negative horizontal displacement at node i . The summation of d_e from $Me+2Le+2$ to i leads to the distance from the level of point 0 to the node i .

Using matrix $[A]$ in Equation (188) and its transposed form in Equation (186), the dynamic-stiffness matrix of the excavated part of the system with rigid interface can be expressed as

$$\begin{Bmatrix} F_x^e \\ M_y^e \\ F_z^e \end{Bmatrix} = [S_{00}^e(\omega)] \begin{Bmatrix} x_0^e \\ \theta_0^e \\ z_0^e \end{Bmatrix} \quad (194)$$

where

$$[S_{00}^e(\omega)] = [A]^T [S_{BB}^e(\omega)] [A] \quad (195)$$

and

$$\begin{Bmatrix} F_x^e \\ M_y^e \\ F_z^e \end{Bmatrix} = [A]^T \{PR_B\} \quad (196)$$

2. Element Stiffness Matrix. The local coordinate and node numbering system of a four-node rectangular element is shown in Figure 25. The element has lengths b_e and d_e along x - and z -axis, respectively. For a plane elastic problem, the element has eight degrees of freedom, two degrees of freedom on each node.

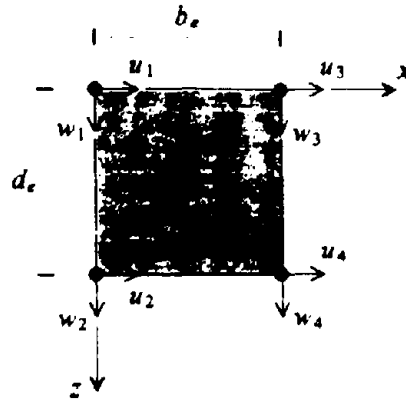


Figure 25. Four-node Rectangular Element

Therefore the displacement pattern can be represented by eight unknown coefficients of the polynomial as

$$u(x, z) = \alpha_1 + \alpha_2 x + \alpha_3 z + \alpha_4 xz \quad (197)$$

$$w(x, z) = \alpha_5 + \alpha_6 x + \alpha_7 z + \alpha_8 xz \quad (198)$$

Substituting the values of nodal coordinates in Equations (197), (198) and then solving for $\{\alpha\}$, displacement shape functions can be expressed in terms of nodal displacements as

$$\begin{Bmatrix} u(x, z) \\ w(x, z) \end{Bmatrix} = [\bar{N}(x, z)] \begin{Bmatrix} u_1 \\ w_1 \\ \vdots \\ u_2 \\ w_2 \\ \vdots \\ u_3 \\ w_3 \\ \vdots \\ u_4 \\ w_4 \end{Bmatrix} \quad (199)$$

with

$$[\bar{N}(x, z)] = \begin{bmatrix} \bar{N}_{(1,1)} & 0 & \bar{N}_{(1,3)} & 0 & \bar{N}_{(1,5)} & 0 & \bar{N}_{(1,7)} & 0 \\ 0 & \bar{N}_{(2,2)} & 0 & \bar{N}_{(2,4)} & 0 & \bar{N}_{(2,6)} & 0 & \bar{N}_{(2,8)} \end{bmatrix} \quad (200)$$

where

$$\bar{N}_{(1,1)} = \bar{N}_{(2,2)} = 1 - \frac{x}{b_e} - \frac{z}{d_e} + \frac{xz}{b_e d_e} \quad (201)$$

$$\bar{N}_{(1,3)} = \bar{N}_{(2,4)} = \frac{z}{d_e} - \frac{xz}{b_e d_e} \quad (202)$$

$$\bar{N}_{(1,5)} = \bar{N}_{(2,6)} = \frac{x}{b_e} - \frac{xz}{b_e d_e} \quad (203)$$

$$\bar{N}_{(1,7)} = \bar{N}_{(2,8)} = \frac{xz}{b_e d_e} \quad (204)$$

The strain-displacement relationship can be expressed as

$$\varepsilon_x = u_{,x}(x, z) \quad (205)$$

$$\varepsilon_z = w_{,z}(x, z) \quad (206)$$

$$\gamma_{xz} = \gamma_{zx} = u_{,z}(x, z) + w_{,x}(x, z) \quad (207)$$

where the normal strain and shear strain amplitudes are denoted by ε and γ , respectively.

The first subscript denotes the direction of the strain component. The second denotes the direction of the infinitesimal area's normal where the strain component is. A comma denotes a partial derivative with respect to the subscript following it.

Using Equation (199), the strains in Equations (205) through (207) can be expressed in terms of nodal displacements as

$$\begin{Bmatrix} \epsilon_x(x, z) \\ \epsilon_z(x, z) \\ \gamma_{xz}(x, z) \end{Bmatrix} = [\bar{B}(x, z)] \begin{Bmatrix} u_1 \\ w_1 \\ \vdots \\ u_i \\ w_i \\ \vdots \\ u_4 \\ w_4 \end{Bmatrix} \quad (208)$$

with

$$[\bar{B}(x, z)] = \begin{bmatrix} \bar{B}_{(1,1)} & 0 & \bar{B}_{(1,3)} & 0 & \bar{B}_{(1,5)} & 0 & \bar{B}_{(1,7)} & 0 \\ 0 & \bar{B}_{(2,2)} & 0 & \bar{B}_{(2,4)} & 0 & \bar{B}_{(2,6)} & 0 & \bar{B}_{(2,8)} \\ \bar{B}_{(3,1)} & \bar{B}_{(3,2)} & \bar{B}_{(3,3)} & \bar{B}_{(3,4)} & \bar{B}_{(3,5)} & \bar{B}_{(3,6)} & \bar{B}_{(3,7)} & \bar{B}_{(3,8)} \end{bmatrix} \quad (209)$$

where

$$\bar{B}_{(1,1)} = \bar{B}_{(3,2)} = -\bar{B}_{(1,5)} = -\bar{B}_{(3,6)} = \frac{-1}{b_e} + \frac{z}{b_e d_e} \quad (210)$$

$$\bar{B}_{(1,3)} = \bar{B}_{(3,4)} = -\bar{B}_{(1,7)} = -\bar{B}_{(3,8)} = \frac{-z}{b_e d_e} \quad (211)$$

$$\bar{B}_{(2,2)} = \bar{B}_{(3,1)} = -\bar{B}_{(2,4)} = -\bar{B}_{(3,3)} = \frac{-1}{d_e} + \frac{x}{b_e d_e} \quad (212)$$

$$\bar{B}_{(2,6)} = \bar{B}_{(3,5)} = -\bar{B}_{(2,8)} = -\bar{B}_{(3,7)} = \frac{-x}{b_e d_e} \quad (213)$$

Normal stress and shear stress amplitudes σ , τ can be obtained in terms of normal strain and shear strain amplitudes ϵ , γ in matrix form as

$$\begin{Bmatrix} \sigma_x \\ \sigma_z \\ \tau_{xz} \end{Bmatrix} = [\bar{D}] \begin{Bmatrix} \epsilon_x \\ \epsilon_z \\ \gamma_{xz} \end{Bmatrix} \quad (214)$$

with

$$[\bar{D}] = \begin{bmatrix} 2\Upsilon + \lambda & \lambda & 0 \\ \lambda & 2\Upsilon + \lambda & 0 \\ 0 & 0 & \Upsilon \end{bmatrix} \quad (215)$$

where

$$\text{the shear modulus of elasticity } \Upsilon = \frac{E}{2(1+\nu)} \quad (216)$$

$$\text{the Lamé constant } \lambda = \frac{\nu E}{(1+\nu)(1-2\nu)} \quad (217)$$

and the letter E represents Young's modulus of elasticity. The symbol ν represents Poisson's ratio.

By using Equations (208) and (214) and applying the principle of virtual work, nodal forces relate to the nodal displacements in terms of the symmetrical element stiffness matrix as

$$\begin{Bmatrix} P_1 \\ R_1 \\ \vdots \\ P_i \\ R_i \\ \vdots \\ P_4 \\ R_4 \end{Bmatrix} = [K^e]_j \begin{Bmatrix} u_1 \\ w_1 \\ \vdots \\ u_i \\ w_i \\ \vdots \\ u_4 \\ w_4 \end{Bmatrix} \quad (218)$$

with

$$[\bar{K}^*]_j = \int_0^{d_e} \int_0^{b_e} [\bar{B}(x, z)]^T [\bar{D}]_j [\bar{B}(x, z)] dx dz$$

$$= \begin{bmatrix} \bar{K}_{(1,1)}^* & \bar{K}_{(1,2)}^* & \bar{K}_{(1,3)}^* & \bar{K}_{(1,4)}^* & \bar{K}_{(1,5)}^* & \bar{K}_{(1,6)}^* & \bar{K}_{(1,7)}^* & \bar{K}_{(1,8)}^* \\ \vdots & \bar{K}_{(2,2)}^* & \bar{K}_{(2,3)}^* & \bar{K}_{(2,4)}^* & \bar{K}_{(2,5)}^* & \bar{K}_{(2,6)}^* & \bar{K}_{(2,7)}^* & \bar{K}_{(2,8)}^* \\ \vdots & \vdots & \bar{K}_{(3,3)}^* & \bar{K}_{(3,4)}^* & \bar{K}_{(3,5)}^* & \bar{K}_{(3,6)}^* & \bar{K}_{(3,7)}^* & \bar{K}_{(3,8)}^* \\ \vdots & \vdots & \vdots & \bar{K}_{(4,4)}^* & \bar{K}_{(4,5)}^* & \bar{K}_{(4,6)}^* & \bar{K}_{(4,7)}^* & \bar{K}_{(4,8)}^* \\ \vdots & \vdots & \vdots & \vdots & \bar{K}_{(5,5)}^* & \bar{K}_{(5,6)}^* & \bar{K}_{(5,7)}^* & \bar{K}_{(5,8)}^* \\ \vdots & \vdots & \vdots & \vdots & \vdots & \bar{K}_{(6,6)}^* & \bar{K}_{(6,7)}^* & \bar{K}_{(6,8)}^* \\ \vdots & \vdots & \vdots & \vdots & \vdots & \vdots & \bar{K}_{(7,7)}^* & \bar{K}_{(7,8)}^* \\ \vdots & \vdots & \vdots & \vdots & \vdots & \vdots & \vdots & \bar{K}_{(8,8)}^* \end{bmatrix} \quad (219)$$

where

$$\bar{K}_{(1,1)}^* = \bar{K}_{(3,3)}^* = \bar{K}_{(5,5)}^* = \bar{K}_{(7,7)}^* = \frac{1}{3} \left[(2\Upsilon_j + \lambda_j) \frac{d_e}{b_e} + \Upsilon_j \frac{b_e}{d_e} \right] \quad (220)$$

$$\bar{K}_{(2,2)}^* = \bar{K}_{(4,4)}^* = \bar{K}_{(6,6)}^* = \bar{K}_{(8,8)}^* = \frac{1}{3} \left[(2\Upsilon_j + \lambda_j) \frac{b_e}{d_e} + \Upsilon_j \frac{d_e}{b_e} \right] \quad (221)$$

$$\bar{K}_{(1,2)}^* = \bar{K}_{(3,6)}^* = \bar{K}_{(4,5)}^* = \bar{K}_{(7,8)}^* = \frac{1}{4} (\Upsilon_j + \lambda_j) \quad (222)$$

$$\bar{K}_{(1,8)}^* = \bar{K}_{(2,7)}^* = \bar{K}_{(3,4)}^* = \bar{K}_{(5,6)}^* = \frac{-1}{4} (\Upsilon_j + \lambda_j) \quad (223)$$

$$\bar{K}_{(1,6)}^* = \bar{K}_{(2,3)}^* = \bar{K}_{(4,7)}^* = \bar{K}_{(5,8)}^* = \frac{1}{4} (\lambda_j - \Upsilon_j) \quad (224)$$

$$\bar{K}_{(1,4)}^* = \bar{K}_{(2,5)}^* = \bar{K}_{(3,8)}^* = \bar{K}_{(6,7)}^* = \frac{-1}{4} (\lambda_j - \Upsilon_j) \quad (225)$$

$$\bar{K}_{(1,3)}^* = \bar{K}_{(5,7)}^* = \frac{1}{6} \left[(2\Upsilon_j + \lambda_j) \frac{d_e}{b_e} - 2\Upsilon_j \frac{b_e}{d_e} \right] \quad (226)$$

$$\bar{K}_{(2,6)}^* = \bar{K}_{(4,8)}^* = \frac{1}{6} \left[(2\Upsilon_j + \lambda_j) \frac{b_e}{d_e} - 2\Upsilon_j \frac{d_e}{b_e} \right] \quad (227)$$

$$\bar{K}_{(2,4)}^e = \bar{K}_{(6,8)}^e = \frac{-1}{6} \left[2(2\gamma_j + \lambda_j) \frac{b_e}{d_e} - \gamma_j \frac{d_e}{b_e} \right] \quad (228)$$

$$\bar{K}_{(1,5)}^e = \bar{K}_{(3,7)}^e = \frac{-1}{6} \left[2(2\gamma_j + \lambda_j) \frac{d_e}{b_e} - \gamma_j \frac{b_e}{d_e} \right] \quad (229)$$

$$\bar{K}_{(1,7)}^e = \bar{K}_{(3,5)}^e = \frac{-1}{6} \left[(2\gamma_j + \lambda_j) \frac{d_e}{b_e} + \gamma_j \frac{b_e}{d_e} \right] \quad (230)$$

$$\bar{K}_{(2,8)}^e = \bar{K}_{(4,6)}^e = \frac{-1}{6} \left[(2\gamma_j + \lambda_j) \frac{b_e}{d_e} + \gamma_j \frac{d_e}{b_e} \right] \quad (231)$$

3. **Element Mass Matrix.** Instead of using lumped mass at each node, consistent mass is considered. The mass of element j distributed to each degree of freedom can be defined as

$$[\bar{M}^e]_j = \int_0^{d_e} \int_0^{b_e} \rho_j [\bar{N}(x, z)]^T [\bar{N}(x, z)] dx dz \quad (232)$$

Inserting Equation (200) into Equation (232) results in the symmetrical element mass matrix as

$$[\bar{M}^e]_j = \rho_j b_e d_e \begin{bmatrix} 1/9 & 0 & 1/18 & 0 & 1/18 & 0 & 1/36 & 0 \\ \vdots & 1/9 & 0 & 1/18 & 0 & 1/18 & 0 & 1/36 \\ \vdots & \vdots & 1/9 & 0 & 1/36 & 0 & 1/18 & 0 \\ \vdots & \vdots & \vdots & 1/9 & 0 & 1/36 & 0 & 1/18 \\ \vdots & \vdots & \vdots & \vdots & 1/9 & 0 & 1/18 & 0 \\ \vdots & \vdots & \vdots & \vdots & \vdots & 1/9 & 0 & 1/18 \\ \vdots & \vdots & \vdots & \vdots & \vdots & \vdots & 1/9 & 0 \\ \vdots & \vdots & \vdots & \vdots & \vdots & \vdots & \vdots & 1/9 \end{bmatrix} \quad (233)$$

C. GROUND SYSTEM'S STIFFNESS AND FLEXIBILITY MATRICES

1. **Dynamic Stiffness Matrix.** In Figure 26, the dynamic-stiffness matrix $[S_{00}^g(\omega)]$ of the unbounded ground system with rigid interface is depicted. It specifies the amplitude of forces F_x^g, M_y^g, F_z^g due to unit amplitude of displacements x_0^g, θ_0^g, z_0^g applied at node 0. These forces, for harmonic motion with excitation frequency ω , are expressed as

$$\begin{Bmatrix} F_x^g \\ M_y^g \\ F_z^g \end{Bmatrix} = [S_{00}^g(\omega)] \begin{Bmatrix} x_0^g \\ \theta_0^g \\ z_0^g \end{Bmatrix} \quad (234)$$

with

$$[S_{00}^g(\omega)] = \begin{bmatrix} S_{xx}^g & S_{x\theta}^g & 0 \\ S_{\theta x}^g & S_{\theta\theta}^g & 0 \\ 0 & 0 & S_{zz}^g \end{bmatrix} \quad (235)$$

where ground system coefficients $S_{xx}^g, S_{x\theta}^g, S_{\theta x}^g, S_{\theta\theta}^g$, and S_{zz}^g are forces corresponding to the first subscript's degree of freedom due to a unit displacement excitation corresponding to the second subscript's degree of freedom. Since the soil domain is assumed to be a linear system, the law of superposition is valid. Thus the dynamic-stiffness matrix of the ground system can be obtained by subtracting that of the excavated part of the system (195) from that of the free-field system (129) as

$$[S_{00}^g(\omega)] = [S_{00}^f(\omega)] - [S_{00}^e(\omega)] \quad (236)$$

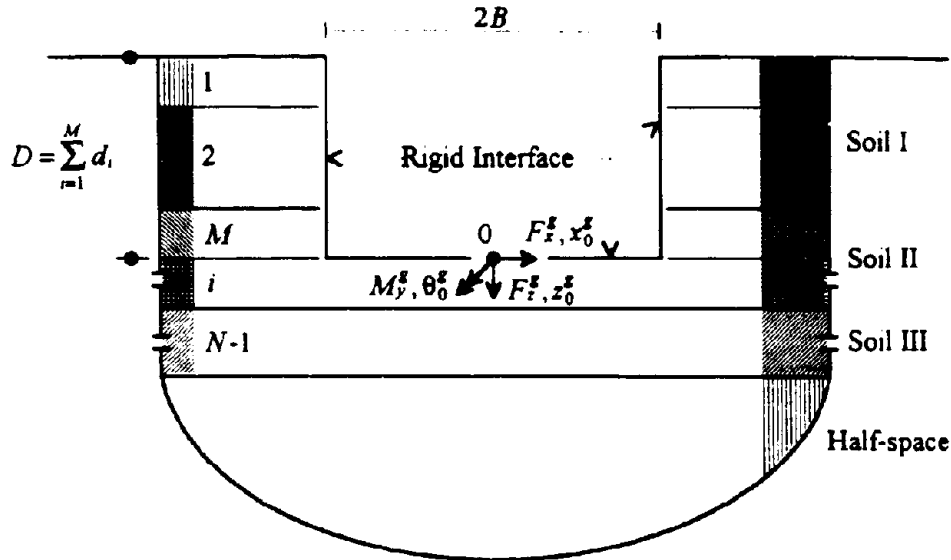


Figure 26. Forces and Displacements of Ground System with Rigid Interface

Near the natural frequency of the system's excavated part, that system's dynamic-stiffness coefficients as well as the free-field system's will be large. Since the dynamic-stiffness coefficients of the ground system involve two large numbers obtained from two different methods, a number of discretizing elements must be chosen carefully in this vicinity.

2. **Time-derivative Dynamic Flexibility Matrix.** Since harmonic motion is represented as $\exp(i\omega t)$, the ground system's force-displacement relationship in Equation (234) can also be written as

$$\exp(i\omega t) \begin{Bmatrix} F_x^e \\ M_y^e \\ F_z^e \end{Bmatrix} = \exp(i\omega t) [S_{00}^e(\omega)] \begin{Bmatrix} x_0^e \\ \theta_0^e \\ z_0^e \end{Bmatrix} \quad (237)$$

where i and t represent $\sqrt{-1}$ and time variable, respectively.

Dynamic-flexibility matrix is the inverse form of dynamic-stiffness matrix. In the case of a ground system with rigid interface (see Figure 26), the dynamic-flexibility matrix specifies amplitude of displacements x_0^g, θ_0^g, z_0^g due to unit amplitude of forces F_x^g, M_y^g, F_z^g applied at node 0 of the rigid interface for harmonic motion with excitation frequency ω . This relationship can be expressed as

$$\exp(i\omega t) \begin{Bmatrix} x_0^g \\ \theta_0^g \\ z_0^g \end{Bmatrix} = \exp(i\omega t) [F_{00}^g(\omega)] \begin{Bmatrix} F_x^g \\ M_y^g \\ F_z^g \end{Bmatrix} \quad (238)$$

with

$$[F_{00}^g(\omega)] = [S_{00}^g(\omega)]^{-1} \quad (239)$$

where $[F_{00}^g(\omega)]$ of dimension 3 by 3 is dynamic-flexibility matrix of ground system with rigid interface for harmonic motion with excitation frequency ω .

Differentiating the displacement-force Equation (238) with respect to time, and omitting term $\exp(i\omega t)$, results in a velocity-force relationship of ground system in harmonic motion as

$$\begin{Bmatrix} \dot{x}_0^g \\ \dot{\theta}_0^g \\ \dot{z}_0^g \end{Bmatrix} = [F_{00}^g(\omega)] \begin{Bmatrix} F_x^g \\ M_y^g \\ F_z^g \end{Bmatrix} \quad (240)$$

where $[F_{00}^g(\omega)]$ is a symbolic form, not a derivative, representing the so-called time-derivative dynamic flexibility matrix of ground system as shown later in Equation (242).

$$\begin{Bmatrix} \dot{x}_0^g \\ \dot{\theta}_0^g \\ \dot{z}_0^g \end{Bmatrix} = i\omega \begin{Bmatrix} x_0^g \\ \theta_0^g \\ z_0^g \end{Bmatrix} \quad (241)$$

$$\begin{aligned} [F_{00}^g(\omega)] &= i\omega[F_{00}^g(\omega)] = i\omega[S_{00}^g(\omega)]^{-1} \\ &= \begin{bmatrix} \dot{F}_{xx}^g & \dot{F}_{x\theta}^g & 0 \\ \dot{F}_{\theta x}^g & \dot{F}_{\theta\theta}^g & 0 \\ 0 & 0 & \dot{F}_{zz}^g \end{bmatrix} \end{aligned} \quad (242)$$

where $[F_{00}^g(\omega)]$ of dimension 3 by 3 specifies amplitude of velocities $\dot{x}_0^g, \dot{\theta}_0^g, \dot{z}_0^g$ due to unit amplitude of forces F_x^g, M_y^g, F_z^g applied at node 0 of the rigid interface for harmonic motion with excitation frequency ω .

3. **Impulse Velocity Matrix.** At node 0 of the rigid interface, the amplitude of velocities $\dot{x}_0^g, \dot{\theta}_0^g, \dot{z}_0^g$ at time t and a series of amplitudes of impulse forces F_x^g, M_y^g, F_z^g are related to impulse velocity matrix of ground system with rigid interface by convolution integral as

$$\begin{Bmatrix} \dot{x}_0^g(t) \\ \dot{\theta}_0^g(t) \\ \dot{z}_0^g(t) \end{Bmatrix} = \int_{-\infty}^{\infty} [F_{00}^g(\tau)] \begin{Bmatrix} F_x^g(t-\tau) \\ M_y^g(t-\tau) \\ F_z^g(t-\tau) \end{Bmatrix} d\tau \quad (243)$$

with

$$[F_{00}^g(\tau)] = \begin{bmatrix} \dot{F}_{xx}^g & \dot{F}_{x\theta}^g & 0 \\ \dot{F}_{\theta x}^g & \dot{F}_{\theta\theta}^g & 0 \\ 0 & 0 & \dot{F}_{zz}^g \end{bmatrix} \quad (244)$$

where $[F_{00}^g]$ is impulse velocity matrix of ground system with rigid interface. Coefficients $\dot{F}_{xx}^g, \dot{F}_{x\theta}^g, \dot{F}_{\theta x}^g, \dot{F}_{\theta\theta}^g,$ and \dot{F}_{zz}^g are velocities, at time τ , corresponding to the first subscript's

degree of freedom due to a unit impulse force, at time equal to zero, corresponding to the second subscript's degree of freedom. Clearly, these coefficients are time-dependent causal functions.

This impulse velocity matrix $[\dot{F}_{00}^g(t)]$ can be obtained by the inverse Fourier transformation of the ground system's time-derivative dynamic flexibility matrix $[F_{00}^g(\omega)]$ in Equation (242) as

$$[\dot{F}_{00}^g(t)] = \frac{1}{2\pi} \int_{-\infty}^{\infty} [F_{00}^g(\omega)] \exp(i\omega t) d\omega \quad (245)$$

where i and π equal to $\sqrt{-1}$ and pi number, respectively.

Since the soil system's dynamic-stiffness matrices and thus the time-derivative dynamic flexibility matrix used in Equation (245) are obtained in discrete-frequency domain, the discrete version of inverse Fourier transform applies as

$$[\dot{F}_{00}^g(n\Delta t)] = \frac{\Delta\omega}{2\pi} \sum_{m=1-NS}^{NS} [F_{00}^g(m\Delta\omega)] \exp(i m\Delta\omega n\Delta t) \quad (246)$$

where Δt and n are time increment and time-instant number, respectively. $\Delta\omega$ and m are frequency increment and frequency number, respectively. NS is a number of sampling steps where $(NS)\Delta\omega$ and $(NS)\Delta t$ equal a truncated frequency Ω_T and time range T_F of impulse velocity function, respectively.

In the discrete version, the time-derivative dynamic flexibility functions $F_{zz}^g(\omega)$, $F_{x0}^g(\omega)$, $F_{0z}^g(\omega)$, $F_{00}^g(\omega)$, $F_{zz}^g(\omega)$ in Equation (242), non-periodic ones, are truncated at an arbitrary frequency. This truncated frequency Ω_T must include all predominant

frequencies of total dynamic system, ground system, and incident waves. As a result of the truncation, band-limited functions, having a frequency range from $-\Omega_T$ to Ω_T , are formed. Then periodic extensions of these band-limited functions, required by the form of Equation (246), are used in the transformation. Therefore, only within time range $[-T_F, T_F]$, is the discrete version in Equation (246) similar to the continuous version in Equation (245).

Truncated frequency Ω_T dictates a size of time increment Δt . Size of frequency increment $\Delta\omega$ depends upon a number of sampling steps, NS . Their relationship can be expressed as

$$\Delta t = \frac{\pi}{\Omega_T} = \frac{\pi}{(NS)\Delta\omega} \quad (247)$$

and

$$\Delta\omega = \frac{\Omega_T}{NS} = \frac{\pi}{(NS)\Delta t} = \frac{\pi}{T_F} \quad (248)$$

According to Equation (247), if truncated frequency Ω_T is too small (not including all predominant frequencies), time increment Δt will be too large for discrete representation of the continuous functions of the entire dynamic system's response, impulse velocity, and earthquake excitation. Since impulse velocity functions attenuate as time goes on and the discrete version's precision is only within a time range $[-T_F, T_F]$ where $T_F = (NS)\Delta t$, this time range must cover all significant ranges of impulse velocity functions and beyond. (From a practical point of view, T_F should double the significant limit of impulse velocity functions to guarantee causality condition). Therefore the

number of sampling steps, NS , needs to be large enough to cover these ranges. According to Equation (248), NS must also be large enough to make frequency increment $\Delta\omega$ small enough for discrete representation of the continuous band-limited functions of time-derivative flexibility functions $\dot{F}_{xx}^g(\omega), \dot{F}_{x\theta}^g(\omega), \dot{F}_{\theta x}^g(\omega), \dot{F}_{\theta\theta}^g(\omega), \dot{F}_{\ddot{x}}^g(\omega)$

Band-limited sequence of the time-derivative flexibility matrix $[F_{00}^g(m\Delta\omega)]$, from frequency $-(NS-1)\Delta\omega$ to $(NS)\Delta\omega$, is used for the transformation in Equation (246). Knowing that the time-derivative flexibility pair corresponding to a positive-negative frequency pair is complex conjugate, the band-limited sequence can be constructed from a given sequence along the positive half of the frequency range. This complex conjugate relationship can be proved by substituting a positive-negative frequency pair in the discrete Fourier transform formula for a causal function. This formula describes time-derivative flexibility matrix as

$$[F_{00}^g(m\Delta\omega)] = \Delta t \sum_{n=0}^{NS} [\dot{F}_{00}^g(n\Delta t)] \exp(-i m \Delta\omega n \Delta t) \quad (249)$$

Substituting $m = l$

$$\begin{aligned} [\dot{F}_{00}^g(l\Delta\omega)] &= \Delta t \sum_{n=0}^{NS} [\dot{F}_{00}^g(n\Delta t)] \exp(-i l \Delta\omega n \Delta t) \\ &= \cos(l \Delta\omega n \Delta t) \Delta t \sum_{n=0}^{NS} [\dot{F}_{00}^g(n\Delta t)] \\ &\quad -i \sin(l \Delta\omega n \Delta t) \Delta t \sum_{n=0}^{NS} [F_{00}^g(n\Delta t)] \end{aligned} \quad (250)$$

Substituting $m = -l$

$$\begin{aligned}
 [F_{00}^g(-l\Delta\omega)] &= \Delta t \sum_{n=0}^{NS} [F_{00}^g(n\Delta t)] \exp(i l \Delta\omega n \Delta t) \\
 &= \cos(l \Delta\omega n \Delta t) \Delta t \sum_{n=0}^{NS} [F_{00}^g(n\Delta t)] \\
 &\quad + i \sin(l \Delta\omega n \Delta t) \Delta t \sum_{n=0}^{NS} [F_{00}^g(n\Delta t)]
 \end{aligned} \tag{251}$$

Equations (250) and (251) always form a complex conjugate pair because signs of their imaginary part are opposite for any integer l .

Phase angle of impulse velocity responses is assumed to be either 0° or 180° .

Impulse velocity functions $\dot{F}_{xx}^g(t)$, $\dot{F}_{x\theta}^g(t)$, $\dot{F}_{\theta x}^g(t)$, $\dot{F}_{\theta\theta}^g(t)$, $\dot{F}_{zz}^g(t)$ are then assumed to be real number. Therefore the following properties are applied.

1. Impulse velocity function $\dot{F}(t)$ can be expressed as the sum of an even part $\dot{F}_e(t)$ and an odd part $\dot{F}_o(t)$.

$$\dot{F}(t) = \dot{F}_e(t) + \dot{F}_o(t) \tag{252}$$

2. The even part $\dot{F}_e(t)$, or conjugate-symmetric one, can be obtained by inverse Fourier transform of the real part of time-derivative flexibility $\dot{F}(\omega)$. If the even part is defined as

$$\dot{F}_e(t) = \dot{F}_e(-t) \quad \text{and} \quad \dot{F}_e(0) = \dot{F}(0) \tag{253}$$

then

$$F_e(t) = \frac{1}{2\pi} \int_{-\infty}^{\infty} \text{Real}(\dot{F}(\omega)) \exp(i\omega t) d\omega \quad (254)$$

3. The odd part $\dot{F}_o(t)$, or conjugate-antisymmetric one, can be obtained by inverse Fourier transform of the imaginary part of time-derivative flexibility $\dot{F}(\omega)$. If the odd part is defined as

$$\dot{F}_o(t) = -\dot{F}_o(-t) \text{ and } \dot{F}_o(0) = 0 \quad (255)$$

then

$$\dot{F}_o(t) = \frac{1}{2\pi} \int_{-\infty}^{\infty} \text{Imag}(\dot{F}(\omega)) \exp(i\omega t) d\omega \quad (256)$$

Impulse velocity function $\dot{F}(t)$ is causal (amplitude of function equals zero for time $t < 0$). Therefore, for $t < 0$, the summation of even and odd parts must be zero. Their relationship can be expressed as

$$\dot{F}_e(t) = -\dot{F}_o(t) \quad \text{for time } t < 0 \quad (257)$$

Using Equations (252), (253), and (255) and the causality condition in Equation (257), impulse velocity function can be expressed in terms of either an even part or an odd part as

$$\dot{F}(t) = 2\dot{F}_e(t)U(t) - \dot{F}_e(0)\delta(t) \quad (258)$$

and

$$\dot{F}(t) = 2\dot{F}_o(t)U(t) + \dot{F}_o(0)\delta(t) \quad (259)$$

where $U(t)$ is a unit step function in the interval of time t greater than or equal to zero. $\delta(t)$ is the Dirac-delta function equal to 1 at time t equal to zero. It should be noted that impulse velocity function $\dot{F}(t)$, for $t=0$, cannot be determined by using the odd part alone [see Equation (259)].

Therefore, by using Equations (254) and (258), impulse velocity function $\dot{F}(t)$ can be determined by using only the real part of $F(\omega)$ as

$$\dot{F}(0) = \frac{1}{2\pi} \int_{-\infty}^{\infty} \text{Real}(F(\omega)) d\omega \quad \text{for time } t = 0 \quad (260)$$

and

$$\dot{F}(t) = \frac{1}{\pi} \int_{-\infty}^{\infty} \text{Real}(F(\omega)) \exp(i\omega t) d\omega \quad \text{for time } t > 0 \quad (261)$$

For a ground system with rigid interface, discrete impulse velocity matrix can be obtained by applying the discrete version of transformation [Equation (246)] and its complex conjugate property [demonstrated in Equations (250) and (251)] to Equations (260) and (261) as

$$\begin{aligned} [\dot{F}_{00}^g(0)] &= \frac{\Delta\omega}{2\pi} \sum_{m=1-N_S}^{N_S} \text{Real}([\dot{F}_{00}^g(m\Delta\omega)]) \\ &= \frac{\Delta\omega}{\pi} \sum_{m=1}^{N_S-1} \text{Real}([\dot{F}_{00}^g(m\Delta\omega)]) + \frac{\Delta\omega}{2\pi} \text{Real}([\dot{F}_{00}^g(\Omega_T)]) \end{aligned} \quad (262)$$

and

$$[F_{00}^g(n\Delta t)] = \frac{\Delta\omega}{\pi} \sum_{m=1-NS}^{NS} \text{Real}([F_{00}^g(m\Delta\omega)]) \exp(i m \Delta\omega n \Delta t)$$

for $n = 1, 2, \dots, NS$ (263)

Note that the static components of the ground system's time-derivative flexibility matrix $[F_{00}^g(\omega = 0)]$ always equal zero [see Equation (242)]. Therefore those of ground system's stiffness matrix need not to be determined. Only the dynamic-stiffness matrices on the positive half of frequency range are needed due to their complex conjugate property. To minimize computing time, Fast Fourier Transform (FFT), an efficient technique of calculating discrete Fourier transform, is employed.

VI. INVESTIGATION OF DYNAMIC STIFFNESS COEFFICIENTS OF SOIL SYSTEMS

A. SCOPE OF INVESTIGATION

1. **Study Parameters and Actual Site Data.** To investigate the influence of soil hysteretic damping, foundation embedment D , and the depth of a soil layer on the rock bed on the dynamic-stiffness matrix, a half-plane and a homogeneous layer with depth H built on the rock are examined by using Poisson's ratio of 0.33. The undamped case and the cases of 0.03, 0.05, and 0.07 damping ratio ζ are investigated. The ratio of embedment to foundation half-width, D/B , and the ratio of layer's depth to foundation half-width, H/B , are varied parametrically.

In addition to the parametric study, the actual site of Takenaka Experimental Building (TEBS) is investigated. The ratio of embedment to half-width, D/B , is chosen to be 0.5. The testing data and calculating data of this site are listed in Table I. P- and S-wave velocities, C_P and C_S , are obtained from the field test. Soil mass density ρ is evaluated from the lab test of soil samples. Soil hysteretic damping ratio ζ is estimated based on the soil type. Shear modulus Υ , Young's modulus E , and Poisson's ratio ν are determined by using the following formulae.

$$\Upsilon = \rho C_S^2 \quad (264)$$

$$E = \frac{\rho C_S^2 (3C_P^2 - 4C_S^2)}{C_P^2 - C_S^2} \quad (265)$$

Table I. Soil Profile at Takenaka Experimental Building Site (TEBS)

Depth (m)	Soil Type	Testing Data				Calculating Data				NO of Divided Layers @ Depth [5]
		P-wave Velocity (m/sec)	S-wave Velocity (m/sec)	Mass Density [2] (gm/cm^3)	Damping Ratio [4]	Shear Modulus (MN/sq.m)	Young's Modulus [1] (MN/sq.m)	Poisson's Ratio [3]	Layer Depth (m)	
0.0 - 1.5	Loam	800	280	1.45	0.070	113.68	325.17	0.430	3.0	[1]=365.83MN/sq.m
1.5 - 2.8	Concrete	800	280	2.00	0.050	156.80	448.51	0.430		[2]=1.71 gm/cu.cm [3]=0.434 [4]=0.060 [5]=4@0.75m
2.8 - 9.0	Silt & Fine sand	1100	160	1.75	0.050	44.80	133.43	0.489	6.0	6@1.00m
9.0 - 11.0	Silty sand	800	90	1.70	0.050	13.77	41.13	0.494	2.0	2@1.00m
11.0 - 12.5	Silt	800	90	1.50	0.050	12.15	36.29	0.494	1.5	2@0.75m
12.5 - 17.5	Silt	1050	90	1.50	0.050	12.15	36.36	0.496	5.0	5@1.00m
17.5 - 21.4	Silt	1050	145	1.50	0.050	31.54	94.00	0.490	3.9	3@1.00m, 1@0.90m
21.4 - 24.0	Silt	1150	190	1.50	0.050	54.15	160.93	0.486	2.6	2@0.90m, 1@0.80m
24.0 - 27.9	Silt	1150	190	1.65	0.050	59.57	177.02	0.486	3.9	3@1.00m, 1@0.90m
27.9 - 33.6	Sandy silt & Clay	800	230	1.55	0.040	82.00	238.60	0.455	5.7	6@0.95m
33.6 - 38.0	Clayey sand & Sandy clay	800	250	1.65	0.035	103.13	298.21	0.446	4.4	4@0.90m, 1@0.80m
38.0 - 44.6	Clay	1300	250	1.55	0.030	96.88	286.90	0.481	6.6	6@0.95m, 1@0.90m
44.6 - 51.8	Fine sand	1500	350	1.75	0.040	214.38	630.78	0.471	7.2	8@0.90m
51.8 - 61.8	Clay & Fine sand	1500	290	1.75	0.035	147.18	435.81	0.481	10.0	10@1.00m
61.8 - 68.0	Sandy gravel	1950	460	2.10	0.045	444.36	1306.90	0.471	Infinity	Half-plane
68.0 - 71.7	Sandy gravel	1950	460	1.85	0.045	391.46	1151.31	0.471		[1]=1064.81MN/sq.m
71.7 - 77.0	Fine sand	1500	410	2.00	0.040	336.20	981.45	0.460		[2]=1.87 gm/cu.cm
77.0 - 78.5	Clay	1500	410	1.50	0.030	252.15	736.09	0.460		[3]=0.468
78.5 - 86.5	Clay & Very fine sand	1500	410	1.75	0.035	294.18	858.77	0.460		[4]=0.039
86.5 - 90.0	Gravel & Top sand	1500	410	2.20	0.050	369.82	1079.60	0.460		[5]=Infinity
90.0 - 96.6	Sandy gravel	2000	480	2.05	0.050	472.32	1388.09	0.469		Avg Shear Modulus = 363.04MN/sq.m
96.6 - 102.8	Clay & Very fine sand	1650	400	1.75	0.035	280.00	822.52	0.469		Avg S-wave Velocity = 440m/sec
102.8 - 116.0	Red Clay	1650	460	1.75	0.030	370.30	1079.69	0.458		
116.0 - 132.0	Very fine sand	1900	410	1.90	0.050	319.39	942.57	0.476		
132.0 - 150.0	Fine sand & Red clay	1900	470	1.80	0.030	397.62	1166.94	0.467		

$$\nu = \frac{E - 2\Upsilon}{2\Upsilon} \quad (266)$$

Soil layers and their properties are simplified as presented in the last column of Table I. The soil of the first three meters depth is treated as 4-layered homogeneous soil, each layer being 0.75 m. The physical properties of this homogeneous medium are obtained by taking the weighting average of the first three soil layers' properties (results shown in the last column of Table I). The soil profile from a depth of 3.00 m to 61.80 m is divided into 62 homogeneous layers as detailed in the last column. The average shear modulus and S-wave velocity of all simplified layers are 94.20 MN/sq.m and 224 m/sec, respectively. Soil underneath 61.80m depth is considered as a half-plane. Again the weighting average is used to determine the properties of this assumed homogeneous domain (results shown in the last column of Table I). Only the soil properties listed in the highlighted columns noted by [1],[2],...[5] are used as data in the code for determining the dynamic-stiffness matrices.

2. **Nondimensionalized Spring and Damping Coefficients.** The various dynamic-stiffness matrices $[S_{00}]$ in Equations (129), (195), and (236) are decomposed as

$$[S_{00}] = [K_{00}]([K(\dot{u}_0)] + \omega \dot{u}_0 [C(\dot{u}_0)]) \quad (267)$$

with

$$[K_{00}] = \pi \Upsilon \begin{bmatrix} 1 & 0 & 0 \\ 0 & B^2 & 0 \\ 0 & 0 & 1 \end{bmatrix} \quad (268)$$

$$[\mathcal{K}(\mu_0)] = \begin{bmatrix} K_x & K_{xy}B & 0 \\ K_{xy}/B & K_y & 0 \\ 0 & 0 & K_z \end{bmatrix} \quad (269)$$

$$[\mathcal{C}(\mu_0)] = \begin{bmatrix} C_x & C_{xy}B & 0 \\ C_{xy}/B & C_y & 0 \\ 0 & 0 & C_z \end{bmatrix} \quad (270)$$

where $[\mathcal{K}_{00}]$ is the arbitrary diagonal static-stiffness matrix. $\bar{\gamma}$ is the average of the soil shear moduli of the calculating system. B is the foundation half-width. $[\mathcal{K}]$ and $[\mathcal{C}]$ are the matrices containing nondimensionalized spring and damping coefficients, respectively. Small letters x and z denote the coefficients in the horizontal and vertical directions; y is used for rotation (rocking) with respect to point 0 of the rigid foundation, and xy represents the coupling between the horizontal direction and rocking. The dimensionless frequency μ_0 is equal to $\omega B/C_S$, where C_S is the average of the soil shear wave velocities of the determining domain. The symbol ι represents $\sqrt{-1}$.

B. INVESTIGATION OF EXCAVATED PART'S COEFFICIENTS

The dynamic-stiffness matrix of the system's excavated part in Equation (195) can be written in the form of a 3 by 3 matrix as

$$[S_{00}^*(\omega)] = \begin{bmatrix} S_{xx}^* & S_{x0}^* & 0 \\ S_{0x}^* & S_{00}^* & 0 \\ 0 & 0 & S_{zz}^* \end{bmatrix} \quad (271)$$

where the first and second subscripts denote the force and unit displacement degrees of freedom, respectively.

Using Equations (267) to (270), the nondimensionalized spring and damping coefficients of the system's excavated part can be obtained as

$$K_x = \frac{Real(S_{xx}^*)}{\pi\gamma} \quad (272)$$

$$C_x = \frac{Imag(S_{xx}^*)}{\pi\gamma d_0} \quad (273)$$

$$K_{xy} = \frac{Real(S_{x\theta}^*)}{\pi\gamma B} = \frac{Real(S_{\theta x}^*)}{\pi\gamma B} \quad (274)$$

$$C_{xy} = \frac{Imag(S_{x\theta}^*)}{\pi\gamma B d_0} = \frac{Imag(S_{\theta x}^*)}{\pi\gamma B d_0} \quad (275)$$

$$K_y = \frac{Real(S_{\theta\theta}^*)}{\pi\gamma B^2} \quad (276)$$

$$C_y = \frac{Imag(S_{\theta\theta}^*)}{\pi\gamma B^2 d_0} \quad (277)$$

$$K_z = \frac{Real(S_{zz}^*)}{\pi\gamma} \quad (278)$$

$$C_z = \frac{Imag(S_{zz}^*)}{\pi\gamma d_0} \quad (279)$$

For $D/B = 0.5, 1.0,$ and $2.0,$ the excavated part of system is finely discretized into 400, 450, and 400 elements, respectively. To create the square elements, the vertical side and the horizontal side of this domain are equally divided into 10 and 40 portions for $D/B = 0.5,$ 15 and 30 portions for $D/B = 1.0,$ and 20 and 20 portions for $D/B = 2.0.$ The 4-node element is employed in the finite element procedure.

1. **Effects of Hysteretic Damping.** As described in Equation (180), the hysteretic damping ζ relates to the dynamic-stiffness coefficients of the system's excavated part as

$$[S_{00}^*(\omega)] = [K^e](1 + 2\zeta i) - \omega^2[M^e] \quad (280)$$

For the system's bounded excavated part, the dimensionless natural frequencies associated with various modes can be determined. In Table II, the natural frequencies in the range of interest (less than 4.0) are presented for the excavated part of the undamped system with $D/B = 2.0$. The antisymmetric mode applies to the horizontal (x) and rocking (y) degrees of freedom. The symmetric mode refers to the vertical (z) degree of freedom. The zero values of K_x , K_y , and K_z correspond to the dimensionless natural frequencies of the system's excavated part having rigid-body constraint with the released degrees of freedom in the horizontal direction, rocking, and vertical direction, respectively.

Table II. Dimensionless Natural Frequencies of Undamped Bounded Domain with $D/B = 2.0$

2.86	2.07	0	0	0
3.04	*	2.97	2.92	3.04
3.94	*	3.48	3.75	*

* out of the interested range

At the frequencies corresponding to the antisymmetric mode (2.86, 3.04, and 3.94 in Figures 27 to 32), the spring and damping coefficients approach infinity. The first two frequencies of this undamped medium are very close. Coefficients approaching infinity are also applied, at frequency 2.07 in Figures 33 and 34, for the symmetric mode. At the frequencies 0, 2.97, and 3.48 in Figure 27, the frequencies 0, 2.92, and 3.75 in Figure 31, and the frequencies 0 and 3.04 in Figure 33, the spring coefficients are equal to zero. These frequencies are the natural frequencies of the medium having a rigid constraint with the released degrees of freedom, the horizontal direction (Figure 27), the rocking (Figure 31), and the vertical direction (Figure 33), respectively. It should be noted that the frequencies corresponding to the second mode of the horizontal and rocking released degrees of freedom (2.97 in Figure 27 and 2.92 in Figure 31, respectively) occur between the two close frequencies corresponding to the antisymmetric mode (2.86 and 3.04).

Figures 27 to 34 also show the influence of various hysteretic damping ratios on the nondimensionalized spring and damping coefficients of the system's excavated part. The damping coefficients of the undamped medium (see Figures 28, 30, 32, and 34) are equal to zero due to no radiation of energy in the bounded domain. For the damping case, all damping coefficients arise as the result of a frictional loss of energy. As the damping ratio increases, the spring coefficients have no significant change except in the vicinity of the natural frequencies (see Figures 27, 29, 31, and 33). In this zone, both spring and damping coefficients are reduced. The damping ratio can cause considerable change in the vibrational mode. Taking the antisymmetric mode as an example, only one natural frequency of the damping medium develops in the narrow frequency range where the two

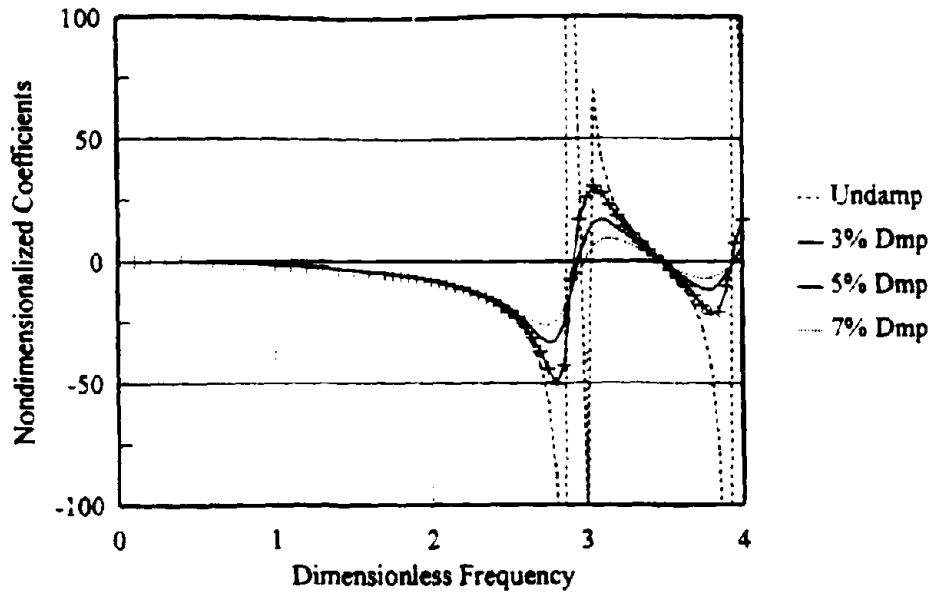


Figure 27. Spring Coefficient (K_x) of Excavated Part of System, $D/B=2.0$, with Indicated Damping Ratio

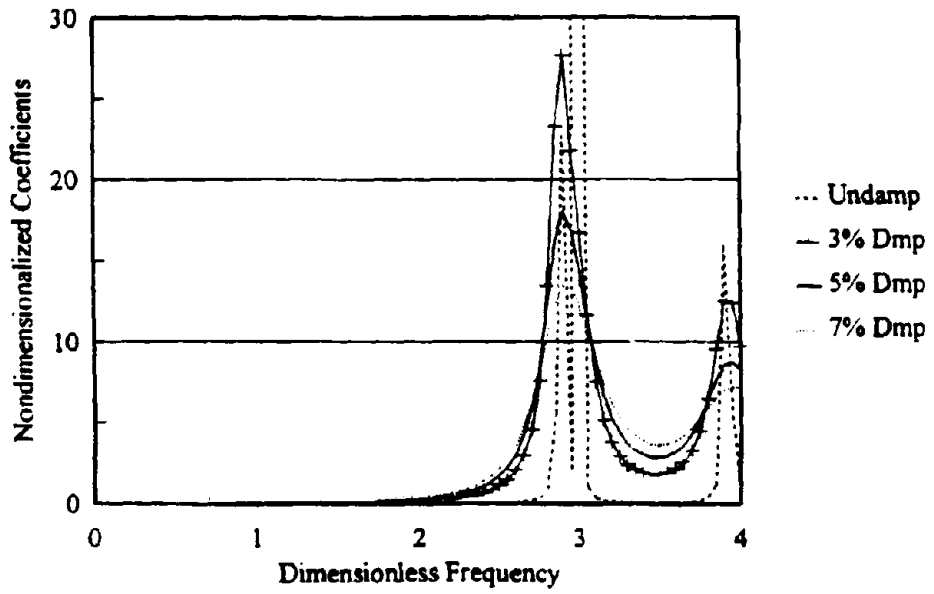


Figure 28. Damping Coefficient (C_x) of Excavated Part of System, $D/B=2.0$, with Indicated Damping Ratio

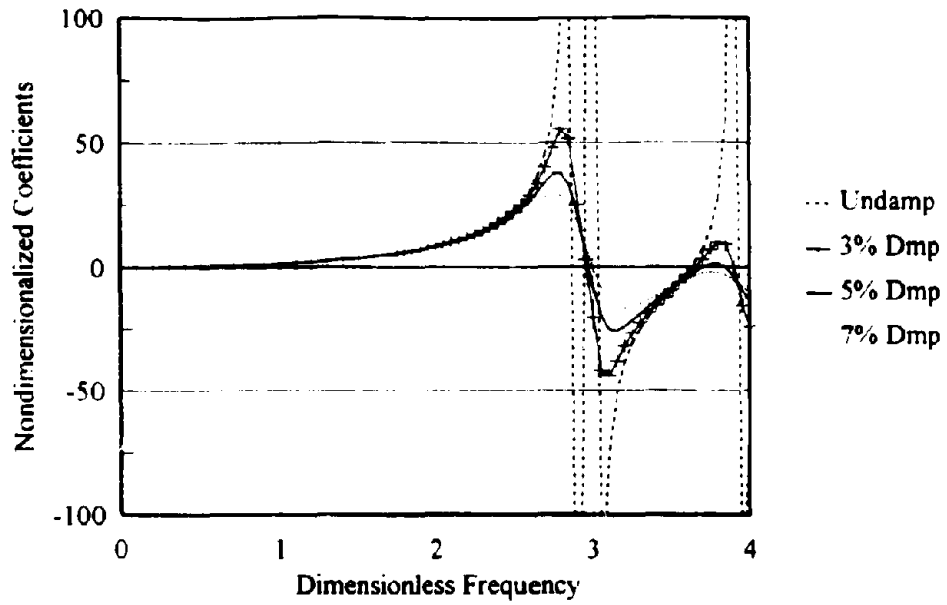


Figure 29. Spring Coefficient (K_{xy}) of Excavated Part of System, $D/B=2.0$, with Indicated Damping Ratio

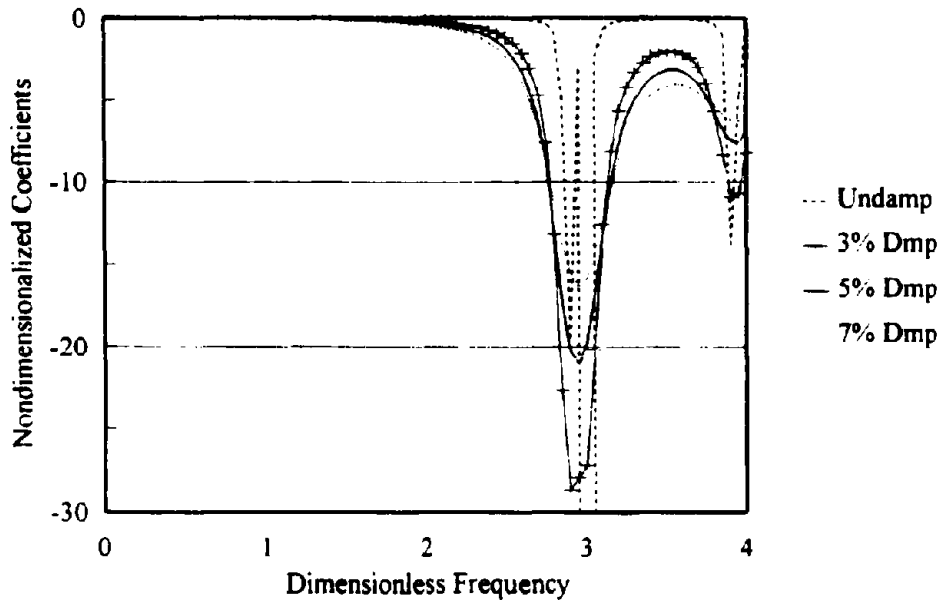


Figure 30. Damping Coefficient (C_{xy}) of Excavated Part of System, $D/B=2.0$, with Indicated Damping Ratio

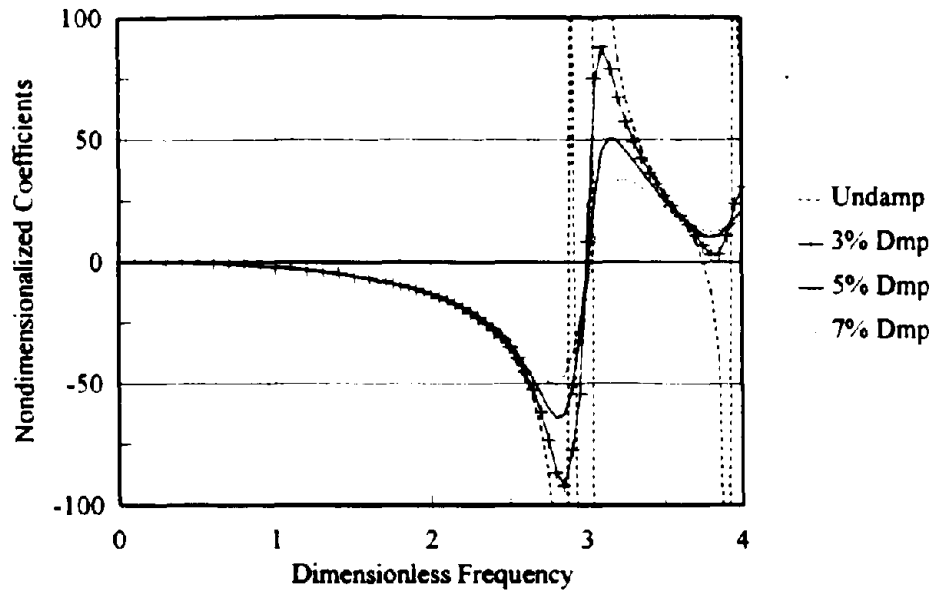


Figure 31. Spring Coefficient (K_y) of Excavated Part of System, $D/B=2.0$, with Indicated Damping Ratio

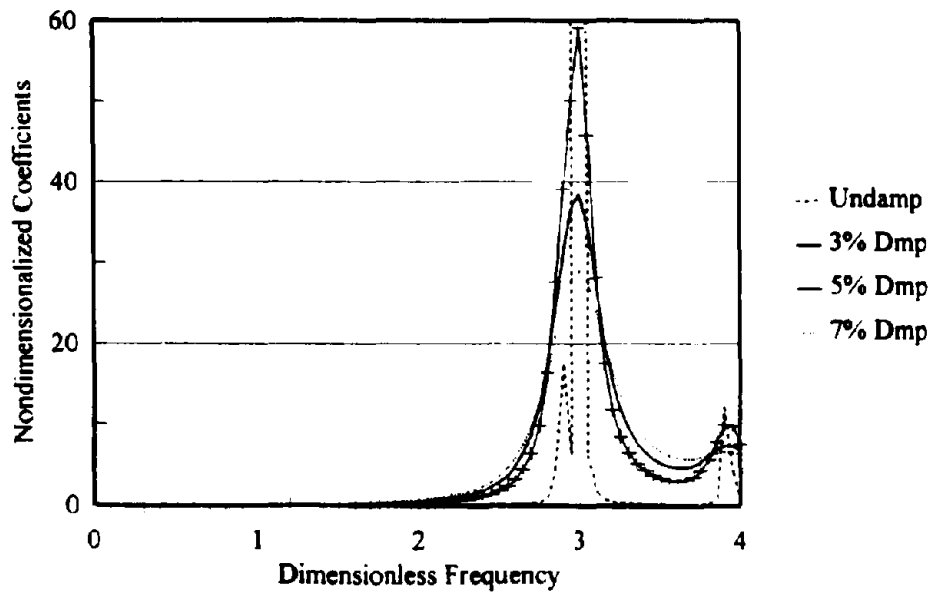


Figure 32. Damping Coefficient (C_y) of Excavated Part of System, $D/B=2.0$, with Indicated Damping Ratio

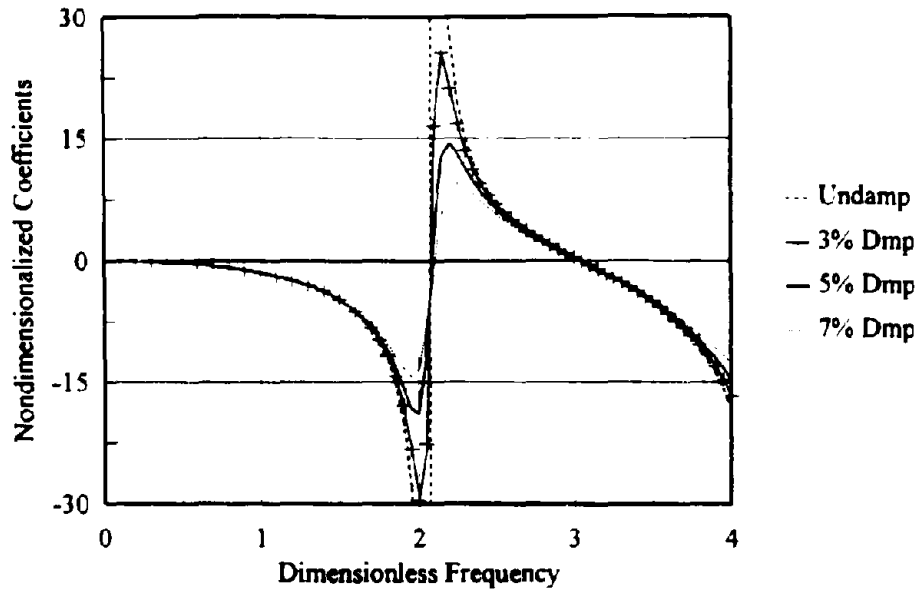


Figure 33. Spring Coefficient (K_z) of Excavated Part of System, $D/B=2.0$, with Indicated Damping Ratio

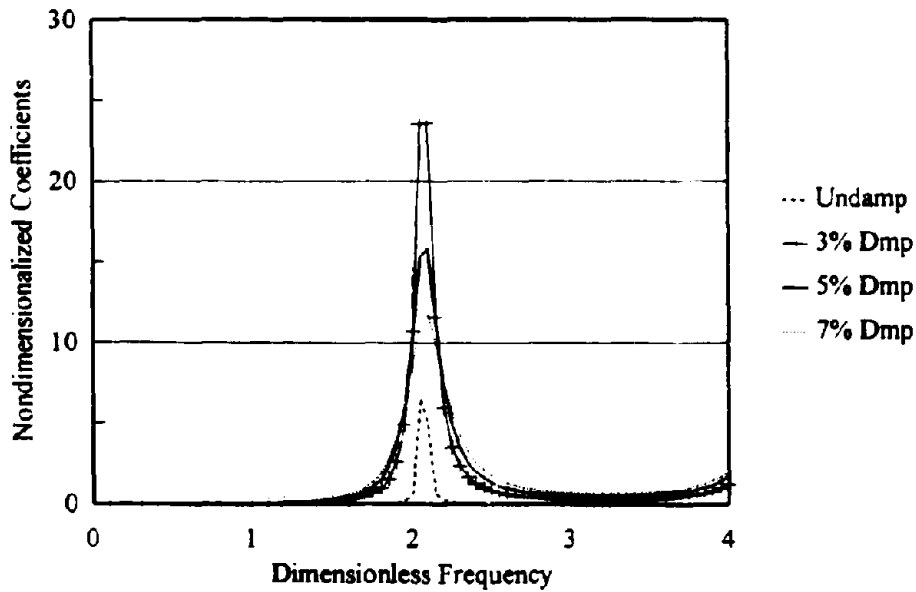


Figure 34. Damping Coefficient (C_z) of Excavated Part of System, $D/B=2.0$, with Indicated Damping Ratio

natural frequencies of the undamped medium (2.86 and 3.04 in Figures 27 to 32) occur. Consequently, the natural frequencies corresponding to the released degrees of freedom between the two (2.97 in Figure 27 and 2.92 in Figure 31) disappear. Also the frequency corresponding to the rocking released degree of freedom in the vicinity of frequency 3.75 in Figure 31 will not occur for the damping case studied.

2. **Effects of Foundation Embedment.** As shown in Figure 23, the foundation embedment D can be expressed as $D = Me * d_e$. The dynamic-stiffness coefficients of the system's excavated part are influenced by the discretized element's length d_e through the element stiffness matrix $[\bar{K}^e]$ in Equation (219), the element mass matrix $[\bar{M}^e]$ in Equation (233), and the transformation matrix $[A]$ in Equations (189), (190), and (193).

In Table I, the hysteretic damping ratio of the actual site ranges from 0.30 to 0.07. Therefore the hysteretic damping ratio of 0.05 is selected for the systems with the foundation embedment to half-width ratios, D/B , equal to 0.5, 1.0, and 2.0. Their nondimensionalized spring and damping coefficients of the systems' excavated part are demonstrated in Figures 35 to 42. In the same set of figures, the coefficients of the actual site (TEBS) are also included. At a particular frequency in the low frequency range (less than the first mode natural frequency), the bigger D/B leads to the larger spring and damping coefficients as the result of the bigger medium. Also in this range, the spring and damping coefficients corresponding to the coupling between the horizontal translation and rocking (see Figures 37 and 38) have the sign opposite to the translational and rocking coefficients (see Figures 35, 36, 39, 40, 41, and 42). The spring coefficients convert to zero when the dimensionless frequency approaches zero (see Figures 35, 37, 39, and 41).

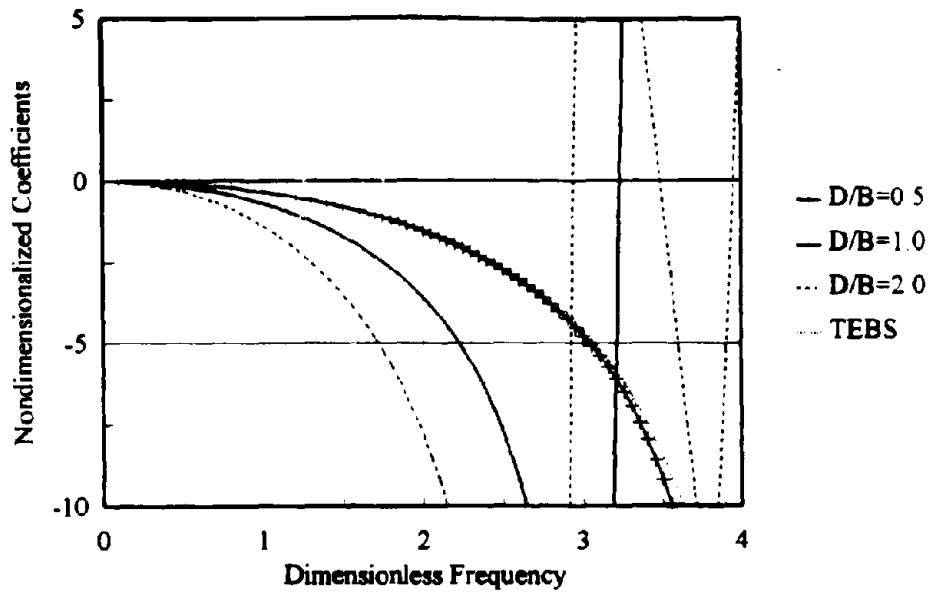


Figure 35. Spring Coefficient (K_x) of Excavated Part of System, Indicated D/B , with 5% Damping Ratio

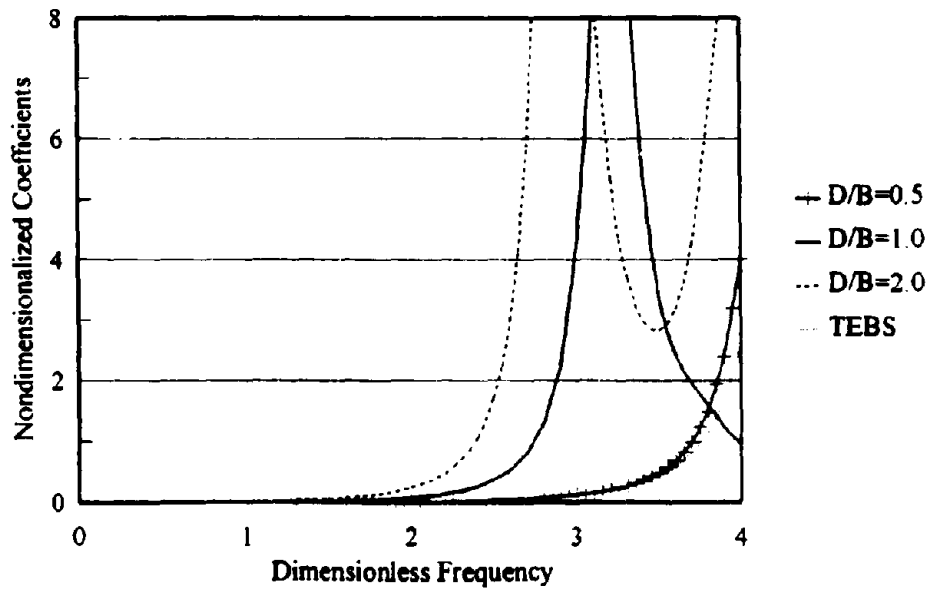


Figure 36. Damping Coefficient (C_x) of Excavated Part of System, Indicated D/B , with 5% Damping Ratio

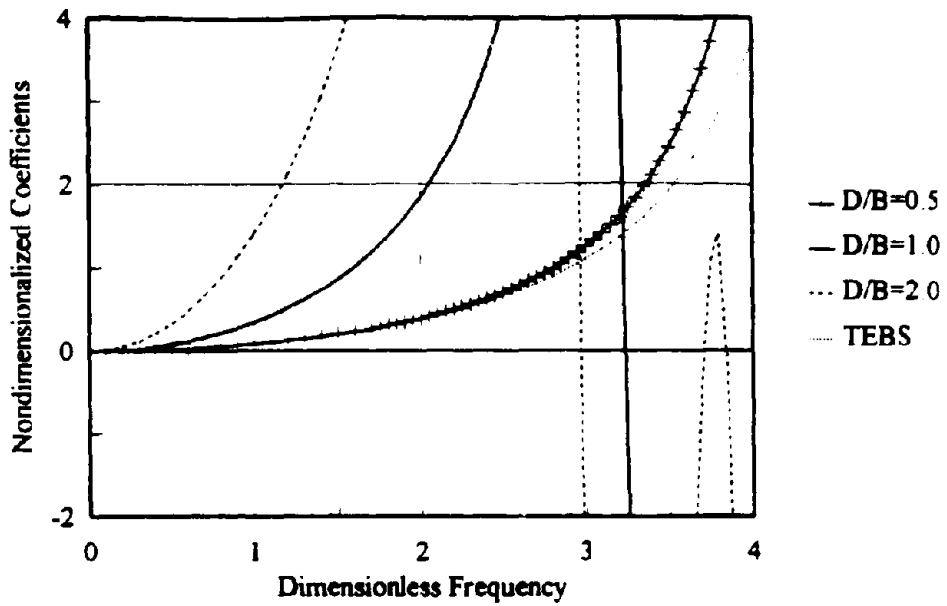


Figure 37. Spring Coefficient (K_{xy}) of Excavated Part of System, Indicated D/B , with 5% Damping Ratio

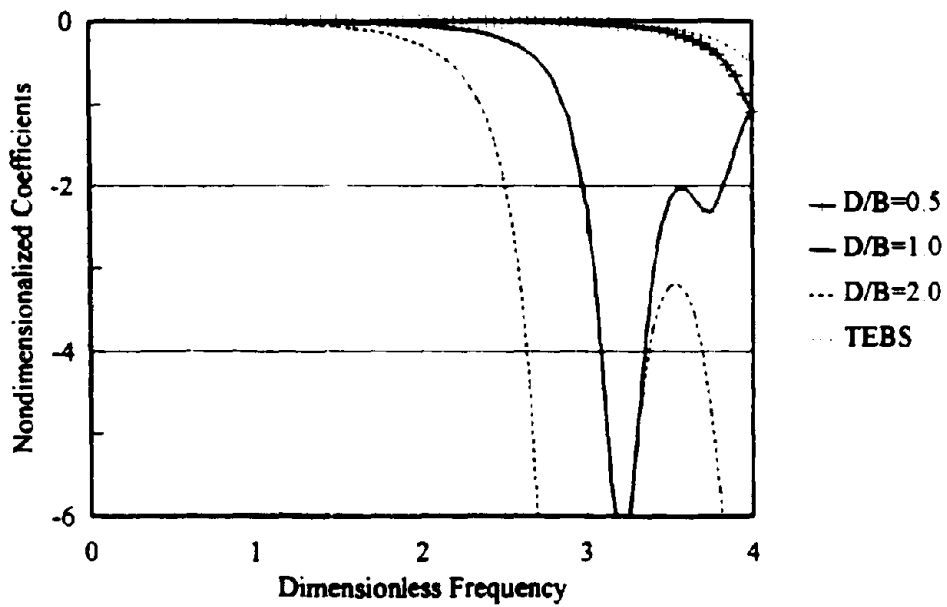


Figure 38. Damping Coefficient (C_{xy}) of Excavated Part of System, Indicated D/B , with 5% Damping Ratio

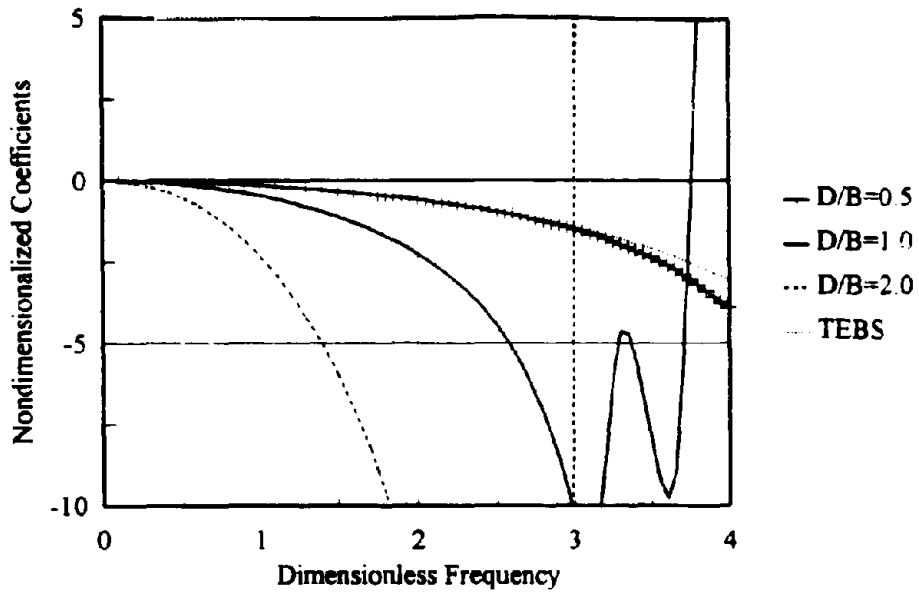


Figure 39. Spring Coefficient (K_y) of Excavated Part of System, Indicated D/B , with 5% Damping Ratio

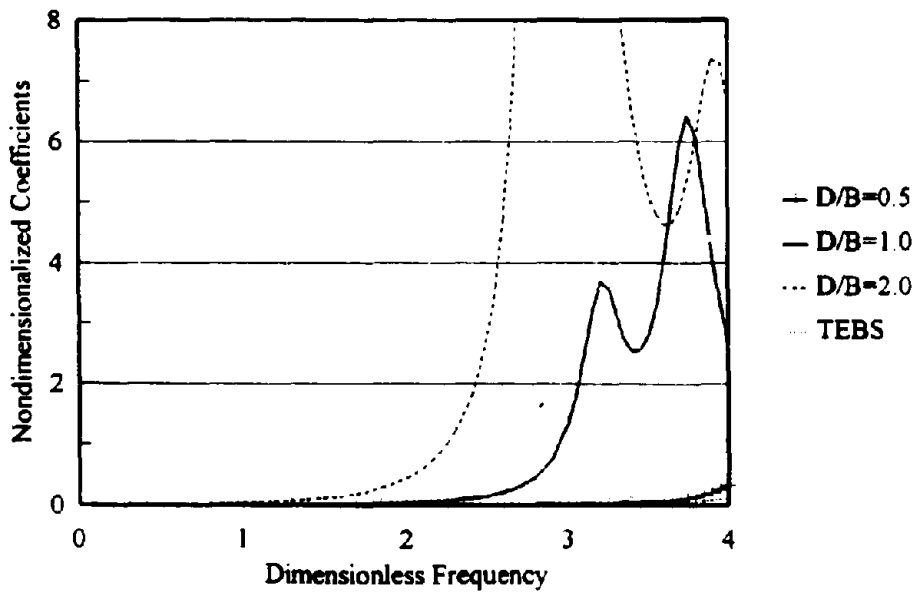


Figure 40. Damping Coefficient (C_y) of Excavated Part of System, Indicated D/B , with 5% Damping Ratio

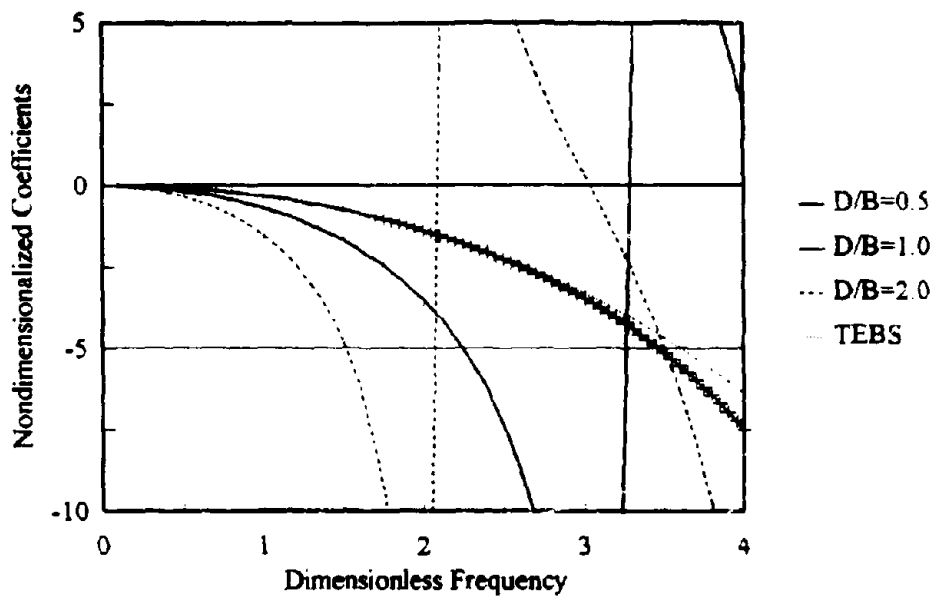


Figure 41. Spring Coefficient (K_z) of Excavated Part of System, Indicated D/B, with 5% Damping Ratio

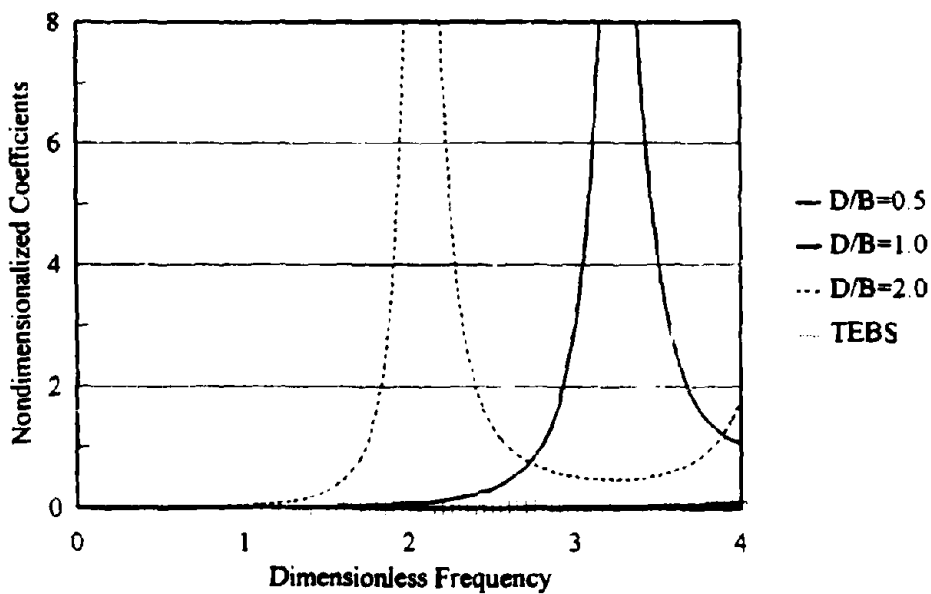


Figure 42. Damping Coefficient (C_z) of Excavated Part of System, Indicated D/B, with 5% Damping Ratio

The damping coefficients in the low frequency range are flatly zero (see Figures 36, 38, 40, and 42). As a point of an almost vertical line in the spring coefficient plot crossing the frequency axis suggests a natural frequency of the system's excavated part, Figures 35, 37, 39, and 41 show that the bigger D/B results in the lower first mode natural frequency. The first mode natural frequencies of the TEBS system's excavated part and the system's excavated part with $D/B = 0.5$ are greater than 4.0; therefore they do not show in these figures. Comparing the horizontal spring and damping coefficients in the low frequency range (see Figures 35 and 36) to the vertical spring and damping coefficients (see Figures 41 and 42), the former are bigger for $D/B = 0.5$, about the same for $D/B = 1.0$, and smaller for $D/B = 2.0$.

As for the actual site (TEBS), all coefficients are very close to those of the $D/B = 0.5$ since the excavated part of the actual site is assumed to be the homogeneous medium having $D/B = 0.5$. The smaller coefficients of the actual site are caused by the difference in the hysteretic damping and Poisson's ratios.

C. INVESTIGATION OF FREE-FIELD SYSTEM COEFFICIENTS

Analogous to the system's excavated part, the dynamic-stiffness matrix of a free-field system in Equation (129) can be expressed as

$$[S_{00}^f(\omega)] = \begin{bmatrix} S_{xx}^f & S_{x\theta}^f & 0 \\ S_{\theta x}^f & S_{\theta\theta}^f & 0 \\ 0 & 0 & S_{zz}^f \end{bmatrix} \quad (281)$$

where the first and second subscripts denote the force and unit displacement degrees of freedom, respectively.

Therefore the nondimensionalized spring and damping coefficients of the free-field system can be determined as

$$K_x = \frac{Real(S'_{xx})}{\pi\gamma} \quad (282)$$

$$C_x = \frac{Imag(S'_{xx})}{\pi\gamma d_0} \quad (283)$$

$$K_{xy} = \frac{Real(S'_{x\theta})}{\pi\gamma B} = \frac{Real(S'_{\theta x})}{\pi\gamma B} \quad (284)$$

$$C_{xy} = \frac{Imag(S'_{x\theta})}{\pi\gamma B d_0} = \frac{Imag(S'_{\theta x})}{\pi\gamma B d_0} \quad (285)$$

$$K_y = \frac{Real(S'_{\theta\theta})}{\pi\gamma B^2} \quad (286)$$

$$C_y = \frac{Imag(S'_{\theta\theta})}{\pi\gamma B^2 d_0} \quad (287)$$

$$K_z = \frac{Real(S'_{zz})}{\pi\gamma} \quad (288)$$

$$C_z = \frac{Imag(S'_{zz})}{\pi\gamma d_0} \quad (289)$$

Two extreme cases of a free-field system, the half-plane and the homogeneous layer with depth H built on a rock, are considered. The rock is defined as the medium having its shear wave velocity ten times faster than that of the topping soil layer. On the vertical and horizontal assumed lines of the boundary element technique (which coincide with the rigid structure-soil interface), 4 by 16 elements, 6 by 12 elements, and 8 by 8

elements are selected for $D/B = 0.5, 1.0,$ and $2.0,$ respectively. The distributed loads vary linearly along the elements with continuity generally enforced at all nodes except the corner one. This leads to a total of 54 nodal forces for all cases, as each element contains four nodal forces.

1. **Effects of Foundation Embedment.** The foundation embedment is equal to $\sum_{i=1}^M d_i$ as shown in Figure 14. The depth d_i of soil layer, where $i = 1, \dots, M,$ effects the dynamic-stiffness coefficients of the free-field system [see Equation (129)] through the element strain-displacement matrix $[\bar{T}]_e$ in Equations (138) and (141) and the element flexibility matrix $[\bar{F}]_e$ in Equations (170) to (178).

Presented in Figures 43 to 50 are the nondimensionalized spring and damping coefficients of the free-field systems comprising the half-plane with the 5% damping ratio and indicated $D/B.$ Those of the free-field system consisting of the TEBS with $D/B = 0.5$ are contained as well. The natural frequencies of the free-field system (see Figure 43, 45, 47 and 49) appear at the same frequencies as those of the system's excavated (see Figures 35, 37, 39, and 41). In contrast to the system's excavated part, the spring coefficients (see Figures 43, 45, 47 and 49) do not transform to zero as the frequency reaches zero. This is an indication of the free-field system's non-zero static stiffness coefficients. In the lower-frequency range (less than 1.0), an increase of the D/B has no significant effect on the horizontal and vertical spring coefficients (see Figures 43 and 49). On the contrary, the rocking spring coefficients increase while the D/B increases (see Figure 47).

In the low frequency range, the damping coefficients (see Figures 44, 46, 48, and 50) are not equal to zero like those of the system's excavated part due to the free-field

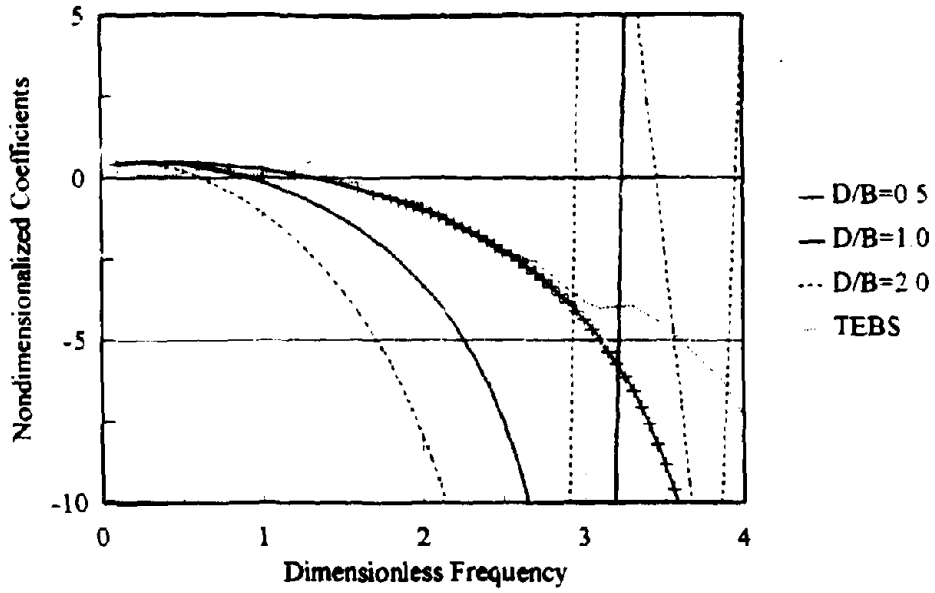


Figure 43. Spring Coefficient (K_x) of Free-field System, Half-plane, Indicated D/B , with 5% Damping Ratio

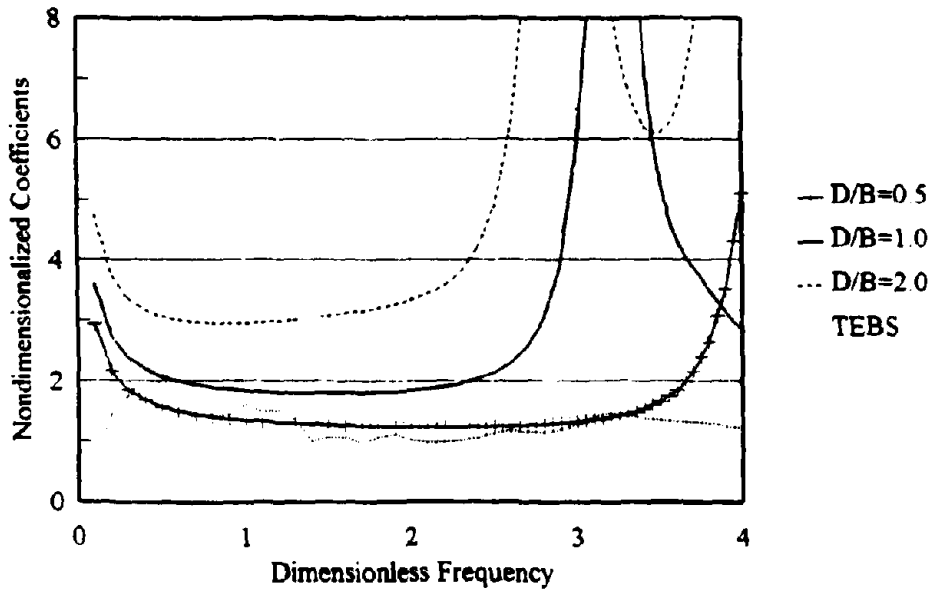


Figure 44. Damping Coefficient (C_x) of Free-field System, Half-plane, Indicated D/B , with 5% Damping Ratio

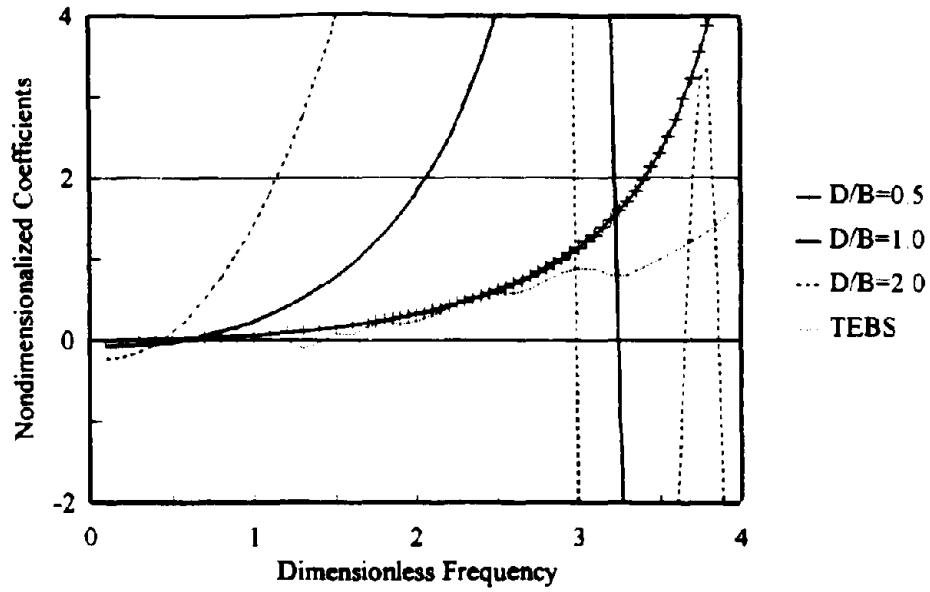


Figure 45. Spring Coefficient (K_{xy}) of Free-field System, Half-plane, Indicated D/B, with 5% Damping Ratio

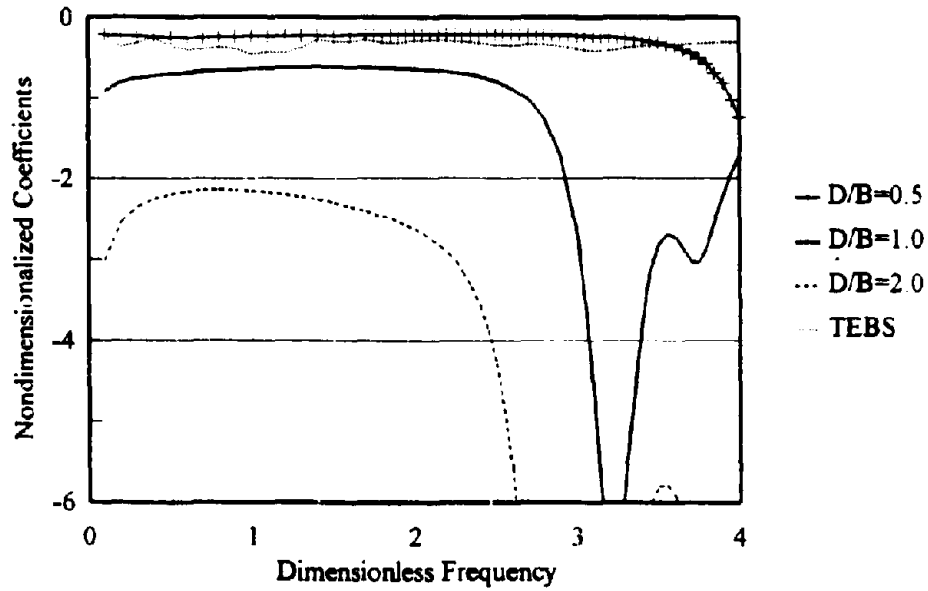


Figure 46. Damping Coefficient (C_{xy}) of Free-field System, Half-plane, Indicated D/B, with 5% Damping Ratio

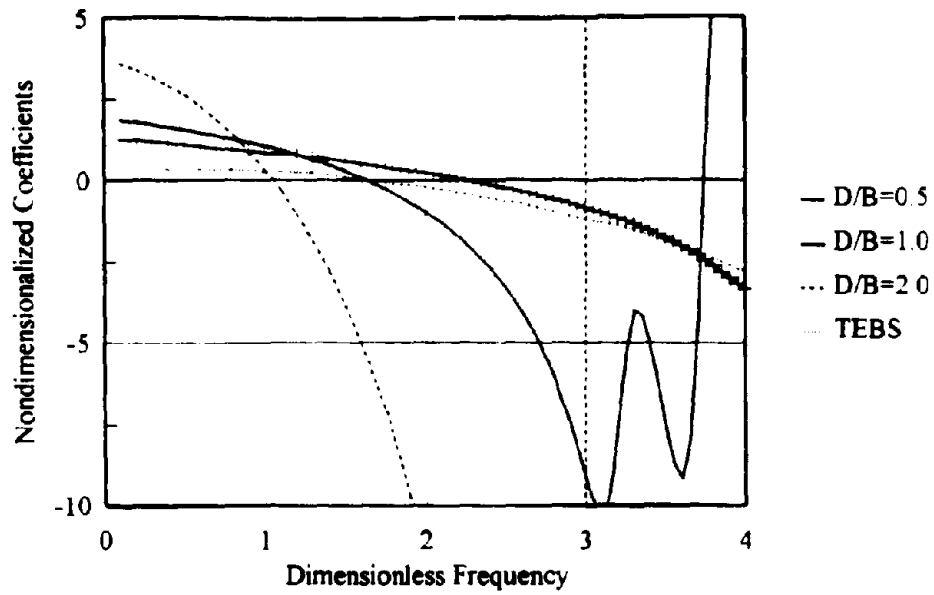


Figure 47. Spring Coefficient (K_y) of Free-field System, Half-plane, Indicated D/B , with 5% Damping Ratio

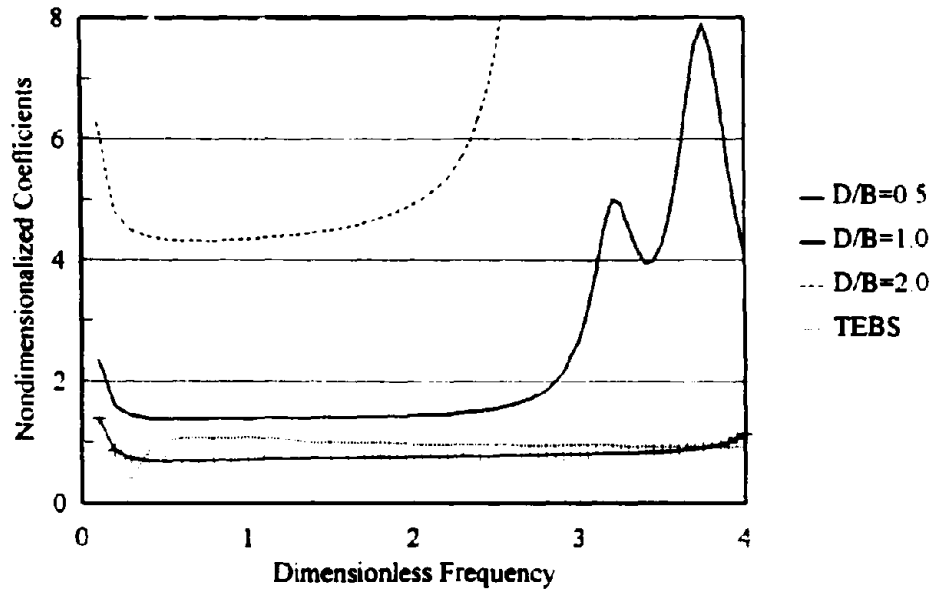


Figure 48. Damping Coefficient (C_y) of Free-field System, Half-plane, Indicated D/B , with 5% Damping Ratio

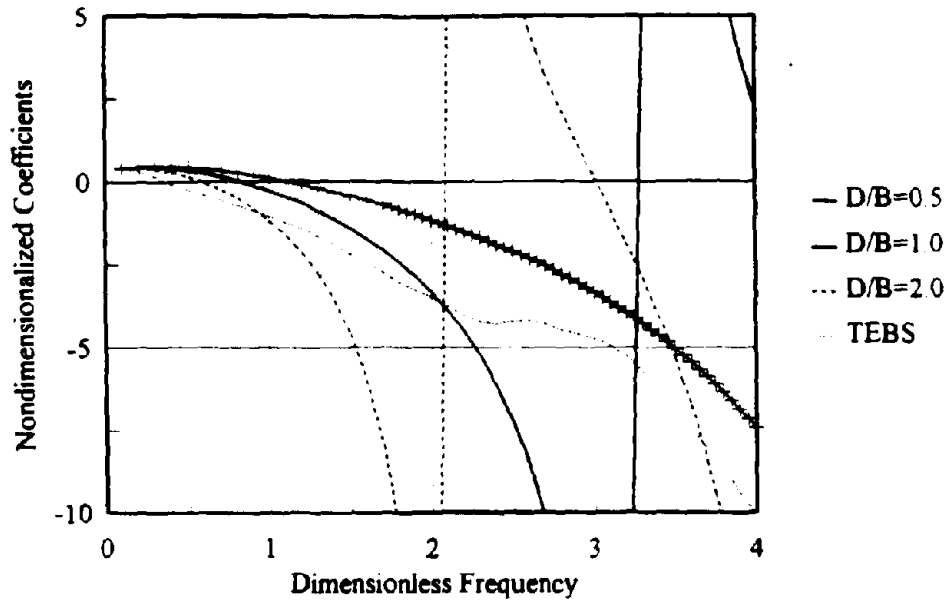


Figure 49. Spring Coefficient (K_z) of Free-field System, Half-plane, Indicated D/B , with 5% Damping Ratio

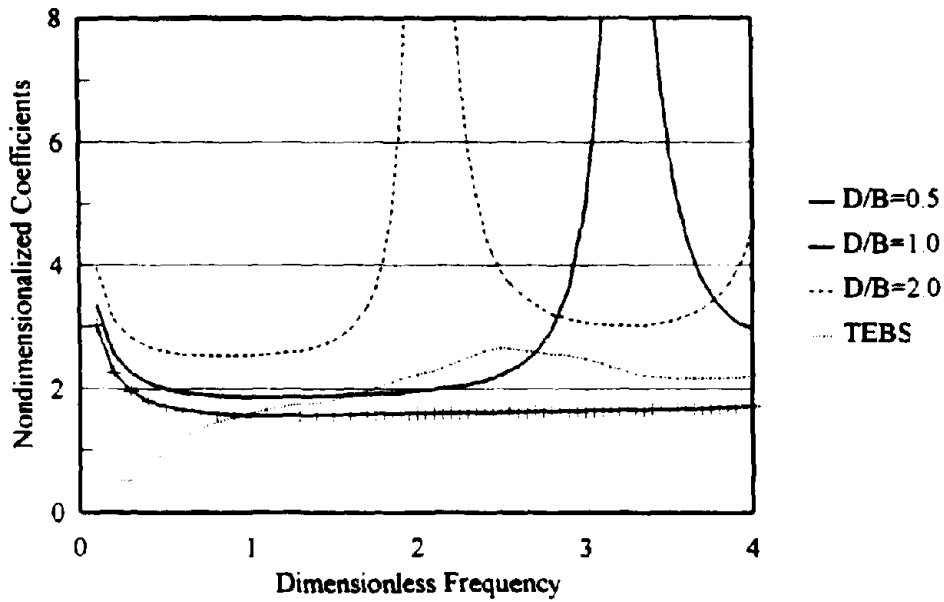


Figure 50. Damping Coefficient (C_z) of Free-field System, Half-plane, Indicated D/B , with 5% Damping Ratio

system's radiation of energy toward infinity. The increase of the horizontal and vertical damping coefficients is proportional to the D/B (see Figures 44 and 50). A nonproportional but more remarkable increase can be seen in the rocking damping coefficients, especially for $D/B = 2.0$ (see Figure 48). Comparing the horizontal damping coefficients (see Figure 44) to the vertical damping coefficients (see Figure 50), the former are greater for $D/B = 2.0$ and about the same for $D/B = 0.5$ and 1.0 . Despite the rising value of the damping coefficients in the very low and narrow frequency range ($0 - 0.2$), the imaginary part of the dynamic-stiffness coefficients (dimensionless frequency times damping coefficients, also see Equation 64) maintains a small value

2. **Effects of Layer's Depth.** Prior to the discussion of the free-field system consisting of the TEBS with $D/B = 0.5$ (nonhomogeneous soil), the influence of the layer's depth on a rock should be understood. As shown in Figure 14, this depth can be expressed as $\sum_{i=1}^{N-1} d_i$. The depth d_i , where $i = 1, \dots, N-1$, has an effect on the layer's dynamic-stiffness matrix $[S_{p-si}^l(k)]$ in Equations (446) and (489) and the total dynamic-stiffness matrix $[S_{p-si}^r(k)]$ in Equation (352). The latter is part of the Green's influence function's formulation as shown in Equations (143) to (147) and (149) to (151). Through these Green's functions, $[\mathbf{uwpr}(x', z)]_i'$ and $[\mathbf{uwpr}(x', z)]_{M,i}'$, the layer's depth on rock affects the element flexibility matrix $[\bar{F}]_i'$ in Equations (170) to (178) and the dynamic-stiffness coefficients of the free-field system in Equation (129).

Shown in Figures 51 to 58 are the nondimensionalized spring and damping coefficients of the free-field systems comprising the layer on rock with the 5% damping ratio and indicated H/B . As the layer's depth to half-width ratio, H/B , decreases (the rock

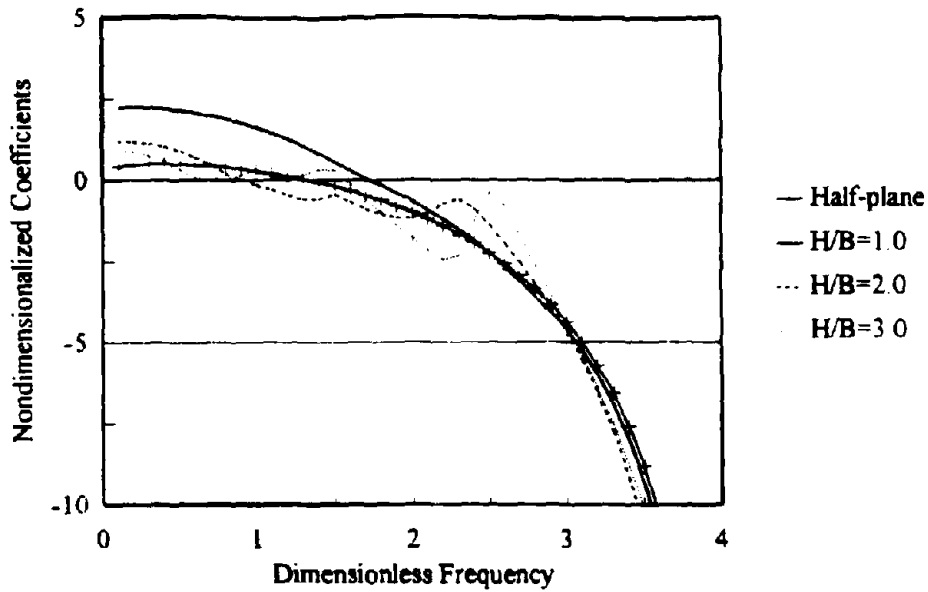


Figure 51. Spring Coefficient (K_x) of Free-field System, Layer on Rock, Indicated H/B , $D/B=0.5$, with 5% Damping Ratio

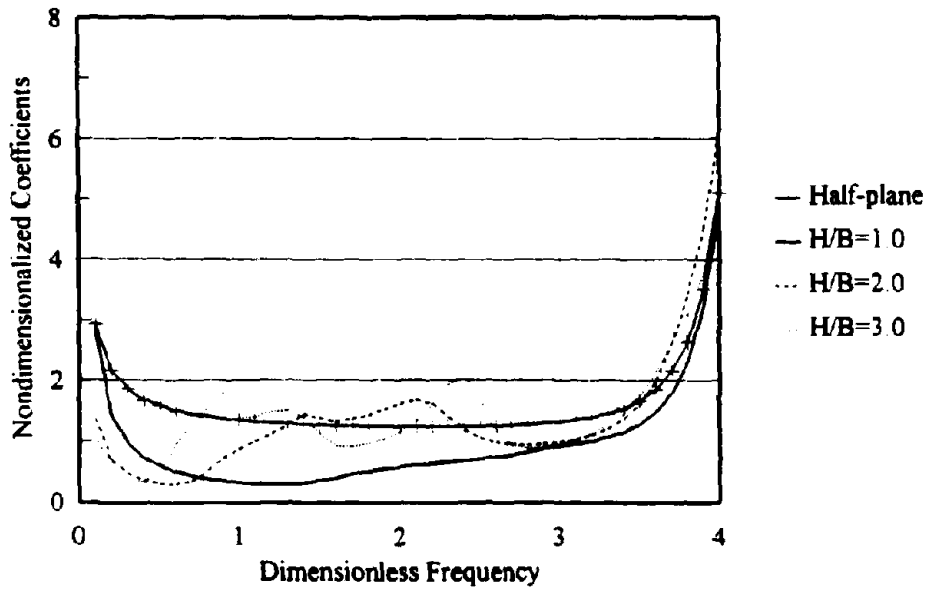


Figure 52. Damping Coefficient (C_x) of Free-field System, Layer on Rock, Indicated H/B , $D/B=0.5$, with 5% Damping Ratio

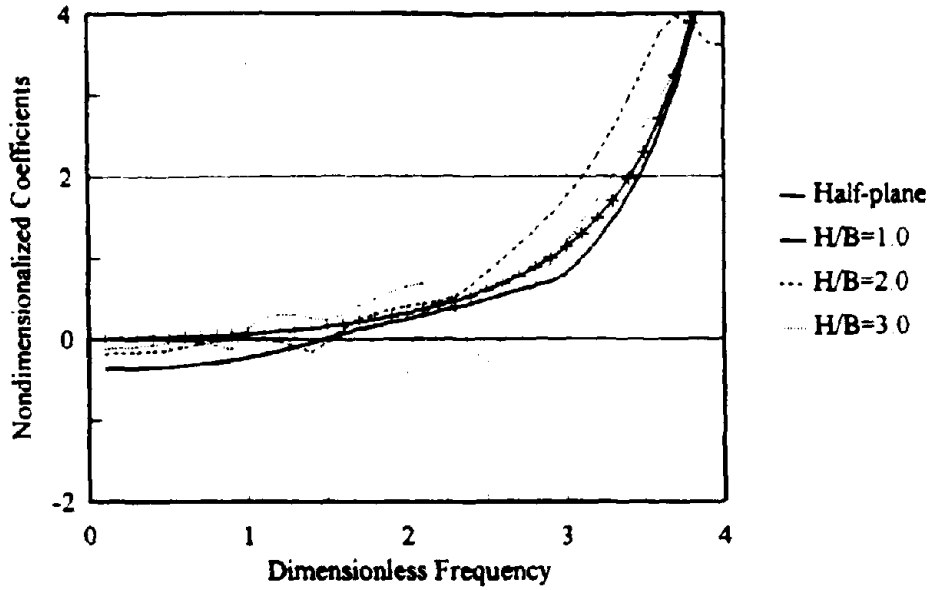


Figure 53. Spring Coefficient (K_{xy}) of Free-field System, Layer on Rock, Indicated H/B , $D/B=0.5$, with 5% Damping Ratio

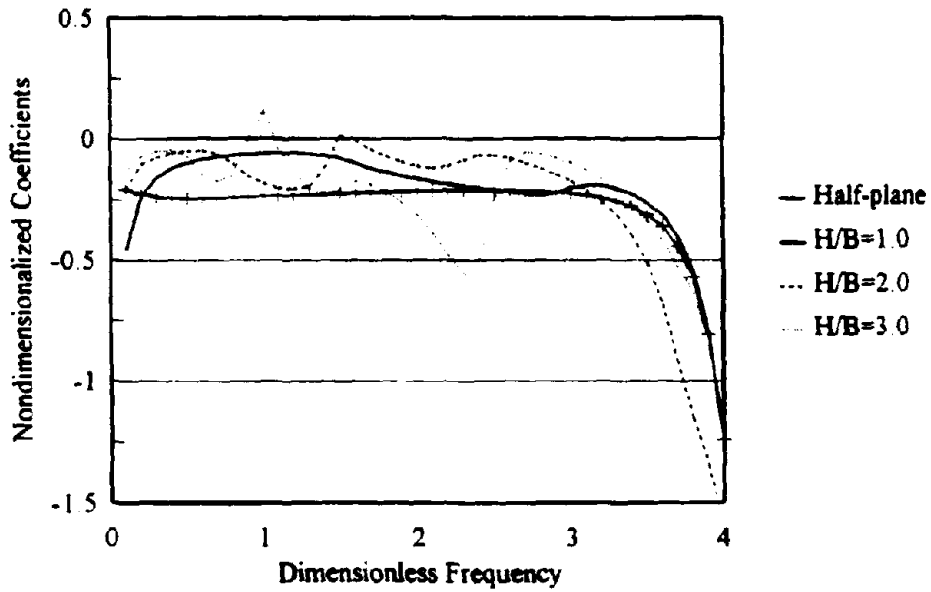


Figure 54. Damping Coefficient (C_{xy}) of Free-field System, Layer on Rock, Indicated H/B , $D/B=0.5$, with 5% Damping Ratio

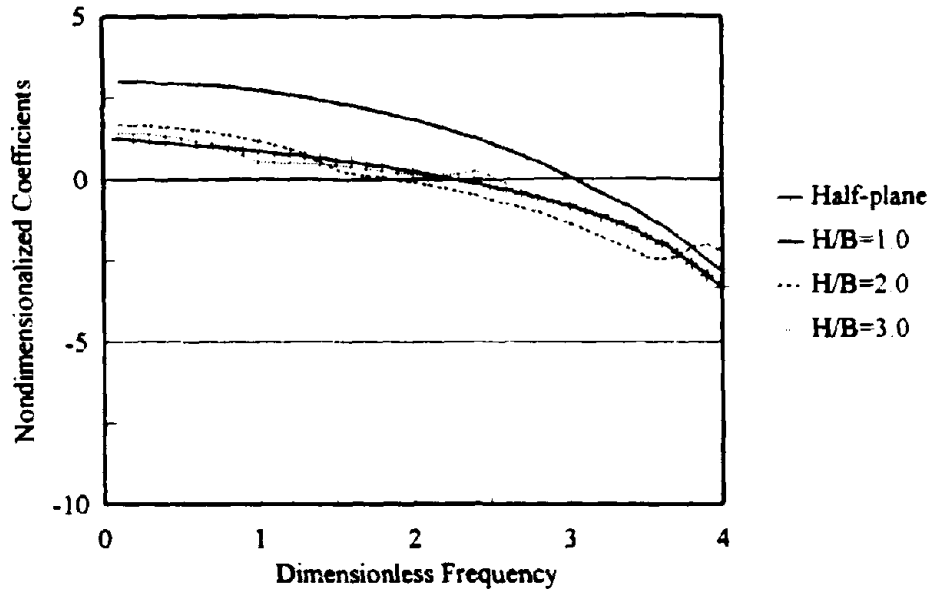


Figure 55. Spring Coefficient (K_y) of Free-field System, Layer on Rock, Indicated H/B , $D/B=0.5$, with 5% Damping Ratio

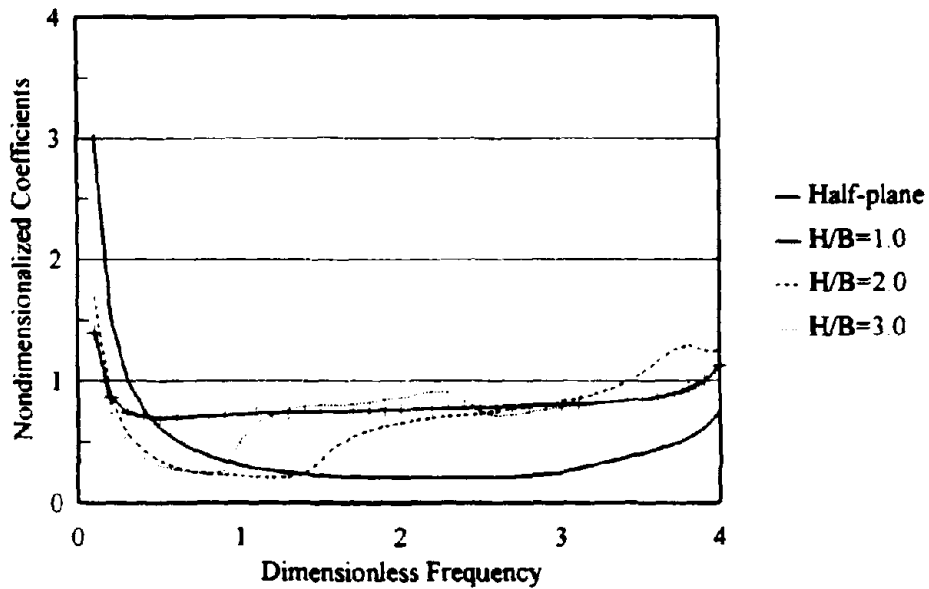


Figure 56 Damping Coefficient (C_y) of Free-field System, Layer on Rock, Indicated H/B , $D/B=0.5$, with 5% Damping Ratio

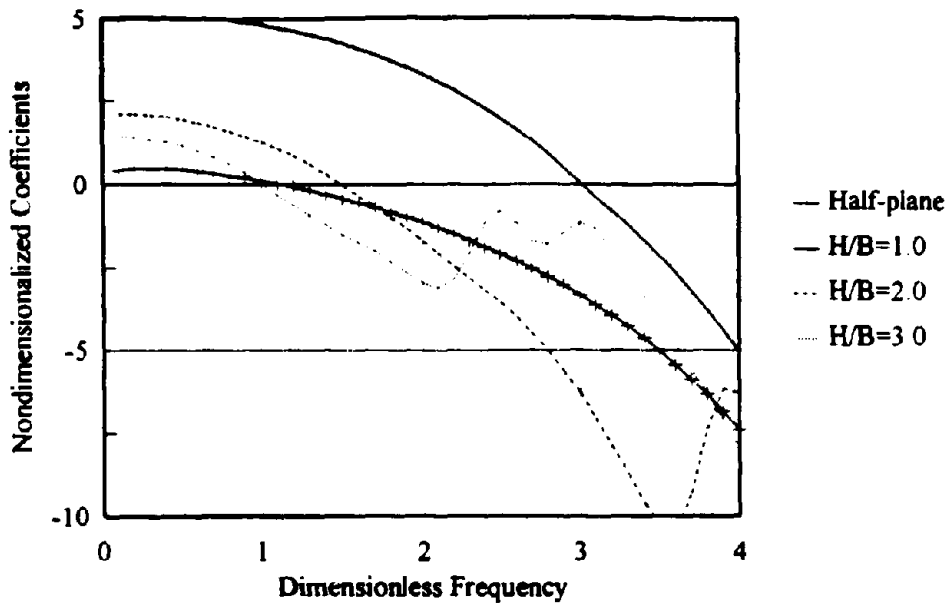


Figure 57. Spring Coefficient (K_z) of Free-field System, Layer on Rock, Indicated H/B , $D/B=0.5$, with 5% Damping Ratio

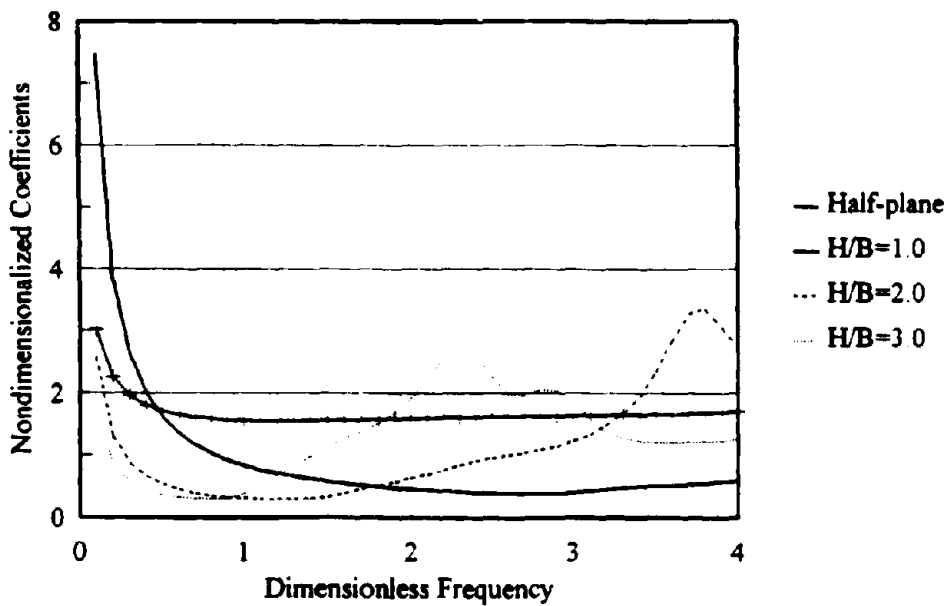


Figure 58. Damping Coefficient (C_z) of Free-field System, Layer on Rock, Indicated H/B , $D/B=0.5$, with 5% Damping Ratio

base comes closer to the surface), the spring coefficients in the lower-frequency range (see Figures 51, 53, 55, and 57) increase. This effect is more noticeable in the vertical direction (see Figure 57). In the same range, all spring coefficients of the layer on a rock are greater than those of the half-plane. As the frequency increases, the spring coefficients corresponding to $H/B = 2.0$ and 3.0 oscillate around those corresponding to the half-plane. This implies a stronger frequency dependence of the former. The smoother spring coefficients are exhibited in a case of the very shallow layer, $H/B = 1.0$. In contrast to the half-plane, a layer on the rock demonstrates a cutoff frequency below which only small amount of energy can be radiated toward infinity. This leads to a small damping coefficient. As shown in Figures 52, 56, and 58, the small damping coefficients can be found below these cutoff frequencies. The corresponding damping coefficients are less than those of the half-plane. In the cases of $H/B = 2.0$ and 3.0 , the damping coefficients corresponding to the horizontal direction and rocking (see Figures 52 and 56) suddenly increase, above the cutoff frequencies, to the levels of those corresponding to half-plane. Gradual increase is found in the coefficient corresponding to the vertical direction. The more shallow layer (smaller H/B) leads to the higher cutoff frequency, especially in the case of $H/B = 1.0$. The latter means a system's energy is trapped within the layer in the wider frequency range.

Turning back to the free-field system consisting of the TEBS with $D/B = 0.5$ in Figures 43 to 50, this system's coefficients are similar to those corresponding to half-plane with $D/B = 0.5$. But stronger frequency dependence of the former is noticeable due to its nonhomogeneous domain. As the average shear wave velocity of the TEBS's half-plane is

about two times faster than that of the thick TEBS's layer (61.8m), the amplitudes of the TEBS's vertical and rocking coefficients are affected and therefore differ from the corresponding amplitudes of the homogeneous half-plane. The cutoff frequencies are quite low and the energy trap range is then barely noticeable.

D. INVESTIGATION OF GROUND SYSTEM COEFFICIENTS

Four parametric cases and one actual site are examined. They are as follows: the 5% damping ratio systems consisting of the half-plane with $D/B = 0.5$ (D5), the half-plane with $D/B = 1.0$ (D10), the layer on a rock having $D/B = 0.5$ and $H/B = 1.0$ (D5H10), the layer on a rock having $D/B = 0.5$ and $H/B = 2.0$ (D5H20), and the actual site with $D/B = 0.5$ (TEBS).

1. Dynamic Stiffness Coefficients. The spring and damping coefficients of a ground system can directly be determined by using an indirect boundary element method (IBEM). But the method requires two Green's influence functions relating to the displacement and surface traction along a structure-soil interface. Since the calculation of the free-field system's coefficients needs only the displacement Green's influence function, it can be simpler to determine the coefficients of system's excavated part by the finite element method (FEM) and then subtract them from those of the free-field system to yield the ground system's coefficients.

Close to the natural frequencies of the system's excavated part, the spring and damping coefficients of both system's excavated part and free-field system are very large. Since the errors inherent in the two different methods (IBEM and FEM) are not consistent, the difference between these two large numbers may yield a problematic result.

No problem is found in the cases of D5, D5H10, D5H20, and TEBS since their systems' fundamental frequency is beyond the range of interest (0 - 4.0). For the D10, the problem arises in the frequency range of 3.0 - 4.0 (see Figures 59 to 66). This problem can be minimized but not eliminated by an increase in a number of the discretizing elements. As an example, for this particular case, the 6 elements on the vertical interface and 12 elements on the horizontal interface in the IBEM increase to 11 and 22 elements, respectively. The D10's coefficients, shown in Figures 59 to 66, are the result of these increasing elements. The remaining problem (the unexpectedly non-smooth coefficients) may be tackled by the function interpolation using values before and after the natural frequency. Since the lower damping ratio produces larger stiffness coefficients, in the vicinity of a natural frequency, of a system's excavated part and a free-field, and the larger D/B tends lower the first natural frequency (as discussed in Subsection B), the subtraction technique is not recommended for such a case because an unacceptable error may arise at the relatively-important low range of frequency.

In the very low frequency range (0 - 0.2), it should be emphasized that the imaginary part of the dynamic-stiffness coefficients (dimensionless frequency times damping coefficients) maintains a small value regardless of the increasing value of the nondimensionalized damping coefficients.

a. Effects of Foundation Embedment. Comparing the coefficients of D5 to those of D10, the foundation embedment barely has an effect on both translational spring coefficients (see Figures 59 and 65). On the contrary, the deeper embedment (D10) leads to a greater rocking spring coefficient (see Figure 63). In both translation directions and

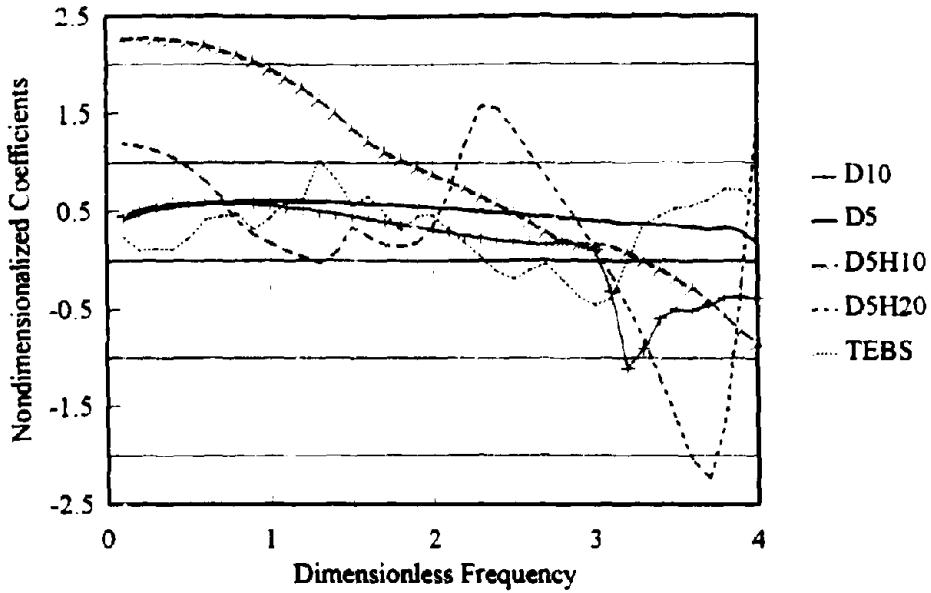


Figure 59. Spring Coefficient (K_x) of Ground System, with 5% Damping Ratio

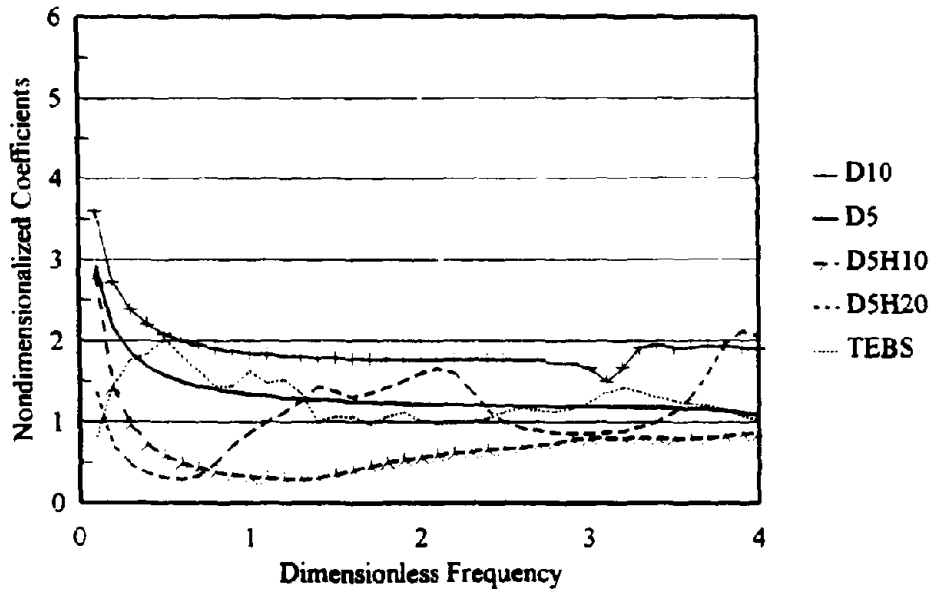


Figure 60. Damping Coefficient (C_x) of Ground System, with 5% Damping Ratio

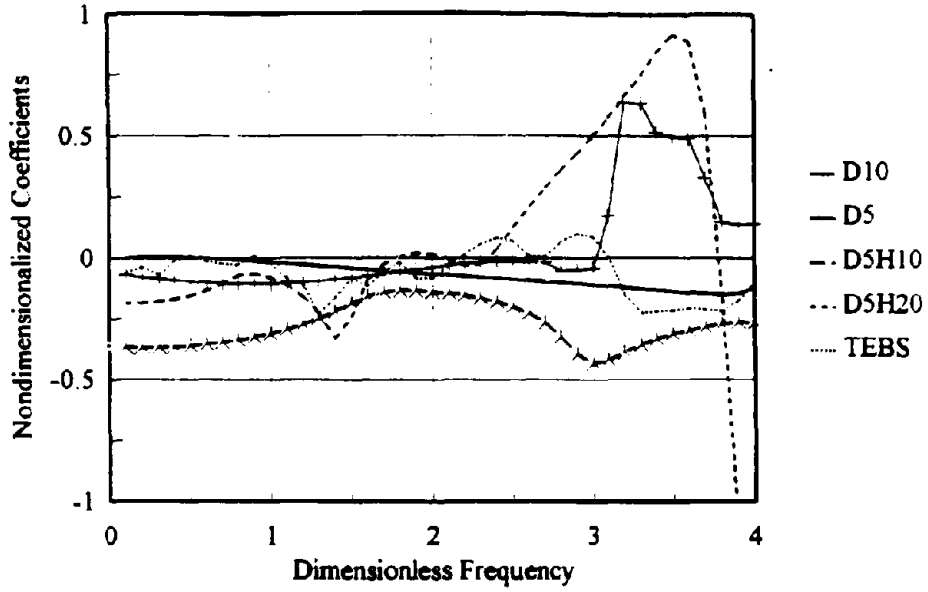


Figure 61. Spring Coefficient (K_{xy}) of Ground System, with 5% Damping Ratio

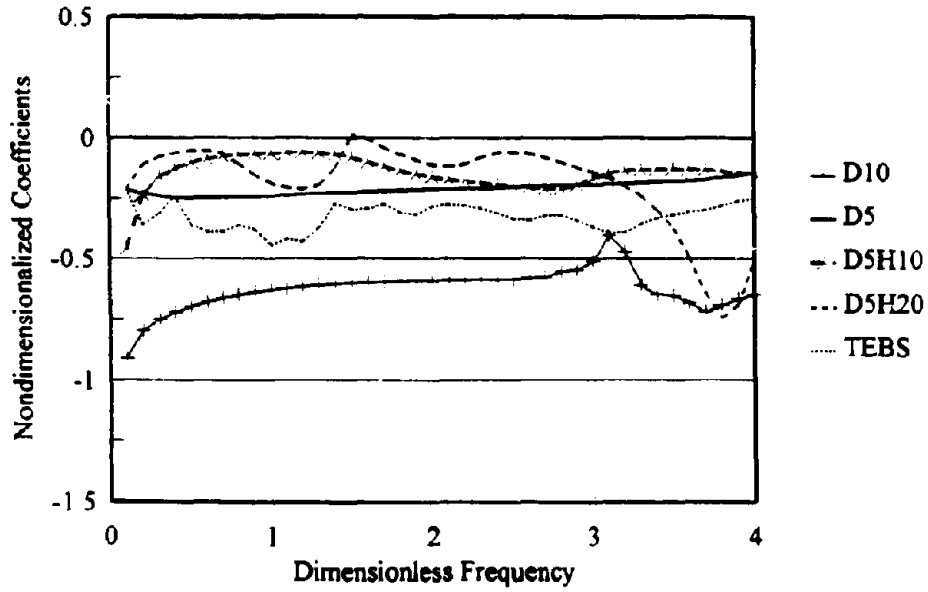


Figure 62. Damping Coefficient (C_{xy}) of Ground System, with 5% Damping Ratio

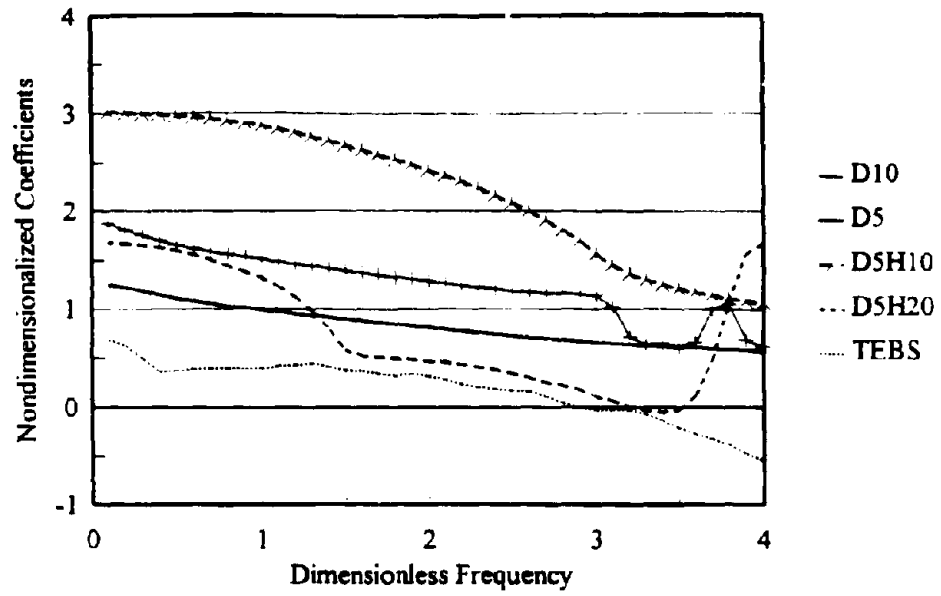


Figure 63. Spring Coefficient (K_y) of Ground System, with 5% Damping Ratio

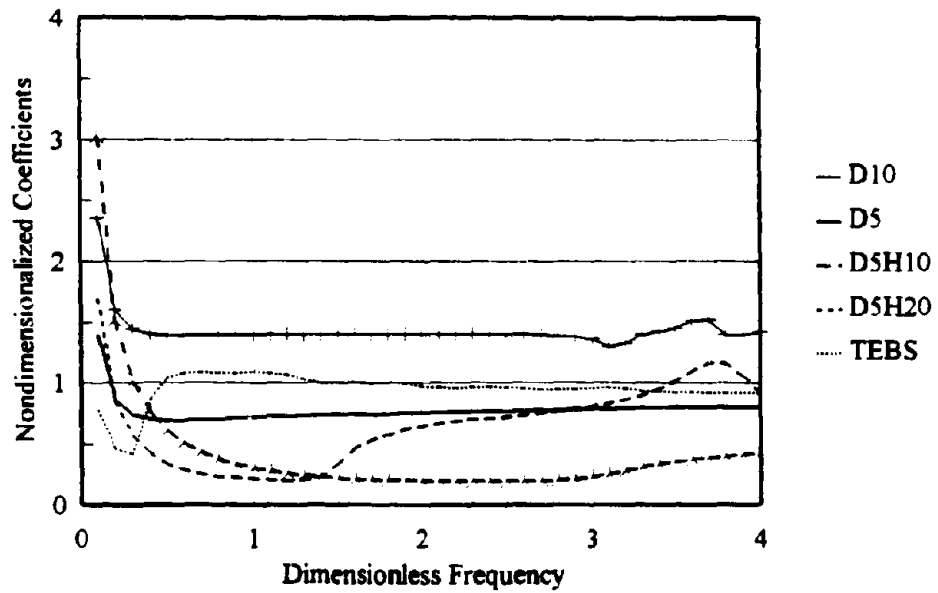


Figure 64. Damping Coefficient (C_y) of Ground System, with 5% Damping Ratio

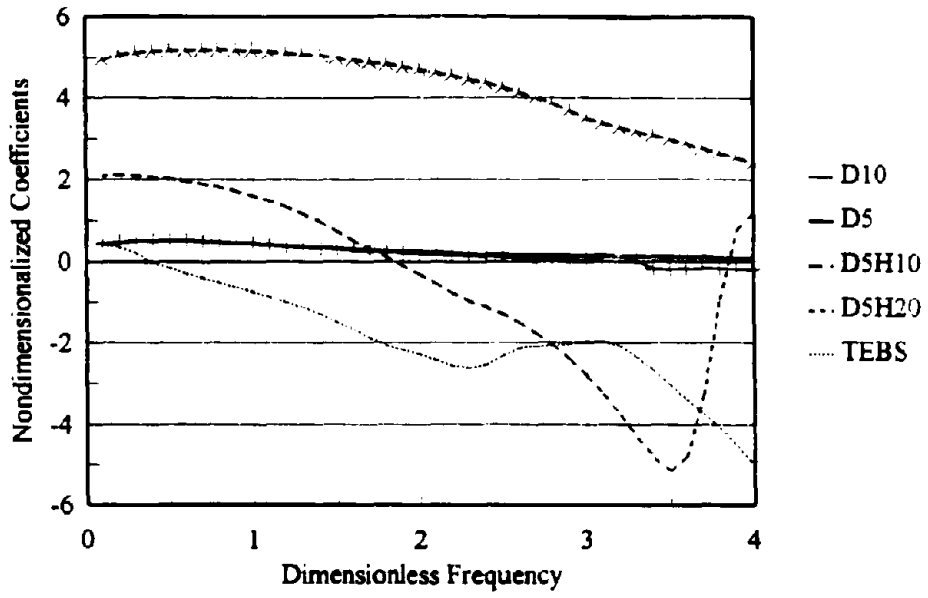


Figure 65. Spring Coefficient (K_z) of Ground System, with 5% Damping Ratio

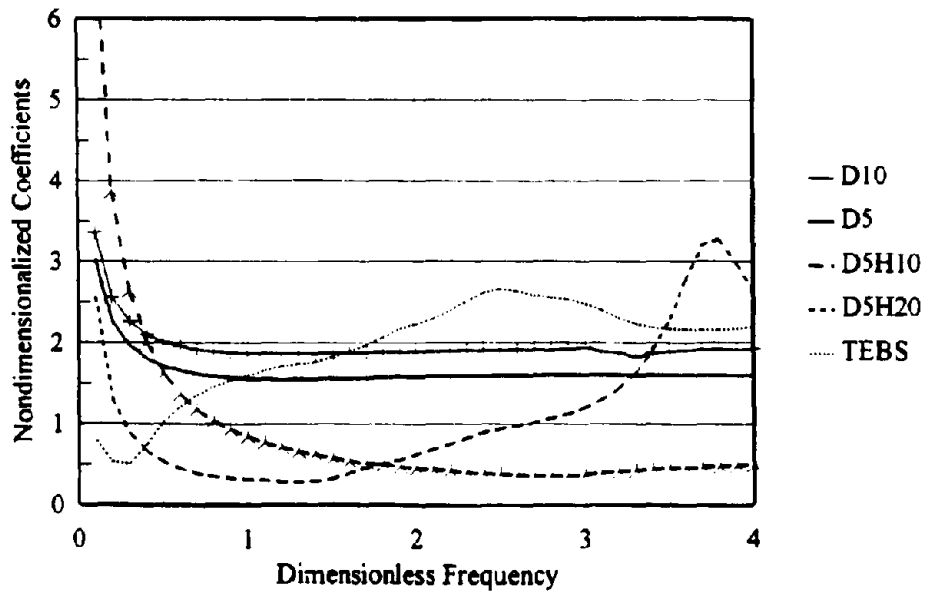


Figure 66. Damping Coefficient (C_z) of Ground System, with 5% Damping Ratio

rocking, the larger damping coefficients of D10 appear (see Figures 60, 64, and 66). A bigger increase is found in the rocking. This phenomenon seems to be consistent with that of the free-field system in the low and lower ranges of frequency because the ground system's coefficients are the difference between the coefficients of the free-field system and the system's excavated part, and the latter convert to zero in these ranges. Of D10's ground system, the horizontal and vertical coefficients are about the same (see Figures 59, 60, 65, and 66) for which the identical behavior is also found in the free-field and the system's excavated part. In the case of the D5's ground system, the horizontal damping coefficient is slightly smaller than the vertical damping coefficient (see Figures 60 and 66) since both coefficients of the free-field system are about the same but the horizontal damping coefficient of the system's excavated part is slightly bigger than the vertical damping coefficients.

b. Effects of Layer's Depth. For D5H10, D5H20, and TESB, the same tendency of the free-field system in the low and lower frequency range is also applied. The D5H10's spring coefficients are greater than those of D5H20, especially in the vertical direction. The former's smaller frequency-dependence is shown. The spring coefficients of both systems are greater than those of D5 (half-plane). The cutoff frequencies exist at the same points as those in the free-field system. Below these frequencies, the damping coefficients of D5H10 and D5H20 are less than those of half-plane. Then beyond the cutoff frequencies, they increase to the level of the half-plane. For D5H20 and TEBS, both spring and damping coefficients display a strong dependence of frequency. In the high

frequency range of D5H20, the large oscillation is clearly demonstrated. The negative spring coefficients occur in the three cases.

2. Time-derivative Flexibility Coefficients. The investigation so far leads to the conclusion that the deeper foundation embedment results in the greater rocking dynamic-stiffness coefficients. To clearly demonstrate the influence of the rocking component in the structure-soil interaction, only the cases of shallow embedment (D5, D5H10, and D5H20) will be explored hereafter. Since the vertical degree of freedom of a shear structure investigated in Section VII is neglected, the corresponding degree of freedom of ground system is omitted as well.

Using the shear modulus Υ of 320.0 MN/sq.m, shear wave velocity C_S of 400.0 m/sec, and foundation half-width B of 3.0 m, the dynamic stiffness coefficients of ground system can be determined from their nondimensionalized coefficients (see Equations 267 to 270). In Figures 67 to 72, the ground system's dynamic stiffness coefficients of D5, D5H10, and D5H20 are illustrated in the range of their system frequency ω equal 0 to 80 Hz. This 80 Hz frequency corresponds to the dimensionless frequency ω_0 of 3.77 as $\omega_0 = \omega B / C_S$. The shape of the dynamic-stiffness coefficients' real part (see Figures 67, 69, and 71) is similar to that of nondimensionalized spring coefficients in the frequency range below 3.77 (see Figures 59, 61, and 63). On the contrary, that of the dynamic-stiffness coefficients' imaginary part (see Figures 68, 70, and 72) is different from that of nondimensionalized damping coefficients (see Figures 60, 62, and 64). Since the imaginary part is the product of system's frequency and damping coefficient, it then increases as a function of frequency. In the case of D5H10 and D5H20 (layer on a rock), the imaginary

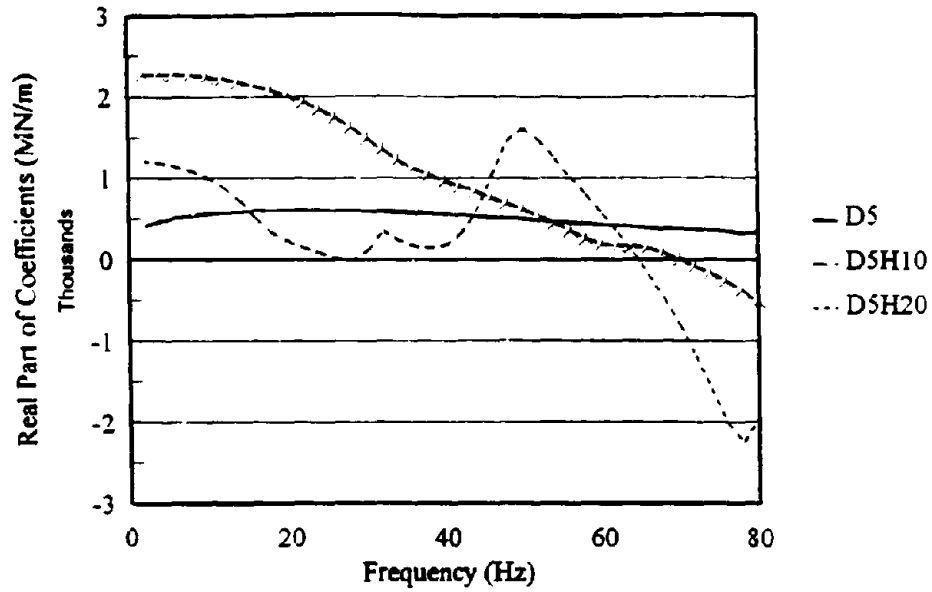


Figure 67. Real Part of Horizontal Dynamic Stiffness Coefficients, Ground System with 5% Damping Ratio

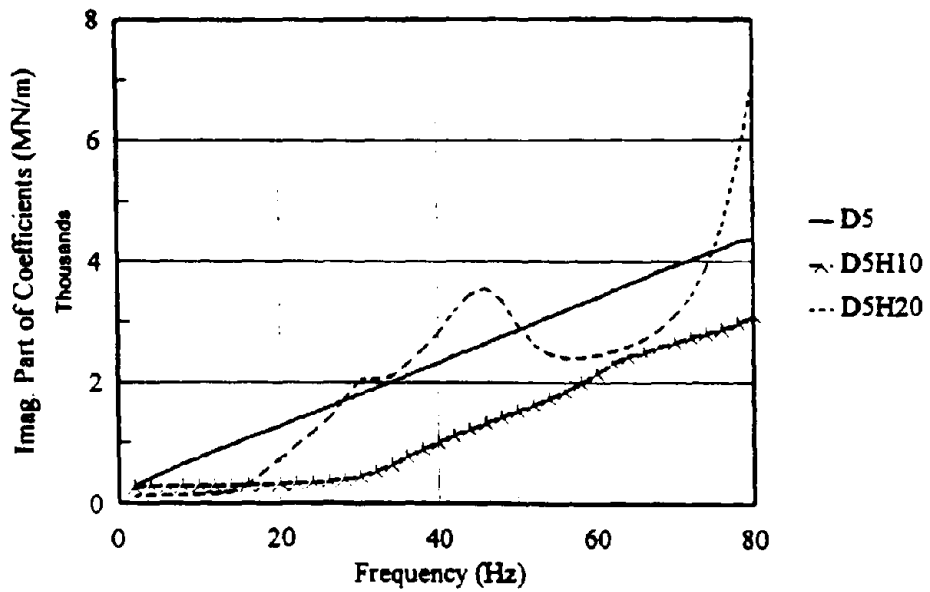


Figure 68. Imaginary Part of Horizontal Dynamic Stiffness Coefficients, Ground System with 5% Damping Ratio

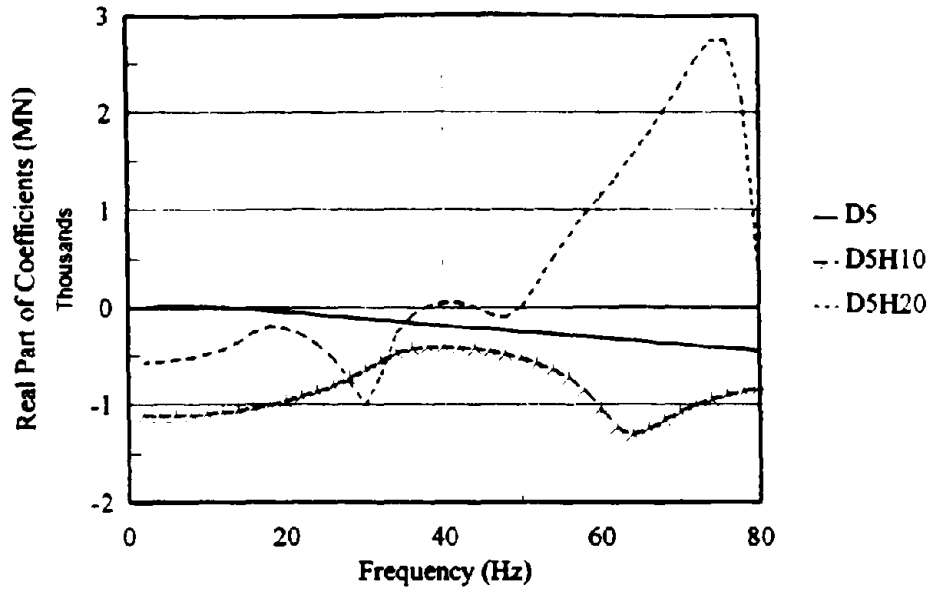


Figure 69. Real Part of Coupling Dynamic Stiffness Coefficients, Ground System with 5% Damping Ratio

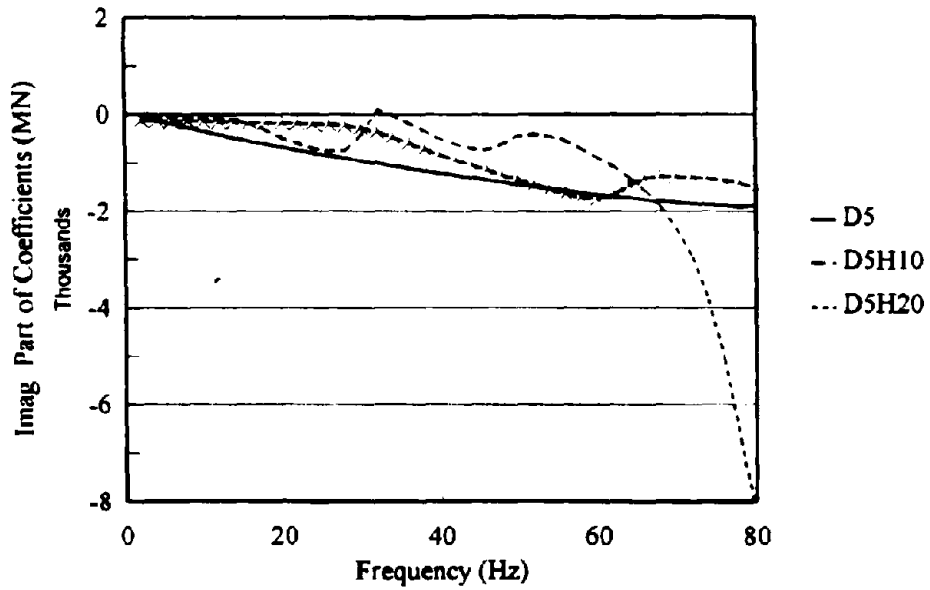


Figure 70. Imaginary Part of Coupling Dynamic Stiffness Coefficients, Ground System with 5% Damping Ratio

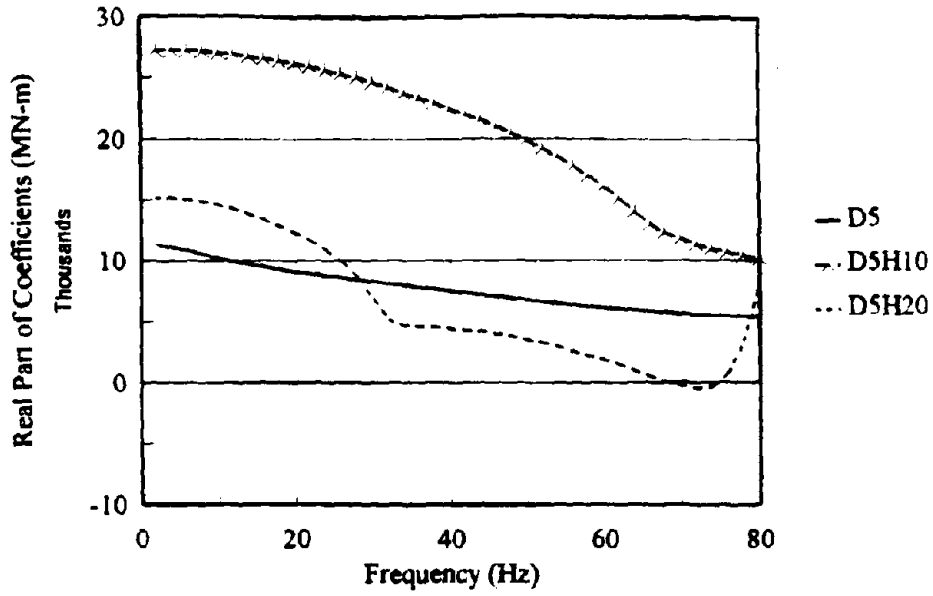


Figure 71. Real Part of Rocking Dynamic Stiffness Coefficients, Ground System with 5% Damping Ratio

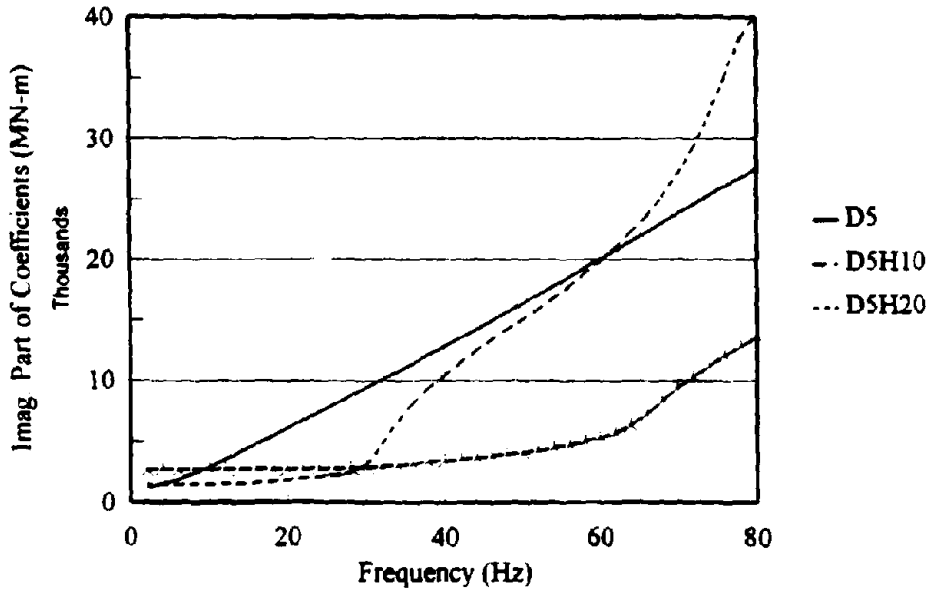


Figure 72. Imaginary Part of Rocking Dynamic Stiffness Coefficients, Ground System with 5% Damping Ratio

part maintains its small value up to their cutoff frequency and then increases as the system's frequency rises.

Time-derivative flexibility coefficients can be obtained as described in Equation (242). First, the inversion of the ground system's dynamic stiffness matrices corresponding to discrete frequencies ranging from 0 to 80 Hz is determined. Then, multiplying the former by their corresponding frequencies and imaginary number results in the desired coefficients. These coefficients of D5, D5H10, and D5H20 are displayed in Figures 73 to 78. All coefficients are equal to zero where their systems' frequencies are also equal to zero. Similar to the ground system's dynamic-stiffness coefficients, the more frequency-dependent coefficients are noticeable in the cases of D5H20. In both D5H10 and D5H20, the small coefficients' real part in the range of low frequency is shown.

3. **Impulse Velocity Coefficients.** An impulse velocity coefficient of time t is a velocity at time t due to impulse force at time equal to 0. To obtain the coefficients, the inverse discrete Fourier transform is applied to the real parts of time-derivative flexibility coefficients in Figures 73, 75, and 77 [Equations (262) and (263)]. The coefficients on the negative side of frequency axis are constructed by forming their complex conjugate pairs. Using the truncated frequency Ω_T of 80 Hz and the sampling step number NS of 160 leads to the frequency increment $\Delta\omega$ of 0.5 Hz, the time increment Δt of 0.00625 sec and then the time range T_F of 1.0 sec [Equations (247) and (248)].

In Figures 79 to 81, the resultant coefficients of D5, D5H10, and D5H20 are shown in the time range of 0 to 0.1 sec. The horizontal impulse velocity coefficients of all three soil conditions, at time $t = 0$, are about the same since the same foundation

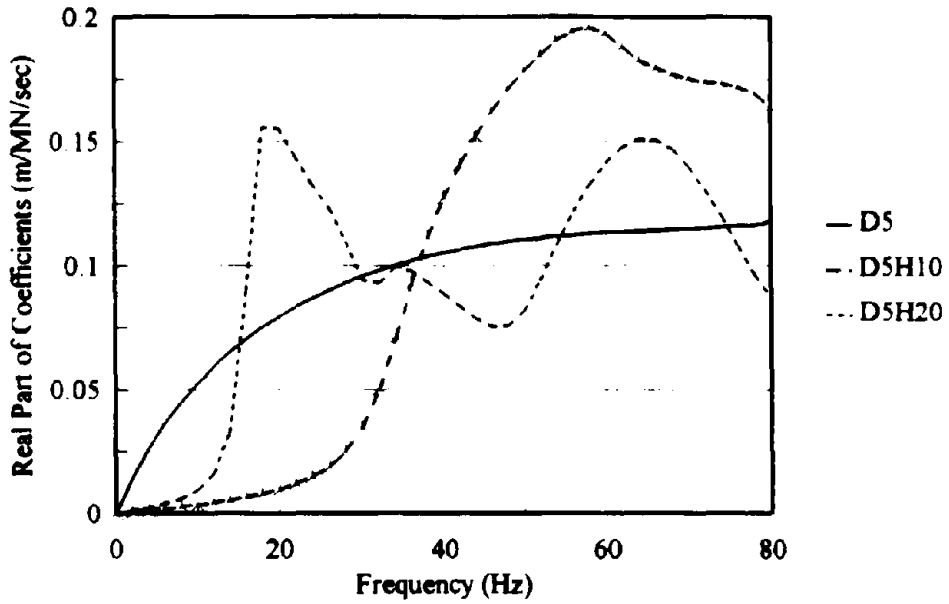


Figure 73. Real Part of Time-derivative Horizontal Flexibility Coefficients, Ground System with 5% Damping Ratio

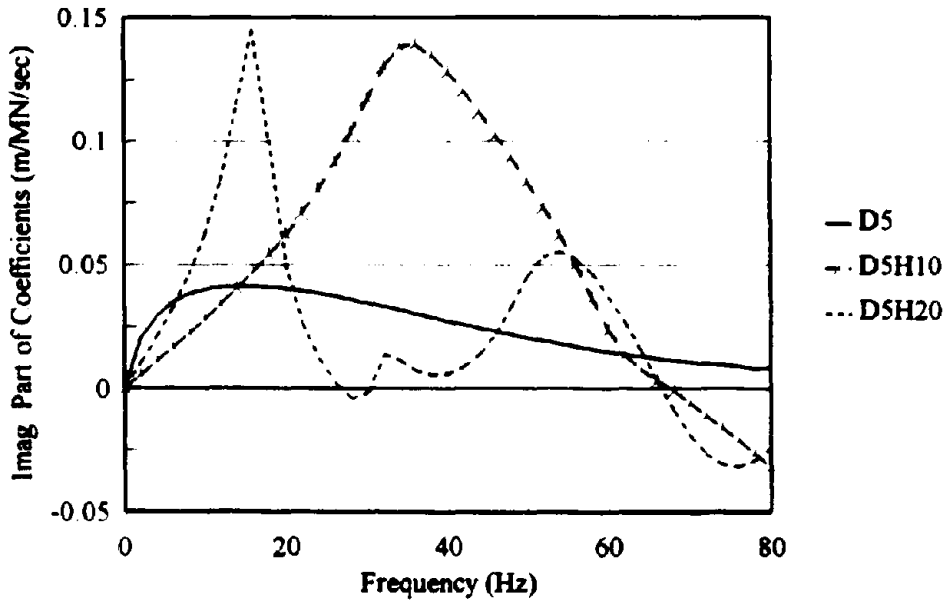


Figure 74. Imaginary Part of Time-derivative Horizontal Flexibility Coefficients, Ground System with 5% Damping Ratio

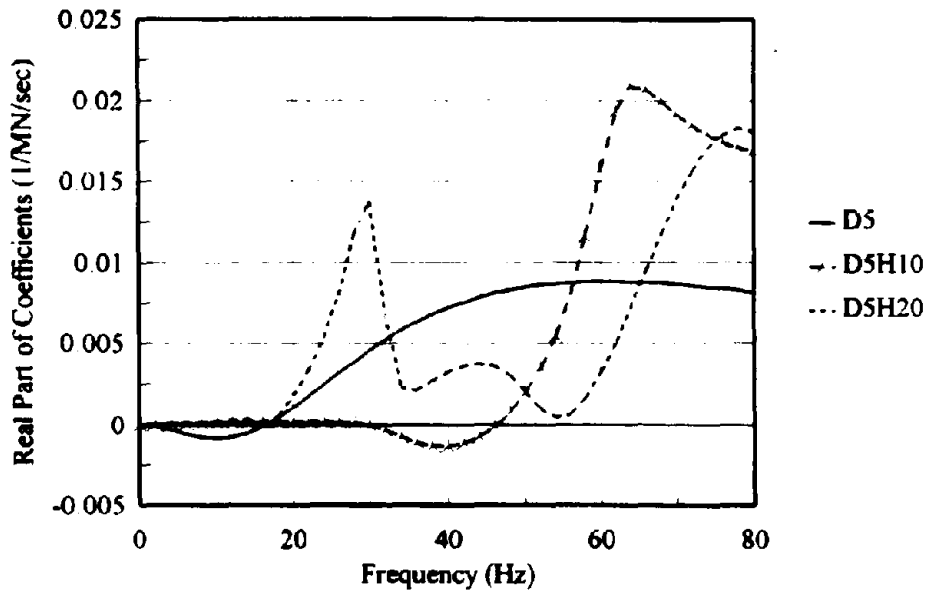


Figure 75. Real Part of Time-derivative Coupling Flexibility Coefficients, Ground System with 5% Damping Ratio

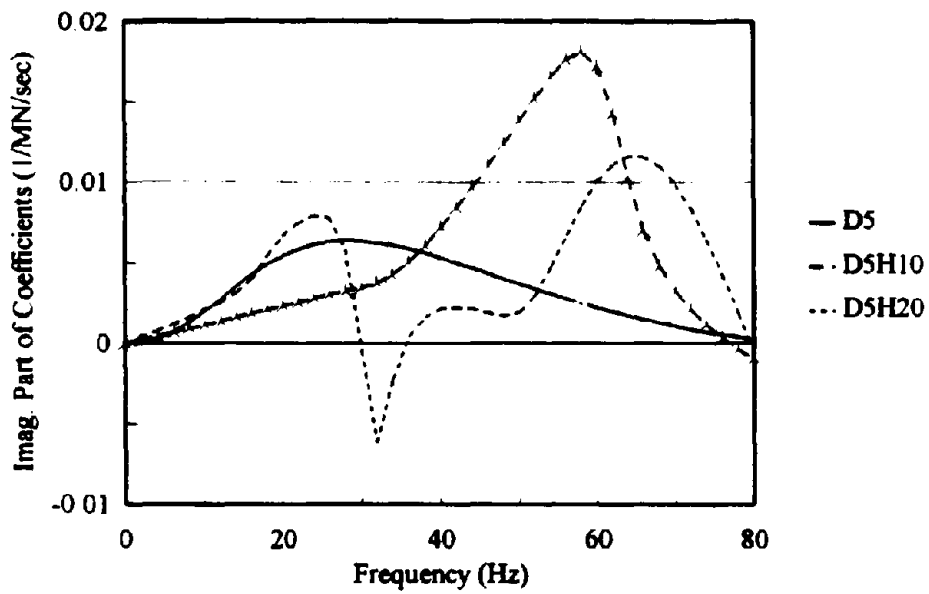


Figure 76. Imaginary Part of Time-derivative Coupling Flexibility Coefficients, Ground System with 5% Damping Ratio

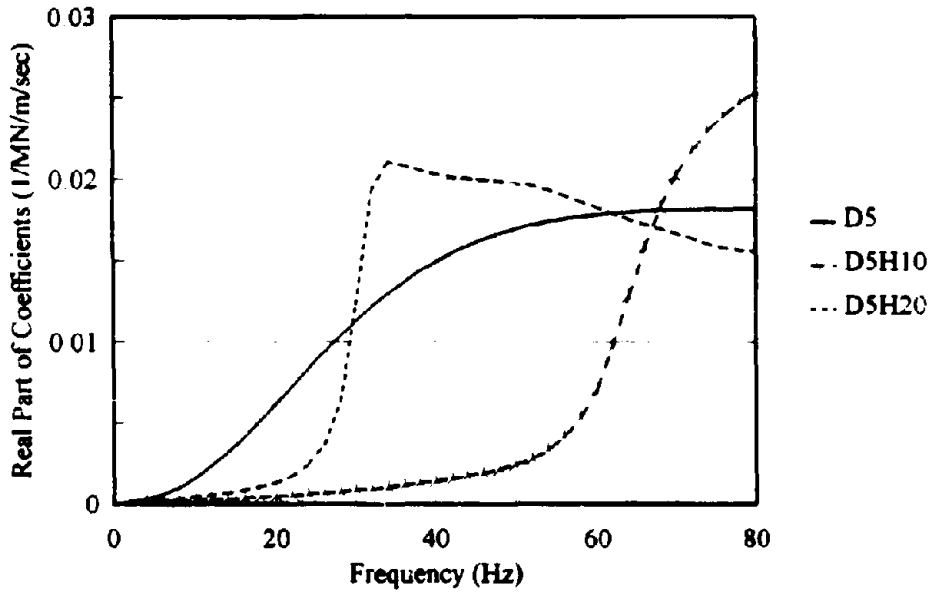


Figure 77. Real Part of Time-derivative Rocking Flexibility Coefficients, Ground System with 5% Damping Ratio

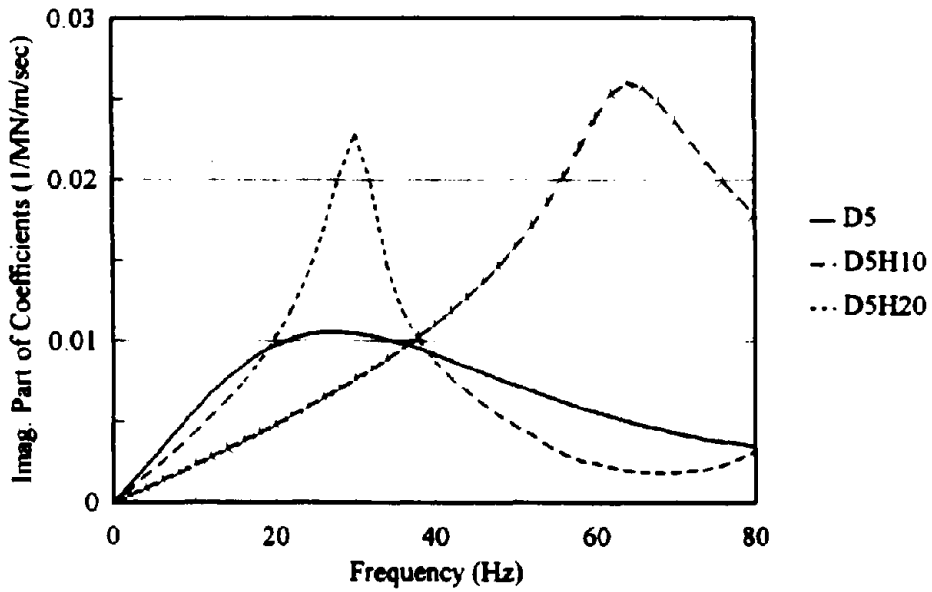


Figure 78. Imaginary Part of Time-derivative Rocking Flexibility Coefficients, Ground System with 5% Damping Ratio

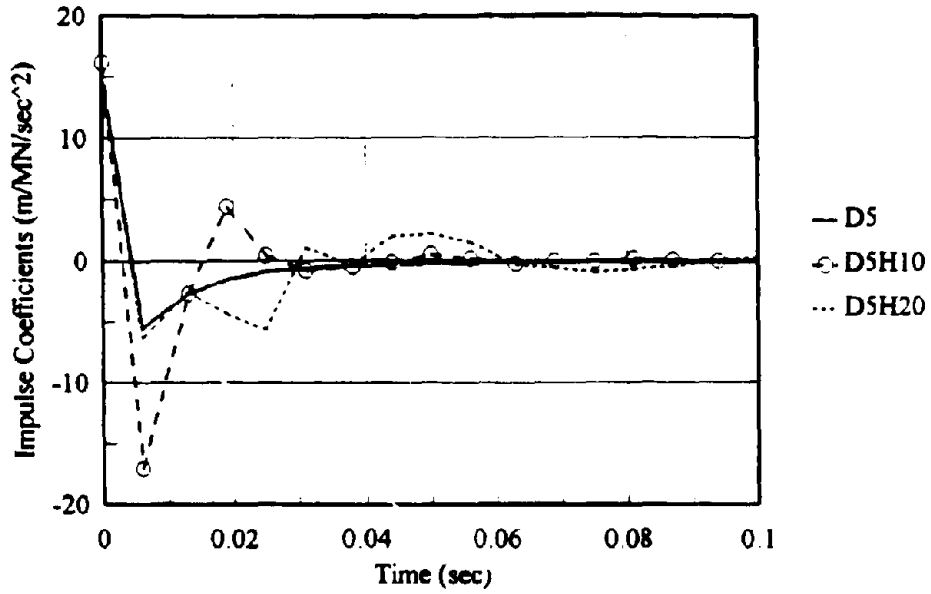


Figure 79. Horizontal Impulse Velocity Coefficients of Ground System, with 5% Damping Ratio

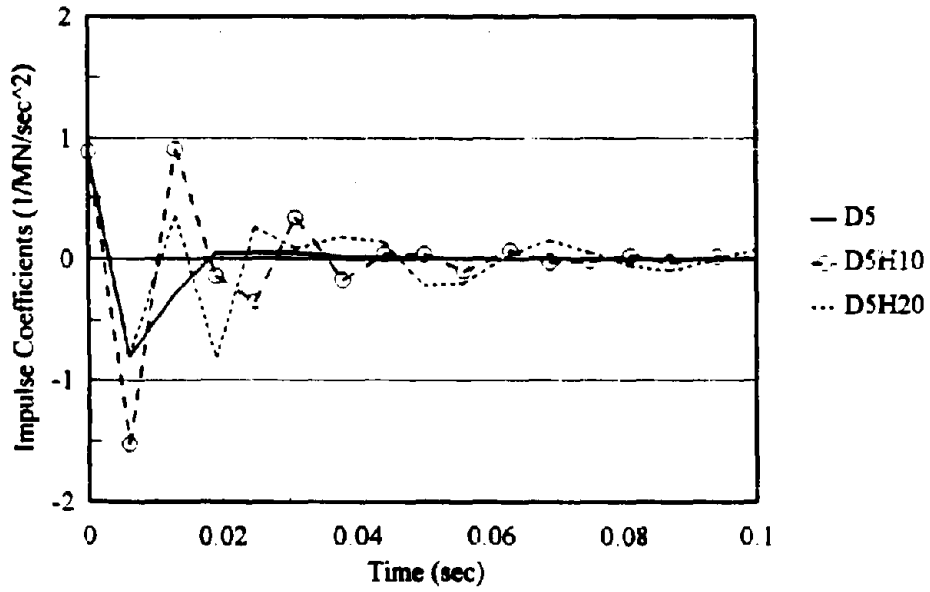


Figure 80. Coupling Impulse Velocity Coefficients of Ground System, with 5% Damping Ratio

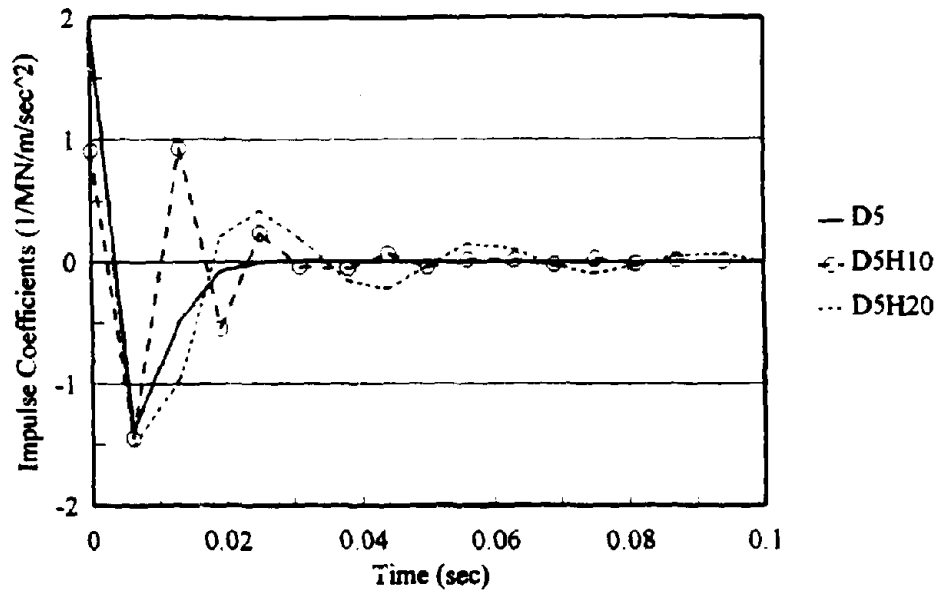


Figure 81. Rocking Impulse Velocity Coefficients of Ground System, with 5% Damping Ratio

embedment and soil type are used. But the rocking coefficient of D5H10 is less than those of D5 and D5H20. The rock base in D5H10 but not in D5H20 has an influence on the rocking component by increasing its stiffness as the former's rock base level is closer to the surface. The coefficients of D5 (half-plane) attenuate faster than D5H10 and D5H20 since more energy in the former propagates toward infinity.

VII. INVESTIGATION OF TOTAL DYNAMIC SYSTEMS WITH AND WITHOUT CONTROL

A. SCOPE OF INVESTIGATION

1. **Concerning Parameters.** In the analysis and design of a dynamic structure-soil interaction system, structure and foundation failure are the primary concern. The former may be categorized into two types; a global failure and a local failure. The local failure will not be discussed here.

Two parameters concerning the structure system's global failure are investigated. First, the failure governed by the system's strain energy is induced by the floor relative displacement excluding rigid motion effect due to foundation rotation. D_s represents the corresponding displacement as the letter s stands for the structure system's strain energy. As depicted in Figure 12, the corresponding displacement (D_s) of a single-story shear structure can be expressed as

$$D_s = x_1^{tg} - x_0^{tg} + h_{c1} \theta_0^{tg} \quad (290)$$

where x_1^{tg} , x_0^{tg} , and θ_0^{tg} are floor translation, foundation translation, and foundation rotation, respectively. Superscript tg indicates the corresponding responses which are of the total dynamic system and relative to those of the ground system. h_{c1} is accumulated height from rotational point 0 to the centroid of floor lumped mass. For a multistory structure, the corresponding displacement (D_s) of the i^{th} floor, where $i = 2, \dots, NO$, can be obtained as

$$D_s(i) = \ddot{x}_i^{ig} - \ddot{x}_{i-1}^{ig} + h_i \ddot{\theta}_0^{ig} \quad (291)$$

where h_i is the i^{th} floor height. Secondly, the floor displacement relative to ground system (\ddot{x}_i^{ig} or D_g) is related to the failure due to a structure collision with adjacent structures, especially for a high slenderness ratio structure. The small letter g of D_g stands for a ground system.

As for a foundation failure, a horizontal interaction force R_x and an interaction moment R_θ as the measurement of the maximum stresses along a structure-soil interface are examined. By extending the free-body diagram in Figure 12 for a multistory shear structure, these forces can be obtained as

$$R_x = -\sum_{i=1}^{NO} m_i (\ddot{x}_i^{ig} + \ddot{x}_0^g) - m_0 (\ddot{x}_0^{ig} + \ddot{x}_0^g - h_{a0} \ddot{\theta}_0^{ig}) \quad (292)$$

$$R_\theta = -\sum_{i=1}^{NO} I_i \ddot{\theta}_0^{ig} - I_0 \ddot{\theta}_0^{ig} + \sum_{i=1}^{NO} m_i h_{ai} (\ddot{x}_i^{ig} + \ddot{x}_0^g) + m_0 h_{a0} (\ddot{x}_0^{ig} + \ddot{x}_0^g - h_{a0} \ddot{\theta}_0^{ig}) \quad (293)$$

where m_i and I_i are the i^{th} floor lumped mass and mass moment of inertia with respect to point 0. m_0 and I_0 are foundation mass and mass moment of inertia with respect to point 0. h_{ai} and h_{a0} are accumulated height from rotational point 0 to the centroid of i^{th} floor lumped mass and foundation mass, respectively. \ddot{x}_i^{ig} and \ddot{x}_0^{ig} are the i^{th} floor and foundation horizontal accelerations, respectively. $\ddot{\theta}_0^{ig}$ is foundation rotational acceleration. Superscript ig indicates all responses are of the total dynamic system and relative to those of the ground system. \ddot{x}_0^g is the horizontal acceleration, at point 0, of the ground system with

rigid interface. Also the interaction forces can be obtained from the ground system's impulse velocity matrix as described in Section III.

In a FIX-model, a horizontal base shear S_{base}^{FIX} and base moment M_{base}^{FIX} are determined and compared with the corresponding forces of an SSI's model, S_{base}^{SSI} and M_{base}^{SSI} , evaluated at the connection between a superstructure and foundation. Using the free body diagrams analogous to that of Figure 12, these forces can be expressed as

$$S_{base}^{FIX} = -\sum_{i=1}^{NO} m_i (\ddot{x}_i^{tb} + \ddot{x}^b) \quad (294)$$

$$M_{base}^{FIX} = \sum_{i=1}^{NO} m_i h_{bi} (\ddot{x}_i^{tb} + \ddot{x}^b) \quad (295)$$

$$S_{base}^{SSI} = -\sum_{i=1}^{NO} m_i (\ddot{x}_i^{ig} + \ddot{x}_0^g) \quad (296)$$

$$M_{base}^{SSI} = -\sum_{i=1}^{NO} I_i \ddot{\theta}_0^g + \sum_{i=1}^{NO} m_i (h_{ai} - h_0) (\ddot{x}_i^{ig} + \ddot{x}_0^g) \quad (297)$$

where \ddot{x}_i^{tb} and \ddot{x}^b are the i^{th} floor acceleration and the horizontal acceleration of the structure-base, respectively. Superscript tb indicates the corresponding responses are of the total dynamic system and relative to that of the structure-base. h_{bi} is the accumulated height from the structure-base to the centroid of the i^{th} floor lumped mass. h_0 is the depth of foundation.

To understand a change in the behavior of a dynamic system, the system's properties such as frequency ratio and damping ratio are also explored. The frequency

ratio is determined by the first translational mode's natural frequency of an SSI-model divided by that of a FIX-model. The plant matrix $[D]$ of a dynamic system (discussed in Section III) yields $N\mathcal{O}$ complex conjugate pairs of eigenvalues $\alpha_i \pm i\beta_i$, and their corresponding eigenvectors $\{a_i\} \pm i\{b_i\}$, where $i = \sqrt{-1}$. Therefore, the i^{th} mode's natural frequency (in radian) and its corresponding damping ratio of the system can be obtained as β_i and $-\alpha_i/\beta_i$, respectively.

2. **Governing Parameters.** Soil condition including embedment to foundation half-width ratio, structure property, type of excitation input, and state weighting matrix $[S]$ (a control parameter) are the governing parameters. The structure properties consist of a fixed-base natural frequency, the i^{th} floor mass ratio \bar{m}_i , a footing mass ratio \bar{m}_0 , and a structure slenderness ratio \bar{h} . The corresponding ratios are defined as follows.

$$\bar{m}_i = \frac{m_i}{\rho B^3} \quad (298)$$

$$\bar{m}_0 = \frac{m_0}{\rho B^3} \quad (299)$$

$$\bar{h} = \frac{h}{B} \quad (300)$$

where m_i, m_0 , and h are the i^{th} floor mass, foundation mass, and structure height, respectively. ρ is soil mass density of the study soil condition. B is foundation half-width. The i^{th} floor and foundation mass moments of inertia, I_i and I_0 , with respect to point 0 are also a substantial structural mass-dependent property and can be expressed as

$$I_i = m_i \left(\frac{W_i^2}{12} + h_{ai}^2 \right) \quad (301)$$

$$I_0 = m_0 \left(\frac{W_f^2}{12} + \frac{h_0^2}{3} \right) \quad (302)$$

where W_s and W_f are structure and foundation width. The latter equals to $2B$. In Equation (302), the centroid of a rectangular foundation is assumed to be at the midpoint of foundation depth.

As for excitation input, 1940 El Centro earthquake acceleration record, north-south component and 1985 Mexico earthquake acceleration record, east-west component are used as horizontal acceleration inputs of a FIX-model (\ddot{x}^b) and an SSI-model (\ddot{x}_0^f). By assuming a vertically incident shear wave and a shallow embedded foundation in an SSI-model, the rotational acceleration, at point 0 of a ground system's rigid interface, is neglected. The first 20 seconds of El Centro earthquake record and the 50-70 seconds of Mexico earthquake record are shown in Figure 82. Their characteristics (see in Figure 83) are specified by the maximum response of a one-degree-of-freedom FIX-model system with 2% damping ratio excited by their time history records.

In a control system, the weighting matrix $[S]$ (discussed in Section IV) is selected as an arbitrary row-matrix where both s_D and s_V on the R^{th} row are equal to s_1 . The s_1 is any real number and varied in order to obtain the optimal performance index. For each controller, R equals $NO-ONC+1$, where ONC is one of the controller's node number which does not allow any two consecutive rows of the matrix to be filled.

B. INVESTIGATION OF SINGLE STORY WITHOUT CONTROL

A shear wave velocity of 400 m/sec and shear modulus of 320 MN/sq.m are used for three types of soil condition, D5, D5H10, and D5H20 (discussed in Section VI) which

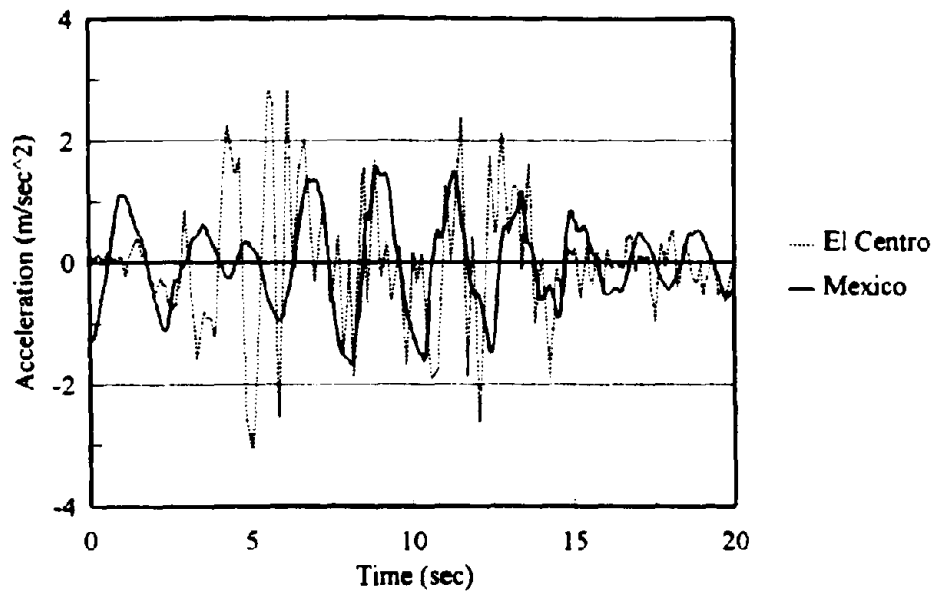


Figure 82. Acceleration Records of 1940 El Centro Earthquake, North-south and 1985 Mexico Earthquake, East-west (50-70sec)

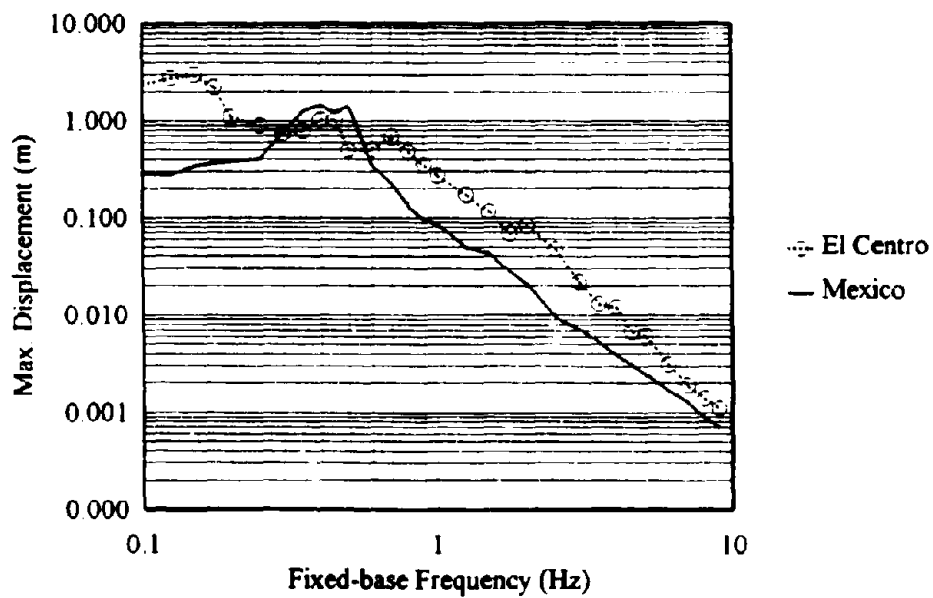


Figure 83. Maximum Displacement Response vs. Fixed-base Frequency, 2% Damping FIX-model, El Centro and Mexico Earthquakes

are designated as S0-, S1-, and S2-soil condition, respectively. These three soil conditions are described as a half-plane, a 3.0-meter depth layer on rock, and a 6.0-meter depth layer on rock, respectively. The foundation embedment and half-width of the named soil conditions are 1.5 m and 3.0 m, respectively.

The FIX-models and SSI-models are considered with 2% damping ratio and natural frequencies of 0.7 Hz, 1.25 Hz, and 3.0 Hz of a fixed-base frame. When the FIX-models of 1.25 Hz and 3.0 Hz are subjected to El Centro earthquake, the maximum displacements of 0.173 m and 0.022 m are produced, respectively (see Figure 83). In the same figure, the maximum responses of 0.224 m and 0.050 m can be obtained for the FIX-models of 0.7 Hz and 1.25 Hz subjected to Mexico earthquake. Therefore the structures with the fixed-base frequency of 3.0 Hz and 1.25 Hz are considered to be stiff structures corresponding to El Centro and Mexico earthquakes, respectively. Those with a frequency of 1.25 Hz and 0.7 Hz are regarded as flexible structures corresponding to the same earthquakes.

Floor mass ratios vary from 1 to 20 while the footing mass ratio is equal to 2. The floor mass ratios of 1 and 20 represent the lightest and heaviest (massive) structure, respectively. For a foundation width of 6.0 m, foundation depth of 1.5 m, and soil mass density of 2.0 gm/cu cm, the specified footing mass ratio yields the foundation mass of 0.108 Kton and the foundation mass moment of inertia of 0.405 Kton-sq.m. Floor masses and mass moments of inertia with respect to point 0, for the floor width of 5.0 m and the indicated structure slenderness ratios, are listed in Table III. Three structure slenderness ratios of 1, 3, and 5, which represent a low-rise, medium-rise, and high-rise structure, are

Table III. Floor Mass and Mass Moment of Inertia

Floor Mass Ratio	Floor Mass (Kton)	Floor Mass Moment of Inertia (Kton-sq m)		
		h1	h3	h5
1	0.054	1.206	6.066	14.814
2	0.108	2.412	12.132	29.628
3	0.162	3.618	18.198	44.442
4	0.216	4.824	24.264	59.256
5	0.270	6.030	30.330	74.070
6	0.324	7.236	36.396	88.884
7	0.378	8.442	42.462	103.698
8	0.432	9.648	48.528	118.512
9	0.486	10.854	54.594	133.326
10	0.540	12.060	60.660	148.140
11	0.594	13.266	66.726	162.954
12	0.648	14.472	72.792	177.768
13	0.702	15.678	78.858	192.582
14	0.756	16.884	84.924	207.396
15	0.810	18.090	90.990	222.210
16	0.864	19.296	97.056	237.024
17	0.918	20.502	103.122	251.838
18	0.972	21.708	109.188	266.652
19	1.026	22.914	115.254	281.466
20	1.080	24.120	121.320	296.280

studied. These ratios are named as h1, h3, and h5, respectively. For the study foundation half-width, they correspond to the floor height of 3.0 m, 9.0 m, and 15.0 m, respectively

1. **Structural Response vs. Time.** The responses of the FIX-model and SSI-model subjected to El Centro earthquake are shown in Figures 84 and 85. The displacement responses D_s and D_g of a SSI-model are compared to the response of a FIX-model. The fixed-base natural frequencies of both models are equal to 1.25 Hz. In SSI-model, the structure having the floor mass ratio of 10 and the slenderness ratio of 5 (h5) sits on a rigid rectangular foundation. The foundation has its mass ratio equal to 2

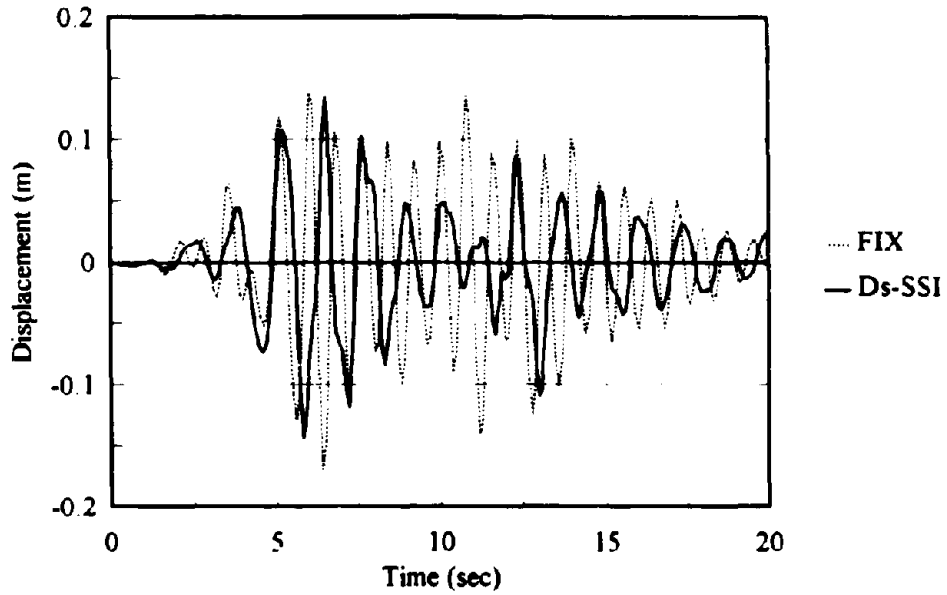


Figure 84. FIX Response and SSI Response (Ds), 5h-slenderness Ratio, $f=1.25\text{Hz}$, Floor & Footing Mass Ratio=10.0 & 2.0, S0-soil Condition, El Centro Earthquake

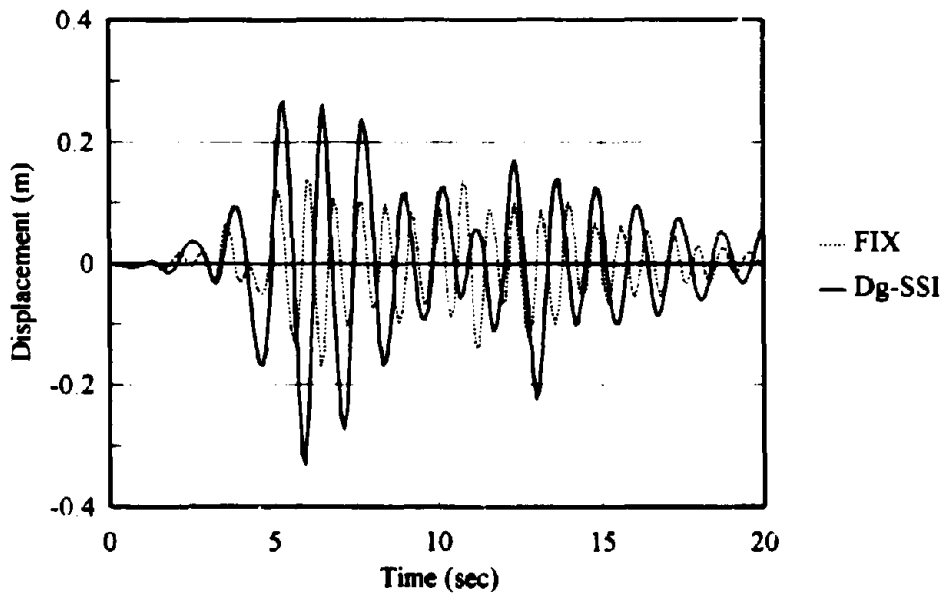


Figure 85. FIX Response and SSI Response (Dg), 5h-slenderness Ratio, $f=1.25\text{Hz}$, Floor & Footing Mass Ratio=10.0 & 2.0, S0-soil Condition, El Centro Earthquake

and is embedded in the S0-soil. The maximum of D_s in Figure 84 (0.146 m at time equal to 5.81 sec) is less than that of the FIX-model's displacement (0.173 m at time equal to 6.42 sec). In Figure 85, the maximum of D_g (0.338 m at time equal to 5.86 sec) is greater than that of the FIX-model's displacement. In both figures, a longer period of response in the SSI-model is noticeable as a result of the system becoming more flexible (system's fundamental frequency reduces from 1.25 Hz in the FIX-model to 1.04 Hz in the SSI-model).

Figures 86 and 87 show the same comparison for the 0.7 Hz fixed-base natural frequency's models subjected to Mexico earthquake. Other structure properties and soil conditions are the same. The maximum of D_s in Figure 86 (0.257 m at time equal to 7.99 sec) and the maximum of D_g in Figure 87 (0.349 m at time equal to 8.01 sec) are greater than that of FIX-model's displacement (0.224 m at time equal to 7.875 sec). The system's fundamental frequency drops from 0.7 Hz in the FIX-model to 0.66 Hz in the SSI-model.

This leads to the conclusion that a dynamic system becomes more flexible when considering structure-soil interaction. Furthermore, the maximum of D_g is greater than that of the FIX-model's displacement as a result of footing translation and rotation. But the maximum of D_s is not necessary greater than that of the FIX-model's displacement.

2. Effects of Floor Mass and Slenderness Ratios. In Figures 88 to 91, the floor mass ratio of SSI-model varies from 1 to 20 but the fixed-base natural frequency is kept constant of 1.25 Hz by adjusting the structural stiffness with the varying masses. Structure slenderness ratios are selected to be h1, h3, and h5. The rigid foundation of mass ratio equal to 2 is embedded in the S0-soil. This system is subjected to El Centro

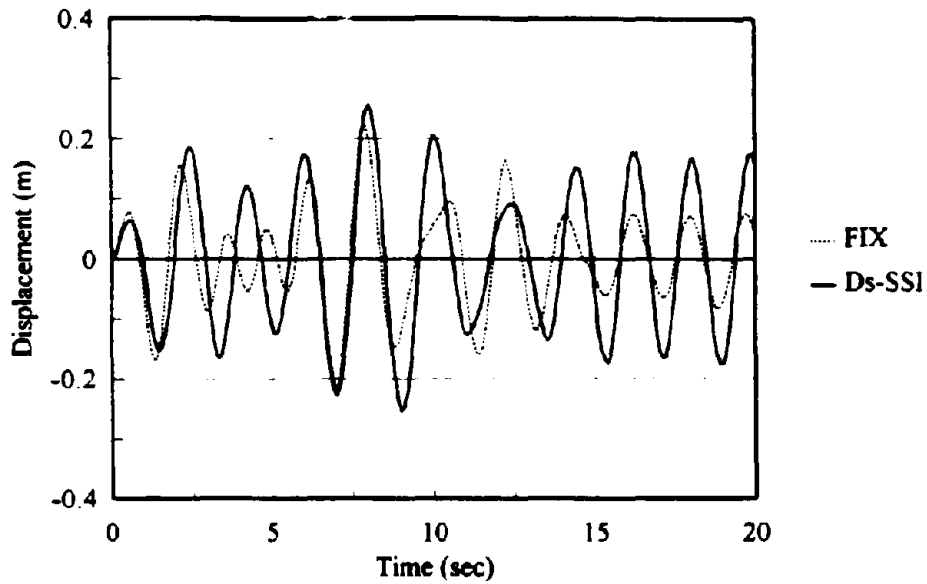


Figure 86. FIX Response and SSI Response (Ds), 5h-slenderness Ratio, $f=0.7\text{Hz}$, Floor & Footing Mass Ratio=10.0 & 2.0, S0-soil Condition, Mexico Earthquake

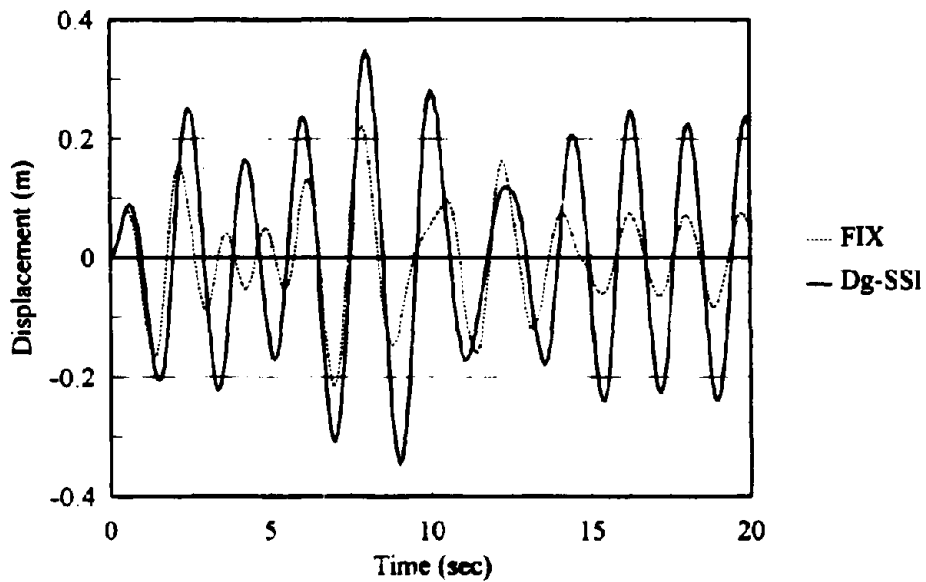


Figure 87. FIX Response and SSI Response (Dg), 5h-slenderness Ratio, $f=0.7\text{Hz}$, Floor & Footing Mass Ratio=10.0 & 2.0, S0-soil Condition, Mexico Earthquake

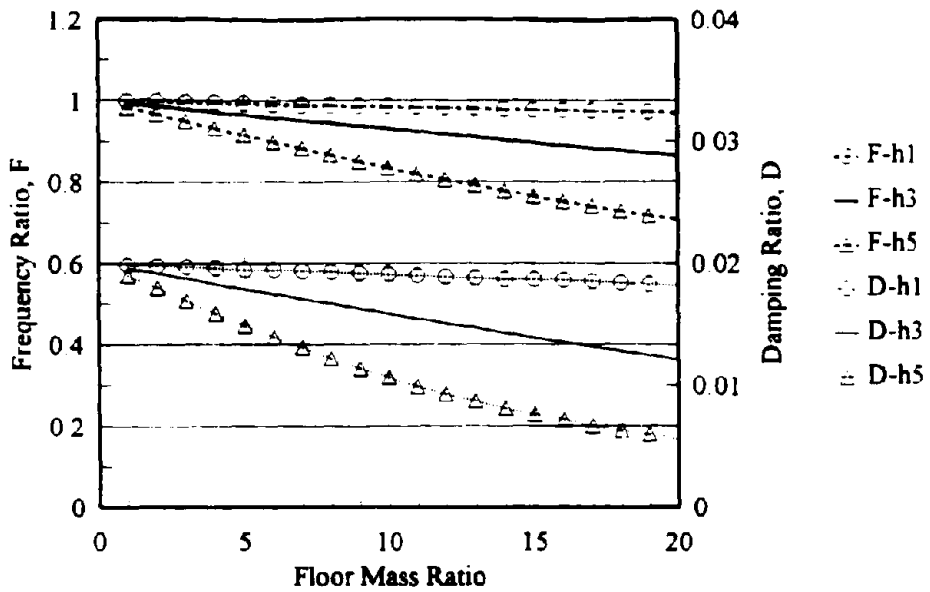


Figure 88. System Properties vs. Floor Mass Ratio, S0-soil Condition, $f=1.25\text{Hz}$, Footing Mass Ratio=2.0, El Centro Earthquake

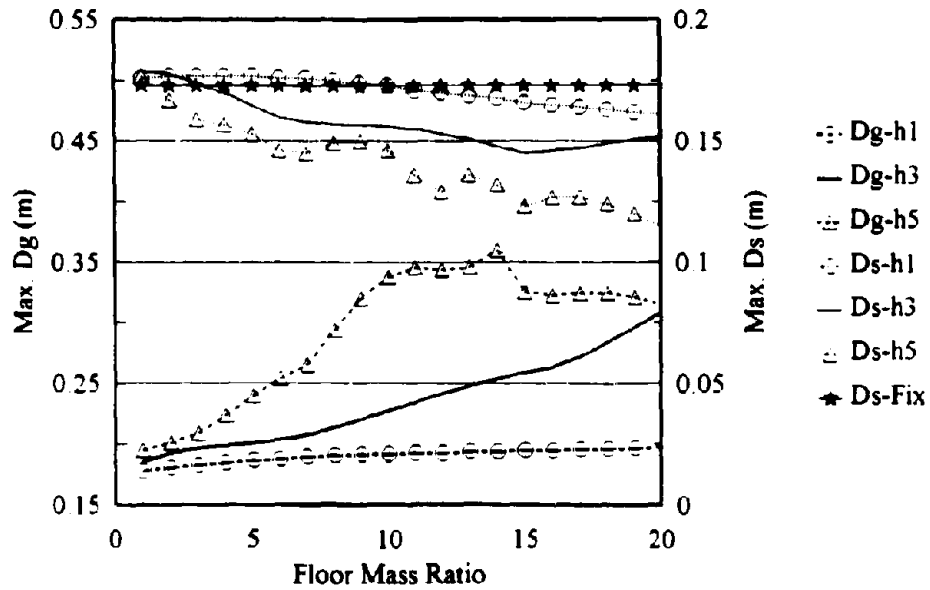


Figure 89. Maximum Responses vs. Floor Mass Ratio, S0-soil Condition, $f=1.25\text{Hz}$, Footing Mass Ratio=2.0, El Centro Earthquake

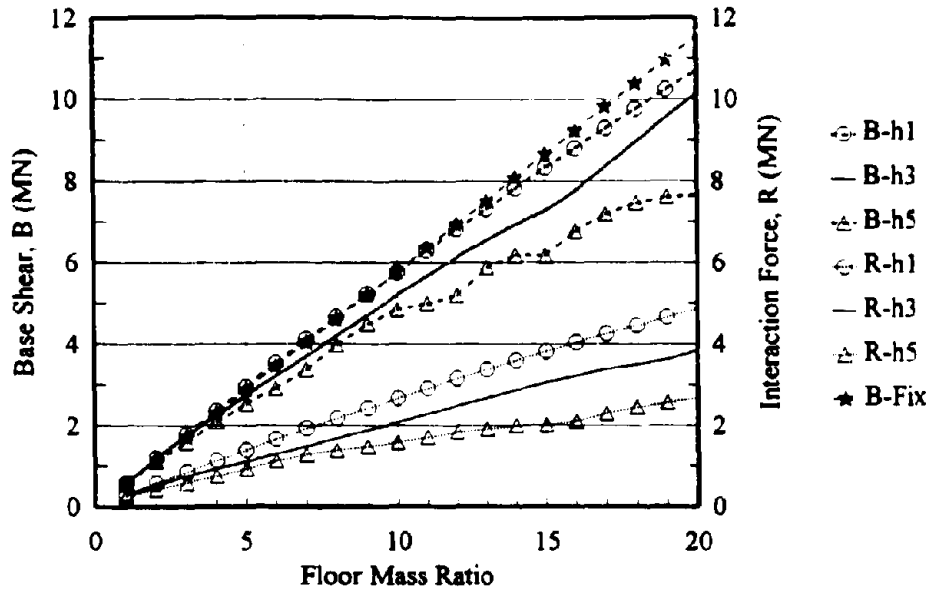


Figure 90. Maximum Horizontal Forces vs. Floor Mass Ratio, S0-soil Condition, $f=1.25\text{Hz}$, Footing Mass Ratio=2.0, El Centro Earthquake

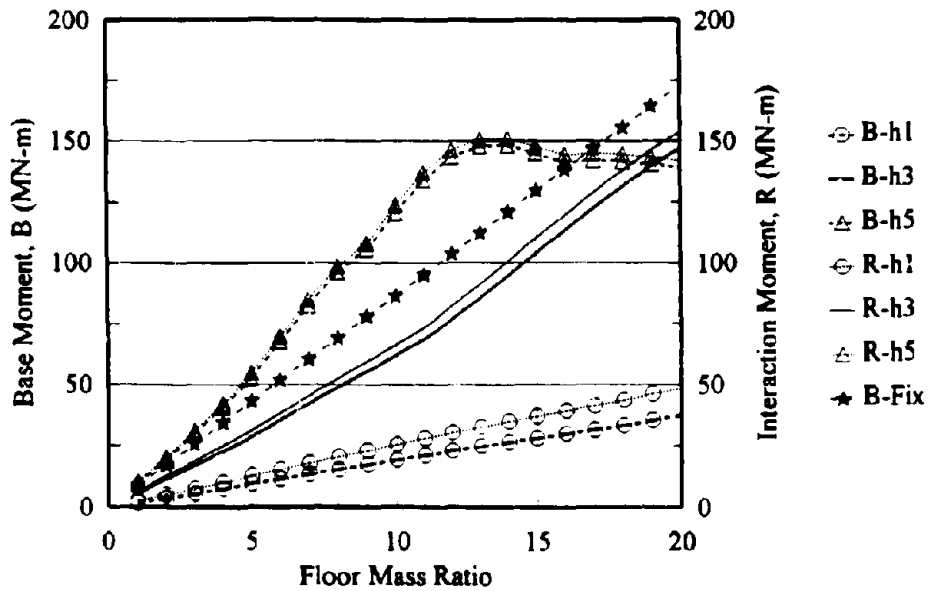


Figure 91. Maximum Moments vs. Floor Mass Ratio, S0-soil Condition, $f=1.25\text{Hz}$, Footing Mass Ratio=2.0, El Centro Earthquake

earthquake. As the floor mass ratio increases, frequency ratio and damping ratio decrease (see Figure 88). The effect is more prominent for higher slenderness ratio. This implies that, for an SSI-model, greater floor mass and height lead to a more flexible system with less damping.

As a single-story SSI-model has three degrees of freedom, its three normal modes include a rigid translational mode, a relative translational mode, and a rigid rocking mode. The rigid translational and rocking modes involve a horizontal translation and rotation of the system's rigid-body. The former reflects a foundation's horizontal translation and then a horizontal interaction force. The latter contributes to a foundation's rotation and then a whole system's rotation. An interaction moment as well as a base moment can be used to describe this rocking component. The relative translational mode involves relative displacement between floor and foundation excluding a rigid-body rotational effect. This relative displacement is equal to D_s and proportional to a base shear. While D_s is only influenced by the relative translational mode, D_g (which is the floor displacement relative to a ground system) is affected by all three modes, the rigid translational, relative translational, and rigid rocking modes.

In Figure 89, the increasing of the maximum D_g but decreasing of the maximum D_s occurs as the floor mass ratio increases. A greater effect is noticeable in the structure with higher slenderness ratio (h_3 and h_5). The maximum D_s of the massive structure (floor mass ratio = 10 to 20) is less than the maximum FIX-model's displacement. Therefore, for the cases studied, greater floor mass and height results in less importance of the relative translational mode but more importance of the rigid rocking mode. The change of the

maximum D_g in the structure with h_5 is less in the floor mass ratio range of 10 to 20 than that of 0 to 10. This phenomena also occurs in its maximum base moment and interaction moment (see Figure 91) since they are the effect of the same cause, foundation rocking. The maximum D_s of the structure with higher slenderness ratio is smaller as is its maximum base shear shown in Figure 90. Therefore, the higher floor height leads to the lesser maximum base shear and horizontal interaction force. The difference between the maximum base shears and horizontal interaction forces is the result of foundation's translations. These maximum base shears and horizontal interaction forces of the SSI-model are less than the maximum base shear of the FIX-model. In contrast, the higher floor height results in the greater maximum base moment and interaction moment as shown in Figure 91. Especially for h_5 -slenderness ratio, the maximum base moment and interaction moment of the SSI-model are greater than the maximum base moment of the FIX-model.

In Figures 92 to 94, the same investigation is also made for 0.7 Hz fixed-base natural frequency's system subjected to Mexico earthquake. In the range of a massive structure (floor mass ratio = 10 to 20) with h_5 -slenderness ratio, a large increase of both maximum D_g and D_s occurs and the maximum D_s is greater than the maximum FIX-model's displacement (see Figure 92). This is due to the dominance of the system's relative translational and rigid rocking mode. As shown in Figure 93, the maximum base shear of the corresponding system is very high which implies the relative translational mode's dominance and thus results in the large maximum D_s . It should be noted that this increase of maximum D_s is inconsistent with the previous cases studied. In the massive

structure range of Figure 94, the larger maximum base moment and interaction moment imply the larger contribution of the rocking mode.

The behavior of a dynamic system depends upon the combination of the system's dominant modes. The influence of floor mass ratio and structure slenderness ratio on these dominant modes is different for various systems. In general, the larger floor mass and slenderness ratios lead to the larger maximum D_g , base moment, and interaction moment as the result of the more foundation rocking. Dominance of the relative translation mode as factors of the floor mass and slenderness ratio is not certain. Therefore, as the ratios rise, the maximum D_s decreases in some cases but increases in others. In most cases, the maximum base shear and horizontal interaction force increase as the slenderness ratio decreases.

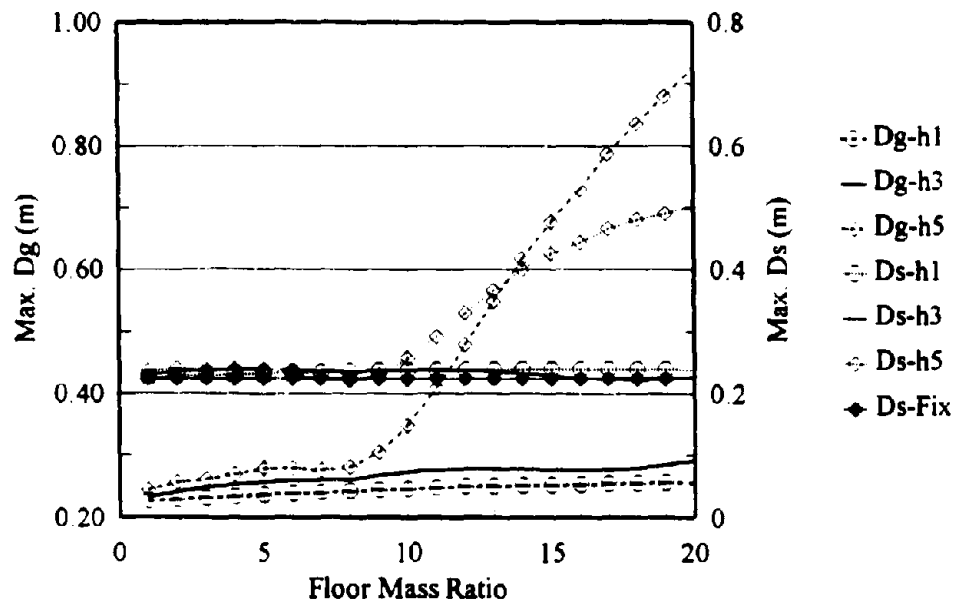


Figure 92. Maximum Responses vs. Floor Mass Ratio, S0-soil Condition, $f=0.70\text{Hz}$, Footing Mass Ratio=2.0, Mexico Earthquake

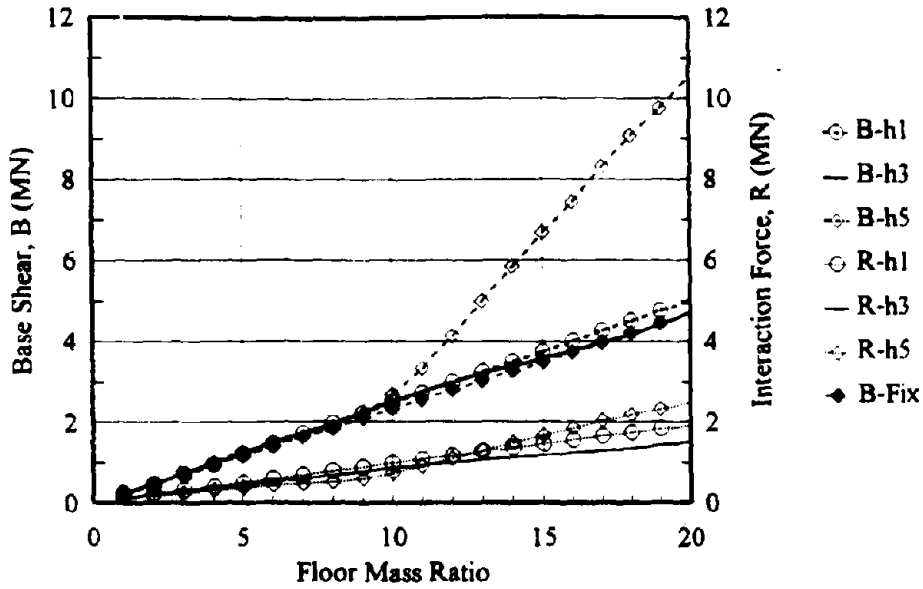


Figure 93. Maximum Horizontal Forces vs. Floor Mass Ratio, S0-soil Condition, $f=0.70\text{Hz}$, Footing Mass Ratio=2.0, Mexico Earthquake

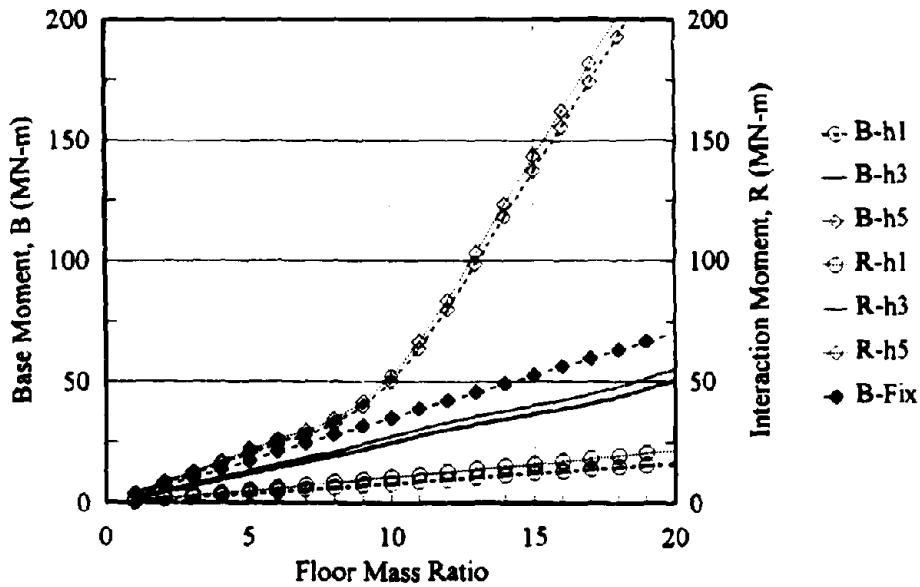


Figure 94. Maximum Moments vs. Floor Mass Ratio, S0-soil Condition, $f=0.70\text{Hz}$, Footing Mass Ratio=2.0, Mexico Earthquake

3. **Effects of Fixed-base Frequency.** Figures 95 to 98 demonstrate the effects of fixed-base frequency (1.25Hz and 3.0Hz) for a high-rise structure (h5- slenderness ratio). The similar demonstration for a low-rise structure (h1-slenderness ratio) is shown in Figures 99 to 102. The S0-soil condition and El Centro earthquake are used. Other structure properties are not changed. Figures 95 and 99 indicate the higher fixed-base frequency ($f_{3.0}$) and the higher slenderness ratio (h5) lead to greater changes in the frequency ratio and damping ratio. The lower frequency ratio is a result of the system becoming more flexible.

In Figure 96, the maximum D_g of the high-rise structures having 1.25 Hz fixed-base frequency (flexible structure) and 3.0 Hz fixed-base frequency (stiff structure) increases as the floor mass ratio rises. The increase in the stiff structure is greater than that in the flexible structure. These increases are roughly proportional to the differences between the FIX-model's and SSI-model's maximum base moments (see Figure 98). This implies that the increases in the maximum of D_g are predominantly a contribution of foundation rocking. For the massive stiff structure (floor mass ratio=15-20 and $f_{3.0}$), the rigid translational mode is also part of the increase of the maximum D_g . In Figure 97, the corresponding system's horizontal interaction force's sharp increase and larger value than the system's base shear hints at the dominance of a rigid translational mode. As the floor mass ratio increases in Figure 96, the decrease of the maximum D_s in the flexible structure ($f_{1.25}$) is more obvious than that in the stiff structure ($f_{3.0}$). Also in Figure 97, the difference between the FIX-model's and SSI-model's maximum base shears of the flexible structure system ($f_{1.25}$) is greater than that of the stiff structure system ($f_{3.0}$). This

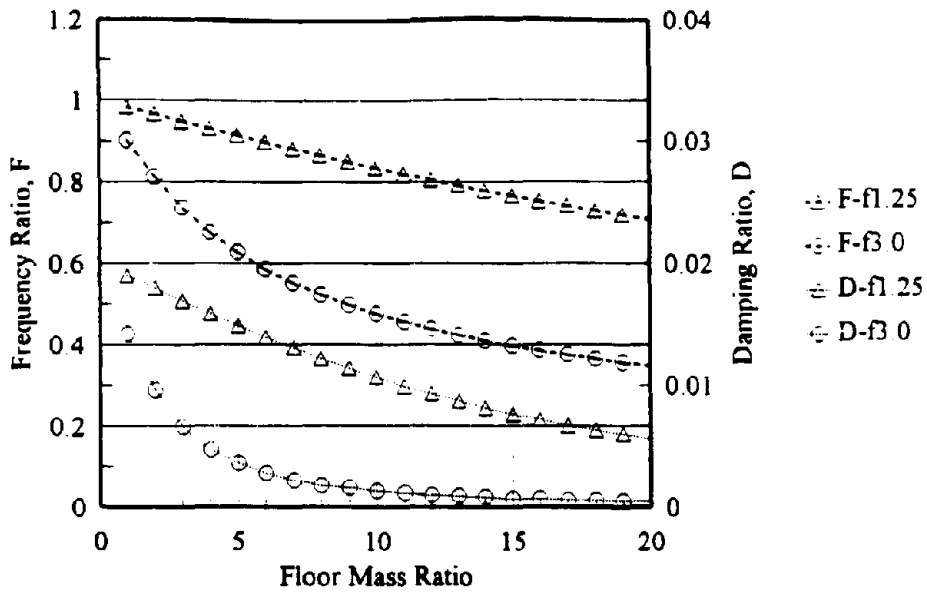


Figure 95. System Properties vs. Floor Mass Ratio, h5-slenderness Ratio, S0-soil Condition, Footing Mass Ratio=2.0, El Centro Earthquake

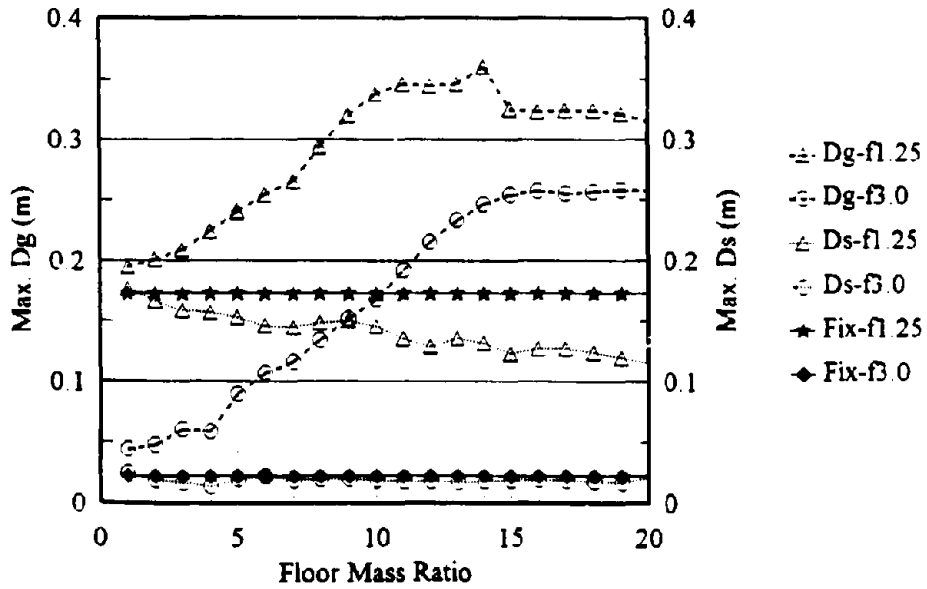


Figure 96. Maximum Responses vs. Floor Mass Ratio, h5-slenderness Ratio, S0-soil Condition, Footing Mass Ratio=2.0, El Centro Earthquake

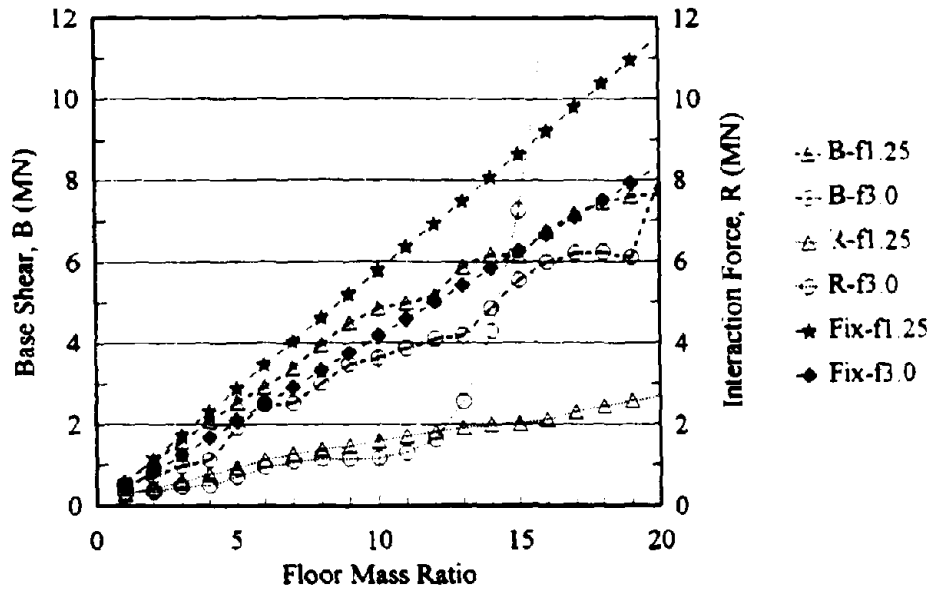


Figure 97. Maximum Horizontal Forces vs. Floor Mass Ratio, S0-soil Condition, h5-slenderness Ratio, Footing Mass Ratio=2.0, El Centro Earthquake

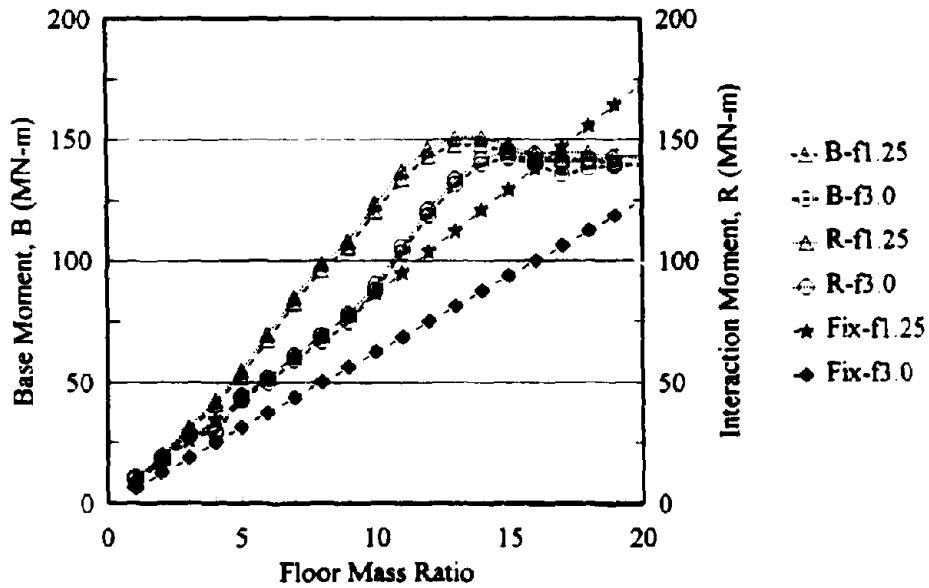


Figure 98. Maximum Moments vs. Floor Mass Ratio, h5-slenderness Ratio, S0-soil Condition, Footing Mass Ratio=2.0, El Centro Earthquake

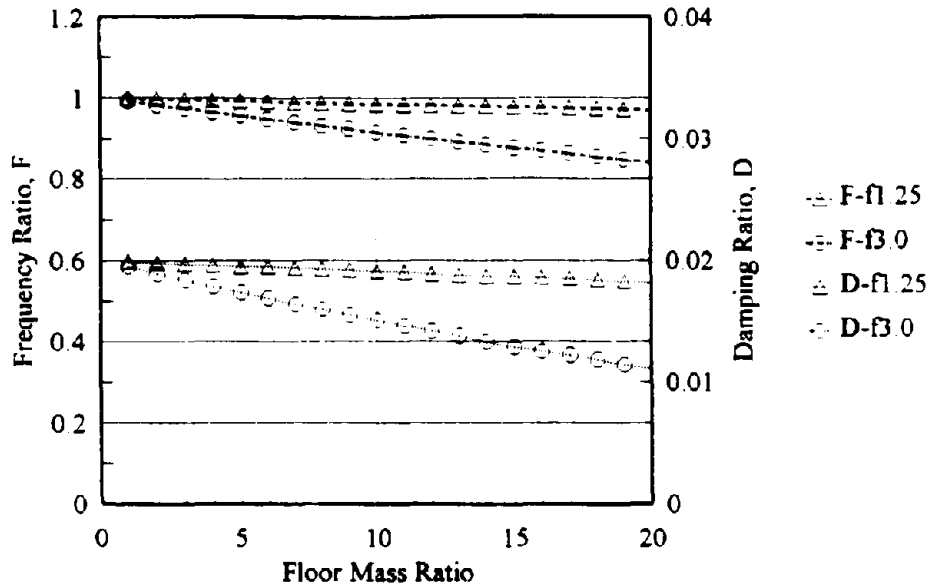


Figure 99. System Properties vs. Floor Mass Ratio, h1-slenderness Ratio, S0-soil Condition, Footing Mass Ratio=2.0, El Centro Earthquake

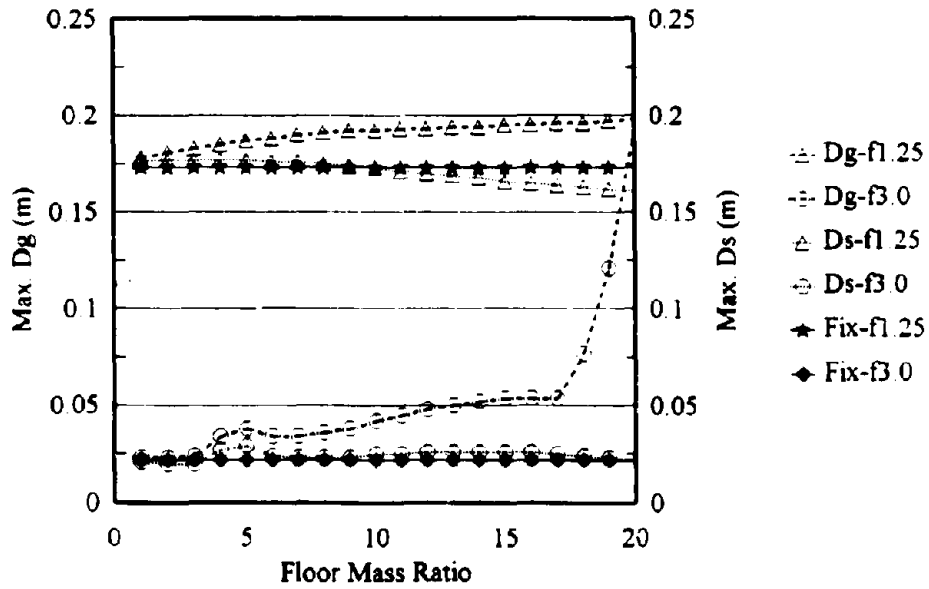


Figure 100. Maximum Responses vs. Floor Mass Ratio, h1-slenderness Ratio, S0-soil Condition, Footing Mass Ratio=2.0, El Centro Earthquake

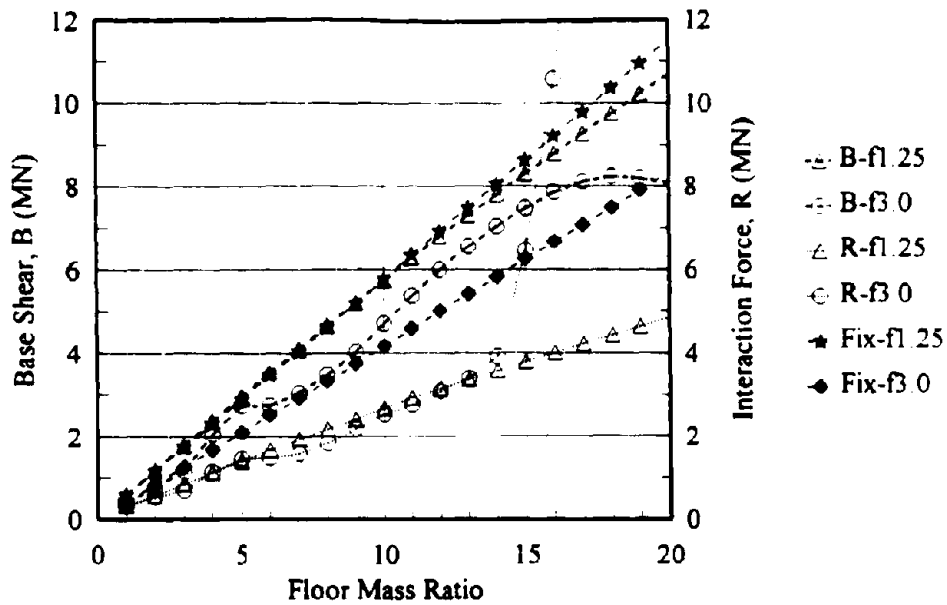


Figure 101. Maximum Horizontal Forces vs. Floor Mass Ratio, S0-soil Condition, h1-slenderness Ratio, Footing Mass Ratio=2.0, El-centro Earthquake

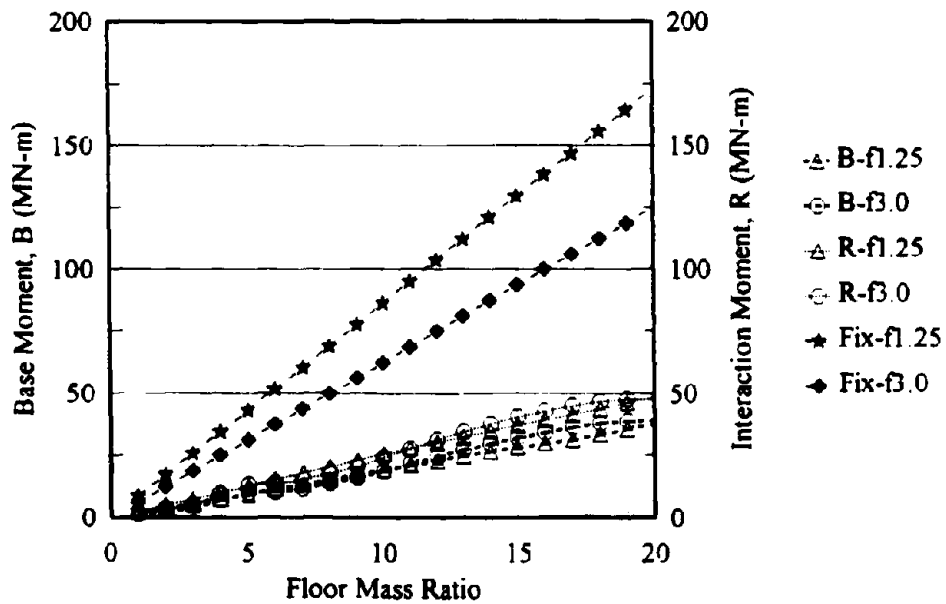


Figure 102. Maximum Moments vs. Floor Mass Ratio, h1-slenderness Ratio, S0-soil Condition, Footing Mass Ratio=2.0, El Centro Earthquake

implies the greater importance of a relative translational mode in the stiff structure system. Both the maximum D_s 's and base shears of the SSI-models are less than those of the FIX-models.

In the low-rise structure (see Figure 100), the increase in the maximum D_g as a function of the floor mass ratio is not as great as that of the high-rise structure since the importance of its rigid rocking mode decreases. This lesser importance of the rocking mode is evidenced by the small values of the maximum base moment and interaction moment in Figure 102. The large increase of the maximum D_g in the massive stiff low-rise structure (see floor mass ratio=18-20, h_1 , and $f_{3.0}$ in Figure 100) is a result of the rigid translational mode's dominance. This occurrence is indicated by the corresponding system's horizontal interaction force's sharp increase and larger value than the system's base shear in Figure 100. The importance of the low-rise structure's relative translational mode increases since the decrease of the maximum D_s as a function of the floor mass ratio is small (see Figure 100). The maximum D_s of the stiff low-rise structure ($f_{3.0}$ and h_1) is even slightly larger than that of the FIX-model's displacement. Also the difference between the FIX-model's and SSI-model's maximum base shears of the low-rise structure (see Figure 101) is smaller than that of the high-rise structure (see Figure 97). Of the stiff low-rise structure (see $f_{3.0}$ and h_1 in Figure 101), the maximum base shear in the SSI-model is even greater than that in the FIX-model.

The stiffer structure (higher fixed-base frequency) results in the smaller responses. Also stiffer structure leads to the greater importance of all modes. Therefore the behavior (D_g) of a flexible high-rise structure is dominated by its rigid rocking mode, a stiff

high-rise structure by its rigid rocking and translational mode, and a massive stiff low-rise structure by its rigid translational mode.

4. Effects of Soil's Layer Depth. In Figures 103 to 106, the influence of different soil conditions (S0, S1, and S2) is demonstrated for the flexible high-rise structure ($f1.25$ and $h5$). The structure properties and input motion are the same as in the previous study. As the floor mass ratio increases, the change in the frequency ratio and damping ratio of the system embedded in S1-soil is less than that of the system embedded in S0-soil and S2-soil (see Figure 103). The change in the ratios of the system embedded in S0-soil and S2-soil is almost the same. This implies that the effect of the rock base in S1-soil condition (shallow soil layer) is important and results in a stiffer system. The same behavior of the system embedded in S0-soil and S2-soil is due to negligible influence of the rock base in S2-soil condition (deeper soil layer) on the system studied.

As a function of the floor mass ratio, the change in the maximum D_s and D_g of the system embedded in S1-soil is less than that of the other two cases (see Figure 104). Since a rigid rocking mode dominates in a flexible high-rise structure, this mode is the main contribution to D_g . Therefore the smaller change in the maximum D_g of the system embedded in S1-soil is due to its smaller foundation rocking. The latter is supported by its smaller maximum base moment and interaction moment in Figure 106. The smaller change in the maximum D_s of the system embedded in S1-soil indicates the greater importance of its system's relative translational mode. Also the smaller difference between the FIX-model's and SSI-model's maximum base shears of the corresponding system is found in Figure 105. In the same figure, the maximum base shear and horizontal interaction force

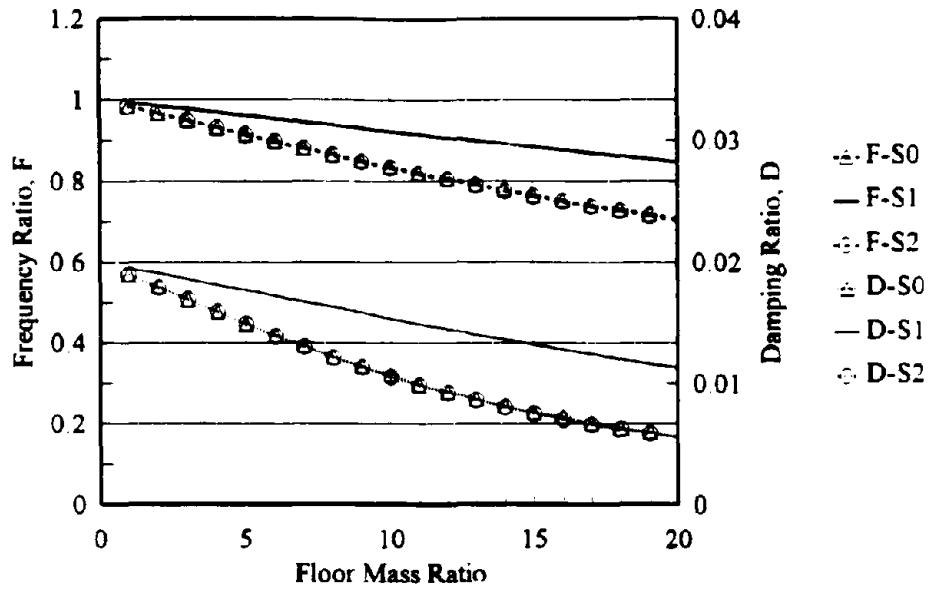


Figure 103. System Properties vs. Floor Mass Ratio, h5-slenderness Ratio, $f=1.25\text{Hz}$, Footing Mass Ratio=2.0, El Centro Earthquake

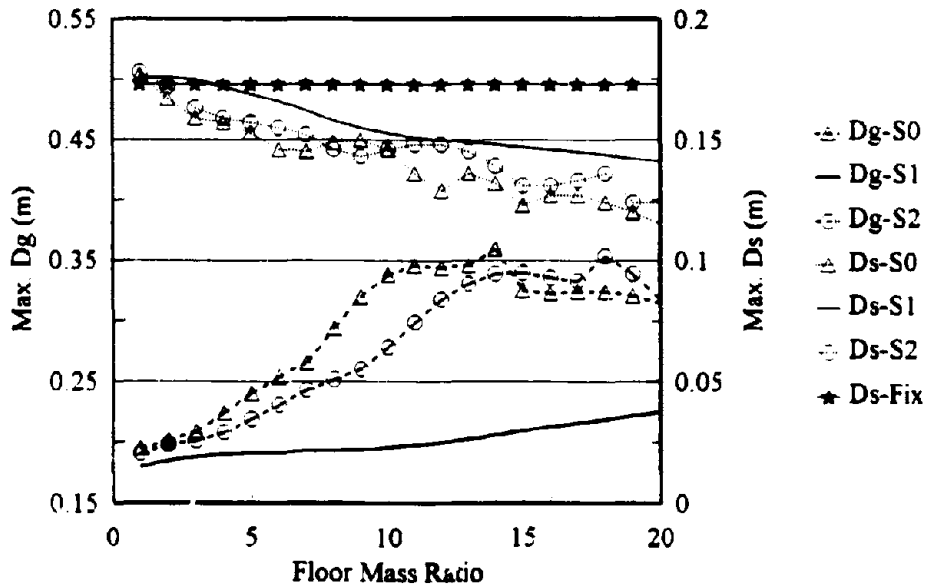


Figure 104. Maximum Responses vs. Floor Mass Ratio, h5-slenderness Ratio, $f=1.25\text{Hz}$, Footing Mass Ratio=2.0, El Centro Earthquake

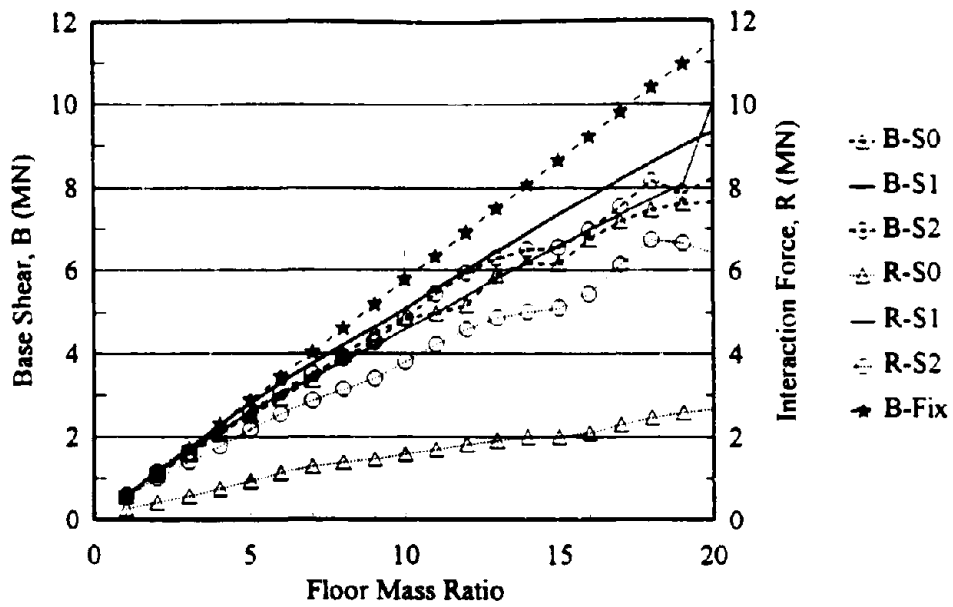


Figure 105. Maximum Horizontal Forces vs. Floor Mass Ratio, $f=1.25\text{Hz}$, $h5\text{-slenderness Ratio}$, Footing Mass Ratio=2.0, El Centro Earthquake

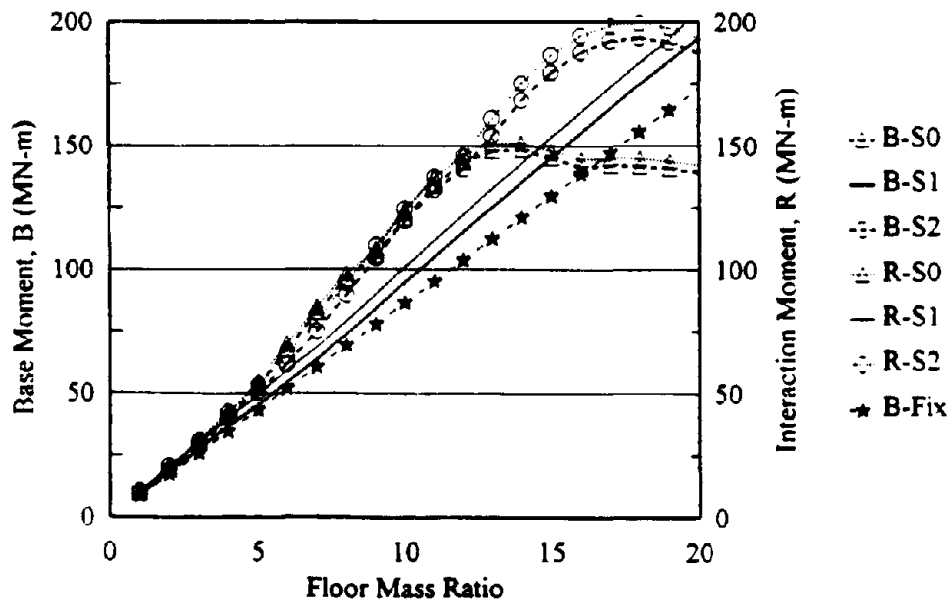


Figure 106. Maximum Moments vs. Floor Mass Ratio, $h5\text{-slenderness Ratio}$, $f=1.25\text{Hz}$, Footing Mass Ratio=2.0, El Centro Earthquake

of the system embedded in S1-soil are closer than those of the other two cases due to the former's less rigid translational motion.

Therefore the system embedded in S1-soil (shallow soil layer) which is considered as the stiffer soil system results in the lesser importance of the rigid translational and rocking mode but the greater importance of the relative translational mode.

C. INVESTIGATION OF 10-STORY STRUCTURE WITH CONTROL

In Figure 107, a dynamic system which is used to demonstrate the influence of structure-soil interaction and control consists of a 10-story shear structure equipped with an active tendon system attached to its foundation and second floor (node no.1). The structure sits on a 6.0 x 6.0 m rigid square foundation having its 3.0-meter depth embedded into a half-plane (D/B=1.0). Structural properties are: each floor mass (m_i) = 10 ton; each floor mass moment of inertia ($I_i - m_i h_{ai}$) = 20.83 ton-sq.m; foundation mass (m_0) = 28.75 ton; foundation mass moment of inertia (I_0) = 172.5 ton-sq.m; floor translational stiffness (k_i) = 1244 MN/m; proportional damping ratios (η_1 and η_2) = 0.02 for the first mode and 0.10 for the second mode; and floor height (h_i) = 3.00 m for every floor. Half-plane properties are: shear modulus of elasticity (γ) = 7.2 MN/sq.m; soil density (ρ) = 2.0 gram/cu.cm; Poisson's ratio (ν) = 0.33; and hysteretic damping ratio (ζ) = 0.04. The shear wave velocity (C_s) is 60 m/sec. The first 20-second 1940 El Centro earthquake acceleration record, north-south component, is selected as the horizontal acceleration at point 0 of the ground system's rigid interface. Since vertically incident shear wave is assumed, the rotational component of the ground system is omitted. As for a

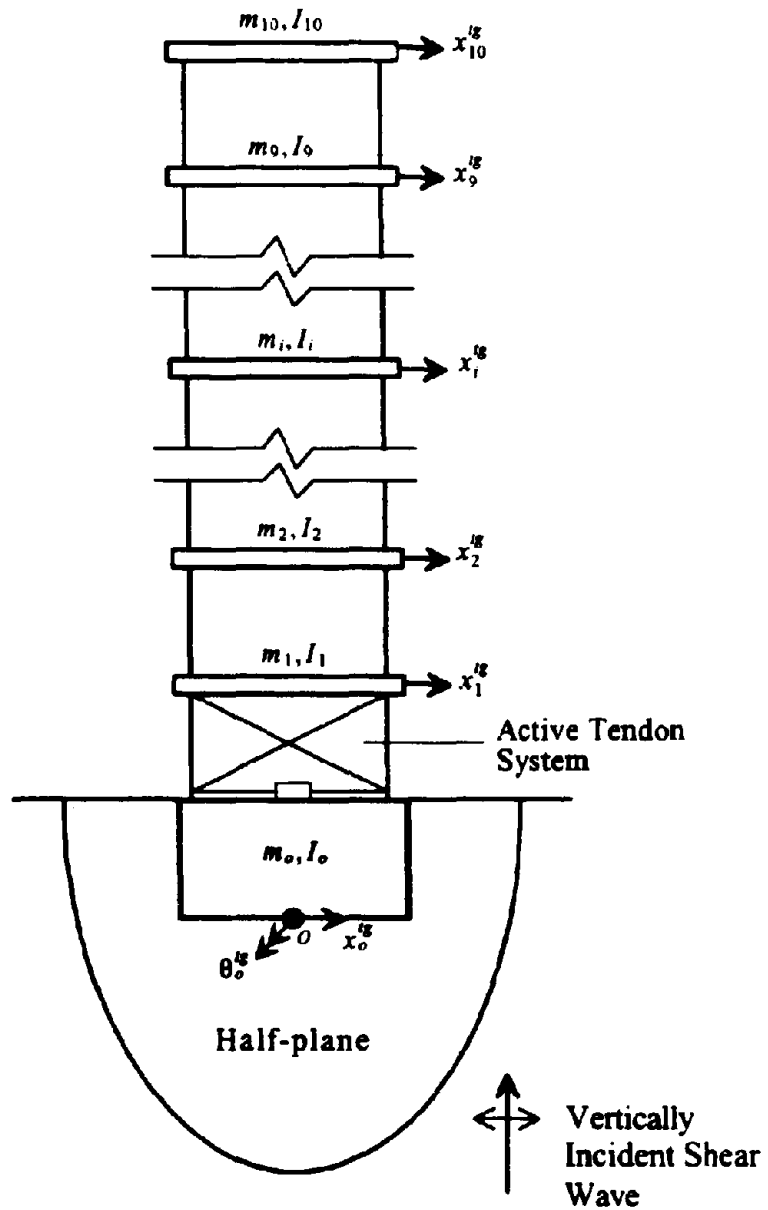


Figure 107. 10-story Shear Structure with Active Tendon System Embedded in Half-plane

one-controller system, the control weighting matrix $[R]$ consists of only one element r . To obtain an optimal performance of the system, $s1/r$ ratio is varied parametrically.

The fundamental system frequency is 2.65 Hz for the FIX-model and 1.15 Hz for the SSI-model. The smaller frequency in the SSI-model is a result of its greater flexibility. In a system with control, its frequency and damping ratio are increased as $s1/r$ ratio reaches an optimal point (the minimum point of performance index). For the FIX-model (see Figure 108), the fundamental system frequency and damping ratio are increased, at the optimal point ($s1/r=0.6$), to 2.85 Hz and 0.36, respectively. For the SSI-model (Figure 109), at the optimal point ($s1/r=0.6$), the fundamental system frequency and damping ratio are increased to 1.19 Hz and 0.15, respectively. This is because control force, which is related to the system's displacement and velocity vector by a gain matrix $[G]$, helps to increase stiffness and damping of the system. It should be noted that this effect is smaller in the SSI-model. Displacement control and velocity control are manipulated by s_D and s_V in the state weighting matrix $[S]$ and therefore in the gain matrix $[G]$, which are chosen to be equal to an arbitrary real number $s1$.

In a system without control, the maximum of the top floor displacement relative to footing is equal to $0.053 \text{ m} \left(x_{10}^{fb} \right)$ for the FIX-model and $1.219 \text{ m} \left(x_{10}^{fg} - x_0^{fg} \right)$ for the SSI-model. The larger displacement in the SSI-model may be a result of foundation rotation θ_0^{fg} since the rigid rocking mode trends to dominate in a flexible high-rise structure. Comparison of the top floor displacement relative to footing $\left(x_{10}^{fb} \right)$ in the FIX-model and the top floor displacement relative to footing excluding rigid motion effect due to foundation rotation $\left(x_{10}^{fg} - x_0^{fg} + h_{a10} \theta_0^{fg} \right)$ in the SSI-model is shown in Figure

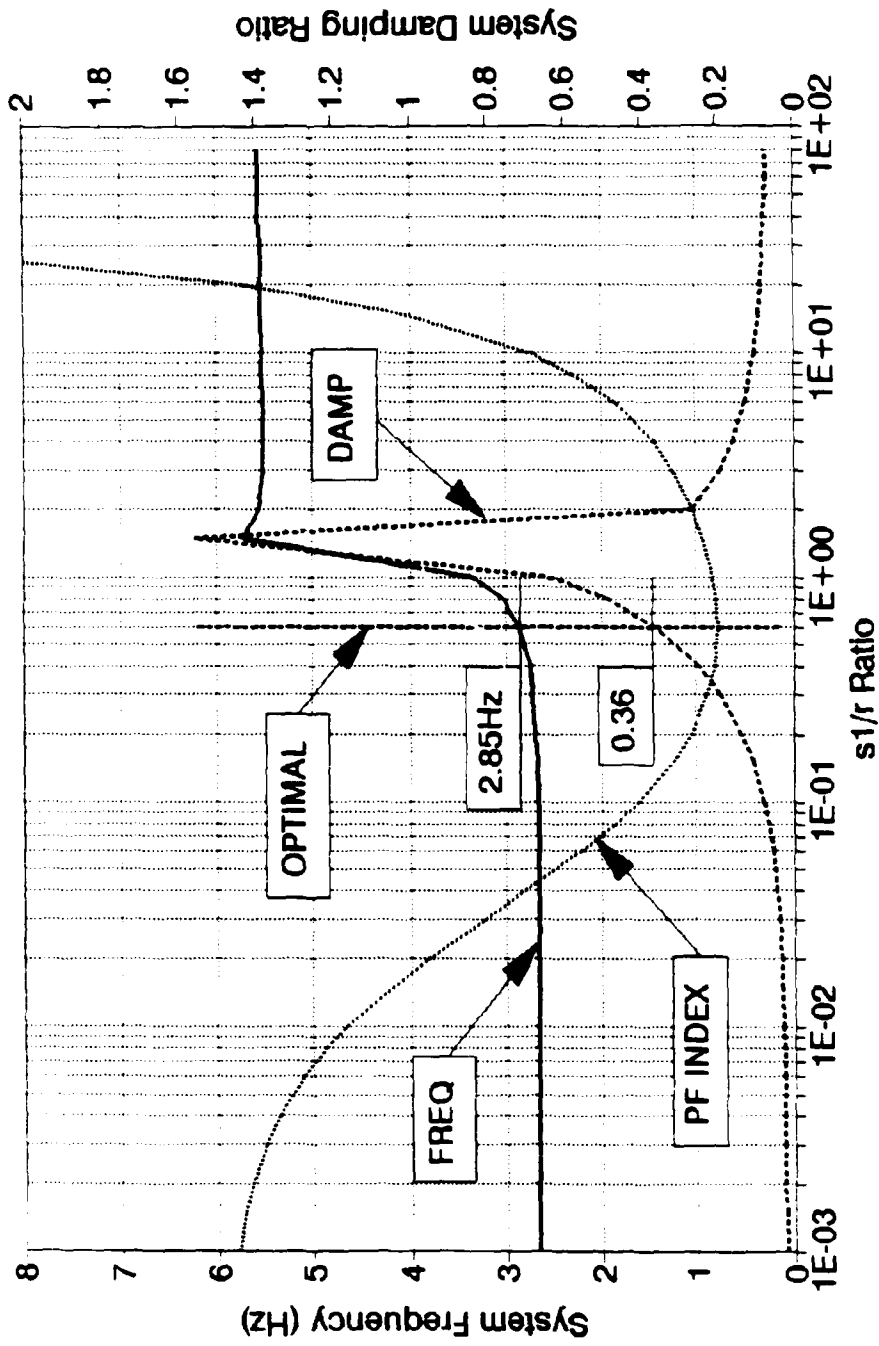


Figure 108 Fundamental Frequency and Damping Ratio vs s1/r Ratio, 10-story Controlled Structure, FIX-model

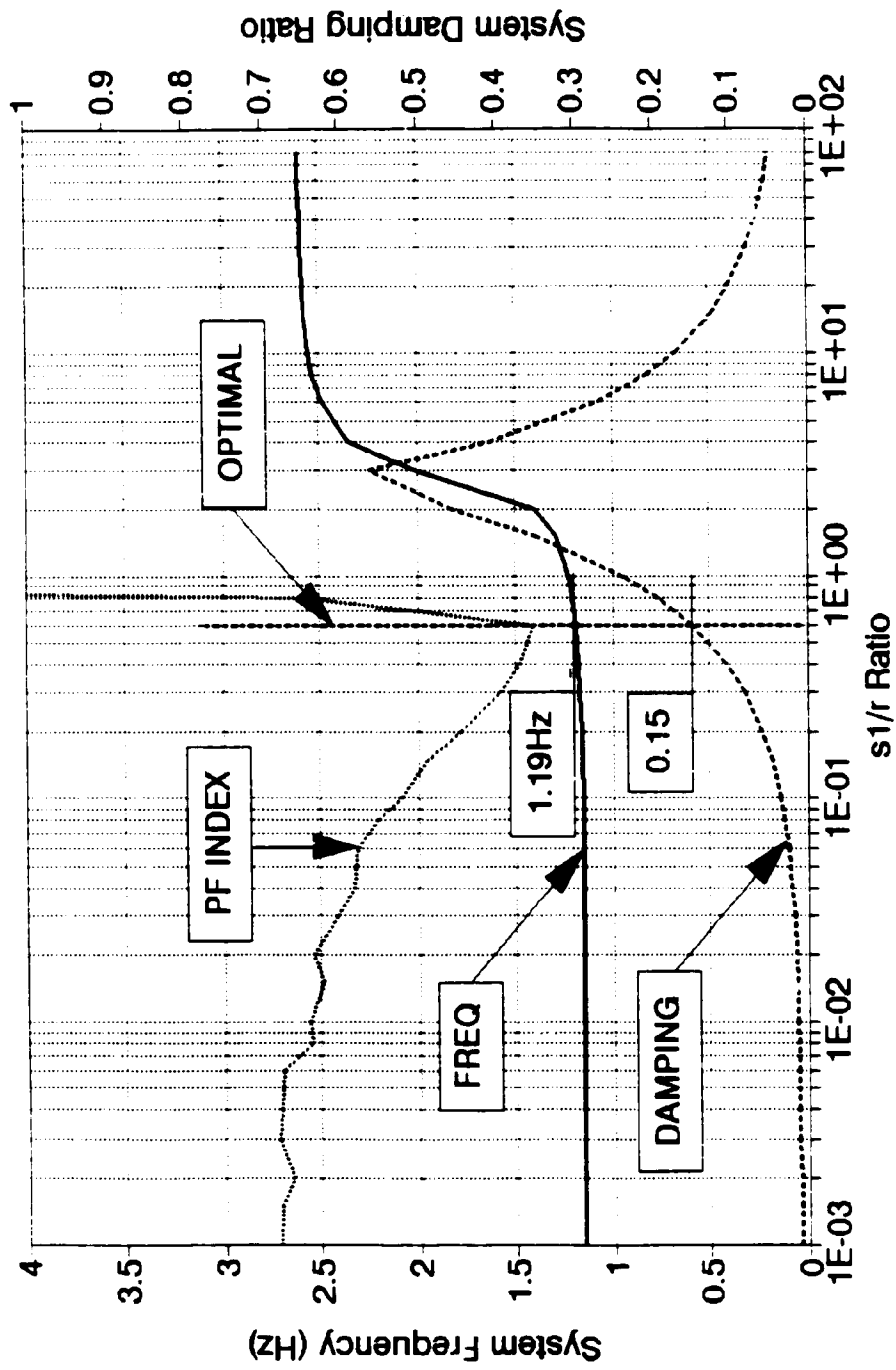


Figure 109. Fundamental Frequency and Damping Ratio vs. s1/r Ratio, 10-story Controlled Structure, SSI-model

110. Without the rotational effect, the envelope of both responses is quite similar. Therefore the larger displacement in the SSI-model as the result of foundation rotation is verified. The FIX-model's period of response is shorter than that of the SSI-model due to its more rigid model.

Figure 111 shows the same comparison for a system with control. The smaller displacement in the FIX-model implies that the study system's control force is more effective in reducing the FIX-model's translational displacement than the SSI-model's relative displacement excluding rotational effect. For the FIX-model with control (see Figure 112), an increase of $s1/r$ ratio results in an increase of the maximum of control force and then a decrease of the maximum of the top floor displacement relative to footing (x_{10}^{tb}). At the optimal point, the maximum displacement is reduced from 0.053 m (without control) to 0.016 m with the maximum control force of 8.68 MN.

For the SSI-model with control (see Figure 113), an increase of $s1/r$ ratio also results in the same manner as the case of the FIX-model. But the change in the maximum of the top floor displacement relative to footing excluding rotational effect (DISP W/O ROT) as a function of $s1/r$ ratio is very small. This indicates that the decrease of displacement relative to footing is mainly the result of the decrease of footing rotation. At the optimal point, the maximum displacement is reduced from 1.219 m (without control) to 0.735 m with the maximum control force of 68.54 MN. The footing rotation is reduced from 0.035 radian (without control) to 0.022 radian as shown in Figure 114. The maximum of relative displacement excluding rotational effect is slightly changed from 0.052 m (without control) to 0.058 m as shown in Figures 110 and 111 for the case of the

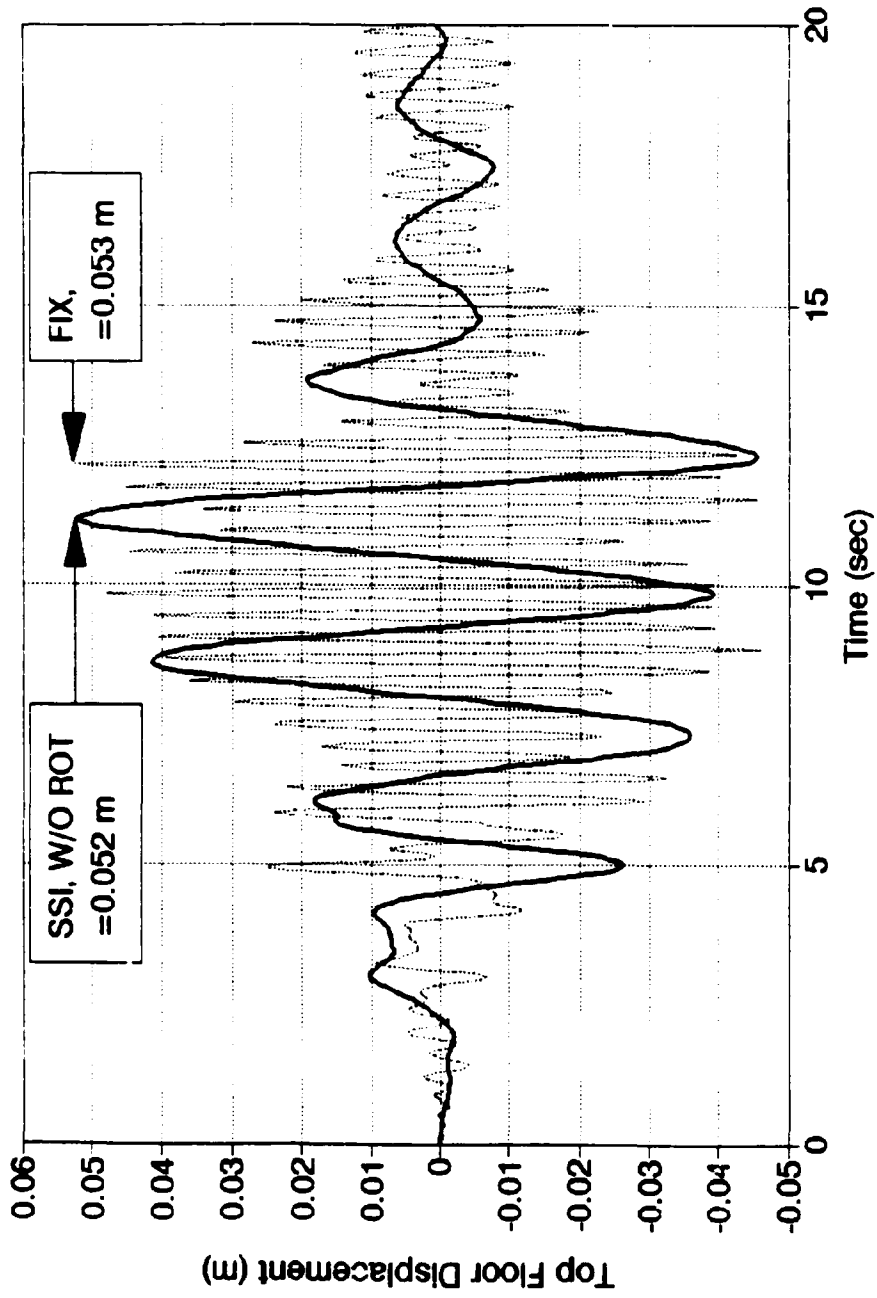


Figure 110. Top Floor Displacement Relative to Footing of FIX-model and SSI-model (Excluding Rotational Effect), without Control

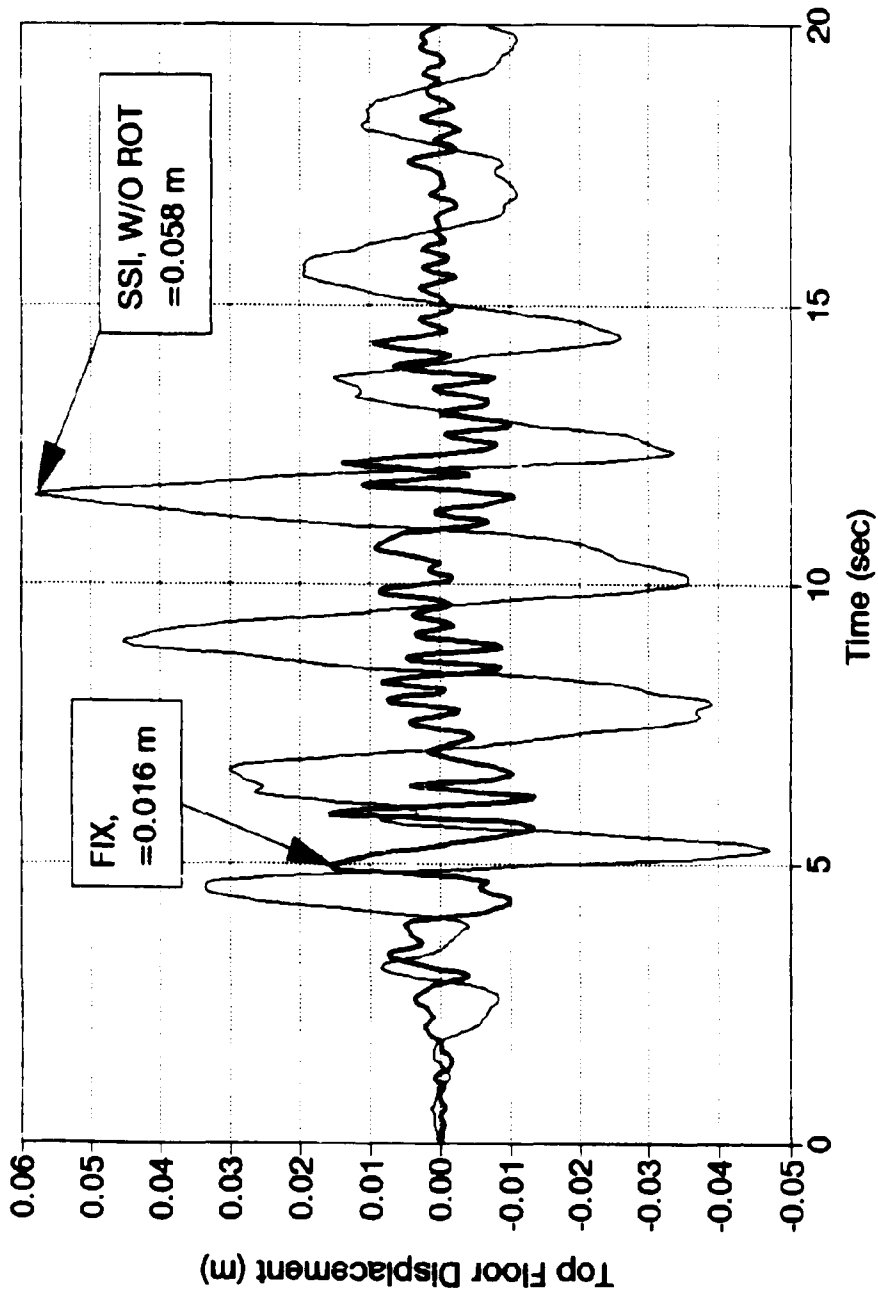


Figure 111 Top Floor Displacement Relative to Footing of FIX-model and SSI-model (Excluding Rotational Effect), with Control ($s/r=0.6$)

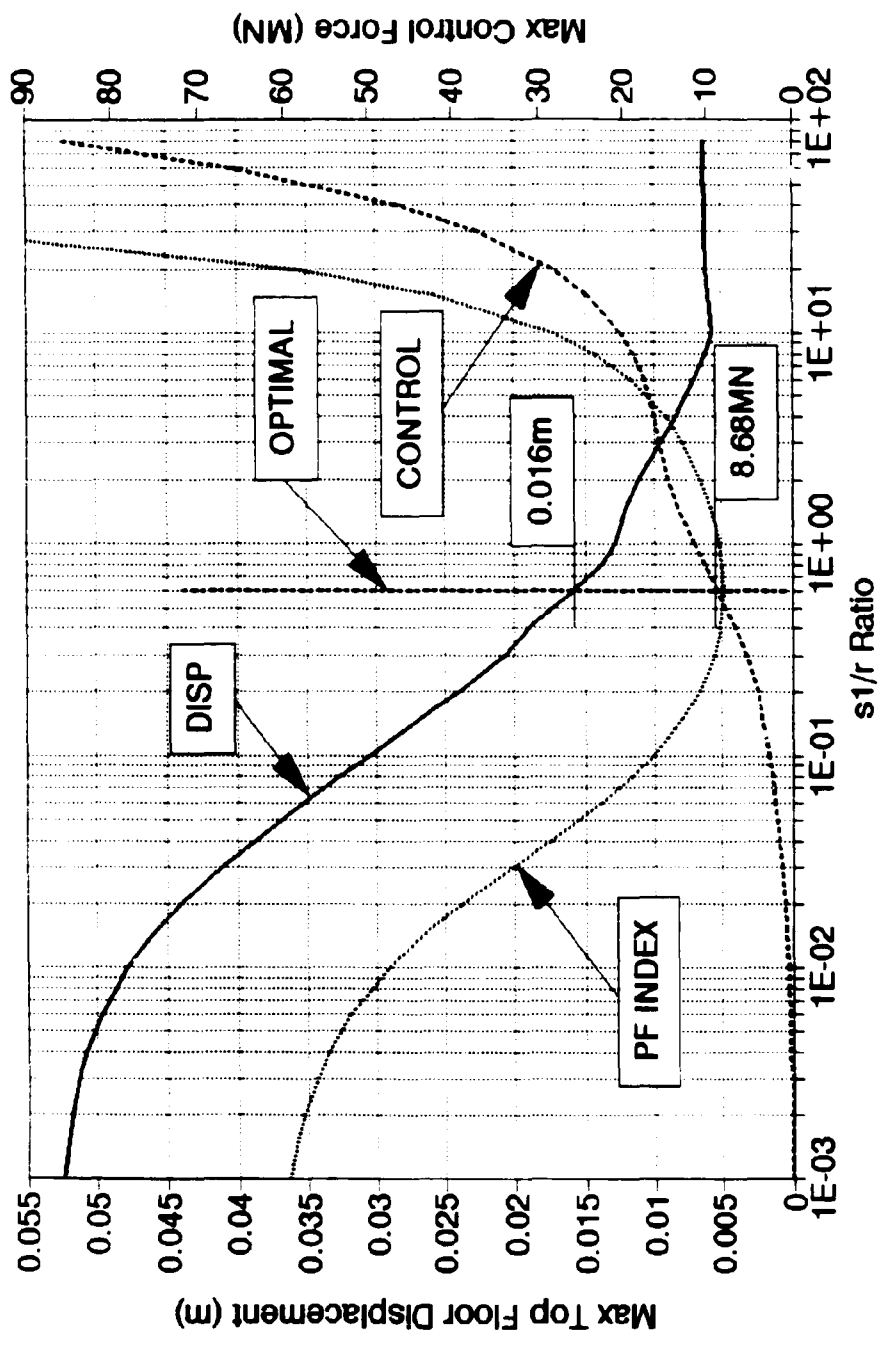


Figure 112 Maximum Top Floor Displacement and Horizontal Control Force vs s1/r Ratio, FIX-model

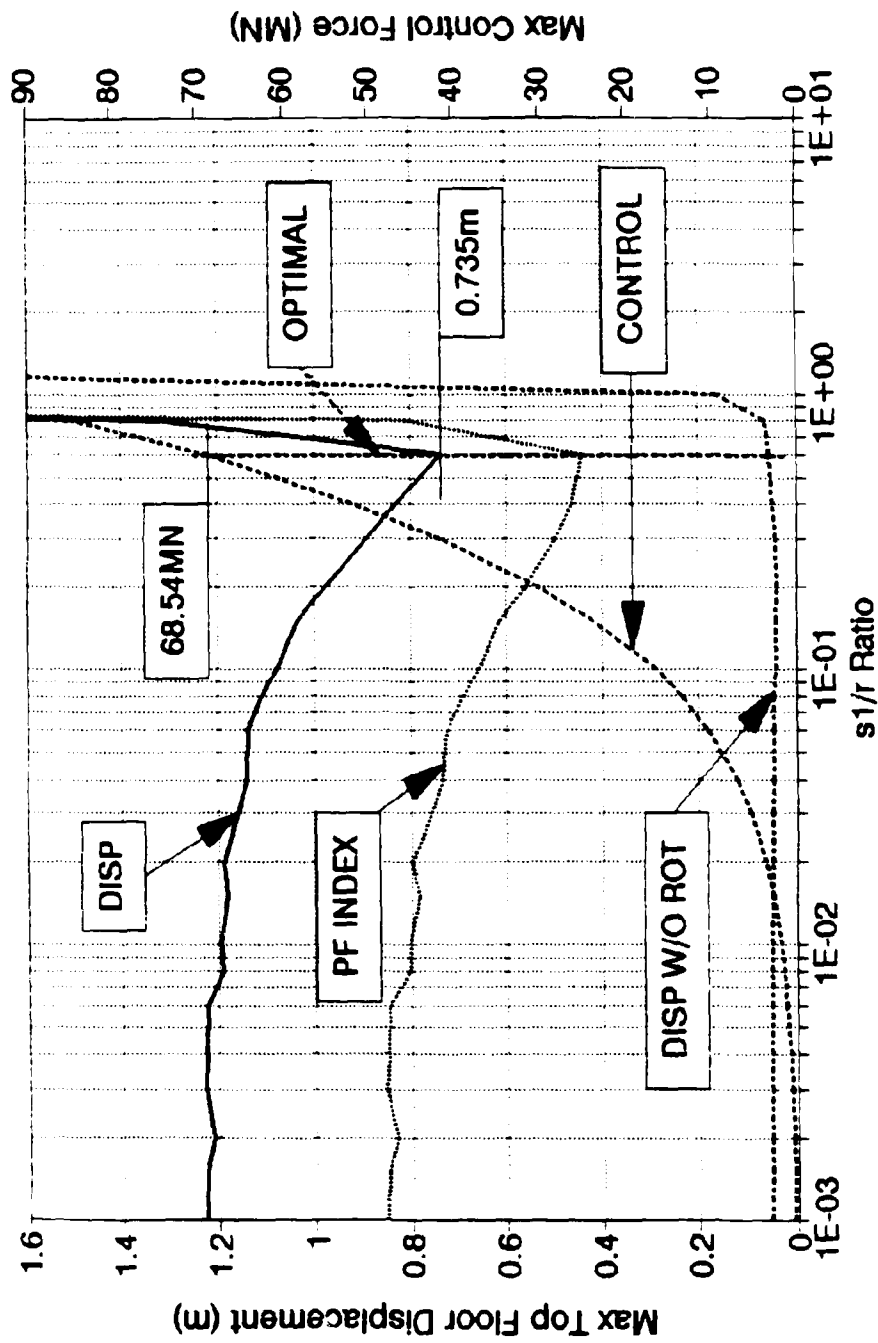


Figure 113. Maximum Top Floor Relative Displacement with and without Rotational Effect and Horizontal Control Force vs. $s1/r$ Ratio, SSI-model

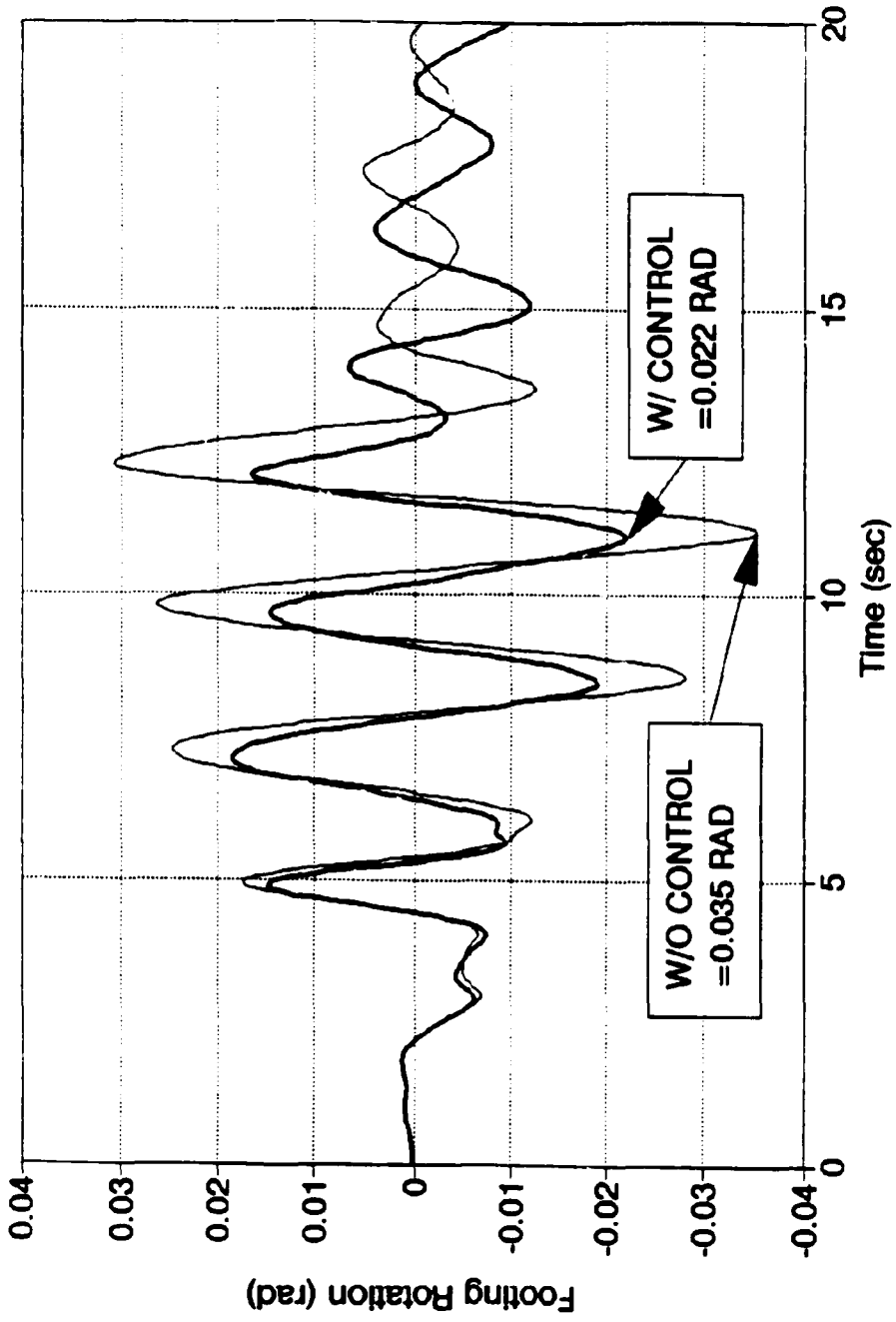


Figure 114. Footing Rotation of System with Control ($s/r=0.6$) and without Control

SSI-model. Since interaction moment and footing rotation are related to the impulse velocity coefficients of ground system by the convolution integral, the former is reduced, as expected, from 66.13 MN-m (without control) to 39.11 MN-m at the optimal point as shown in Figure 115. Also in the same figure, the horizontal interaction force is reduced from 1.51 MN (without control) to 1.37 MN.

Therefore the active tendon system, attached to the foundation and second floor of a structure embedded in a soft soil, limits structural responses by mean of reducing foundation rotation. Its control force also reduces a horizontal interaction force and interaction moment. This active system is not so effective in reducing relative floor translation. To limit structural responses even more, the second active system on the upper floor is recommended.

Since the foundation degrees of freedom in an SSI-model distinguish this model's behavior from a FIX-model's, the responses of these two models are different and thus require different control forces. The control force required in the SSI-model is greater than that in the FIX-model as a result of the former's larger response. Furthermore, an additional amount of control force is needed to limit the movement of foundation. Even in a closed-loop control, the structural responses are directly measured by response sensors, the control force determined by a FIX-model's gain matrix may not be large enough to limit the foundation movement and thus the structural responses. Moreover, the control force set by the FIX-model's gain matrix is dictated only by floor translations. By using the SSI-model's gain matrix, a suitable control force is determined as the functions of both floor and foundation responses.

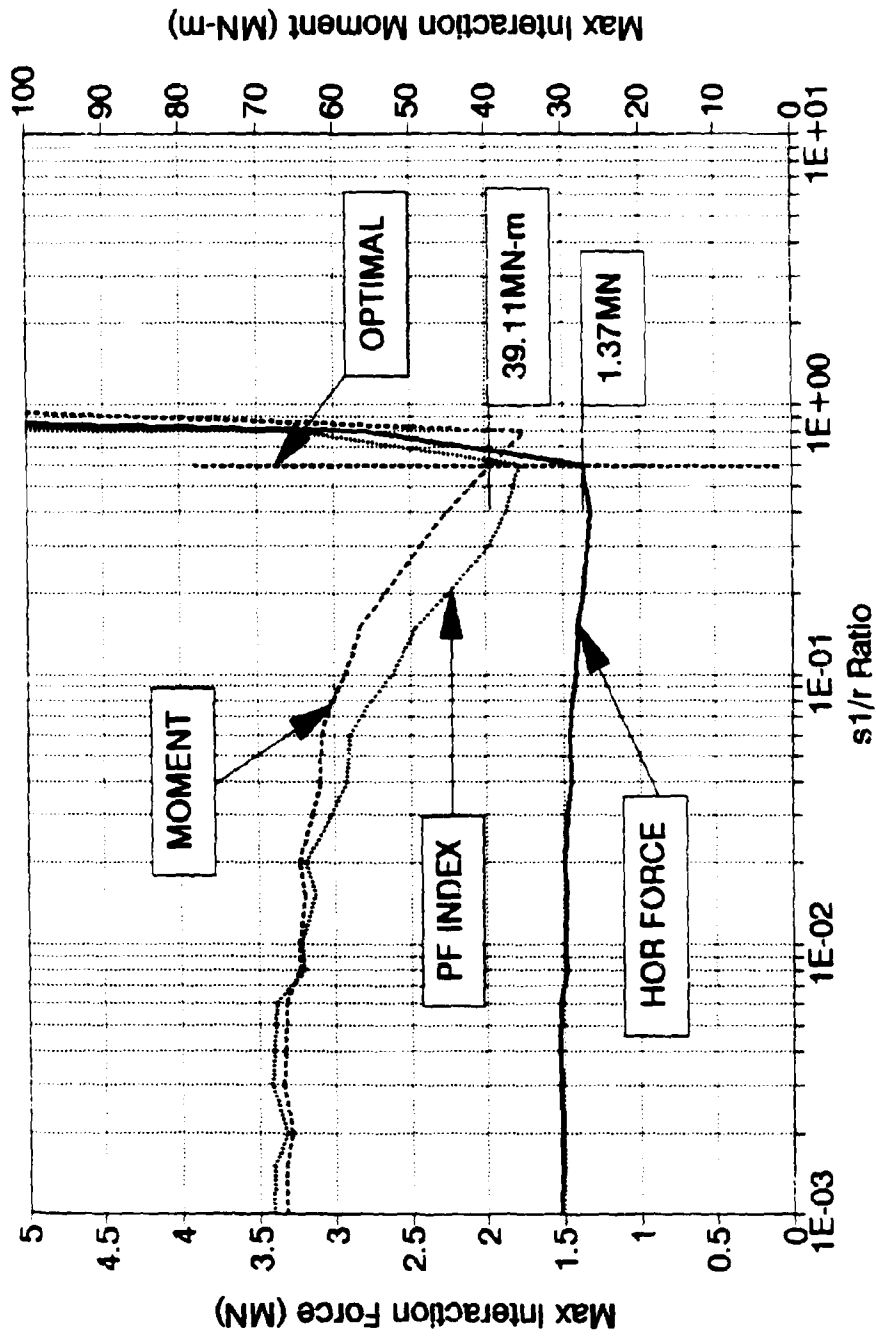


Figure 115 Maximum Horizontal Interaction Force and Interaction Moment vs. s1/r Ratio, SSI-model

VIII. CONCLUSIONS

A. MATHEMATICAL MODELS

Four mathematical models of a multistory seismic shear structure were presented. First, a fixed-base model (FIX) is valid where the structure is placed on rock. If the structure is founded on soft soil, a second model, so-called structure-soil interaction model (SSI), may appropriately be employed. An integrated active tendon control to limit dynamic system's response results in other two models, a FIX-model with control and SSI-model with control.

The SSI-model can be applied to a seismic structure with a rigid rectangular mat foundation embedded in an unbounded soil. The unbounded soil domain is modeled as unbounded horizontal layers stacked on a half-space (layered half-space). An isotropic viscoelastic property of soil may vary with depth but remain constant within the individual layers. The indirect boundary element method is applied to unbounded part of soil (free-field system), while the finite element method with 4-node rectangular element is employed to bounded part (system's excavated part). In the indirect boundary element method, an adaptive quadrature integration technique is used in a Green's influence function's transformation from the k wave-number domain to space domain. For the integration along a boundary (foundation-soil interface), Simpson's method is employed. The frequency-dependent time-derivative flexibility coefficient of ground system is determined and then, by using the discrete Fourier transformation (or fast Fourier transform) with causality condition, an impulse velocity coefficient is obtained. By virtue

of the soil coefficient's time derivative, its static component is not required. In a discrete time fashion, a structure-soil interaction force is computed through the convolution integral of the impulse velocity coefficient. This coefficient relates the difference of the ground system's and foundation's responses to the interaction force. Since vertically incident shear wave and shallow foundation are assumed, the rotational component of the ground system's response is neglected.

In the integrated control systems, the concept of a generalized optimal active control is applied. The optimal control rules of both FDX-model and SSI-model are developed based on the generalized performance indexes (objective functional) in which an endpoint state vector is included. Euler's equation and transversality condition are enforced to obtain an optimal solution. This results in the constant feedback gain matrices (control laws) which are neither a function of time nor time increment. The weighting matrix $[S]$ associated with the endpoint state vector is chosen to be either a row matrix or a symmetrical matrix. Since this weighting matrix is integrated into the gain matrix, the displacement control and velocity control are manipulated by the weighting elements $(S_D, \gamma_D$ and $S_V, \gamma_V)$ corresponding to a system's displacement vector and velocity vector, respectively. In the SSI-model with control, foundation responses (translation and rocking) are included in the state vector and then dictate control force. Therefore, in a closed-loop control, not only a response sensor on each floor but also an innovative sensor for a foundation is needed. The foundation sensor may detect the pressure (or stress or strain) at a foundation-soil interface and then convert to the foundation's response relative to the ground system.

To obtain a system's response, the state equation is transformed into its canonical form and the first-order differential equation is then solved by applying the trapezoidal rule. For all cases (FIX-model and SSI-model with or without control), this technique is implemented on the basis of time domain.

B. STUDY OF SOIL SYSTEMS

In the indirect boundary element method (IBEM), the calculation of the frequency-dependent dynamic stiffness coefficients in the free-field system needs only the displacement Green's influence function. Unlike the finite element method (FEM), this method does not require the fictitious boundary and interior nodes for an unbounded soil. Therefore it is simpler to determine the coefficients of system's excavated part (bounded domain) by the finite element method and then subtract them from those of the free-field system to yield the corresponding coefficients of the ground system. Since the errors inherent in the two different methods (IBEM and FEM) are not consistent, this subtraction technique may yield problematic results in the vicinity of the natural frequency. Therefore the technique is not recommended in cases of small damping and high foundation embedment to half-width ratio (D/B). In such cases, the indirect boundary element method, which requires Green's influence functions for both displacement and surface traction, should directly be applied to the ground system.

Parametric studies of dynamic stiffness coefficients were made on various soil systems to investigate the influence of soil hysteretic damping ζ , foundation embedment D , and the depth H of a soil layer on rock. An investigation of the actual site (Takenaka

Experimental Building Site or TEBS) was also presented. These results can be summarized as follows.

1. **System's Excavated Part.** Since there is no radiation of energy in a bounded domain, the damping coefficient of undamped medium is zero. For a damping case, the damping coefficient arises as the result of frictional loss. The spring coefficient has no significant change as the hysteretic damping ratio increases. In the vicinity of the natural frequency, both spring and damping coefficients change as the reverse function of the damping ratio. The damping ratio can cause considerable change in the vibrational mode. The spring and damping coefficients convert to zero where their dimensionless frequency approaches zero. Thus their static component ($\omega=0$) of the system's excavated part is equal to zero. The bigger D/B results in a lower first mode natural frequency.

For the actual site (TEBS), its coefficients are very close to those of the homogeneous system having $D/B = 0.5$, since the excavated part of the actual site is assumed to be the homogeneous medium having $D/B = 0.5$. The difference is due to the hysteretic damping and Poisson's ratio used in actual site and homogeneous medium.

2. **Free-field System.** Two types of free-field systems were investigated. The influence of foundation embedment D was based on a free-field system with a homogeneous half-plane. Then the effect of layer's depth was studied in a free-field system comprising a homogeneous layer with depth H built on rock base.

The natural frequencies of the free-field system are the same as those of the system's excavated part. In contrast to the system's excavated part, the spring and damping coefficients do not transform to zero as their frequency reaches zero. This indicates the

non-zero static stiffness coefficient of the free-field system. The increase of D/B has no significant effect on the horizontal and vertical spring coefficients. On the contrary, in the low frequency range (less than the first mode's natural frequency) the rocking spring coefficients increase while D/B increases. Due to the free-field system's radiation of energy toward infinity, the damping coefficient is not equal to zero. The increase of the horizontal and vertical damping coefficients is proportional to D/B . More remarkable increase can be seen in the rocking damping coefficient, especially for $D/B = 2.0$.

As depth H of the layer decreases, the spring coefficients in the low frequency range increase. The effect is more noticeable in the vertical direction. The spring coefficients of the system with a layer on rock are greater than those of the system with a half-plane. For $H/B = 2.0$ and 3.0 ($H =$ layer's depth and $B =$ foundation half-width), the spring coefficients have a stronger frequency-dependence. A smoother spring coefficient is found in the case of a very shallow layer ($H/B=1.0$). In contrast to the system with half-plane, the one with a layer on rock demonstrates a cutoff frequency below which only a small amount of energy can be radiated toward infinity. This leads to small damping coefficients below that frequency. The corresponding coefficients are less than those of the half-plane medium. A bigger H/B leads to a smaller cutoff frequency.

For the actual site (TEBS), the strongly frequency-dependent coefficients of this nonhomogeneous domain are expected. Amplitudes of the coefficients are close to those of the homogeneous half-plane having the same D/B , except in the vertical direction and rocking as a result of the TEBS's half-plane. The level of TEBS's half-plane, in which

average shear wave velocity is about 2 times faster than that of topping layers, is quite deep (61.8m). Therefore the cutoff frequency is very low.

3. **Ground System.** The behavior of this system's coefficients tends to be the same as that of the free-field coefficients in the low frequency range. The foundation embedment barely has any effect on both horizontal and vertical spring coefficients. On the contrary, the deeper embedment leads to stronger rocking spring coefficients. For both translation directions and rocking, the larger damping coefficients are found in the deeper foundation embedment. A greater effect appears in the rocking. As for depth of soil layer on rock base, spring coefficients of the more shallow layer system are greater, especially in a vertical direction. Spring coefficients of the system comprising a layer on rock base are larger than those of the system with a half-plane. But the system's damping coefficients are smaller below a cutoff frequency and then increase to the level of those corresponding to a half-plane medium. The cutoff frequency exists at the same point as that in the free-field system. Both spring and damping coefficients display a strong dependence of frequency, except in the case of a very shallow layer. In a high frequency range, a large oscillation is demonstrated and the negative spring coefficients occur to a greater extent. For the actual site (TEBS), the same conclusion in the free-field system is applied here.

Therefore, for an embedded foundation, the assumption of a surface foundation is too conservative. This is because foundation embedment does increase damping coefficients and rocking spring coefficient. As for impulse velocity coefficients, the coefficients of the system with a half-plane attenuate faster than those corresponding to a layer on rock medium since more energy in the half-plane propagates toward infinity. The

rock base of a very shallow layer has an effect on a rocking impulse velocity coefficient as its dynamic-stiffness coefficient is stronger.

C. BEHAVIOR OF TOTAL DYNAMIC SYSTEMS

1. System without Control. In an SSI-model, two types of displacement concerning structural failure were investigated. D_s is defined as floor relative displacement excluding rigid motion effect due to foundation rotation. D_g is floor displacement relative to ground system. The former is related to a structure system's strain energy. The latter concerns the structure collision with an adjacent system. Regarding foundation failure, a horizontal interaction force and interaction moment as the measurement of maximum stresses along a structure-soil interface were examined. In a single-story SSI-model, three normal modes include a rigid translational mode, relative translational mode, and rigid rocking mode. A base shear and D_s are directly effected by the dominance of a relative translational mode while D_g is influenced by the dominance of every mode. A base moment and interaction moment are dominated by the rigid rocking mode much as a horizontal interaction force is controlled by the rigid and relative translational modes. In a FIX-model, a floor relative displacement, base shear, and base moment were compared to the corresponding responses of the SSI-model.

The longer period of response in the SSI-model is noticeable as a result of the system becoming more flexible. The maximum of D_g is always bigger than that of the FIX-model's floor relative displacement due to foundation translation and rotation. The maximum of D_s and base shear may be larger or smaller than that of the FIX-model's floor

relative displacement and base shear, respectively. The former are larger in the case of a relative translational mode's dominance .

In the SSI-model, its greater floor mass and/or height result in a more flexible system as well as the more importance of a rigid rocking mode. The latter leads to the larger maximum for D_g , base moment, and interaction moment. In the case of a high-rise structure, this maximum base moment is larger than that of a FIX-model. On the contrary, the translational modes tend to dominate in a low-rise structure, which leads to the greater maximum of D_s , base shear, and horizontal interaction force. Therefore, both translational and rocking modes potentially dominate in a massive low-rise structure such as a nuclear reactor, and then produce a large response. The dominant mode of a similar dynamic system subjected to different seismic excitation could also be different. This leads to a distinct structural responses.

The fixed-base natural frequency of a dynamic system is used as a relative indicator whether a structure is stiff or flexible. In general, a stiff structure leads to a smaller response but greater importance of every mode, especially a rigid translation mode. Therefore, in a stiff high-rise structure, a large response is caused by the dominance of both rigid rocking and translational modes. The dominance of a rigid translational mode is found in a massive stiff low-rise structure. Also a stiffer structure results in a bigger change in the total dynamic system's frequency.

To some extent, the level of rock base has an influence on a flexible high-rise structure. The rigid rocking mode is normally important for the flexible high-rise structure embedded in soil (half-plane). This importance is reduced in the case of a shallow soil

layer on rock as the result of its smaller rocking impulse velocity coefficient. In turn, this leads to the smaller maximum of D_g , base moment, and interaction moment. For a stiffer soil system, the greater importance of a relative translational mode but lesser importance of a rigid translational mode is described. In contrast to a stiff structure system mentioned in the previous paragraph, a stiff soil system leads to a smaller change in the total system's frequency.

2. **System with Control.** A flexible high-rise structure with an active tendon system attached to its foundation and second floor was investigated. As the structure (without control) interacts with soil, the total dynamic system predictably becomes more flexible (smaller system's frequency). Dominance of its rigid rocking mode leads to a large foundation rotation and thus greater floor translation than that of a FIX-model. In a closed-loop control, its control force (which is the function of displacement and velocity) strengthens the system's stiffness and damping. Therefore the frequency and damping ratio of an integrated control system are increased. A lesser impact is noticeable in the SSI-model. For the control system used in this study, structural response is limited by means of reducing foundation rocking rather than relative floor translation as done in the FIX-model. Consequently, this control system's interaction moment is greatly reduced as is its horizontal interaction force to a lesser extent. In order to reduce the floor translation without rotational effect, a second active tendon control on an upper floor is recommended. The larger control force in an SSI-model is required to limit its larger response and foundation movement. Even this larger response is directly detected by response sensors in a closed-loop control. A control force calculated by a FIX-model's

gain matrix may not be large enough to limit the response of a structure on soft soil. Proper control force as a function of floor translation, foundation translation and foundation rotation can be determined by using an SSI-model's gain matrix.

APPENDIX A

GREEN'S INFLUENCE FUNCTION

In the indirect boundary element method, a so-called fundamental solution is needed for an applied load acting on a continuous system. In order to determine the dynamic stiffness of the free-field system in Subsection A of Section V, displacements $u_{pr}(x,z)$ and $w_{pr}(x,z)$, on the assumed line which subsequently forms the structure-soil interface, are needed for the applied distributed loads acting on the same line of a continuous soil system.

1. Displacements in k -domain for Loads on Vertical Line.

As shown in Figure 116, the horizontal linearly distributed load $p(x,z)$, with nodal values of p_j and p_{j+1} , and the vertical linearly distributed load $r(x,z)$, with nodal values of r_j and r_{j+1} , act on part of the vertical assumed line between node j and node $j+1$ in x - and z -direction, respectively. The procedure to determine the displacements is divided into two parts. In part I (superscript I) as shown in Figure 117, an additional horizontal interface needs to be introduced through node j . The introduced layer j on which the distributed loads act is fixed at the interfaces. Corresponding reaction forces, $P_j^I(k)$, $P_{j+1}^I(k)$ and $R_j^I(k)$, $R_{j+1}^I(k)$ in x - and z -direction, are calculated to achieve this condition whereby local displacements $u_{pr}^I(k,z)$ and $w_{pr}^I(k,z)$, between the nodes, are determined. In part II (superscript II) as shown in Figure 118, amplitudes of the reaction forces are then applied at the nodes of the total soil system with the opposite direction; displacements $u_{pr}^{II}(k,z)$ and $w_{pr}^{II}(k,z)$ along the vertical assumed line are calculated. To find global displacements $u_{pr}(k,z)$ and $w_{pr}(k,z)$, local displacements (part I) have to be superimposed on them (part II). Subscript pr indicates that displacements u and w in x - and z -direction are the result of both applied distributed loads p and r .

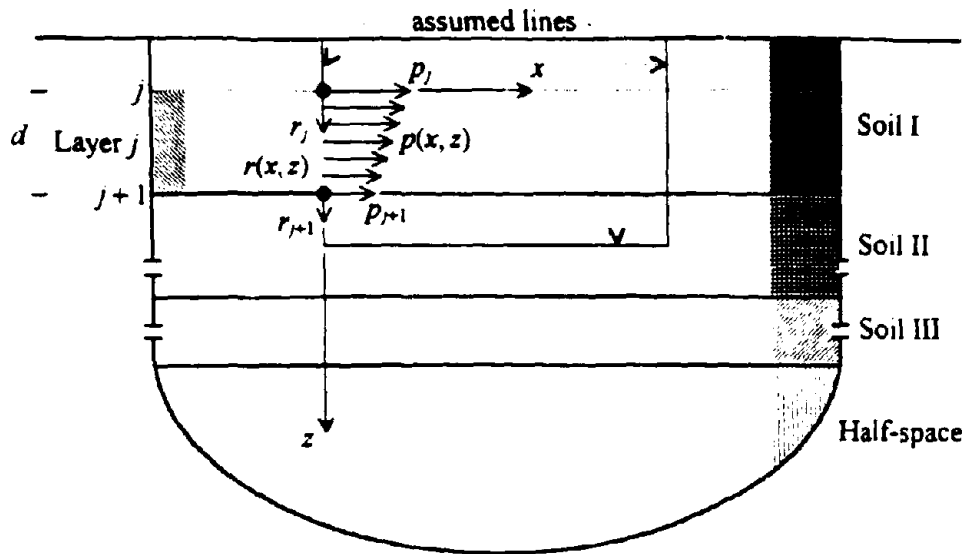


Figure 116. Linearly Distributed Loads on Vertical Assumed Line

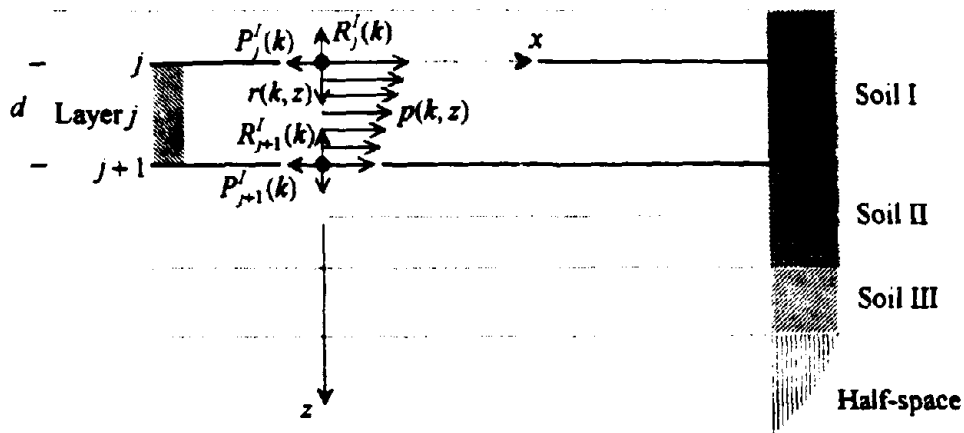


Figure 117. Loaded Layer with Reaction Forces (Part I)

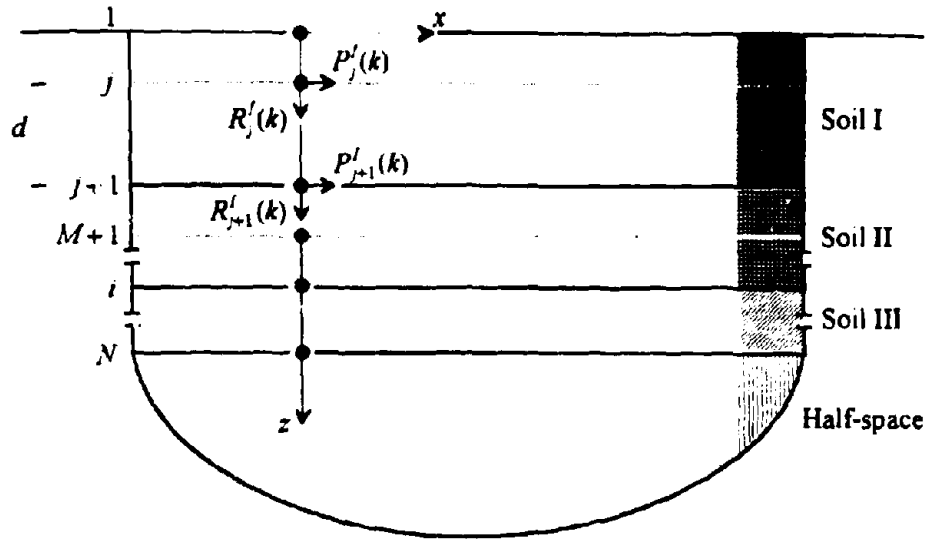


Figure 118. Total Soil System with External Forces (Part II)

a. **Fixed Layer (Part I).** For harmonic excitation with frequency ω , the dynamic-equilibrium equations of loaded layer j (see Figure 116) in Cartesian coordinates x and z can be written as

$$\sigma_{xx}(x, z) + \tau_{xz}(x, z) = -\rho\omega^2 u(x, z) - p(x, z) \quad (303)$$

$$\tau_{zx}(x, z) + \sigma_{zz}(x, z) = -\rho\omega^2 w(x, z) - r(x, z) \quad (304)$$

Normal stress and shear stress amplitudes are denoted as σ and τ , respectively. The first subscript denotes the direction of the stress component. The second one denotes the direction of the infinitesimal area's normal that the stress component acts on. A comma denotes a partial derivative with respect to the subscript following it. The letter ρ represents the mass density. Displacement amplitudes $u(x, z)$ and $w(x, z)$ are in x - and z -direction, respectively. Linearly distributed loads $p(x, z)$ and $r(x, z)$ can be expressed as

$$p(x, z) = \left[p_j + (p_{j+1} - p_j) \frac{z}{d} \right] \delta(x) \quad (305)$$

$$r(x, z) = \left[r_j + (r_{j+1} - r_j) \frac{z}{d} \right] \delta(x) \quad (306)$$

where the letter d represents the depth of the loaded layer j and $\delta(x)$ represents the Dirac-delta function equal to 1 at $x = 0$ and 0 where $x \neq 0$.

By using the stress-strain relationship (Hook's law) and strain-displacement relationship, the normal stress and shear stress amplitudes can be expressed as

$$\sigma_x(x, z) = [2\Upsilon^* + \lambda^*] u_x(x, z) + \lambda^* w_z(x, z) \quad (307)$$

$$\sigma_z(x, z) = [2\Upsilon^* + \lambda^*] w_z(x, z) + \lambda^* u_x(x, z) \quad (308)$$

$$\tau_{xz}(x, z) = \tau_{zx}(x, z) = \Upsilon^* [u_x(x, z) + w_x(x, z)] \quad (309)$$

where the complex shear modulus Υ^* and the complex Lamé constant λ^* [Equations (512), (519), and (535)] can be expressed as the functions of Young's modulus of elasticity E , Poisson's ratio ν , and the ratio of the linear hysteretic damping ζ as follows

$$\Upsilon^* = \frac{(1 + 2i\zeta)}{2(1 + \nu)} E \quad \text{and} \quad \lambda^* = \frac{\nu(1 + 2i\zeta)}{(1 + \nu)(1 - 2\nu)} E \quad (310)$$

As discussed in Equations (568) to (571), the x - z plane displacement equations of layer can be derived and expressed as follows

$$u(x, z) = u(k, z) \exp(-i\alpha x) \quad (311)$$

$$w(x, z) = w(k, z) \exp(-i\alpha x) \quad (312)$$

with

$$u(k, z) = l_x [A_P \exp(ukfz) + B_P \exp(-ukfz)] - m_x s [A_{SV} \exp(uksz) - B_{SV} \exp(-uksz)] \quad (313)$$

$$w(k, z) = -l_x f [A_P \exp(ukfz) - B_P \exp(-ukfz)] - m_x [A_{SV} \exp(uksz) + B_{SV} \exp(-uksz)] \quad (314)$$

where $l_x/C_P = m_x/C_S$ needs to be enforced.

The symbol ι represents $\sqrt{-1}$. The scalar k represents the wave number which is equal to ω/C . The letter C stands for phase velocity which is equal to C_P/l_x and C_S/m_x . C_P and C_S represent P- and S-wave velocities, and are equal to $\sqrt{(2\Upsilon^* + \lambda^*)/\rho}$ and $\sqrt{\Upsilon^*/\rho}$, respectively. Scalars l_x and m_x may be considered propagating directional cosines to the x -axis ($=\cos \psi_P$ and $=\cos \psi_S$) of the P- and S-wave, respectively. Algebraically, they are equal to kC_P/ω and kC_S/ω , respectively, which can be real, imaginary, or complex numbers. Therefore this interpretation holds only for real values smaller than or equal to 1. Scalars f and s are $\sqrt{1/l_x^2 - 1}$ and $\sqrt{1/m_x^2 - 1}$, respectively. A_P and A_{SV} are the amplitudes of the P- and SV-wave traveling in the negative z -direction (incident waves). B_P and B_{SV} are the amplitudes of the P- and SV-wave traveling in the positive z -direction (reflected waves).

Substituting the stresses in Equations (307) through (309) and the displacements in Equations (311) and (312) into the dynamic-equilibrium Equations (303) and (304) results in

$$\begin{aligned} \{\Gamma^* u_{\underline{z}}(k, z) - \mathcal{U}[\Gamma^* + \lambda^*]w_{\underline{z}}(k, z) - k^2[2\Gamma^* + \lambda^*]u(k, z)\}\exp(-\mathcal{U}\alpha) = \\ -\rho\omega^2 u(k, z)\exp(-\mathcal{U}\alpha) - p(x, z) \end{aligned} \quad (315)$$

$$\begin{aligned} \{-k^2\Gamma^* w(k, z) - \mathcal{U}[\Gamma^* + \lambda^*]u_{\underline{z}}(k, z) + [2\Gamma^* + \lambda^*]w_{\underline{z}}(k, z)\}\exp(-\mathcal{U}\alpha) = \\ -\rho\omega^2 w(k, z)\exp(-\mathcal{U}\alpha) - r(x, z) \end{aligned} \quad (316)$$

Distributed loads $p(x, z)$ and $r(x, z)$, defined in Equations (305) and (306), are then expanded in the x -direction into Fourier integrals, with term $\exp(-\mathcal{U}\alpha)$, as

$$p(k, z) = \frac{1}{2\pi} \int_{-\infty}^{\infty} p(x, z)\exp(\mathcal{U}\alpha)\alpha d\alpha = \frac{1}{2\pi} \left[p_j + (p_{j+1} - p_j) \frac{z}{d} \right] \quad (317)$$

$$r(k, z) = \frac{1}{2\pi} \int_{-\infty}^{\infty} r(x, z)\exp(\mathcal{U}\alpha)\alpha d\alpha = \frac{1}{2\pi} \left[r_j + (r_{j+1} - r_j) \frac{z}{d} \right] \quad (318)$$

Thus, using Equations (315) to (318) and omitting term $\exp(-\mathcal{U}\alpha)$, the equilibrium equations of loaded layer, for harmonic motion in k -domain, can be written as

$$\begin{aligned} \Gamma^* u_{\underline{z}}(k, z) - \mathcal{U}[\Gamma^* + \lambda^*]w_{\underline{z}}(k, z) - k^2[2\Gamma^* + \lambda^*]u(k, z) = \\ -\rho\omega^2 u(k, z) - \frac{1}{2\pi} \left[p_j + (p_{j+1} - p_j) \frac{z}{d} \right] \end{aligned} \quad (319)$$

$$\begin{aligned} -k^2\Gamma^* w(k, z) - \mathcal{U}[\Gamma^* + \lambda^*]u_{\underline{z}}(k, z) + [2\Gamma^* + \lambda^*]w_{\underline{z}}(k, z) = \\ -\rho\omega^2 w(k, z) - \frac{1}{2\pi} \left[r_j + (r_{j+1} - r_j) \frac{z}{d} \right] \end{aligned} \quad (320)$$

By inspection, the particular solutions (superscript P) of Equations (319) and (320) can be obtained and written in matrix form as

$$\begin{Bmatrix} u^p(k, z) \\ w^p(k, z) \end{Bmatrix}_j = [uwpr^p(k, z)]_j \begin{Bmatrix} p_j \\ r_j \\ p_{j+1} \\ r_{j+1} \end{Bmatrix} \quad (321)$$

with

$$[uwpr^p(k, z)]_j = \frac{1}{2\pi} \begin{bmatrix} -(1-z/d)\bar{A}(k) & \bar{B}(k) & -(z/d)\bar{A}(k) & -\bar{B}(k) \\ \bar{B}(k) & -(1-z/d)\bar{C}(k) & -\bar{B}(k) & -(z/d)\bar{C}(k) \end{bmatrix} \quad (322)$$

where

$$\bar{A}(k) = \frac{1}{k^2 \gamma^* j^2 \bar{D}}, \quad \bar{B}(k) = \frac{1(1-1/\bar{D})}{k^3 \gamma^* d j^2 s^2}, \quad \bar{C}(k) = \frac{1}{k^2 \gamma^* s^2}, \quad \bar{D} = \frac{C_p^2}{C_s^2} \quad (323)$$

and the j subscription for vectors or matrices denotes that they are associated with distributed loads on and/or physical properties of layer j .

At the top (node j , $z=0$) and the bottom (node $j+1$, $z=d$) of loaded layer j , the particular parts of corresponding displacements can be obtained as

$$\begin{Bmatrix} u_j^p(k) \\ w_j^p(k) \\ u_{j+1}^p(k) \\ w_{j+1}^p(k) \end{Bmatrix} = [uwpr^p(k)]_j \begin{Bmatrix} p_j \\ r_j \\ p_{j+1} \\ r_{j+1} \end{Bmatrix} \quad (324)$$

with

$$[uwpr^p(k)]_j = \frac{1}{2\pi} \begin{bmatrix} -\bar{A}(k) & \bar{B}(k) & 0 & -\bar{B}(k) \\ \bar{B}(k) & -\bar{C}(k) & -\bar{B}(k) & 0 \\ 0 & \bar{B}(k) & -\bar{A}(k) & -\bar{B}(k) \\ \bar{B}(k) & 0 & -\bar{B}(k) & -\bar{C}(k) \end{bmatrix} \quad (325)$$

where the subscript * denotes that the given matrix yields nodal values

Based on Equations (308), (309), (311), (312), and (321), on any z -planes ($z=\text{constant}$) the particular parts in k -domain of the normal stress in z -direction and of the shear stress in x -direction can be obtained as

$$\begin{aligned} \sigma_z^p(k, z) &= [2Y^* + \lambda^*]w_z^p(k, z) - \nu k \lambda^* u^p(k, z) \\ &= \frac{Y^*}{2\pi d} \left[\begin{array}{cc} \nu k \bar{A}(k)(\bar{D}-2)(d-z) & -\nu k d \bar{B}(k)(\bar{D}-2) + \bar{C}(k)\bar{D} \\ \nu k \bar{A}(k)(\bar{D}-2)z & \nu k d \bar{B}(k)(\bar{D}-2) - \bar{C}(k)\bar{D} \end{array} \right] \begin{Bmatrix} p_j \\ r_j \\ p_{j+1} \\ r_{j+1} \end{Bmatrix} \end{aligned} \quad (326)$$

$$\begin{aligned} \tau_{xz}^p(k, z) &= Y^* [u_z^p(k, z) - \nu k w^p(k, z)] \\ &= \frac{Y^*}{2\pi d} \left[\begin{array}{cc} \bar{A}(k) - \nu k d \bar{B}(k) & \nu k \bar{C}(k)(d-z) \\ -\bar{A}(k) + \nu k d \bar{B}(k) & \nu k \bar{C}(k)z \end{array} \right] \begin{Bmatrix} p_j \\ r_j \\ p_{j+1} \\ r_{j+1} \end{Bmatrix} \end{aligned} \quad (327)$$

The particular parts of reactions at the top and bottom of the loaded layer are defined as $P_j^p(k) = -\tau_{xz}^p(k, 0)$, $R_j^p(k) = -\sigma_z^p(k, 0)$, $P_{j+1}^p(k) = \tau_{xz}^p(k, d)$ and $R_{j+1}^p(k) = \sigma_z^p(k, d)$. By using Equations (326) and (327), they can be obtained in matrix form as

$$\begin{Bmatrix} P_j^p(k) \\ R_j^p(k) \\ P_{j+1}^p(k) \\ R_{j+1}^p(k) \end{Bmatrix} = [PRpr^p(k)]_j \begin{Bmatrix} p_j \\ r_j \\ p_{j+1} \\ r_{j+1} \end{Bmatrix} \quad (328)$$

with

$$[PRpr^p(k)]_j = \frac{\Upsilon^*}{2\pi d} \begin{bmatrix} [PRpr_{(1,1)}^p] & [PRpr_{(1,2)}^p] \\ [PRpr_{(2,1)}^p] & [PRpr_{(2,2)}^p] \end{bmatrix} \quad (329)$$

where

$$[PRpr_{(1,1)}^p] = \begin{bmatrix} -\bar{A}(k) + \nu kd\bar{B}(k) & -\nu kd\bar{C}(k) \\ -\nu kd\bar{A}(k)(\bar{D}-2) & \nu kd\bar{B}(k)(\bar{D}-2) - \bar{C}(k)\bar{D} \end{bmatrix} \quad (330)$$

$$[PRpr_{(1,2)}^p] = [PRpr_{(2,1)}^p] = \begin{bmatrix} \bar{A}(k) - \nu kd\bar{B}(k) & 0 \\ 0 & -\nu kd\bar{B}(k)(\bar{D}-2) + \bar{C}(k)\bar{D} \end{bmatrix} \quad (331)$$

$$[PRpr_{(2,2)}^p] = \begin{bmatrix} -\bar{A}(k) + \nu kd\bar{B}(k) & \nu kd\bar{C}(k) \\ \nu kd\bar{A}(k)(\bar{D}-2) & \nu kd\bar{B}(k)(\bar{D}-2) - \bar{C}(k)\bar{D} \end{bmatrix} \quad (332)$$

To complete the first part of the procedure, the homogeneous parts (superscript H) of the displacements and reactions will be determined and superimposed on the particular ones. Boundary conditions at node j and node $j+1$ of the homogeneous Equations (313) and (314) must be equal to the negative values of $u_j^p(k)$, $w_j^p(k)$, $u_{j+1}^p(k)$, and $w_{j+1}^p(k)$ in order to fix those two interfaces of the loaded layer. The homogeneous Equations (313) and (314) can be rewritten into matrix form in terms of the unknowns A_p , B_p , A_{SIV} and B_{SIV} as

$$\begin{Bmatrix} u(k, z) \\ w(k, z) \end{Bmatrix}_j = [uwAB(k, z)]_j \begin{Bmatrix} A_P \\ B_P \\ A_{SV} \\ B_{SV} \end{Bmatrix} \quad (333)$$

with

$$[uwAB(k, z)]_j = \begin{bmatrix} l_x \exp(kfz) & l_x \exp(-kfz) & -m_x s \exp(ksz) & m_x s \exp(-ksz) \\ -l_x f \exp(kfz) & l_x f \exp(-kfz) & -m_x \exp(ksz) & -m_x \exp(-ksz) \end{bmatrix} \quad (334)$$

By using Equation (333), the unknowns A_P , B_P , A_{SV} and B_{SV} can be expressed in terms of four boundary conditions at the top and bottom of the layer as

$$\begin{Bmatrix} A_P \\ B_P \\ A_{SV} \\ B_{SV} \end{Bmatrix}_j = [uwAB_*(k)]_j^{-1} \begin{Bmatrix} u_j(k) \\ w_j(k) \\ u_{j+1}(k) \\ w_{j+1}(k) \end{Bmatrix} \quad (335)$$

with

$$[uwAB_*(k)]_j = \begin{bmatrix} [uwAB_{(1,1)}] & [uwAB_{(1,2)}] \\ [uwAB_{(2,1)}] & [uwAB_{(2,2)}] \end{bmatrix} \quad (336)$$

where

$$[uwAB_{(1,1)}] = l_x \begin{bmatrix} 1 & 1 \\ -f & f \end{bmatrix} \quad (337)$$

$$[uwAB_{(1,2)}] = m_x \begin{bmatrix} -s & s \\ -1 & -1 \end{bmatrix} \quad (338)$$

$$[uwAB_{(2.1)}] = l_x \begin{bmatrix} \exp(ukfd) & \exp(-ukfd) \\ -f \exp(ukfd) & f \exp(-ukfd) \end{bmatrix} \quad (339)$$

$$[uwAB_{(2.2)}] = m_x \begin{bmatrix} -s \exp(uksd) & s \exp(-uksd) \\ -\exp(uksd) & -\exp(-uksd) \end{bmatrix} \quad (340)$$

Knowing the boundary conditions and then using Equations (324), (333) and (335), the homogeneous parts of the displacements can be obtained as

$$\begin{Bmatrix} u^H(k, z) \\ w^H(k, z) \end{Bmatrix}_j = [uwpr^H(k, z)]_j \begin{Bmatrix} p_j \\ r_j \\ p_{j+1} \\ r_{j+1} \end{Bmatrix} \quad (341)$$

with

$$[uwpr^H(k, z)]_j = -[uwAB(k, z)]_j [uwAB_*(k)]_j^{-1} [uwpr^P(k)]_j \quad (342)$$

Local displacements (part I) are the summation of the particular parts in Equation (321) and the homogeneous parts in Equation (341) which can be expressed as

$$\begin{Bmatrix} u_{pr}^I(k, z) \\ w_{pr}^I(k, z) \end{Bmatrix}_j = [uwpr^I(k, z)]_j \begin{Bmatrix} p_j \\ r_j \\ p_{j+1} \\ r_{j+1} \end{Bmatrix} \quad (343)$$

with

$$\begin{aligned} [uwpr^I(k, z)]_j &= [uwpr^P(k, z)]_j + [uwpr^H(k, z)]_j \\ &= [uwpr^P(k, z)]_j - [uwAB(k, z)]_j [uwAB_*(k)]_j^{-1} [uwpr^P(k)]_j \end{aligned} \quad (344)$$

Homogeneous parts of the reaction forces can be determined by using the dynamic stiffness of the horizontal layer in k -domain. As shown in Equation (445), external forces and nodal displacements of layer j are related to its stiffness matrix as

$$\begin{Bmatrix} P_j(k) \\ R_j(k) \\ P_{j+1}(k) \\ R_{j+1}(k) \end{Bmatrix} = [S_{P-SV}^L(k)]_j \begin{Bmatrix} u_j(k) \\ w_j(k) \\ u_{j+1}(k) \\ w_{j+1}(k) \end{Bmatrix} \quad (345)$$

By substituting negative values of the particular parts of the nodal displacements into Equation (345), homogeneous parts of the reactions can be obtained as

$$\begin{Bmatrix} P_j^H(k) \\ R_j^H(k) \\ P_{j+1}^H(k) \\ R_{j+1}^H(k) \end{Bmatrix} = [PRpr^H(k)]_j \begin{Bmatrix} p_j \\ r_j \\ p_{j+1} \\ r_{j+1} \end{Bmatrix} \quad (346)$$

with

$$[PRpr^H(k)]_j = -[S_{P-SV}^L(k)]_j [uwpr^P(k)]_j \quad (347)$$

For loaded layer j , the reaction forces (see Figure 117) to counterbalance the linearly distributed loads and fix the interfaces can be obtained by combining Equations (328) and (346) as

$$\begin{Bmatrix} P_j^I(k) \\ R_j^I(k) \\ P_{j+1}^I(k) \\ R_{j+1}^I(k) \end{Bmatrix} = [PRpr^I(k)]_j \begin{Bmatrix} p_j \\ r_j \\ p_{j+1} \\ r_{j+1} \end{Bmatrix} \quad (348)$$

with

$$\begin{aligned}
 [PRpr^L(k)]_j &= [PRpr^P(k)]_j + [PRpr^H(k)]_j \\
 &= [PRpr^P(k)]_j - [S_{P-SV}^L(k)]_j [uwpr^P(k)]_j
 \end{aligned}
 \tag{349}$$

b. **Free Layer (Part II).** The dynamic-stiffness matrix $[S_{P-SV}^T(k)]$ of the total soil system which consists of $N-1$ layers and a half-space (see Figure 119) is first assembled by using the direct stiffness approach. In the assembling process, the stiffness matrices of two adjacent layers and half-space are overlapped on the matrix's elements corresponding to the same node. Superscript T stands for the total soil system.

In Equations (445) and (488), the dynamic-stiffness matrices $[S_{P-SV}^L(k)]$, of any horizontal layer i , for $i=1,2,\dots,N-1$, relate displacement amplitudes u and w at node i and node $i+1$ to load amplitudes P and R at the same nodes. The force-displacement

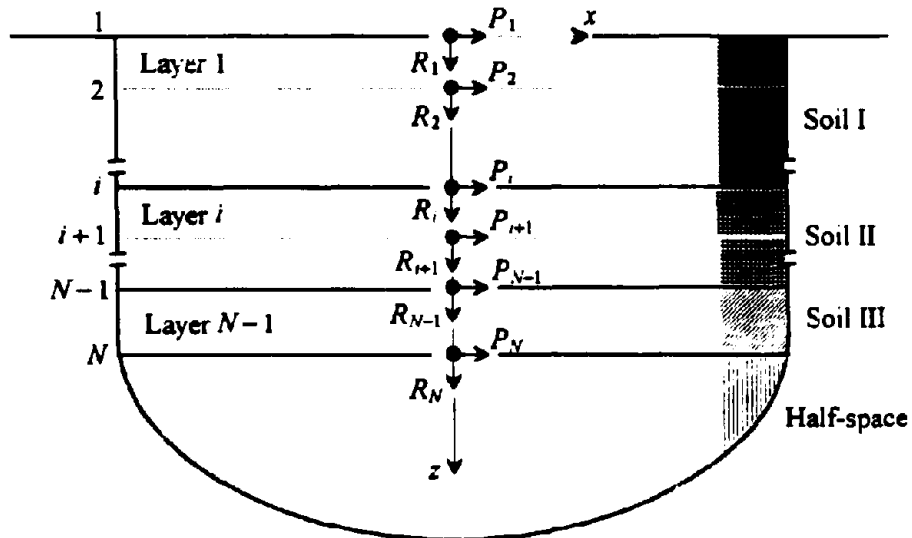


Figure 119. Total Soil System in k -domain

relationship of the half-space can be obtained by the dynamic-stiffness matrices $[S_{P-SV}^R(k)]$ in Equations (460), (468), and (501). Both relationships can be expressed as follows

$$\begin{Bmatrix} P_i(k) \\ R_i(k) \\ P_{i+1}(k) \\ R_{i+1}(k) \end{Bmatrix} = [S_{P-SV}^L(k)] \begin{Bmatrix} u_i(k) \\ w_i(k) \\ u_{i+1}(k) \\ w_{i+1}(k) \end{Bmatrix} \quad (350)$$

$$\begin{Bmatrix} P_0(k) \\ R_0(k) \end{Bmatrix} = [S_{P-SV}^R(k)] \begin{Bmatrix} u_0(k) \\ w_0(k) \end{Bmatrix} \quad (351)$$

As shown in Equations (311) and (312), the variation of displacement amplitudes $u(x,z)$ and $w(x,z)$ in the x -direction is determined by wave number k and is thus constant with depth for the layer. Boundary conditions at the interface of two adjacent layers and half-space force the value of k to be constant for the total soil system. For a given frequency ω , phase velocity C has to be constant ($C=\omega/k$) for all layers and half-space. After determining $[S_{P-SV}^L(k)]$, and $[S_{P-SV}^R(k)]$ by taking this into consideration, the total dynamic-stiffness matrix in k -domain $[S_{P-SV}^T(k)]$ can be assembled and expressed as

$$\begin{Bmatrix} P_1(k) \\ R_1(k) \\ \vdots \\ P_i(k) \\ R_i(k) \\ \vdots \\ P_N(k) \\ R_N(k) \end{Bmatrix} = [S_{P-SV}^T(k)] \begin{Bmatrix} u_1(k) \\ w_1(k) \\ \vdots \\ u_i(k) \\ w_i(k) \\ \vdots \\ u_N(k) \\ w_N(k) \end{Bmatrix} \quad (352)$$

For the distributed loads acting on the vertical assumed line of any layer j between node j and node $j+1$, reactions at the corresponding nodes were determined in part I as

shown in Equation (348). Applying these forces in the opposite direction at the same nodes to the total soil system (see Figure 118), nodal displacements at any node i and node $i+1$ can be calculated. Using Equation (348) and (352), they can be expressed as

$$\begin{Bmatrix} u_i^{II}(k) \\ w_i^{II}(k) \\ u_{i+1}^{II}(k) \\ w_{i+1}^{II}(k) \end{Bmatrix} = [uwpr_r^I(k)]_j' \begin{Bmatrix} p_j \\ r_j \\ p_{j+1} \\ r_{j+1} \end{Bmatrix} \quad (353)$$

with

$$\begin{aligned} [uwpr_r^I(k)]_j' &= -SUB_{ij} \left([S_{p-SV}^T(k)]^{-1} \right) [PRpr_r^I(k)]_j \\ &= -SUB_{ij} \left([S_{p-SV}^T(k)]^{-1} \right) \\ &\quad \left([PRpr_r^P(k)]_j - [S_{p-SV}^L(k)]_j [uwpr_r^P(k)]_j \right) \end{aligned} \quad (354)$$

where $SUB_{ij} \left([S_{p-SV}^T(k)]^{-1} \right)$ is the submatrix of dimension 4 by 4, comprising the coefficients in the matrix $[S_{p-SV}^T(k)]^{-1}$ from row $4i-3^{\text{th}}$ to row $4i^{\text{th}}$ and column $4j-3^{\text{th}}$ to column $4j^{\text{th}}$ and $[PRpr_r^I(k)]_j$ is shown in Equation (349). The i superscription for vectors or matrices indicates that they are associated with layer r 's displacements.

Displacements $u_{pr}^{II}(k, z)$ and $w_{pr}^{II}(k, z)$ between node i and node $i+1$ are determined by using nodal displacements in Equation (353) as the boundary conditions of homogeneous Equations (313) and (314). Using Equations (333), (335) and (353), the displacement vector in part II can be obtained as

$$\begin{Bmatrix} u_{pr}^{II}(k, z) \\ w_{pr}^{II}(k, z) \end{Bmatrix}' = [uwpr^{II}(k, z)]_j' \begin{Bmatrix} p_j \\ r_j \\ p_{j+1} \\ r_{j+1} \end{Bmatrix} \quad (355)$$

with

$$\begin{aligned} [uwpr^{II}(k, z)]_j' &= [uwAB(k, z)]_j [uwAB_*(k)]_j^{-1} [uwpr_*^{II}(k)]_j' \\ &= -[uwAB(k, z)]_j [uwAB_*(k)]_j^{-1} SUB_j \left([S_{P-SV}^I(k)]^{-1} \right) \\ &\quad \left([PRpr_*^P(k)]_j - [S_{P-SV}^L(k)]_j [uwpr_*^P(k)]_j \right) \end{aligned} \quad (356)$$

c. **Global Displacements.** Along the vertical line in any layer i , for $i=1, 2, \dots, M$ where M = number of layers along the vertical assumed line, on which no distributed loads act ($i \neq j$), global displacements $u_{pr}(k, z)$ and $w_{pr}(k, z)$ are equal to the displacements determined in part II (355) and can be written as

$$\begin{Bmatrix} u_{pr}(k, z) \\ w_{pr}(k, z) \end{Bmatrix}' = \begin{Bmatrix} u_{pr}^{II}(k, z) \\ w_{pr}^{II}(k, z) \end{Bmatrix}' = [uwpr(k, z)]_j' \begin{Bmatrix} p_j \\ r_j \\ p_{j+1} \\ r_{j+1} \end{Bmatrix} \quad (357)$$

with

$$\begin{aligned} [uwpr(k, z)]_j' &= -[uwAB(k, z)]_j [uwAB_*(k)]_j^{-1} SUB_j \left([S_{P-SV}^I(k)]^{-1} \right) \\ &\quad \left([PRpr_*^P(k)]_j - [S_{P-SV}^L(k)]_j [uwpr_*^P(k)]_j \right) \end{aligned} \quad (358)$$

Along the vertical line in any layer i on which the distributed loads act ($i=j$), global displacements $u_{pr}(k, z)$ and $w_{pr}(k, z)$ are the combination of displacements obtained in part I (343) and part II (355), and can be expressed as

$$\begin{Bmatrix} u_{pr}(k, z) \\ w_{pr}(k, z) \end{Bmatrix}_j^{i=j} = \begin{Bmatrix} u'_{pr}(k, z) \\ w'_{pr}(k, z) \end{Bmatrix}_j + \begin{Bmatrix} u''_{pr}(k, z) \\ w''_{pr}(k, z) \end{Bmatrix}_j = [uwpr(k, z)]_j^{i=j} \begin{Bmatrix} p_j \\ r_j \\ p_{j+1} \\ r_{j+1} \end{Bmatrix} \quad (359)$$

with

$$\begin{aligned} [uwpr(k, z)]_j^{i=j} &= [uwpr^p(k, z)]_j - [uwAB(k, z)]_j [uwAB \cdot (k)]_j^{-1} [uwpr^p(k)]_j \\ &\quad - [uwAB(k, z)]_j [uwAB \cdot (k)]_j^{-1} SUB_{ij} \left([S_{p-SV}^T(k)]^{-1} \right) \\ &\quad \left([PRpr^p(k)]_j - [S_{p-SV}^L(k)]_j [uwpr^p(k)]_j \right) \end{aligned} \quad (360)$$

2. Displacements in k -domain for Loads on Horizontal Line.

As shown in Figure 120, the horizontal linearly distributed load $p(x)$, with nodal values of p_l and p_{l+1} in x -direction, and the vertical linearly distributed load $r(x)$, with nodal values of r_l and r_{l+1} in z -direction, act on part of the horizontal assumed line between node l and node $l+1$, which lies underneath layer M . Since the distributed loads act on the horizontal interface, not between the interfaces, the first part of the procedure mentioned in the previous subsection is not required.

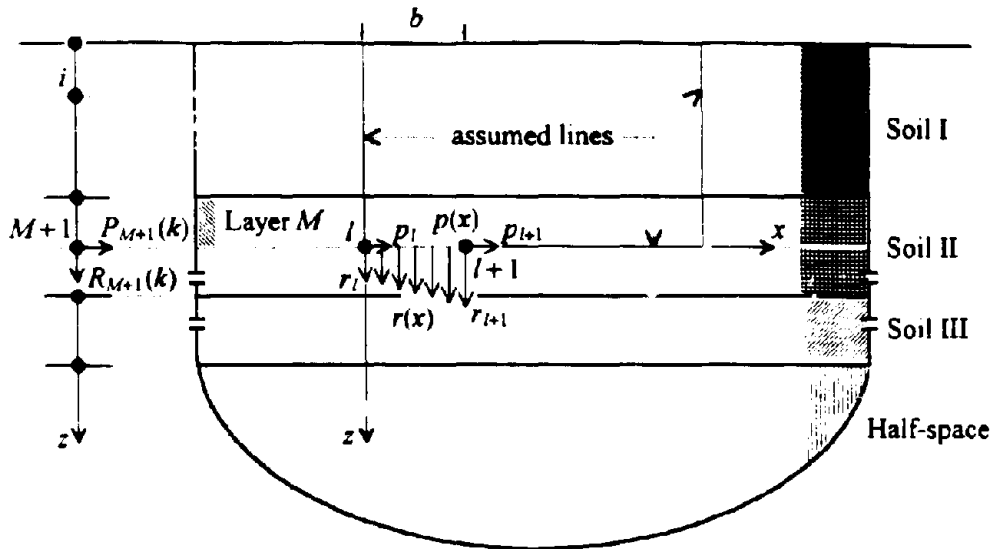


Figure 120. Linearly Distributed Loads on Horizontal Assumed Line

Linearly distributed loads $p(x)$ and $r(x)$ can be expressed in matrix form as

$$\begin{Bmatrix} p(x) \\ r(x) \end{Bmatrix} = \begin{bmatrix} (1-x/b) & 0 & x/b & 0 \\ 0 & (1-x/b) & 0 & x/b \end{bmatrix} \begin{Bmatrix} p_l \\ r_l \\ p_{l+1} \\ r_{l+1} \end{Bmatrix} \quad (361)$$

where the letter b is the length between node l and node $l+1$. Then the distributed loads are expanded in the x -direction into Fourier integrals, with term $\exp(-i\alpha x)$, as

$$\begin{Bmatrix} P_{M+1}(k) \\ R_{M+1}(k) \end{Bmatrix} = \frac{1}{2\pi} \int_0^b \begin{Bmatrix} p(x) \\ r(x) \end{Bmatrix} \exp(i\alpha x) dx$$

$$= [PRpr_*(k)]_{M,l} \begin{Bmatrix} p_l \\ r_l \\ p_{l+1} \\ r_{l+1} \end{Bmatrix} \quad (362)$$

with

$$[PRpr_*(k)]_{M,l} = \frac{1}{2\pi} \begin{bmatrix} Pp_l & 0 & Pp_{l+1} & 0 \\ 0 & Rr_l & 0 & Rr_{l+1} \end{bmatrix} \quad (363)$$

where

$$Pp_l = Rr_l = \frac{1}{k} [1 - \exp(ukb)] - \frac{1}{k^2 b} [\exp(ukb)(1 - ukb) - 1] \quad (364)$$

$$Pp_{l+1} = Rr_{l+1} = \frac{1}{k^2 b} [\exp(ukb)(1 - ukb) - 1] \quad (365)$$

The M,l subscription for vectors and matrices denotes that they are associated with distributed loads on the horizontal element between node l and node $l+1$ which are on the horizontal interface underneath layer M .

These external loads are then applied to the total soil system at node $M+1$ corresponding to the horizontal assumed line (see Figure 120). By using the total dynamic-stiffness matrix $[S_{P-SV}^T(k)]$ mentioned in Equation (352) and the external loads in Equation (362), nodal displacements at any node i and node $i+1$ on vertical line can be obtained as

$$\begin{Bmatrix} u_i(k) \\ w_i(k) \\ u_{i+1}(k) \\ w_{i+1}(k) \end{Bmatrix}_{M,l} = [uwpr_*(k)]_{M,l}^i \begin{Bmatrix} p_l \\ r_l \\ p_{l+1} \\ r_{l+1} \end{Bmatrix} \quad (366)$$

with

$$[uwpr_*(k)]_{M,l}^i = sub_{iM} \left([S_{P-SV}^T(k)]^{-1} \right) [PRpr_*(k)]_{M,l} \quad (367)$$

where $sub_M([S_{P-SV}^T(k)]^{-1})$ is the submatrix of dimension 4 by 2. This dimension comprises elements in the matrix $[S_{P-SV}^T(k)]^{-1}$ from row $4i-3^{th}$ to row $4i^{th}$ and column $4M-1^{th}$ to column $4M^{th}$. $[PRpr_i(k)]$ can be obtained from Equation (363). The i superscription for vectors or matrices indicates that they are associated with layer i 's displacements.

Analogous to part II of displacements for loads on the vertical assumed line in the previous subsection, displacements $u_{pr}(k,z)$ and $w_{pr}(k,z)$ between node i and node $i+1$ are calculated by using nodal displacements in Equation (366) as the boundary conditions of displacement Equations (313) and (314). Using Equations (333), (335) and (366), the displacement vector can be obtained as

$$\begin{Bmatrix} u_{pr}(k,z) \\ w_{pr}(k,z) \end{Bmatrix}_{M,i}^i = [uwpr(k,z)]_{M,i}^i \begin{Bmatrix} p_i \\ r_i \\ p_{i+1} \\ r_{i+1} \end{Bmatrix} \quad (368)$$

with

$$\begin{aligned} [uwpr(k,z)]_{M,i}^i &= [uwAB(k,z)]_i [uwAB_i(k)]_i^{-1} [wpr_i(k)]_{M,i}^i \\ &= [uwAB(k,z)]_i [uwAB_i(k)]_i^{-1} \\ &\quad sub_M([S_{P-SV}^T(k)]^{-1}) [PRpr_i(k)]_{M,i} \end{aligned} \quad (369)$$

3. Displacements for Vertically Incident Wave.

a. Loads on Vertical Line. A procedure is analogous to Subsection 1. For the vertically incident waves which correspond to a zero wave number k , displacement equations [see Equations (572) and (573) of Appendix C] can be expressed as

$$u(x, z)^{k=0} = -A_{SV} \exp\left(\frac{1\omega}{C_S} z\right) + B_{SV} \exp\left(-\frac{1\omega}{C_S} z\right) \quad (370)$$

$$w(x, z)^{k=0} = -A_P \exp\left(\frac{1\omega}{C_P} z\right) + B_P \exp\left(-\frac{1\omega}{C_P} z\right) \quad (371)$$

Using stress Equations (308) and (309) and displacement Equations (370) and (371), the dynamic-equilibrium Equations (303) and (304) for loaded layer j can be reformulated as

$$\Upsilon^* u_{,z}(z) = -\rho\omega^2 u(z) - \frac{1}{2\pi} \left[p_j + (p_{j+1} - p_j) \frac{z}{d} \right] \quad (372)$$

$$[2\Upsilon^* + \lambda^*] w_{,z}(z) = -\rho\omega^2 w(z) - \frac{1}{2\pi} \left[r_j + (r_{j+1} - r_j) \frac{z}{d} \right] \quad (373)$$

Displacements in Equations (372) and (373) are uncoupled. By inspection, the particular solutions of these equations can be obtained in matrix form as

$$\begin{Bmatrix} u^p(z) \\ w^p(z) \end{Bmatrix}_j = [uwp^p(z)]_j^{k=0} \begin{Bmatrix} p_j \\ r_j \\ p_{j+1} \\ r_{j+1} \end{Bmatrix} \quad (374)$$

with

$$[uwpr^p(z)]_j^{k=0} = \frac{-C_S^2}{2\pi\omega^2\Upsilon^*} \begin{bmatrix} 1-z/d & 0 & z/d & 0 \\ 0 & 1-z/d & 0 & z/d \end{bmatrix} \quad (375)$$

At the top (node $j, z = 0$) and bottom (node $j+1, z = d$) of the loaded layer, the particular parts of corresponding displacements can be obtained as

$$\begin{Bmatrix} u_j^p \\ w_j^p \\ u_{j+1}^p \\ w_{j+1}^p \end{Bmatrix} = [uwpr^p]_j^{k=0} \begin{Bmatrix} p_j \\ r_j \\ p_{j+1} \\ r_{j+1} \end{Bmatrix} \quad (376)$$

with

$$[uwpr^p]_j^{k=0} = \frac{-C_S^2}{2\pi\omega^2\Upsilon^*} \begin{bmatrix} 1 & 0 & 0 & 0 \\ 0 & 1 & 0 & 0 \\ 0 & 0 & 1 & 0 \\ 0 & 0 & 0 & 1 \end{bmatrix} \quad (377)$$

Based on Equations (308), (309), and (374), on any z -planes ($z=\text{constant}$) the particular parts of the normal stress in z -direction and the shear stress in x -direction can be obtained as

$$\sigma_z^p(z) = [2\Upsilon^* + \lambda^*]w_z^p(z) = \frac{C_P^2}{2\pi\omega^2 d}(r_j - r_{j+1}) \quad (378)$$

$$\tau_{xz}^p(z) = \Upsilon^*u_z^p(z) = \frac{C_S^2}{2\pi\omega^2 d}(p_j - p_{j+1}) \quad (379)$$

By using Equations (378) and (379), the particular parts of reactions at the top and bottom of the loaded layer can be obtained in matrix form as

$$\begin{Bmatrix} P_j^p \\ R_j^p \\ P_{j+1}^p \\ R_{j+1}^p \end{Bmatrix} = [PRPr^p]_j^{k=0} \begin{Bmatrix} p_j \\ r_j \\ p_{j+1} \\ r_{j+1} \end{Bmatrix} \quad (380)$$

with

$$[PRPr^p]_j^{k=0} = \frac{1}{2\pi\omega^2 d} \begin{bmatrix} -C_S^2 & 0 & C_S^2 & 0 \\ 0 & -C_P^2 & 0 & C_P^2 \\ C_S^2 & 0 & -C_S^2 & 0 \\ 0 & C_P^2 & 0 & -C_P^2 \end{bmatrix} \quad (381)$$

Homogeneous Equations (370) and (371) can be rewritten in matrix form in terms of the unknowns A_p , B_p , A_{SV} , and B_{SV} as

$$\begin{Bmatrix} z(z) \\ w(z) \end{Bmatrix}_j = [uwAB(z)]_j^{k=0} \begin{Bmatrix} A_p \\ B_p \\ A_{SV} \\ B_{SV} \end{Bmatrix} \quad (382)$$

with

$$[uwAB(z)]_j^{k=0} = \begin{bmatrix} 0 & 0 & -\exp(i\omega z/C_S) & \exp(-i\omega z/C_S) \\ -\exp(i\omega z/C_P) & \exp(-i\omega z/C_P) & 0 & 0 \end{bmatrix} \quad (383)$$

By using Equation (382), the unknowns A_p , B_p , A_{SV} , and B_{SV} can be expressed in terms of four boundary conditions at the top and bottom of the layer as

$$\begin{Bmatrix} A_P \\ B_P \\ A_{SV} \\ B_{SV} \end{Bmatrix}_j = [uwAB_*]_j^{hom0} \begin{Bmatrix} u_j \\ w_j \\ u_{j+1} \\ w_{j+1} \end{Bmatrix} \quad (384)$$

with

$$[uwAB_*]_j^{hom0} = \begin{bmatrix} 0 & 0 & -1 & 1 \\ -1 & 1 & 0 & 0 \\ 0 & 0 & -\exp(i\omega d/C_S) & \exp(-i\omega d/C_S) \\ -\exp(i\omega d/C_P) & \exp(-i\omega d/C_P) & 0 & 0 \end{bmatrix} \quad (385)$$

Knowing the boundary conditions which equal the negative values of u_j^P , w_j^P , u_{j+1}^P , w_{j+1}^P and then using Equations (376), (382), and (384), the homogeneous parts of the displacements can be obtained as

$$\begin{Bmatrix} u^H(z) \\ w^H(z) \end{Bmatrix}_j = [uwpr^H(z)]_j^{hom0} \begin{Bmatrix} p_j \\ r_j \\ p_{j+1} \\ r_{j+1} \end{Bmatrix} \quad (386)$$

with

$$\begin{aligned} [uwpr^H(z)]_j^{hom0} &= -[uwAB_*]_j^{hom0} [uwAB_*]_j^{hom0}^{-1} [uwpr_*^P]_j^{hom0} \\ &= \frac{C_S^2}{2\pi\omega^2\Upsilon^*} \begin{bmatrix} uwpr_{(1,1)}^H & 0 & uwpr_{(1,2)}^H & 0 \\ 0 & uwpr_{(2,2)}^H & 0 & uwpr_{(2,4)}^H \end{bmatrix} \end{aligned} \quad (387)$$

where

$$uwpr_{(1,1)}^H = \frac{\sin [\omega(d-z)/C_S]}{\sin (\omega d/C_S)} \quad (388)$$

$$uwpr_{(1,3)}^H = \frac{\sin (\omega z/C_S)}{\sin (\omega d/C_S)} \quad (389)$$

$$uwpr_{(2,2)}^H = \frac{\sin [\omega(d-z)/C_P]}{\sin (\omega d/C_P)} \quad (390)$$

$$uwpr_{(2,4)}^H = \frac{\sin (\omega z/C_P)}{\sin (\omega d/C_P)} \quad (391)$$

Local displacements for $k=0$ are the summation of the particular parts in Equation (374) and the homogeneous parts in Equation (387) which can be expressed as

$$\left\{ \begin{array}{l} u_{pr}^l(z) \\ w_{pr}^l(z) \end{array} \right\}_j = [uwpr^l(z)]_j^{k=0} \left\{ \begin{array}{l} p_j \\ r_j \\ p_{j+1} \\ r_{j+1} \end{array} \right\} \quad (392)$$

with

$$\begin{aligned} [uwpr^l(z)]_j^{k=0} &= [uwpr^p(z)]_j^{k=0} + [uwpr^H(z)]_j^{k=0} \\ &= \frac{C_S^2}{2\pi\omega^2\Upsilon^0} \left[\begin{array}{cccc} uwpr_{(1,1)}^l & 0 & uwpr_{(1,3)}^l & 0 \\ 0 & uwpr_{(2,2)}^l & 0 & uwpr_{(2,4)}^l \end{array} \right] \end{aligned} \quad (393)$$

where

$$uwpr_{(1,1)}^l = \frac{\sin [\omega(d-z)/C_S]}{\sin (\omega d/C_S)} + \frac{z}{d} - 1 \quad (394)$$

$$uwpr_{(1,3)}^l = \frac{\sin (\omega z/C_S)}{\sin (\omega d/C_S)} - \frac{z}{d} \quad (395)$$

$$uwpr_{(2,2)}^j = \frac{\sin[\omega(d-z)/C_p]}{\sin(\omega d/C_p)} + \frac{z}{d} - 1 \quad (396)$$

$$uwpr_{(2,4)}^j = \frac{\sin(\omega z/C_p)}{\sin(\omega d/C_p)} - \frac{z}{d} \quad (397)$$

As shown in Equation (488), external forces and nodal displacements of layer j , for $k = 0$, are related to its stiffness matrix as

$$\begin{Bmatrix} P_j \\ R_j \\ P_{j+1} \\ R_{j+1} \end{Bmatrix} = [S_{P-SV}^L]_j^{k=0} \begin{Bmatrix} u_j \\ w_j \\ u_{j+1} \\ w_{j+1} \end{Bmatrix} \quad (398)$$

By substituting negative values of the particular parts of nodal displacements (376) into Equation (398), the homogeneous parts of the reactions can be obtained as

$$\begin{Bmatrix} P_j^H \\ R_j^H \\ P_{j+1}^H \\ R_{j+1}^H \end{Bmatrix} = [PRpr_*^H]_j^{k=0} \begin{Bmatrix} P_j \\ r_j \\ P_{j+1} \\ r_{j+1} \end{Bmatrix} \quad (399)$$

with

$$\begin{aligned} [PRpr_*^H]_j^{k=0} &= -[S_{P-SV}^L]_j^{k=0} [uwpr_*^p]_j^{k=0} \\ &= \frac{C_S}{2\pi\omega} \begin{bmatrix} PRpr_{(1,1)}^H & 0 & PRpr_{(1,3)}^H & 0 \\ 0 & PRpr_{(2,2)}^H & 0 & PRpr_{(2,4)}^H \\ PRpr_{(3,1)}^H & 0 & PRpr_{(3,3)}^H & 0 \\ 0 & PRpr_{(4,2)}^H & 0 & PRpr_{(4,4)}^H \end{bmatrix} \end{aligned} \quad (400)$$

where

$$PRpr_{(1,1)}^H = PRpr_{(3,3)}^H = \cot\left(\frac{\omega d}{C_S}\right) \quad (401)$$

$$PRpr_{(1,3)}^H = PRpr_{(3,1)}^H = \frac{-1}{\sin(\omega d/C_S)} \quad (402)$$

$$PRpr_{(2,2)}^H = PRpr_{(4,4)}^H = \left(\frac{C_P}{C_S}\right) \cot\left(\frac{\omega d}{C_P}\right) \quad (403)$$

$$PRpr_{(2,4)}^H = PRpr_{(4,2)}^H = \left(\frac{C_P}{C_S}\right) \frac{-1}{\sin(\omega d/C_P)} \quad (404)$$

For loaded layer j , the reaction forces for $k=0$ (see Figure 117) to counterbalance linearly distributed loads and fix the interfaces can be obtained by combining Equations (380) and (399) as

$$\begin{Bmatrix} P_j^I \\ R_j^I \\ P_{j+1}^I \\ R_{j+1}^I \end{Bmatrix} = [PRpr_{\cdot}^I]_j^{k=0} \begin{Bmatrix} P_j \\ r_j \\ P_{j+1} \\ r_{j+1} \end{Bmatrix} \quad (405)$$

with

$$\begin{aligned} [PRpr_{\cdot}^I]_j^{k=0} &= [PRpr_{\cdot}^{P_1}]_j^{k=0} + [PRpr_{\cdot}^H]_j^{k=0} \\ &= \frac{C_S}{2\pi\omega} \begin{bmatrix} PRpr_{(1,1)}^I & 0 & PRpr_{(1,3)}^I & 0 \\ 0 & PRpr_{(2,2)}^I & 0 & PRpr_{(2,4)}^I \\ PRpr_{(3,1)}^I & 0 & PRpr_{(3,3)}^I & 0 \\ 0 & PRpr_{(4,2)}^I & 0 & PRpr_{(4,4)}^I \end{bmatrix} \end{aligned} \quad (406)$$

where

$$PRpr_{(1,1)}^I = PRpr_{(3,3)}^I = \cot\left(\frac{\omega d}{C_S}\right) - \frac{C_S}{\omega d} \quad (407)$$

$$PRpr_{(1,3)}^i = PRpr_{(3,1)}^i = \frac{-1}{\sin(\omega d/C_S)} + \frac{C_S}{\omega d} \quad (408)$$

$$PRpr_{(2,2)}^i = PRpr_{(4,4)}^i = \left(\frac{C_P}{C_S}\right) \cot\left(\frac{\omega d}{C_P}\right) - \frac{C_P^2}{C_S \omega d} \quad (409)$$

$$PRpr_{(2,4)}^i = PRpr_{(4,2)}^i = \left(\frac{C_P}{C_S}\right) \frac{-1}{\sin(\omega d/C_P)} + \frac{C_P^2}{C_S \omega d} \quad (410)$$

Analogous to the derivation of Equation (357), global displacements $u_{pr}(k=0,z)$ and $w_{pr}(k=0,z)$ along the vertical line in any layer i , on which no distributed loads act ($i \neq j$), can be expressed as

$$\begin{Bmatrix} u_{pr}(k=0,z) \\ w_{pr}(k=0,z) \end{Bmatrix}_j^{i,ny} = [uwpr(k=0,z)]_j^{i,ny} \begin{Bmatrix} p_j \\ r_j \\ p_{j+1} \\ r_{j+1} \end{Bmatrix} \quad (411)$$

with

$$[uwpr(k=0,z)]_j^{i,ny} = -[uwAB(z)]_i^{k=0} [uwAB_*]_i^{k=0}]^{-1} SUB_{ij} \left(\left[[S_{P-SV}^T]^{k=0} \right]^{-1} \right) [PRpr_*]_j^{k=0} \quad (412)$$

where $[PRpr_*]_j^{k=0}$ can be obtained from Equation (406).

And similar to the derivation of Equation (359), global displacements $u_{pr}(k=0,z)$ and $w_{pr}(k=0,z)$ along the vertical line in any layer i , on which the distributed loads act ($i=j$), can be expressed as

$$\begin{Bmatrix} u_{pr}(k=0, z) \\ w_{pr}(k=0, z) \end{Bmatrix}_j^{i,uy} = [uwpr(k=0, z)]_j^{i,uy} \begin{Bmatrix} p_j \\ r_j \\ p_{j+1} \\ r_{j+1} \end{Bmatrix} \quad (413)$$

with

$$\begin{aligned} [uwpr(k=0, z)]_j^{i,uy} &= [uwpr'(z)]_j^{k=0} - [uwAB(z)]_i^{k=0} [[uwAB.]_i^{k=0}]^{-1} \\ &\quad SUB_{ij} \left(\left([[S_{P-SV}^T]^{k=0}]^{-1} \right) [PRpr']_j^{k=0} \right) \end{aligned} \quad (414)$$

where $[uwpr'(z)]_j^{k=0}$ and $[PRpr']_j^{k=0}$ can be obtained from Equations (393) and (406), respectively.

b. Loads on Horizontal Line. Analogous to Subsection 2, external loads $P(k=0)$ and $R(k=0)$ can be formulated as

$$\begin{aligned} \begin{Bmatrix} P_{M+1}(k=0) \\ R_{M+1}(k=0) \end{Bmatrix} &= \frac{1}{2\pi} \int_0^b \begin{Bmatrix} p(x) \\ r(x) \end{Bmatrix} dx \\ &= [PRpr.]_{M,l}^{k=0} \begin{Bmatrix} p_l \\ r_l \\ p_{l+1} \\ r_{l+1} \end{Bmatrix} \end{aligned} \quad (415)$$

with

$$[PRpr.]_{M,l}^{k=0} = \frac{b}{4\pi} \begin{bmatrix} 1 & 0 & 1 & 0 \\ 0 & 1 & 0 & 1 \end{bmatrix} \quad (416)$$

Similar to the derivation of Equation (368), displacements $u_{pr}(k=0, z)$ and $w_{pr}(k=0, z)$ between node i and node $i+1$, for loads on horizontal element l underneath layer M , can be expressed as

$$\begin{Bmatrix} u_{pr}(k=0, z) \\ w_{pr}(k=0, z) \end{Bmatrix}'_{M,l} = [uwpr(k=0, z)]'_{M,l} \begin{Bmatrix} p_l \\ r_l \\ p_{l+1} \\ r_{l+1} \end{Bmatrix} \quad (417)$$

with

$$[uwpr(k=0, z)]'_{M,l} = [uwAB(z)]_i^{k=0} [[uwAB\cdot]_i^{k=0}]^{-1} sub_M \left(\left[[S_{P-SV}^T]^{k=0} \right]^{-1} \right) [PRpr\cdot]_{M,l}^{k=0} \quad (418)$$

4. Green's Influence Functions in Space Domain.

In the previous subsections, displacements were determined in k -domain. The inverse Fourier transform needs to be formulated in order to obtain Green's influence functions in the space domain. The z -axis is based on the local z -axis of layer i . The x' -axis is based on the local x -axis of layer j for distributed loads on vertical interface, and of element l for distributed loads on horizontal interface.

Green's influence function in any layer i on x' - z plane, for the linearly distributed loads on the vertical assumed line in any layer j , can be expressed as

$$\begin{Bmatrix} u_{pr}(x', z) \\ w_{pr}(x', z) \end{Bmatrix}'_j = [uwpr(x', z)]'_j \begin{Bmatrix} p_j \\ r_j \\ p_{j+1} \\ r_{j+1} \end{Bmatrix} \quad (419)$$

with

$$[\mathbf{uwpr}(x', z)]_j' = \int_{-\infty}^{\infty} [\mathbf{uwpr}(k, z)]_j' \exp(-ikx') dk \quad (420)$$

where $[\mathbf{uwpr}(k, z)]_j'$ can be obtained from Equation (358) or (360) for non-zero wave numbers k and from Equation (412) or (414) for a zero wave number k . Bold letters in the matrix indicate that the corresponding matrix is in the space domain.

As for linearly distributed loads on the horizontal element with any node l and node $l+1$, which are on the horizontal interface underneath layer M . Green's influence function in any layer i on x' - z plane can be expressed as

$$\left\{ \begin{array}{c} u_{pr}(x', z) \\ w_{pr}(x', z) \end{array} \right\}_{M,i}' = [\mathbf{uwpr}(x', z)]_{M,i}' \left\{ \begin{array}{c} p_l \\ r_l \\ p_{l+1} \\ r_{l+1} \end{array} \right\} \quad (421)$$

with

$$[\mathbf{uwpr}(x', z)]_{M,i}' = \int_{-\infty}^{\infty} [\mathbf{uwpr}(k, z)]_{M,i}' \exp(-ikx') dk \quad (422)$$

where $[\mathbf{uwpr}(k, z)]_{M,i}'$ can be obtained from Equation (369) for non-zero wave numbers k and from Equation (418) for a zero wave number k .

APPENDIX B

STIFFNESS MATRICES OF LAYER AND HALF-PLANE

In order to formulate Green's influence function described in Appendix A, the dynamic-stiffness matrices of individual components, a horizontal layer and a half-plane, are needed. In this appendix, the force-displacement relationship in k -domain for harmonic excitation of both basic components is derived.

1. Dynamic-stiffness Coefficients of Horizontal Layer.

In Figure 121, the horizontal layer i of depth d , extending to infinity in both x -directions, has constant material properties. Origin of the local coordinate system with the z -axis pointing downward is located at the top of the layer. As discussed in Equations (568) to (571), the in-plane displacement equations of a layer can be expressed as

$$u(x, z) = u(k, z)\exp(-ikx) \quad (423)$$

$$w(x, z) = w(k, z)\exp(-ikx) \quad (424)$$

with

$$u(k, z) = I_x[A_P \exp(ikfz) + B_P \exp(-ikfz)] \\ -m_x s [A_{SV} \exp(ksz) - B_{SV} \exp(-ksz)] \quad (425)$$

$$w(k, z) = -I_x f [A_P \exp(ikfz) - B_P \exp(-ikfz)] \\ -m_x [A_{SV} \exp(ksz) + B_{SV} \exp(-ksz)] \quad (426)$$

where $I_x/C_P = m_x/C_S$ needs to be enforced.

The symbol ι represents $\sqrt{-1}$. The scalar k represents the wave number which is equal to ω/C . The letter C stands for phase velocity which is equal to C_P/I_x and C_S/m_x .

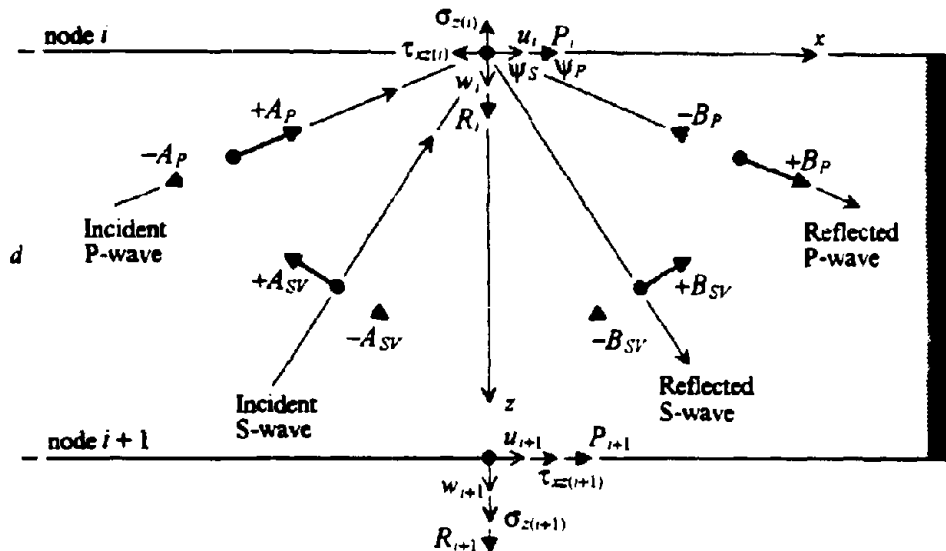


Figure 121. Displacements, Stresses, and External Forces on Layer i

C_p and C_s represent P- and S-wave velocities and are equal to $\sqrt{(2\Upsilon^* + \lambda^*)/\rho}$ and $\sqrt{\Upsilon^*/\rho}$, respectively. Υ^* and λ^* are the complex shear modulus and the complex Lamé constant, respectively. ρ represents the mass density. Scalars l_x and m_x may be considered propagating directional cosines to the x -axis ($=\cos \psi_p$ and $=\cos \psi_s$) of the P- and S-wave, respectively. Algebraically, they are equal to kC_p/ω and kC_s/ω , respectively, which can be real, imaginary, or complex numbers. Therefore this interpretation holds only for real values that are smaller than or equal to 1. Scalars f and s are $\sqrt{1/l_x^2 - 1}$ and $\sqrt{1/m_x^2 - 1}$, respectively. A_p and A_{sv} are amplitudes of the P- and SV-wave traveling in the negative z -direction (incident waves). B_p and B_{sv} are amplitudes of the P- and SV-wave traveling in the positive z -direction (reflected waves).

By using the stress-strain relationship (Hook's law) and strain-displacement relationship, normal stress and shear stress amplitudes on the horizontal interface can be obtained as follows

$$\sigma_z(x, z) = [2\Upsilon^* + \lambda^*]w_z(x, z) + \lambda^*u_x(x, z) \quad (427)$$

$$\tau_{xz}(x, z) = \Upsilon^*[u_z(x, z) + w_x(x, z)] \quad (428)$$

Normal stress and shear stress amplitudes are denoted as σ and τ , respectively. The first subscript denotes the direction of the stress component. The second one denotes the direction of the infinitesimal area's normal that the stress component acts on. A comma denotes a partial derivative with respect to the subscript following it.

Substituting the displacements in Equations (423), (424), (425) and (426) into Equations (427) and (428) and omitting term $\exp(-ikx)$, normal stress and shear stress amplitudes in k -domain can be expressed as

$$\begin{aligned} \sigma_z(k, z) &= [2\Upsilon^* + \lambda^*]w_z(k, z) - ik\lambda^*u(k, z) \\ &= -ik[2\Upsilon^* + \lambda^*] \left\{ I_x f^2 [A_P \exp(ikfz) + B_P \exp(-ikfz)] \right. \\ &\quad \left. + m_{xs} [A_{SV} \exp(iks z) - B_{SV} \exp(-iks z)] \right\} \\ &\quad - ik\lambda^* \left\{ I_x [A_P \exp(ikfz) + B_P \exp(-ikfz)] \right. \\ &\quad \left. - m_{xs} [A_{SV} \exp(iks z) - B_{SV} \exp(-iks z)] \right\} \end{aligned}$$

$$\begin{aligned}
&= ik\Upsilon^* \left\{ I_x(1-s^2)[A_P \exp(ikfz) + B_P \exp(-ikfz)] \right. \\
&\quad \left. - 2m_x s [A_{SV} \exp(uksz) - B_{SV} \exp(-uksz)] \right\} \quad (429)
\end{aligned}$$

$$\begin{aligned}
\tau_{xz}(k, z) &= \Upsilon^* [u_z(k, z) - kw(k, z)] \\
&= ik\Upsilon^* \left\{ I_x f [A_P \exp(ikfz) - B_P \exp(-ikfz)] \right. \\
&\quad \left. - m_x s^2 [A_{SV} \exp(uksz) + B_{SV} \exp(-uksz)] \right. \\
&\quad \left. + I_x f [A_P \exp(ikfz) - B_P \exp(-ikfz)] \right. \\
&\quad \left. + m_x [A_{SV} \exp(uksz) + B_{SV} \exp(-uksz)] \right\} \\
&= ik\Upsilon^* \left\{ 2I_x f [A_P \exp(ikfz) - B_P \exp(-ikfz)] \right. \\
&\quad \left. + m_x (1-s^2) [A_{SV} \exp(uksz) + B_{SV} \exp(-uksz)] \right\} \quad (430)
\end{aligned}$$

By using Equations (425), (426), (429), and (430), displacements and stresses at the top (node $i, z=0$) of layer i can be expressed in matrix form in terms of wave amplitudes A_P , B_P , A_{SV} , and B_{SV} as

$$\begin{Bmatrix} u_i(k) \\ w_i(k) \\ \tau_{xz(i)}(k) \\ \sigma_{z(i)}(k) \end{Bmatrix} = [u\omega\tau\sigma AB_i(k)]^{k\omega_0} \begin{Bmatrix} A_P \\ B_P \\ A_{SV} \\ B_{SV} \end{Bmatrix} \quad (431)$$

with

$$[u\omega\tau\sigma AB_i(k)]^{k\omega_0} = \begin{bmatrix} [u\omega\tau\sigma AB_i^{(1,1)}] & [u\omega\tau\sigma AB_i^{(1,2)}] \\ [u\omega\tau\sigma AB_i^{(2,1)}] & [u\omega\tau\sigma AB_i^{(2,2)}] \end{bmatrix} \quad (432)$$

where

$$[i\omega\tau\sigma AB_i^{(1,1)}] = I_x \begin{bmatrix} 1 & 1 \\ -f & f \end{bmatrix} \quad (433)$$

$$[i\omega\tau\sigma AB_i^{(1,2)}] = m_x \begin{bmatrix} -s & s \\ -1 & -1 \end{bmatrix} \quad (434)$$

$$[i\omega\tau\sigma AB_i^{(2,1)}] = ikI_x \Upsilon^* \begin{bmatrix} 2f & -2f \\ 1-s^2 & 1-s^2 \end{bmatrix} \quad (435)$$

$$[i\omega\tau\sigma AB_i^{(2,2)}] = ikm_x \Upsilon^* \begin{bmatrix} 1-s^2 & 1-s^2 \\ -2s & 2s \end{bmatrix} \quad (436)$$

At the bottom (node $i+1$, $z=d$) of layer i , displacements and stresses can be expressed in terms of the wave amplitudes A_p , B_p , A_{SV} , and B_{SV} as

$$\begin{Bmatrix} u_{i+1}(k) \\ w_{i+1}(k) \\ \tau_{xz(i+1)}(k) \\ \sigma_{zz(i+1)}(k) \end{Bmatrix} = [i\omega\tau\sigma AB_{i+1}(k)]^{k=d} \begin{Bmatrix} A_p \\ B_p \\ A_{SV} \\ B_{SV} \end{Bmatrix} \quad (437)$$

with

$$[i\omega\tau\sigma AB_{i+1}(k)]^{k=d} = \begin{bmatrix} [i\omega\tau\sigma AB_{i+1}^{(1,1)}] & [i\omega\tau\sigma AB_{i+1}^{(1,2)}] \\ [i\omega\tau\sigma AB_{i+1}^{(2,1)}] & [i\omega\tau\sigma AB_{i+1}^{(2,2)}] \end{bmatrix} \quad (438)$$

where

$$[i\omega\tau\sigma AB_{i+1}^{(1,1)}] = I_x \begin{bmatrix} \exp(ukfd) & \exp(-ukfd) \\ -f \exp(ukfd) & f \exp(-ukfd) \end{bmatrix} \quad (439)$$

$$[uw\tau\sigma AB_{i+1}^{(1,2)}] = m_x \begin{bmatrix} -s \exp(ksd) & s \exp(-ksd) \\ -\exp(ksd) & -\exp(-ksd) \end{bmatrix} \quad (440)$$

$$[uw\tau\sigma AB_{i+1}^{(2,1)}] = kI_x \Gamma^* \begin{bmatrix} 2f \exp(kfd) & -2f \exp(-kfd) \\ (1-s^2) \exp(kfd) & (1-s^2) \exp(-kfd) \end{bmatrix} \quad (441)$$

$$[uw\tau\sigma AB_{i+1}^{(2,2)}] = km_x \Gamma^* \begin{bmatrix} (1-s^2) \exp(ksd) & (1-s^2) \exp(-ksd) \\ -2s \exp(ksd) & 2s \exp(-ksd) \end{bmatrix} \quad (442)$$

Using Equations (431) and (437), displacement and stress amplitudes at node $i+1$ are expressed as a function of those at node i by the transfer matrix as

$$\begin{Bmatrix} u_{i+1}(k) \\ w_{i+1}(k) \\ \tau_{xz(i+1)}(k) \\ \sigma_{z(i+1)}(k) \end{Bmatrix} = [uw\tau\sigma_{i+1}^{i+1}(k)]^{k\omega} \begin{Bmatrix} u_i(k) \\ w_i(k) \\ \tau_{xz(i)}(k) \\ \sigma_{z(i)}(k) \end{Bmatrix} \quad (443)$$

with

$$[uw\tau\sigma_{i+1}^{i+1}(k)]^{k\omega} = [uw\tau\sigma AB_{i+1}(k)]^{k\omega} [uw\tau\sigma AB_i(k)]^{k\omega}{}^{-1} \quad (444)$$

When assembling the stiffness matrix, applied loads are defined in the global-coordinate system. The local system used to define the stresses is opposite to it on the negative side of a layer. Therefore, as shown in Figure 121, introducing external load amplitudes $P_i = -\tau_{xz(i)}$, $R_i = -\sigma_{z(i)}$, $P_{i+1} = \tau_{xz(i+1)}$, and $R_{i+1} = \sigma_{z(i+1)}$ into Equation (444) and performing a partial inversion leads to the dynamic-stiffness matrix of a horizontal layer as

$$\begin{Bmatrix} P_i(k) \\ R_i(k) \\ P_{i+1}(k) \\ R_{i+1}(k) \end{Bmatrix} = [S_{P-S}^L(k)]_i^{k\omega} \begin{Bmatrix} u_i(k) \\ w_i(k) \\ u_{i+1}(k) \\ w_{i+1}(k) \end{Bmatrix} \quad (445)$$

with

$$[S_{P-SV}^L(k)]_i^{kno} = Cof \begin{bmatrix} S_{11} & S_{12} & S_{13} & S_{14} \\ S_{21} & S_{22} & S_{23} & S_{24} \\ S_{31} & S_{32} & S_{33} & S_{34} \\ S_{41} & S_{42} & S_{43} & S_{44} \end{bmatrix} \quad (446)$$

where

$$Cof = \frac{(1+s^2)k\Upsilon^*}{2[1 - \cos(kfd)\cos(ksd)] + (fs + 1/fs)\sin(kfd)\sin(ksd)} \quad (447)$$

$$S_{11} = S_{33} = \frac{1}{s} \cos(kfd)\sin(ksd) + f \sin(kfd)\cos(ksd) \quad (448)$$

$$S_{12} = -S_{21} = -S_{34} = S_{43} = \frac{(3-s^2)\iota}{(1+s^2)} [1 - \cos(kfd)\cos(ksd)] \\ + \frac{(1+2f^2s^2-s^2)\iota}{fs(1+s^2)} \sin(kfd)\sin(ksd) \quad (449)$$

$$S_{13} = S_{31} = -f \sin(kfd) - \frac{1}{s} \sin(ksd) \quad (450)$$

$$S_{14} = -S_{41} = S_{23} = -S_{32} = \iota [\cos(kfd) - \cos(ksd)] \quad (451)$$

$$S_{22} = S_{44} = \frac{1}{f} \sin(kfd)\cos(ksd) + s [\cos(kfd)\sin(ksd)] \quad (452)$$

$$S_{24} = S_{42} = \frac{-1}{f} \sin(kfd) - s [\sin(ksd)] \quad (453)$$

Superscript L stands for horizontal layer i and subscript $P-SV$ indicates the corresponding stiffness matrix associated with P- and SV-wave.

2. Dynamic-stiffness Coefficients of Half-plane.

A half-plane can be regarded as a horizontal layer with depth approaching infinity. Applying an external load at the free surface of a half-plane, only waves traveling in the positive z -direction (outgoing waves) are developed as shown in Figure 122. The radiation condition states that no energy can propagate from infinity toward the free surface. Therefore the incoming waves with amplitudes A_p and A_{sv} in Equations (425) and (426) are excluded.

a. Positive Wave Number k . The in-plane displacement equations for a positive wave number k can be expressed as

$$u(k, z) = l_x B_p \exp(-kz) + m_x B_{sv} \exp(-ksz) \quad (454)$$

$$w(k, z) = l_x f B_p \exp(-kz) - m_x B_{sv} \exp(-ksz) \quad (455)$$

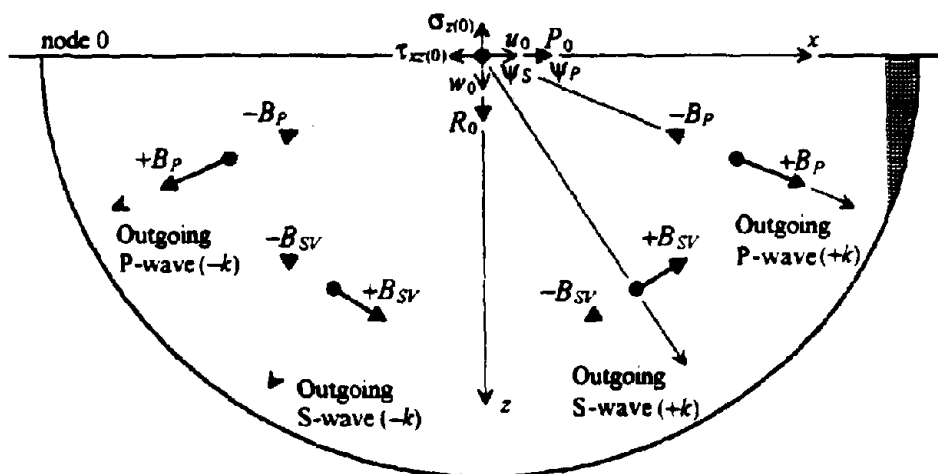


Figure 122. Displacements, Stresses, and External Forces on Half-plane

Substituting displacement Equations (423), (424), (454), and (455) into stress Equations (427) and (428), and omitting term $\exp(-\lambda z)$, the stress amplitudes in k -domain can be expressed as

$$\begin{aligned}\sigma_z(k, z) &= [2\Upsilon^* + \lambda^*]w_z(k, z) - \lambda^*u(k, z) \\ &= \lambda^*\Upsilon^*[I_x(1-s^2)B_P \exp(-\lambda fz) + 2sm_x B_{SV} \exp(-\lambda sz)]\end{aligned}\quad (456)$$

$$\begin{aligned}\tau_{xz}(k, z) &= \Upsilon^*[u_x(k, z) - \lambda w(k, z)] \\ &= \lambda^*\Upsilon^*[-2I_x f B_P \exp(-\lambda fz) + m_x(1-s^2)B_{SV} \exp(-\lambda sz)]\end{aligned}\quad (457)$$

At node 0 ($z=0$) on the surface of a half-plane, displacements and external forces ($P_0 = -\tau_{xz(0)}$, $R_0 = -\sigma_{z(0)}$) in Figure 122 can be expressed in terms of wave amplitudes B_P and B_{SV} as

$$\begin{Bmatrix} u_0(k) \\ w_0(k) \end{Bmatrix} = \begin{bmatrix} I_x & m_x s \\ I_x f & -m_x \end{bmatrix} \begin{Bmatrix} B_P \\ B_{SV} \end{Bmatrix}\quad (458)$$

$$\begin{Bmatrix} P_0(k) \\ R_0(k) \end{Bmatrix} = \lambda^*\Upsilon^* \begin{bmatrix} 2I_x f & -m_x(1-s^2) \\ -I_x(1-s^2) & -2m_x s \end{bmatrix} \begin{Bmatrix} B_P \\ B_{SV} \end{Bmatrix}\quad (459)$$

Eliminating B_P , B_{SV} in Equations (458) and (459), the dynamic-stiffness matrix of a half-plane, for a positive non-zero k , can be expressed as

$$\begin{Bmatrix} P_0(k) \\ R_0(k) \end{Bmatrix} = [S_{P-SV}^R(k)]^{-1} \begin{Bmatrix} u_0(k) \\ w_0(k) \end{Bmatrix}\quad (460)$$

with

$$\begin{aligned}
[S_{P-SV}^R(k)]^{k>0} &= \mathcal{U}k\Upsilon^* \begin{bmatrix} 2l_x f & -m_x(1-s^2) \\ -l_x(1-s^2) & -2m_x s \end{bmatrix} \begin{bmatrix} l_x & m_x s \\ l_x f & -m_x \end{bmatrix}^{-1} \\
&= \mathcal{U}k\Upsilon^* \begin{bmatrix} f(1+s^2)/(1+fs) & 2 - [(1+s^2)/(1+fs)] \\ -2 + [(1+s^2)/(1+fs)] & s(1+s^2)/(1+fs) \end{bmatrix} \quad (461)
\end{aligned}$$

As the half-plane is used mainly to represent rock bed, a superscript R is introduced. Subscript $P-SV$ indicates that the corresponding stiffness matrix is associated with P- and SV-wave.

b. Negative Wave Number k . The displacement equations having the outgoing waves (propagating in the positive z -direction and the negative x -direction as shown in Figure 122) with amplitudes B_P and B_{SV} can be expressed as

$$u(k, z) = l_x B_P \exp(\mathcal{U}kz) - m_x s B_{SV} \exp(\mathcal{U}ksz) \quad (462)$$

$$w(k, z) = -l_x f B_P \exp(\mathcal{U}kz) - m_x B_{SV} \exp(\mathcal{U}ksz) \quad (463)$$

Substituting displacement Equations (423), (424), (462), and (463) into stress Equations (427) and (428), and omitting term $\exp(-\mathcal{U}kx)$, normal stress and shear stress amplitudes can be expressed as

$$\sigma_z(k, z) = \mathcal{U}k\Upsilon^* [l_x(1-s^2)B_P \exp(\mathcal{U}kz) - 2sm_x B_{SV} \exp(\mathcal{U}ksz)] \quad (464)$$

$$\tau_{xz}(k, z) = \mathcal{U}k\Upsilon^* [2l_x f B_P \exp(\mathcal{U}kz) + m_x(1-s^2)B_{SV} \exp(\mathcal{U}ksz)] \quad (465)$$

At node 0 ($z=0$) on the surface of a half-plane, the displacements and external forces ($P_0 = -\tau_{xz(0)}$, $R_0 = -\sigma_{z(0)}$) shown in Figure 122 can be expressed as

$$\begin{Bmatrix} u_0(k) \\ w_0(k) \end{Bmatrix} = \begin{bmatrix} l_x & -m_x s \\ -l_x f & -m_x \end{bmatrix} \begin{Bmatrix} B_P \\ B_{SV} \end{Bmatrix} \quad (466)$$

$$\begin{Bmatrix} P_0(k) \\ R_0(k) \end{Bmatrix} = i k \Upsilon^* \begin{bmatrix} -2l_x f & -m_x(1-s^2) \\ -l_x(1-s^2) & 2m_x s \end{bmatrix} \begin{Bmatrix} B_P \\ B_{SV} \end{Bmatrix} \quad (467)$$

Eliminating B_P, B_{SV} in Equations (466) and (467), the dynamic-stiffness matrix of half-plane, for a negative k , can be expressed as

$$\begin{Bmatrix} P_0(k) \\ R_0(k) \end{Bmatrix} = [S_{P-SV}^R(k)]^{k<0} \begin{Bmatrix} u_0(k) \\ w_0(k) \end{Bmatrix} \quad (468)$$

with

$$\begin{aligned} [S_{P-SV}^R(k)]^{k<0} &= i k \Upsilon^* \begin{bmatrix} -2l_x f & -m_x(1-s^2) \\ -l_x(1-s^2) & 2m_x s \end{bmatrix} \left[\begin{bmatrix} l_x & -m_x s \\ -l_x f & -m_x \end{bmatrix} \right]^{-1} \\ &= i k \Upsilon^* \begin{bmatrix} -f(1+s^2)/(1+fs) & 2-[(1+s^2)/(1+fs)] \\ -2+[(1+s^2)/(1+fs)] & -s(1+s^2)/(1+fs) \end{bmatrix} \end{aligned} \quad (469)$$

3. Dynamic-stiffness Coefficients for Vertically Incident Wave.

a. **Horizontal Layer.** This special case corresponds to a zero wave number k .

The derivation is analogous to Subsection 1, except the in-plane displacement equations of a layer [Equations (572) and (573)] can be expressed as

$$u(x, z)^{k=0} = -A_{SV} \exp\left(\frac{i\omega}{C_S} z\right) + B_{SV} \exp\left(-\frac{i\omega}{C_S} z\right) \quad (470)$$

$$w(x, z)^{k=0} = -A_P \exp\left(\frac{i\omega}{C_P} z\right) + B_P \exp\left(-\frac{i\omega}{C_P} z\right) \quad (471)$$

Using the displacements in Equations (470) and (471) and the stresses in Equations (427) and (428), normal stress and shear stress amplitudes can be expressed as

$$\begin{aligned}\sigma_z(z) &= [2\Upsilon^* + \lambda^*]w_z(x, z) \\ &= -\frac{i\omega C_P}{C_S^2}\Upsilon^* \left[A_P \exp\left(\frac{i\omega}{C_P}z\right) + B_P \exp\left(-\frac{i\omega}{C_P}z\right) \right]\end{aligned}\quad (472)$$

$$\begin{aligned}\tau_{xz}(z) &= \Upsilon^* u_z(x, z) \\ &= -\frac{i\omega}{C_S}\Upsilon^* \left[A_{SV} \exp\left(\frac{i\omega}{C_S}z\right) + B_{SV} \exp\left(-\frac{i\omega}{C_S}z\right) \right]\end{aligned}\quad (473)$$

Using Equations (470) to (473), the displacements and the stresses at node i ($z=0$) can be expressed as

$$\begin{Bmatrix} u_i \\ w_i \\ \tau_{xz(i)} \\ \sigma_{z(i)} \end{Bmatrix} = [i\omega\tau\sigma AB_i]^{k=0} \begin{Bmatrix} A_P \\ B_P \\ A_{SV} \\ B_{SV} \end{Bmatrix}\quad (474)$$

with

$$[i\omega\tau\sigma AB_i]^{k=0} = \begin{bmatrix} [i\omega\tau\sigma AB_i^{(1,1)}] & [i\omega\tau\sigma AB_i^{(1,2)}] \\ [i\omega\tau\sigma AB_i^{(2,1)}] & [i\omega\tau\sigma AB_i^{(2,2)}] \end{bmatrix}\quad (475)$$

where

$$[i\omega\tau\sigma AB_i^{(1,1)}] = \begin{bmatrix} 0 & 0 \\ -1 & 1 \end{bmatrix}\quad (476)$$

$$[i\omega\tau\sigma AB_i^{(1,2)}] = \begin{bmatrix} -1 & 1 \\ 0 & 0 \end{bmatrix}\quad (477)$$

$$[u\omega\tau\sigma_{AB_i}^{(2,1)}] = \frac{i\omega C_P}{C_S^2} \gamma^* \begin{bmatrix} 0 & 0 \\ 1 & 1 \end{bmatrix} \quad (478)$$

$$[u\omega\tau\sigma_{AB_i}^{(2,2)}] = \frac{i\omega}{C_S} \gamma^* \begin{bmatrix} 1 & 1 \\ 0 & 0 \end{bmatrix} \quad (479)$$

At node $i+1$ ($z=d$) the displacements and the stresses can be expressed as

$$\begin{Bmatrix} u_{i+1} \\ w_{i+1} \\ \tau_{xz(i+1)} \\ \sigma_{z(i+1)} \end{Bmatrix} = [u\omega\tau\sigma_{AB_{i+1}}]^{k=0} \begin{Bmatrix} A_P \\ B_P \\ A_{SV} \\ B_{SV} \end{Bmatrix} \quad (480)$$

with

$$[u\omega\tau\sigma_{AB_{i+1}}]^{k=0} = \begin{bmatrix} [u\omega\tau\sigma_{AB_{i+1}}^{(1,1)}] & [u\omega\tau\sigma_{AB_{i+1}}^{(1,2)}] \\ [u\omega\tau\sigma_{AB_{i+1}}^{(2,1)}] & [u\omega\tau\sigma_{AB_{i+1}}^{(2,2)}] \end{bmatrix} \quad (481)$$

where

$$[u\omega\tau\sigma_{AB_{i+1}}^{(1,1)}] = \begin{bmatrix} 0 & 0 \\ -\exp(i\omega d/C_P) & \exp(-i\omega d/C_P) \end{bmatrix} \quad (482)$$

$$[u\omega\tau\sigma_{AB_{i+1}}^{(1,2)}] = \begin{bmatrix} -\exp(i\omega d/C_S) & \exp(-i\omega d/C_S) \\ 0 & 0 \end{bmatrix} \quad (483)$$

$$[u\omega\tau\sigma_{AB_{i+1}}^{(2,1)}] = \frac{i\omega C_P}{C_S^2} \gamma^* \begin{bmatrix} 0 & 0 \\ \exp(i\omega d/C_P) & \exp(-i\omega d/C_P) \end{bmatrix} \quad (484)$$

$$[u\omega\tau\sigma_{AB_{i+1}}^{(2,2)}] = \frac{i\omega}{C_S} \gamma^* \begin{bmatrix} \exp(i\omega d/C_S) & \exp(-i\omega d/C_S) \\ 0 & 0 \end{bmatrix} \quad (485)$$

Using Equations (474) and (480), the displacement and stress amplitudes at node $i+1$ are expressed as a function of those at node i by the transfer matrix as

$$\begin{Bmatrix} u_{i+1} \\ w_{i+1} \\ \tau_{xz(i+1)} \\ \sigma_{z(i+1)} \end{Bmatrix} = [u w \tau \sigma]_i^{i+1, k=0} \begin{Bmatrix} u_i \\ w_i \\ \tau_{xz(i)} \\ \sigma_{z(i)} \end{Bmatrix} \quad (486)$$

with

$$[u w \tau \sigma]_i^{i+1, k=0} = [u w \tau \sigma A B]_{i+1, k=0} [u w \tau \sigma A B]_{i, k=0}^{-1} \quad (487)$$

Introducing external load amplitudes $P_i = -\tau_{xz(i)}$, $R_i = -\sigma_{z(i)}$, $P_{i+1} = \tau_{xz(i+1)}$, and $R_{i+1} = \sigma_{z(i+1)}$ into Equation (486), and performing a partial inversion leads to the dynamic-stiffness matrix of a layer ($k=0$) as

$$\begin{Bmatrix} P_i \\ R_i \\ P_{i+1} \\ R_{i+1} \end{Bmatrix} = [S_{P-SV}^L]_i^{k=0} \begin{Bmatrix} u_i \\ w_i \\ u_{i+1} \\ w_{i+1} \end{Bmatrix} \quad (488)$$

with

$$[S_{P-SV}^L]_i^{k=0} = Cof \begin{bmatrix} S_{11} & 0 & S_{13} & 0 \\ 0 & S_{22} & 0 & S_{24} \\ S_{31} & 0 & S_{33} & 0 \\ 0 & S_{42} & 0 & S_{44} \end{bmatrix} \quad (489)$$

where

$$Cof = \frac{\omega}{C_S} \Upsilon^* \quad (490)$$

$$S_{11} = S_{33} = \cot\left(\frac{\omega d}{C_S}\right) \quad (491)$$

$$S_{13} = S_{31} = \frac{-1}{\sin(\omega d/C_S)} \quad (492)$$

$$S_{22} = S_{44} = \left(\frac{C_P}{C_S}\right) \cot\left(\frac{\omega d}{C_P}\right) \quad (493)$$

$$S_{24} = S_{42} = \left(\frac{C_P}{C_S}\right) \frac{-1}{\sin(\omega d/C_P)} \quad (494)$$

b. **Half-plane.** Analogous to Subsection 2, only the outgoing waves with amplitudes B_P and B_{SV} are developed. Therefore the displacements in Equations (470) and (471) are reduced to

$$u(x, z)^{k=0} = B_{SV} \exp\left(-\frac{i\omega}{C_S} z\right) \quad (495)$$

$$w(x, z)^{k=0} = B_P \exp\left(-\frac{i\omega}{C_P} z\right) \quad (496)$$

Using the displacements in Equations (495) and (496) and the stresses in Equations (427) and (428), the normal stress and shear stress amplitudes can be expressed as

$$\sigma_z(z) = -\frac{i\omega C_P}{C_S^2} \Upsilon^* B_P \exp\left(-\frac{i\omega}{C_P} z\right) \quad (497)$$

$$\tau_{xz}(z) = -\frac{i\omega}{C_S} \Upsilon^* B_{SV} \exp\left(-\frac{i\omega}{C_S} z\right) \quad (498)$$

At node 0 ($z=0$) on the surface of a half-plane, the displacements and external forces ($P_0 = -\tau_{z(0)}, R_0 = -\sigma_{x(0)}$) can be expressed as

$$\begin{Bmatrix} u_0 \\ w_0 \end{Bmatrix} = \begin{bmatrix} 0 & 1 \\ 1 & 0 \end{bmatrix} \begin{Bmatrix} B_P \\ B_{SV} \end{Bmatrix} \quad (499)$$

$$\begin{Bmatrix} P_0 \\ R_0 \end{Bmatrix} = \frac{1\omega}{C_S} \Upsilon^* \begin{bmatrix} 0 & 1 \\ C_P/C_S & 0 \end{bmatrix} \begin{Bmatrix} B_P \\ B_{SV} \end{Bmatrix} \quad (500)$$

Using Equations (499) and (500), the dynamic-stiffness matrix of a half-plane, for $k=0$, can be expressed as

$$\begin{Bmatrix} P_0 \\ R_0 \end{Bmatrix} = [S_{P-SV}^R]^{k=0} \begin{Bmatrix} u_0 \\ w_0 \end{Bmatrix} \quad (501)$$

with

$$[S_{P-SV}^R]^{k=0} = \frac{1\omega}{C_S} \Upsilon^* \begin{bmatrix} 1 & 0 \\ 0 & C_P/C_S \end{bmatrix} \quad (502)$$

APPENDIX C

WAVE EQUATIONS IN CARTESIAN COORDINATES

The fundamental equations of elastodynamics relevant to the establishment of the formulations related to soil system are crucial and are summarized in this appendix.

1. Dynamic-equilibrium Equation.

The infinitesimal cube, shown in Figure 123, is assumed to be an isotropic homogeneous elastic medium with hysteretic damping. For harmonic excitation with frequency ω , the dynamic-equilibrium equations without body forces can be expressed as

$$\sigma_{xx}(x, y, z) + \tau_{xy,y}(x, y, z) + \tau_{xz,z}(x, y, z) = -\rho\omega^2 u(x, y, z) \quad (503)$$

$$\tau_{yx,x}(x, y, z) + \sigma_{yy}(x, y, z) + \tau_{yz,z}(x, y, z) = -\rho\omega^2 v(x, y, z) \quad (504)$$

$$\tau_{zx,x}(x, y, z) + \tau_{zy,y}(x, y, z) + \sigma_{zz}(x, y, z) = -\rho\omega^2 w(x, y, z) \quad (505)$$

Normal stress and shear stress amplitudes are denoted as σ and τ , respectively.

The first subscript denotes the direction of the stress component. The second one denotes

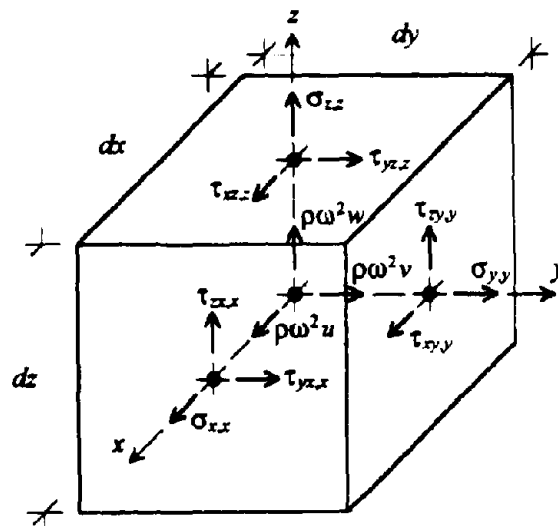


Figure 123. Infinitesimal Cube in Harmonic Motion

the direction of the infinitesimal area's normal on which the stress component acts. A comma denotes a partial derivative with respect to the subscript following it. The letter ρ represents the mass density. Displacements u , v , and w are in x -, y -, and z -direction, respectively. All amplitudes are a function of x , y , and z .

Hook's law, the constitutive equation, is specified as

$$\epsilon_x = \frac{1}{E}(\sigma_x - \nu\sigma_y - \nu\sigma_z) \quad (506)$$

$$\epsilon_y = \frac{1}{E}(-\nu\sigma_x + \sigma_y - \nu\sigma_z) \quad (507)$$

$$\epsilon_z = \frac{1}{E}(-\nu\sigma_x - \nu\sigma_y + \sigma_z) \quad (508)$$

$$\gamma_{xy} = \gamma_{yx} = \frac{\tau_{xy}}{Y} = \frac{\tau_{yx}}{Y} \quad (509)$$

$$\gamma_{xz} = \gamma_{zx} = \frac{\tau_{xz}}{Y} = \frac{\tau_{zx}}{Y} \quad (510)$$

$$\gamma_{yz} = \gamma_{zy} = \frac{\tau_{yz}}{Y} = \frac{\tau_{zy}}{Y} \quad (511)$$

where the normal strain and shear strain amplitudes are denoted by ϵ and γ , respectively.

Shear modulus Y can be expressed as a function of Young's modulus of elasticity E and

Poisson's ratio ν as

$$Y = \frac{E}{2(1 + \nu)} \quad (512)$$

Stress amplitudes in Equations (506) to (511) can be written in terms of strain amplitudes as

$$\sigma_x = (2\Upsilon + \lambda)\epsilon_x + \lambda(\epsilon_y + \epsilon_z) \quad (513)$$

$$\sigma_y = (2\Upsilon + \lambda)\epsilon_y + \lambda(\epsilon_x + \epsilon_z) \quad (514)$$

$$\sigma_z = (2\Upsilon + \lambda)\epsilon_z + \lambda(\epsilon_x + \epsilon_y) \quad (515)$$

$$\tau_{xy} = \tau_{yx} = \Upsilon\gamma_{xy} = \Upsilon\gamma_{yx} \quad (516)$$

$$\tau_{xz} = \tau_{zx} = \Upsilon\gamma_{xz} = \Upsilon\gamma_{zx} \quad (517)$$

$$\tau_{yz} = \tau_{zy} = \Upsilon\gamma_{yz} = \Upsilon\gamma_{zy} \quad (518)$$

where the Lamé constant λ is expressed as

$$\lambda = \frac{\nu E}{(1 + \nu)(1 - 2\nu)} \quad (519)$$

Strain-displacement equations are formulated as

$$\epsilon_x = u_x(x, y, z) \quad (520)$$

$$\epsilon_y = v_y(x, y, z) \quad (521)$$

$$\epsilon_z = w_z(x, y, z) \quad (522)$$

$$\gamma_{xy} = \gamma_{yx} = u_y(x, y, z) + v_x(x, y, z) \quad (523)$$

$$\gamma_{xz} = \gamma_{zx} = u_z(x, y, z) + w_x(x, y, z) \quad (524)$$

$$\gamma_{yz} = \gamma_{zy} = v_z(x, y, z) + w_y(x, y, z) \quad (525)$$

Substituting the stress-strain relationship in Equations (513) to (518) and the strain-displacement relationship in Equations (520) to (525) into the equilibrium Equations (503), (504), and (505) leads to

$$(2\Upsilon + \lambda)u_{xx} + \lambda(v_{yx} + w_{zx}) + \Upsilon(u_{yy} + v_{xy} + u_{zz} + w_{xz}) = -\rho\omega^2 u \quad (526)$$

$$(2\Upsilon + \lambda)v_{yy} + \lambda(u_{xy} + w_{zy}) + \Upsilon(v_{xx} + u_{yz} + v_{zz} + w_{yz}) = -\rho\omega^2 v \quad (527)$$

$$(2\Upsilon + \lambda)w_{zz} + \lambda(u_{xz} + v_{yz}) + \Upsilon(w_{xx} + u_{zy} + w_{yy} + v_{zy}) = -\rho\omega^2 w \quad (528)$$

In order to uncouple the displacements in Equations (526), (527), and (528) and to identify the different types of waves, the volumetric strain with amplitude e and the rotational-strain vector $\{\Omega\}$ with amplitudes Ω_x , Ω_y , and Ω_z are introduced as

$$e(x, y, z) = u_x + v_y + w_z \quad (529)$$

$$\{\Omega(x, y, z)\} = \begin{Bmatrix} \Omega_x \\ \Omega_y \\ \Omega_z \end{Bmatrix} = \frac{1}{2} \begin{Bmatrix} w_y - v_z \\ u_z - w_x \\ v_x - u_y \end{Bmatrix} \quad (530)$$

Note that

$$\Omega_{xx} + \Omega_{yy} + \Omega_{zz} = 0 \quad (531)$$

By using Equations (529), (530), and (531), dynamic-equilibrium Equations (526), (527), and (528) can be rewritten as

$$(2\Upsilon + \lambda)e_x + 2\Upsilon(\Omega_{yz} - \Omega_{zy}) = -\rho\omega^2 u \quad (532)$$

$$(2\Upsilon + \lambda)e_y + 2\Upsilon(\Omega_{zx} - \Omega_{xz}) = -\rho\omega^2 v \quad (533)$$

$$(2\Upsilon + \lambda)e_z + 2\Upsilon(\Omega_{xy} - \Omega_{yx}) = -\rho\omega^2 w \quad (534)$$

The material damping occurring in a soil system involves frictional loss of energy or linear hysteretic damping. The effect of material damping, which may differ for various types of waves, is assumed to be the same. This frequency-independent property can be incorporated by replacing the elastic material constants with the corresponding complex ones. Complex shear modulus Υ^* and complex Lamé constant λ^* can be expressed as

$$\Upsilon^* = (1 + 2i\zeta)\Upsilon \quad \text{and} \quad \lambda^* = (1 + 2i\zeta)\lambda \quad (535)$$

where symbols ζ and i represent the ratio of linear hysteretic damping and $\sqrt{-1}$, respectively. Replacing the elastic material constants in Equations (532), (533), and (534) with the complex ones leads to

$$(2\Upsilon^* + \lambda^*)e_x + 2\Upsilon^*(\Omega_{yx} - \Omega_{xy}) = -\rho\omega^2 u \quad (536)$$

$$(2\Upsilon^* + \lambda^*)e_y + 2\Upsilon^*(\Omega_{zx} - \Omega_{xz}) = -\rho\omega^2 v \quad (537)$$

$$(2\Upsilon^* + \lambda^*)e_z + 2\Upsilon^*(\Omega_{xy} - \Omega_{yx}) = -\rho\omega^2 w \quad (538)$$

Eliminating rotational strains Ω_x , Ω_y , and Ω_z by differentiating Equation (536) with respect to x , Equation (537) with respect to y , and Equation (538) with respect to z , and then adding these three relationships leads to

$$(2\Upsilon^* + \lambda^*)(e_{xx} + e_{yy} + e_{zz}) = -\rho\omega^2 e$$

$$e_{xx} + e_{yy} + e_{zz} = -\frac{\omega^2}{C_p^2} e \quad (539)$$

where the dilatational wave velocity is specified as

$$C_P = \sqrt{\frac{(2\Upsilon^* + \lambda^*)}{\rho}} \quad (540)$$

Eliminating volumetric strain e by differentiating Equation (537) with respect to z and Equation (538) with respect to y , subtracting these two expressions, and noting that the derivative of Equation (531) with respect to x also vanishes, results in

$$\begin{aligned} \Upsilon^*(\Omega_{x,xx} + \Omega_{x,yy} + \Omega_{x,zz}) &= -\rho\omega^2\Omega_x \\ \Omega_{x,xx} + \Omega_{x,yy} + \Omega_{x,zz} &= -\frac{\omega^2}{C_S^2}\Omega_x \end{aligned} \quad (541)$$

where the shear wave velocity is defined as

$$C_S = \sqrt{\frac{\Upsilon^*}{\rho}} \quad (542)$$

Analogously, two other expressions can result as

$$\Omega_{y,xx} + \Omega_{y,yy} + \Omega_{y,zz} = -\frac{\omega^2}{C_S^2}\Omega_y \quad (543)$$

$$\Omega_{z,xx} + \Omega_{z,yy} + \Omega_{z,zz} = -\frac{\omega^2}{C_S^2}\Omega_z \quad (544)$$

Putting Equations (541), (543), and (544) together becomes

$$\{\Omega\}_{,xx} + \{\Omega\}_{,yy} + \{\Omega\}_{,zz} = -\frac{\omega^2}{C_S^2}\{\Omega\} \quad (545)$$

Therefore, for harmonic excitation, the equations of motion are specified in Equations (539) and (545) with the unknown amplitudes of the volumetric strain e and the rotational-strain vector $\{\Omega\}$, respectively. These wave equations are linear partial differential equations of second order.

2. Primary-wave Equation.

As the P-wave (primary wave or dilatational wave) travels, it alternately compresses and dilates the medium (see Figure 124). The volumetric strain e defined in Equation (529) can be used to describe this behavior. To find the unknown amplitude of the volumetric strain for Equation (539), the following trial function is assumed.

$$e(x, y, z) = -\frac{1\omega}{C_p} A_p \exp \left[-\frac{1\omega}{C_p} (l_x x + l_y y + l_z z) \right] \quad (546)$$

The trial function (546) satisfies the wave Equation (539) only if $l_x^2 + l_y^2 + l_z^2 = 1$. These three scalars l_x , l_y , and l_z may be considered the direction cosines of the wave propagation's direction. The trial function [Equation (546)] is multiplied by $l_x^2 + l_y^2 + l_z^2$ which is equal to 1. Using Equation (529), the former are then expanded and grouped into \ominus, \otimes, \oplus corresponding to $u_x, v_y,$ and w_z , respectively. Integrating each group (\ominus, \otimes, \oplus), leads to displacements $u_p, v_p,$ and w_p (see Figure 125) corresponding to x-, y-, and z- direction, respectively.

$$\begin{aligned} e = u_x + v_y + w_z &= -\frac{1\omega}{C_p} (l_x^2 + l_y^2 + l_z^2) A_p \exp \left[-\frac{1\omega}{C_p} (l_x x + l_y y + l_z z) \right] \Rightarrow \\ \Rightarrow u_x &= -\frac{1\omega}{C_p} l_x^2 A_p \exp \left[-\frac{1\omega}{C_p} (l_x x + l_y y + l_z z) \right] \rightarrow \ominus \end{aligned}$$

$$\Rightarrow v_y = -\frac{i\omega}{C_p} l_y^2 A_p \exp\left[-\frac{i\omega}{C_p}(l_x x + l_y y + l_z z)\right] \rightarrow \otimes$$

$$\Rightarrow w_z = -\frac{i\omega}{C_p} l_z^2 A_p \exp\left[-\frac{i\omega}{C_p}(l_x x + l_y y + l_z z)\right] \rightarrow \oplus$$

$$\otimes \rightarrow u_p = l_x A_p \exp\left[-\frac{i\omega}{C_p}(l_x x + l_y y + l_z z)\right] \quad (C.45)$$

$$\oplus \rightarrow v_p = l_y A_p \exp\left[-\frac{i\omega}{C_p}(l_x x + l_y y + l_z z)\right] \quad (C.46)$$

$$\oplus \rightarrow w_p = l_z A_p \exp\left[-\frac{i\omega}{C_p}(l_x x + l_y y + l_z z)\right] \quad (C.47)$$

At $x = y = z = 0$, the amplitude of P-wave equal to A_p is defined an initial condition. Therefore, in x -, y -, and z -direction, amplitudes of the wave at the same location are equal to $l_x A_p$, $l_y A_p$, and $l_z A_p$, respectively. By enforcing these conditions, the integration constants in Equations (C.45), (C.46), and (C.47) are equal to zero. Subscript P indicates that the corresponding displacements are associated with P-wave. Equations (C.45), (C.46), and (C.47) also show the P-wave amplitude is constant over a plane perpendicular to the direction of propagation. The velocity of propagation C_p is constant and depends on material properties only.

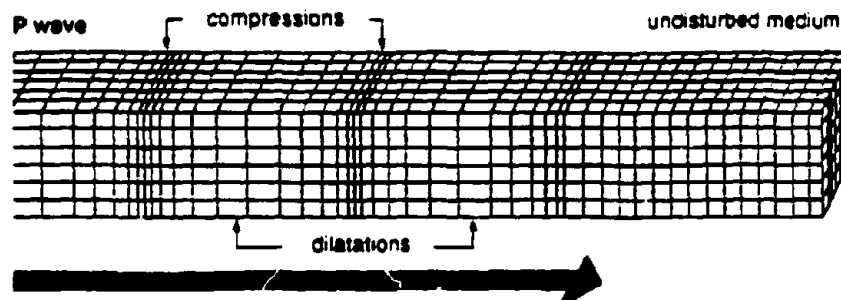


Figure 124. Cross Section of Incident P-wave

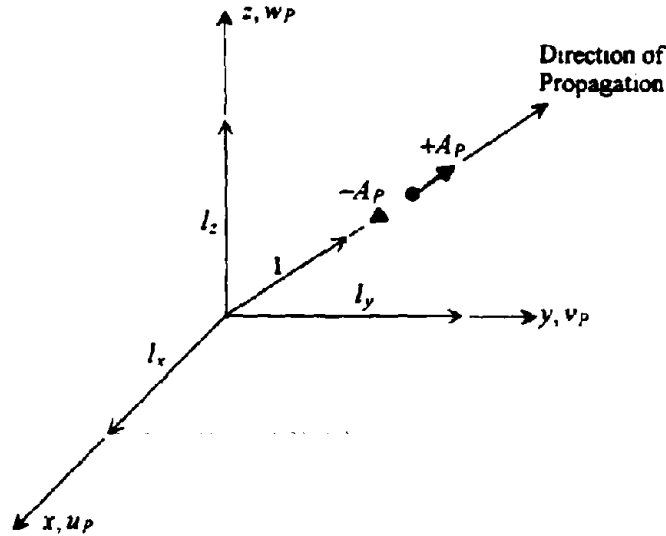


Figure 125. Displacements Associated with Incident P-wave

3. Secondary-wave Equation.

As the S-wave (secondary wave or distortional wave) propagates, it shears the medium sideways at right angles to the direction of propagation (see Figure 126). The rotational-strain vector $\{\Omega\}$ defined in Equation (530) can be used to interpret this behavior. To find the unknown amplitudes of the rotational-strain vector for Equation (545), the trial vector is assumed as

$$\{\Omega(x, y, z)\} = -\frac{1\omega}{2C_S} \{C\} \exp\left[-\frac{1\omega}{C_S}(m_x x + m_y y + m_z z)\right] \quad (550)$$

The trial vector in Equation (550) satisfies equilibrium Equation (545), only if $m_x^2 + m_y^2 + m_z^2 = 1$ and $m_x C_x + m_y C_y + m_z C_z = 0$ where C_x , C_y and C_z are components of vector $\{C\}$. Direction cosines m_x , m_y and m_z in the former specify the direction of

propagation. Since the scalar product in the latter vanishes, vector $\{C\}$ and thus $\{\Omega\}$ are perpendicular to the direction of propagation. Applying $m_x^2 + m_y^2 + m_z^2 = 1$, $m_x C_x + m_y C_y + m_z C_z = 0$ and Equation (530) to the trial vector [Equation (550)], each row of the trial vector is expanded and separated into groups. These groups correspond to $u_y, u_z(\ominus)$, $v_x, v_z(\otimes)$, and $w_x, w_y(\oplus)$, respectively. Then, integrating each group (\ominus, \otimes, \oplus) and setting its integration constant to zero results in displacements u_s, v_s , and w_s corresponding to x -, y -, and z -direction, respectively.

First row multiplied by 2

$$\begin{aligned}
 2\Omega_x = w_y - v_z &= -\frac{i\omega}{C_S} [C_x(m_x^2 + m_y^2 + m_z^2) - m_x(m_x C_x + m_y C_y + m_z C_z)] \\
 &\quad \exp\left[-\frac{i\omega}{C_S}(m_x x + m_y y + m_z z)\right] \Rightarrow \\
 \Rightarrow w_y &= -\frac{i\omega}{C_S} m_y (m_y C_x - m_x C_y) \exp\left[-\frac{i\omega}{C_S}(m_x x + m_y y + m_z z)\right] \rightarrow \oplus \\
 \Rightarrow v_z &= -\frac{i\omega}{C_S} m_z (m_x C_z - m_z C_x) \exp\left[-\frac{i\omega}{C_S}(m_x x + m_y y + m_z z)\right] \rightarrow \otimes
 \end{aligned}$$

Second row multiplied by 2

$$\begin{aligned}
 2\Omega_y = u_z - w_x &= -\frac{i\omega}{C_S} [C_y(m_x^2 + m_y^2 + m_z^2) - m_y(m_x C_x + m_y C_y + m_z C_z)] \\
 &\quad \exp\left[-\frac{i\omega}{C_S}(m_x x + m_y y + m_z z)\right] \Rightarrow \\
 \Rightarrow u_z &= -\frac{i\omega}{C_S} m_z (m_z C_y - m_y C_z) \exp\left[-\frac{i\omega}{C_S}(m_x x + m_y y + m_z z)\right] \rightarrow \ominus \\
 \Rightarrow w_x &= -\frac{i\omega}{C_S} m_x (m_y C_x - m_x C_y) \exp\left[-\frac{i\omega}{C_S}(m_x x + m_y y + m_z z)\right] \rightarrow \oplus
 \end{aligned}$$

Third row multiplied by 2

$$2\Omega_z = v_x - u_y = -\frac{1\omega}{C_S} [C_z(m_x^2 + m_y^2 + m_z^2) - m_z(m_x C_x + m_y C_y + m_z C_z)]$$

$$\exp\left[-\frac{1\omega}{C_S}(m_x x + m_y y + m_z z)\right] \Rightarrow$$

$$\Rightarrow v_x = -\frac{1\omega}{C_S} m_x (m_x C_z - m_z C_x) \exp\left[-\frac{1\omega}{C_S}(m_x x + m_y y + m_z z)\right] \rightarrow \otimes$$

$$\Rightarrow u_y = -\frac{1\omega}{C_S} m_y (m_z C_y - m_y C_z) \exp\left[-\frac{1\omega}{C_S}(m_x x + m_y y + m_z z)\right] \rightarrow \ominus$$

Displacements

$$\ominus \rightarrow u_S = (m_z C_y - m_y C_z) \exp\left[-\frac{1\omega}{C_S}(m_x x + m_x y + m_z z)\right] \quad (551)$$

$$\otimes \rightarrow v_S = (m_x C_z - m_z C_x) \exp\left[-\frac{1\omega}{C_S}(m_x x + m_x y + m_z z)\right] \quad (552)$$

$$\oplus \rightarrow w_S = (m_y C_x - m_x C_y) \exp\left[-\frac{1\omega}{C_S}(m_x x + m_x y + m_z z)\right] \quad (553)$$

Subscript S indicates that the corresponding displacements are associated with S-wave. Equations (551), (552), and (553) show that the displacement amplitudes are proportional to the components of the vector product of $\{C\}$ and the direction of propagation. It follows that the particle motion of S-wave lies in the plane perpendicular to the direction of propagation and is constant over this plane. The material-dependent velocity of propagation C_S is constant.

By using geometric consideration in Figure 127, the displacement vector can be further decomposed into a horizontal component with amplitude A_{SH} , lying in the plane

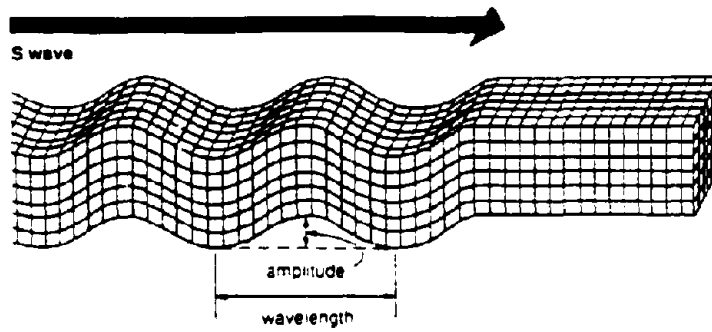


Figure 126. Cross Section of Incident S-wave

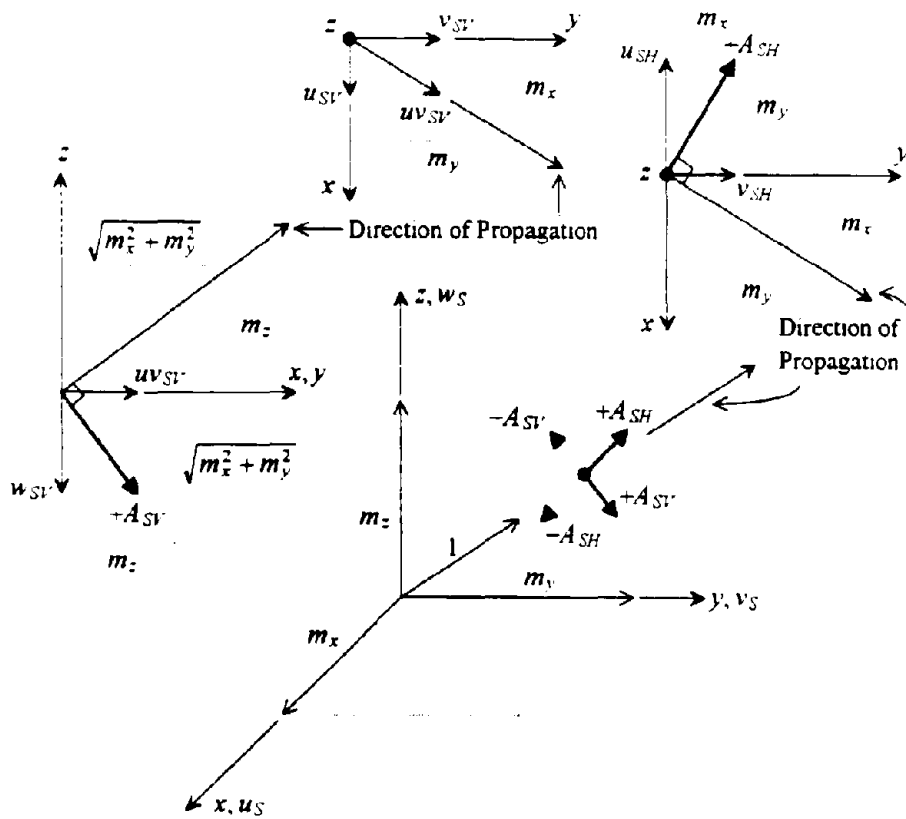


Figure 127. Displacements Associated with Incident S-wave

which is parallel to x - y plane, and into a component with amplitude A_{SV} , lying in the plane which contains the vertical z -axis and direction of propagation.

$$A_{SH} = \frac{C_z}{\sqrt{m_x^2 + m_y^2}} \quad (554)$$

$$A_{SV} = \frac{m_x C_y - m_y C_x}{\sqrt{m_x^2 + m_y^2}} \quad (555)$$

where A_{SH} and A_{SV} are the amplitudes of SH- and SV-wave at the point where $x = y = z = 0$, respectively. The displacements (see Figure 127) can be reformulated in terms of these amplitudes as

$$u_S = u_{SH} + u_{SV} = \frac{-m_y A_{SH} + m_x m_z A_{SV}}{\sqrt{m_x^2 + m_y^2}} \exp\left[-\frac{i\omega}{C_S}(m_x x + m_y y + m_z z)\right] \quad (556)$$

$$v_S = v_{SH} + v_{SV} = \frac{m_x A_{SH} + m_y m_z A_{SV}}{\sqrt{m_x^2 + m_y^2}} \exp\left[-\frac{i\omega}{C_S}(m_x x + m_y y + m_z z)\right] \quad (557)$$

$$w_S = w_{SV} = -\sqrt{m_x^2 + m_y^2} A_{SV} \exp\left[-\frac{i\omega}{C_S}(m_x x + m_y y + m_z z)\right] \quad (558)$$

As described in Equations (540) and (542), P- and S-wave velocities are equal to $\sqrt{(2Y^* + \lambda^*)/\rho}$ and $\sqrt{Y^*/\rho}$, respectively. The always larger numerator of the former leads to P-wave velocity being faster than S-wave velocity. Therefore, at an observation point on the surface, amplitude of P-wave is first recorded and then that of S-wave as shown in Figure 128.

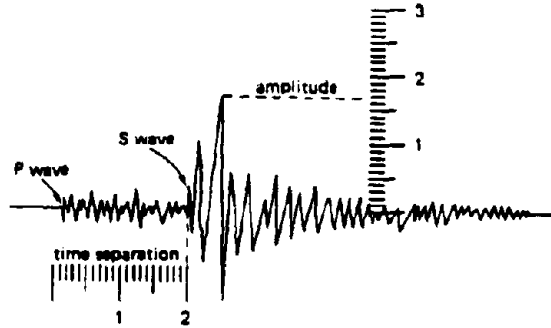


Figure 128. Typical Earthquake Record

4. In-plane Displacement Equation for Horizontal Layer.

The origin of the local coordinate system with the z -axis pointing downward is located at the top of the horizontal layer as shown in Figure 129. Assuming the directions of propagation of the P- and S-wave lie in the same vertical plane, say the x - z plane, leads to $l_y = m_y = 0$. Adding the displacements caused by P-wave (C.45) and (C.47) and S-wave (C.54) and (C.56) in x - and z -direction, the total motion can be expressed as

$$u(x, z) = l_x A_P \exp \left[-\frac{i\omega}{C_P} (l_x x + l_z z) \right] + m_z A_{SV} \exp \left[-\frac{i\omega}{C_S} (m_x x + m_z z) \right] \quad (C.57)$$

$$w(x, z) = l_z A_P \exp \left[-\frac{i\omega}{C_P} (l_x x + l_z z) \right] - m_x A_{SV} \exp \left[-\frac{i\omega}{C_S} (m_x x + m_z z) \right] \quad (C.58)$$

In-plane displacements with amplitudes u and w depend only on the P- and SV-wave. The out-of-plane displacement with amplitude v (perpendicular to x - z plane), caused by the SH-wave, is independent of u , w and not mentioned here. The form of Equations (C.57) and (C.58) compels the boundary conditions at the top and bottom of the layer to vary as $\exp(-i\omega l_x x / C_P)$ and as $\exp(-i\omega m_x x / C_S)$. To achieve the same variation with x , the following condition needs to be imposed.

$$\frac{l_x}{C_P} = \frac{m_x}{C_S} \quad (561)$$

As a total of four boundary conditions has to be satisfied (displacements with amplitudes u and w at top and bottom of layer), a second P- and SV-wave with the same variation in x is introduced (see Figure 129). Since $l_y = 0$, for any value of l_x , l_z can be selected as $\pm\sqrt{1-l_x^2}$. The value l_x equals $\cos \psi_p$, whereby ψ_p is the angle of incidence of the P-wave measured from x -axis. This interpretation holds only for a real value which is smaller than or equal to 1. Analogously, m_x can be chosen as $\pm\sqrt{1-m_x^2}$ with $m_x = \cos \psi_s$, whereby ψ_s is the angle of incidence of the S-wave measured from x -axis. Substituting l_x and m_x into Equations (559) and (560) leads to

$$u(x, z) = l_x \left[A_P \exp\left(\omega \frac{\sqrt{1-l_x^2}}{C_P} z\right) + B_P \exp\left(-\omega \frac{\sqrt{1-l_x^2}}{C_P} z\right) \right] \exp\left(-\omega \frac{l_x}{C_P} x\right) - \sqrt{1-m_x^2} \left[A_{SV} \exp\left(\omega \frac{\sqrt{1-m_x^2}}{C_S} z\right) - B_{SV} \exp\left(-\omega \frac{\sqrt{1-m_x^2}}{C_S} z\right) \right] \exp\left(-\omega \frac{m_x}{C_S} x\right) \quad (562)$$

$$w(x, z) = -\sqrt{1-l_x^2} \left[A_P \exp\left(\omega \frac{\sqrt{1-l_x^2}}{C_P} z\right) - B_P \exp\left(-\omega \frac{\sqrt{1-l_x^2}}{C_P} z\right) \right] \exp\left(-\omega \frac{l_x}{C_P} x\right) - m_x \left[A_{SV} \exp\left(\omega \frac{\sqrt{1-m_x^2}}{C_S} z\right) + B_{SV} \exp\left(-\omega \frac{\sqrt{1-m_x^2}}{C_S} z\right) \right] \exp\left(-\omega \frac{m_x}{C_S} x\right) \quad (563)$$

where A_P , A_{SV} and B_P , B_{SV} are amplitudes of waves traveling in the negative and positive z -direction, respectively (see Figure 129). Definitions of A_P and A_{SV} here differ from Equations (559) and (560) where they are defined as the amplitudes of general waves. For convenience, the following notation is introduced.

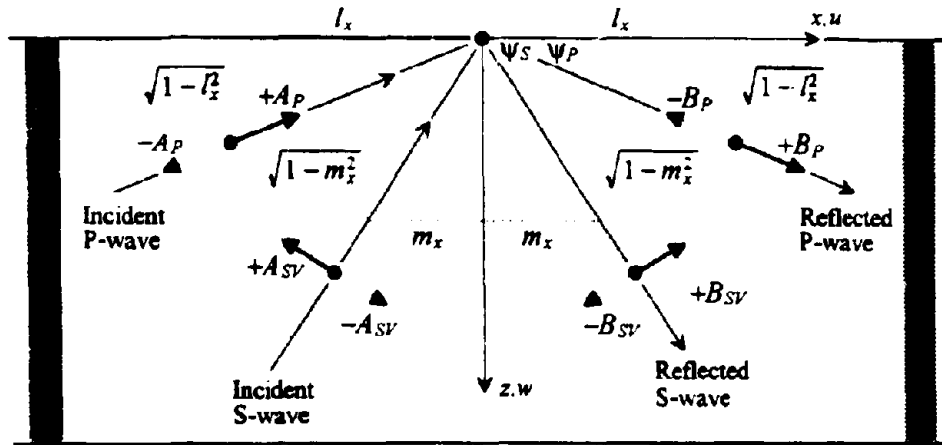


Figure 129. In-plane Displacements for a Horizontal Layer

$$\text{Phase velocity : } C = \frac{C_P}{l_x} = \frac{C_S}{m_x} \quad (564)$$

$$\text{Wave number : } k = \frac{\omega}{C} \quad (565)$$

$$\text{Scalar } f : f = \sqrt{\frac{1}{l_x^2} - 1} \quad (566)$$

$$\text{Scalar } s : s = \sqrt{\frac{1}{m_x^2} - 1} \quad (567)$$

Using Equations (564) through (567), the in-plane displacements in Equations (562) and (563) can be rewritten as

$$u(x, z) = u(k, z) \exp(-l_x x) \quad (568)$$

$$w(x, z) = w(k, z) \exp(-l_x x) \quad (569)$$

with

$$u(k, z) = l_x [A_p \exp(ukfz) + B_p \exp(-ukfz)] - m_x s [A_{SV} \exp(uksz) - B_{SV} \exp(-uksz)] \quad (570)$$

$$w(k, z) = -l_x f [A_p \exp(ukfz) - B_p \exp(-ukfz)] - m_x [A_{SV} \exp(uksz) + B_{SV} \exp(-uksz)] \quad (571)$$

where $l_x/C_p = m_x/C_s$ needs to be enforced. Displacements $u(k, z)$ and $w(k, z)$ in Equations (568) and (569) can be interpreted as the amplitudes of waves propagating in the positive x -direction (for a positive wave number k) with phase velocity C .

For the vertically incident wave, the angle of incident $\psi_p = \psi_s = 90^\circ$ ($l_x = m_x = 0$). Therefore the phase velocity C equals infinity and $k=0$. Since $l_x = m_x = 0$, the in-plane displacements in Equations (562) and (563) can be reformulated as

$$u(x, z)^{k=0} = -A_{SV} \exp\left(\frac{i\omega}{C_s} z\right) + B_{SV} \exp\left(-\frac{i\omega}{C_s} z\right) \quad (572)$$

$$w(x, z)^{k=0} = -A_p \exp\left(\frac{i\omega}{C_p} z\right) + B_p \exp\left(-\frac{i\omega}{C_p} z\right) \quad (573)$$

In this special case, it should be noted that the displacements have no variation in x -direction.

REFERENCES

- Alam, S. and S. Baba (1993), "Robust Active Optimal Control Scheme Including Soil-structure Interaction," Journal of Structural Engineering, 119, 2533-51.
- Burden, R.L. and J.D. Faires (1988), Numerical Analysis, PWS-KENT Publishing Company, Boston, 184-189.
- Cheng, F.Y. and C.P. Pantelides (1986), "Optimum Seismic Structural Design with Tendon and Mass Damper Controls and Random Process," Proc. Structures Congress, Recent Developments in Structural Optimization, ASCE, F.Y. Cheng, ed., New Orleans, 40-53.
- Cheng, F.Y. (1988), "Response Control Based on Structural Optimization and its Combination with Active Protection," theme paper, Proc. of 9th World Conference on Earthquake Engineering, Tokyo/Kyoto, Vol.VIII, 471-476.
- Cheng, F.Y., P. Tian, and S. Suthiwong (1992), "Generalized Optimal Active Control Algorithm of Seismic Structures and Related Soil-Structure Formulation," Computational Mechanics in Structural Engineering-Recent Developments and Future Trends, eds. F.Y. Cheng and Fu Z.Z., Elsevier Applied Science, 49-62.
- Cheng, F.Y. and P. Tian (1993), "Generalized Optimal Active Control Algorithm with Weighting Matrix Configuration, Stability and Time-delay," International Journal of Structural Engineering and Mechanics, Vol.1, No.1, 119-135.
- Cheng, F.Y. and S. Suthiwong (1994), "Active Control of Building Structures on Mat Foundation Embedded in Unbounded Soil," Proc. 5th U.S. National Conference on Earthquake Engineering, Chicago, 1043-1054.
- Cheng, F.Y., S. Suthiwong, and P. Tian (1994), "Generalized Optimal Active Control with Embedded and Half-space Soil-structure Interaction," Proc. 11th Conference on Analysis and Computation (formerly Electronic Computation Conference), ASCE, F.Y. Cheng, ed., 337-346.
- Hayashi, Y. and H. Katukura (1990), "Effective Time-domain Soil-structure Interaction Analysis Based on FFT Algorithm with Causality Condition." Earthquake Engineering and Structural Dynamics, 19, 693-708.

Smith, H.A. W.H. Wu, and R.I. Borja (1994), "Structural Control Considering Soil-structure Interaction Effects," Earthquake Engineering and Structural Dynamics, 23, 609-626.

Soong, T.T. (1990), Active Structural Control: Theory and Practice, Longman, London, and Wiley, New York.

Wolf, J.P. and G.R. Darbre (1983), "Dynamic-stiffness Matrix of Embedded and Pile Foundations by Indirect Boundary Element Method," Trans. 7th International Conference on Structural mechanics Reactor Technology, Chicago, Paper K11/1, K(b), 245-258.

Wolf, J.P. and G.R. Darbre (1984a), "Dynamic-stiffness Matrix of Soil by the Boundary-element Method: Conceptual Aspects," Earthquake Engineering and Structural Dynamics, 12, 385-400.

Wolf, J.P. and G.R. Darbre (1984b), "Dynamic-stiffness Matrix of Soil by the Boundary-element Method: Embedded Foundation," Earthquake Engineering and Structural Dynamics, 12, 401-406.

Wong, H.L. and J.E. Luco (1991), "Structural Control Including Soil-structure Interaction Effects," Journal of Engineering Mechanics, 117, 2237-50.

Yang, J.N., A. Akbarpour, and P. Ghaemmaghami (1987), Instantaneous Optimal Control Laws for Building Structures under Earthquake Excitations, Technical Report, National Center for Earthquake Engineering Research, NCEER-TR-87-0007.

BIBLIOGRAPHY

Bathe, K.J. (1982), Finite Element Procedures in Engineering Analysis, Prentice-Hall, New Jersey, 527-532.

Kausel, E. and J.M. Roesset (1981), "Stiffness Matrices for Layered Soils," Bulletin of the Seismological Society of America, 71, 1743-1761.

Papoulis, A. (1977), Signal Analysis, McGraw-Hill, New York.

Oppenheim, A.V. and R.W. Schaffer (1989), Discrete-time Signal Processing, Prentice-Hall, New Jersey, 20, 664-670.

Rockey, K.C., H.R. Evans, and D.W. Griffiths (1983), The Finite Element Method: A Basic Introduction for Engineers, John Wiley & Sons, New York, .

Schultz, D.G. and J.L. Melsa (1967), State Functions and Linear Control Systems, McGraw-Hill, New York, 197-254.

Wolf, J.P. (1985), Dynamic Soil-structure Interaction, Prentice-Hall, New Jersey.

REPORT DOCUMENTATION PAGE		1. REPORT NO. Structural Series 96-2	2.	3. Recipient's Accession No.
4. Title and Subtitle Active Control for Seismic-Resistant Structures on Embedded Foundation in Layered Half-Space				5. Report Date August 1996
7. Author(s) Franklin Y. Cheng and Sukit Suthiwong				6. Performing Organization Rept. No. Structural Series
9. Performing Organization Name and Address Department of Civil Engineering University of Missouri-Rolla Rolla, MO 65409-0030				10. Project/Task/Work Unit No.
12. Sponsoring Organization Name and Address National Science Foundation 4201 Wilson Blvd. Arlington, VA 22230				11. Contract(C) or Grant(G) No. (C) NSF BCS 9302201 (G) NCEER R-35696
				13. Type of Report & Period Covered Final (partial)
14.				
15. Supplementary Notes				
16. Abstract (Limit: 200 words) The response behavior of seismically excited frame structures with active control and boundless soil is investigated. Mathematical models based on the existence or absence of structure-soil interaction (SSI) and/or control are presented. With SSI consideration, the frequency-dependent property of unbounded nonhomogeneous soil and foundation embedment is applied. Optimal closed-loop laws are established based on the generalized performance index. In the control system considering SSI effects, foundation translation and rocking are included in the control rule. Algorithms are implemented in the time domain. Studies indicate the strong influence of foundation embedment and depth of soil layer on soil-rocking coefficients and consequently on structural response. In a certain structure, additional modes as a result of the foundation's degrees of freedom dominate and hence result in distinct structural response behavior. For example, the rocking mode is important in a massive and/or high-rise structure while the translation mode dominates in a low-rise structure. In a massive low-rise structure such as a nuclear reactor, the combination of these two dominant modes leads to large structural responses. In the control system including SSI effects, reduction of structural response is a result of the decrease in foundation rocking rather than relative floor translation which occurs where the structure is fixed at its base. Furthermore, the effect of control force in strengthening the system's stiffness and damping is reduced in the case of a structure founded on soft soil.				
17. Document Analysis a. Descriptors				
Active control		Foundation	Closed loop	
Earthquake		Rocking	Performance Index	
Half-space		Embedment		
Soil Structure Interaction		Optimization		
b. Identifiers/Open-Ended Terms				
c. COSATI Field/Group				
18. Availability Statement		19. Security Class (This Report) Unclassified	21. No. of Pages 295	
		20. Security Class (This Page) Unclassified	22. Price	